UNIVERSITY OF CALIFORNIA SAN DIEGO

# Low Valent Iron Isocyanide Complexes: Multinuclear Mimics of Metal Surfaces and Mononuclear Analogues of Classical Organometallic Systems

A dissertation submitted in partial satisfaction of the requirements
for the degree Doctor of Philosophy

in

Chemistry

by

Myles Joseph Drance

Committee in charge:

Professor Joshua S. Figueroa, Chair
Professor Clifford P. Kubiak
Professor Darren J. Lipomi
Professor Joseph M. O'Connor
Professor F. Akif Tezcan

The Dissertation of Myles Joseph Drance is approved, and it is acceptable in quality and form for publication on microfilm and electronically:

_____

_____

_____

_____

_____

Chair

University of California San Diego

2020

DEDICATION

*For my parents, Michael and Patricia.*

# EPIGRAPH

Imagination is more important than knowledge.
Knowledge is limited. Imagination encircles the world.

Albert Einstein

TABLE OF CONTENTS

LIST OF FIGURES

LIST OF SCHEMES

LIST OF TABLES

ACKNOWLEDGMENTS

Grad school is often presented as an endeavor rooted in individualism, but it is impossible to complete this long journey alone. I am incredibly fortunate to have met many amazing people over the years who have contributed to my personal and intellectual growth. I hope these next few pages come close to conveying how appreciative I am to each and every one of you.

I must first thank my advisor, Josh Figueroa, for taking a chance on an indecisive first year 64 months ago. I came into grad school wanting to contribute to solving the world's energy crisis, but I wound up joining one of the most fundamental and un-applied research labs in the department. Your intense passion for chemistry immediately drew me in during that Thursday recruitment dinner at Rock Bottom. I knew I wanted to be in a high-energy environment surrounded by other motivated individuals, and your lab was the best fit. I quickly grew to love "Figueroa Chemistry" that truly pushes boundaries and expands chemical space. You gave me the freedom to pursue targets I wanted and pushed me to dive deep in order to understand systems better than anyone else. Your excellent mentorship in my research experience has been complemented by invaluable conversations on academic life that have undoubtedly shaped my view of the leader I hope to be in my future career. For your generosity at Pizza Port/Porter's/Soda & Swine/The Loft, the invitations to ACS afterparties, and the intellectual and personal coaching, I am forever grateful.

Probably the greatest factor that led me to join the Figueroa group was the next-level caliber of students. No one has been more influential to my growth as a chemist than Charles Mokhtarzadeh. Chuck, you are one of the most helpful people I've ever met, which was immediately apparent when you guided me through the synthesis of $Na[Fe_4(\mu^4\text{-}N)(CO)_{12}]$ early in my first year. I quickly learned to "trust in Chuck", and my air-free technique greatly improved.

Watching you make some otherworldly molecules was a huge inspiration during our overlapping years. I have tried to carry on this chemical fearlessness throughout grad school, and I'll make sure that many chemists in my future know of the fabled Chuck. Brandon Barnett's ability to frame a project and get all the data before Josh had to ask was unparalleled. I owe you a tremendous debt of gratitude for helping me develop my writing style and the ability to find the story the data want to tell. I especially want to thank you for your assistance in my postdoc application process and the applications to fellowships that followed. You have been so responsive despite all your own stresses, and I can't wait to see what you accomplish at UofR. Doug Agnew was a model of efficiency and focus that I still have a lot to learn from. You and I had painfully different tastes in music, but that made it feel like an accomplishment the two or three times we agreed on a song playing in lab. Thank you for the help in preparing for my candidacy exam and reviewing my postdoc application package.

I want to thank Kyle Mandla for the countless late nights and coffee cart escapes made over the almost four years we worked together. Our agreements and disagreements over chemistry, life, politics, and everything in between have been transformative both professionally and personally making me a better chemist and a more thoughtful person. You and Joanne Chan were the best labmates I could've asked for. Joanne, you've been such a good friend and confidant. I appreciate you going on walks to get coffee with me especially when you didn't even want any coffee. Our conversations during these breaks and in the lab were always so helpful. It was a privilege going through grad school with you. Mike and Alejandra kept the fire going when they joined the lab. Mike's enthusiasm about everything is an amazing presence that helps keep things lighthearted. Although sometimes annoying, your jokes and excitability really kept me going through some difficult times. Thank you for not letting grad school crush your spirit. Alejandra,

I've admired your intense focus since the beginning. You've really done a great job turning a bunch of loose pieces left over from Doug into a cool research program, and I'm glad we've gotten closer in the past couple years.

Simply put, Vincent Wang is a machine. We knew you were hardcore ever since your single-day roundtrip flight from NY to CA for your interview… But you far exceeded expectations not only in your work ethic and research capabilities but also in being a great person. You fit the lab perfectly, kept me motivated through everything, and continue to be a great resource to the entire lab. Kudos to Haeun, Ritchie, and Adam for braving the two year gap of students in our lab. I can't imagine how much more difficult the transition to graduate life is without second or third year mentors, but you've all made it work. I've enjoyed watching your progress, and I look forward to seeing what you all achieve. Same to you, Krista. Your energy fits the Figueroa group well, and if you keep up the intensity and curiosity, you will do amazing things. My sincerest thanks again to all of my former and current labmates.

I would like to also thank my committee, Professors Darren Lipomi, Cliff Kubiak, Joe O'Connor, and Akif Tezcan for their insightful questions and suggestions during departmental exams and my defense. Professors Arnie Rheingold and Guy Bertrand, your letters of support helped me secure my top choice postdoc position in addition to an Arnold O. Beckman Postdoctoral Fellowship. I hope I'm able to convey my indebtedness for these incredible opportunities. Of course, our world-class X-ray diffraction facility has led to so many incredible discoveries, and I am so fortunate to have had access with assistance from the "dream team" of crystallography, Arnie, Milan, and Curtis. Anthony Mrse has been a huge help in figuring out different NMR experiments, always engaging in interesting conversation every step of the way. You've all taught me so much. Additionally, I am grateful to UCSD Inorganic Chemistry as a

whole for being such a brilliant, friendly, hard-working, and welcoming group of people. To the members of the Bertrand group, I thank you for the healthy competition and allowing me to crash your coffee and lunch breaks. Cory Weinstein and Daniel Tolentino were friendly resources to me ever since my first lab rotation. Mo, thank you for assistance with CV and your willingness to engage. “ALLEZ PSG!” Rudy, getting to know you has been a treat, and your brilliance coupled with humility and approachability make you a fantastic role model. Jesse, I’ve enjoyed growing with you through grad school, and I look forward to watching your continued success. Thank you Profs. Jeff Rinehart, Valerie Schmidt, and Alina Schimpf for your candid advice and generosity in offering a glimpse into life as an assistant professor. I thank Jeremy Hilgar for giving crash courses on EasySpin and MATLAB and being a dependably good person after breaking through the tough exterior. Ryan Holland also contributed greatly to my growth through many helpful and stimulating conversations about research, politics, and life.

I could go on for a hundred pages thanking my friends outside of lab for their kindness and recounting so many amazing memories, but I owe a special shout out to Nick Forsch, Kim McCabe, Naneki McCallum, Matt Nattichia, Pauline Olsen, Sarah Mishek, and Leo Gallo who I could rely on during my personal struggles, especially in my second year, and were there for me as I came through a happier and fuller person. Thanks also to the rest of our first-year crew (Yanice, Allie, Eunice, Jeff, Jon, Dan, Ben, Mitchell) and the Beeramar folks the year below us. You’ve all made grad school a lot more fun than I could’ve imagined.

I had no idea I would be going to grad school when I first started undergrad, but my professors at Colgate University fostered a rich, collaborative environment that encouraged me to pursue my passions. I didn’t know at the time how remarkable my advisor Prof. Anthony Chianese was, but he was an excellent mentor, developing in me a strong foundation in organometallic

research. Prof. Ephraim Woods was super important in my early pedagogical development. The amount of care he put into his classes will always stick with me. The same can be said for many of my earlier science teachers throughout grade school. To Mr. McInnes, Mr. Wallace, Mr. Zenyuh, and Mr. Murphy, thank you.

Almost three years ago, I met an amazing individual who has taught me to be more caring and selfless. Carlos De La Torre, your kindness, fun-loving attitude, and ability to make a room smile have helped keep me grounded through so many intense ups and downs. I love you for everything you continue to do for me.

My family has been a constant source of strength for my entire life. Even though I'm the first to pursue a PhD or a career in research, they've always sought to help in any way they can. I thank my brother for leading by example wanting to be the best at what he does. And I cannot come close to expressing my gratitude and love to my parents, for whom I dedicate this dissertation. Thank you for allowing me to find my own passions and pushing me to stay on track when I needed it. Your love, strength, and support have been my safety net in life. You've done so much for me in my nearly 28 years that the least I can do is dedicate my accomplishments to you. All my love to you, Mom and Dad.

To everyone above and to those I have forgotten to mention, thank you for everything.

**Chapter 2**: This chapter is adapted with permission from Drance, M. J.; Mokhtarzadeh, C. C.; Melaimi, M.; Agnew, D. W.; Moore, C. E.; Rheingold, A. L.; Figueroa, J. S. "Controlled Expansion of a Strong-Field Iron-Nitride Cluster: Multi-Site Ligand Substitution as a Strategy for Activating Interstitial Nitride Nucleophilicity" *Angewandte Chemie, International Edition* **2018**, *57*, 13057–13061. Copyright 2018 Wiley-VCH, Weinheim. Permission to include published material in this dissertation has been obtained from all coauthors. The dissertation author is the first author of this paper. Prof. M. J. Tauber is also acknowledged for assistance with EPR measurements.

**Chapter 3**: This chapter is adapted with permission from Drance, M. J.; Sears, J. D.; Mrse, A. M.; Moore, C. E.; Rheingold, A. L.; Neidig, M. L.; Figueroa, J. S. "Terminal Coordination of Diatomic Boron Monofluoride to Iron" *Science*, **2019**, *363*, 1203–1205. Copyright 2019 The Authors. Permission to include published material in this dissertation has been obtained from all coauthors. The dissertation author is the first author of this paper. Prof. C. C. Cummins, Prof. G. Debelouchina, and Dr. B. R. Barnett are also thanked for helpful discussions.

**Chapter 4**: This chapter is currently in preparation as a manuscript by Drance, M. J.; Sears, J. D.; Gembicky, M; Rheingold, A. L.; Neidig, M. L.; Figueroa, J. S. The dissertation author is the first author of this paper.

**Chapter 5**: This chapter is currently in preparation as a manuscript by Drance, M. J.; Gembicky, M; Rheingold, A. L.; Figueroa, J. S. The dissertation author is the first author of this paper.

VITA

2014 Bachelor of Arts, Chemistry, Colgate University

2016 Master of Science, Chemistry, University of California San Diego

2020 Doctor of Philosophy, Chemistry, University of California San Diego

PUBLICATIONS

**Drance, M. J.**; Sears, J. D.; Mrse, A. A.; Moore, C. E.; Rheingold, A. L.; Neidig, M. L.; Figueroa, J. S. "Terminal Coordination of Diatomic Boron Monofluoride to Iron", *Science* **2019**, *363*, 1203-1205.

**Drance, M. J.**; Mokhtarzadeh, C. C.; Melaimi, M.; Agnew, D. W.; Moore, C. E.; Rheingold, A. L.; Figueroa, J. S. "Controlled Expansion of a Strong-Field Iron Nitride Cluster: Multi-Site Ligand Substitution as a Strategy for Activating Interstitial Nitride Nucleophilicity" *Angewandte Chemie, International Edition* **2018**, *57*, 6853-6857 (Cover Article).

Kim, D.; Le, L.; **Drance, M. J.**; Jensen, K. H.; Bogdanovski, K.; Cervarich, T. N.; Barnard, M. G.; Pudalov, N. J.; Knapp, S. M.; Chianese, A. R. "Ester Hydrogenation Catalyzed by CNN-Pincer Complexes of Ruthenium," *Organometallics* **2016**, *35*, 982-989.

Chianese, A. R.; **Drance, M. J.**; Jensen, K. H.; McCollom, S. P.; Yusufova, N.; Shaner, S. E.; Shopov, D. Y.; Tendler, J. A. "Acceptorless Alkane Dehydrogenation Catalyzed by Iridium CCC-Pincer Complexes," *Organometallics* **2014**, *33*, 457-464.

ABSTRACT OF THE DISSERTATION

**Low Valent Iron Isocyanide Complexes: Multinuclear Mimics of Metal Surfaces and Mononuclear Analogues of Classical Organometallic Systems**

by

Myles Joseph Drance

Doctor of Philosophy in Chemistry

University of California San Diego, 2020

Professor Joshua S. Figueroa, Chair

This dissertation details the utilization of anionic, nucleophilic iron complexes supported by *m*-terphenyl isocyanide and carbonyl ligands to address longstanding questions in organometallic and inorganic chemistry. Chapter 1 offers a brief account of the development of low valent transition-metal chemistry with carbon monoxide (CO) and isocyanides in mononuclear and multinuclear systems. Metal carbonyl clusters gained popularity as molecular surrogates for reactive sites on heterogeneous catalyst surfaces, and some successes and shortcomings of this cluster-surface analogy are revisited in Chapter 2. The synthesis and reactivity of the tetra-iron

nitrido cluster $[Fe(\mu^4\text{-}N)(CO)_8(CNAr^{Mes2})_4]^-$ ($Ar^{Mes2}$ = 2,6-(2,4,6-$Me_3C_6H_2)_2C_6H_3$) is contrasted with the less electron-rich all-carbonyl congener $[Fe(\mu^4\text{-}N)(CO)_{12}]^-$. Ligand substitution is shown to impart nucleophilicity to the interstitial nitride, and this characteristic enables rational cluster expansion with main-group and transition-metal ions to yield unsaturated sites. The resulting clusters were found to display surface-like reactivity through coordination-sphere-dependent atom rearrangement and metal-metal cooperativity.

The remaining three chapters stem from $K_2[Fe(CO)_2(CNAr^{Tripp2})_2]$ ($Ar^{Tripp2}$ = 2,6-(2,4,6-(*i*-Pr)$_3C_6H_2)_2C_6H_3$). In Chapter 3, this metalate is used to generate $Fe(BF)(CO)_2(CNAr^{Tripp2})_2$, the first stable terminal fluoroborylene complex. Importantly, the isoelectronic species $Fe(N_2)(CO)_2(CNAr^{Tripp2})_2$ and $Fe(CO)_3(CNAr^{Tripp2})_2$ are also described allowing for the direct comparison of neutral 10 valence-electron ligands. Single-crystal X-ray diffraction, nuclear magnetic resonance, infrared, and Mössbauer spectroscopic studies demonstrate that the terminal BF ligand possesses particularly strong σ-donor and π-acceptor properties in accord with theoretical predictions. Density functional theory and electron-density topology calculations support this conclusion. The reactivity of $Fe(BF)(CO)_2(CNAr^{Tripp2})_2$ is discussed in Chapter 4. Like all terminal borylene ligands, coordinated BF is shown to be electrophilic at boron, forming Lewis acid-base adducts with various nucleophiles. However, the fluoroborylene ligand can be derivatized further than other borylenes and converted stepwise into aminoborylene and iminoboryl moieties. Additionally, BF can be transformed directly to the oxoboryl anion $[BO]^-$. The last chapter presents efforts toward an analogue of the unsaturated binary metal carbonyl $Fe(CO)_4$. Unusual solvent binding and bond activations suggest that $Fe(N_2)(CO)_2(CNAr^{Tripp2})_2$ may indeed serve as a masked functional analogue of $Fe(CO)_4$.

# Chapter 1

# Carbon Monoxide and Isocyanides as Ligands to Transition Metals

## 1.1 A Brief History of Late Transition-Metal Carbonyls

A major scientific discovery at the turn of the 20th century was brought about by the astute observation by Mond, Langer, and Quincke that nickel corroded in the presence of impure carbon dioxide.[1,2] The contaminant that led to corrosion was carbon monoxide (CO), and the volatile product formed was $Ni(CO)_4$, the first homoleptic metal carbonyl complex. Although an 1868 description of $PtCl_2(CO)_2$ was the first report of a compound featuring CO as a ligand,[3] $Ni(CO)_4$ quickly garnered more attention in spite of its extreme toxicity for its ease of preparation and utility in the purification of nickel.[4] One year later, Mond and Berthelot independently synthesized $Fe(CO)_5$ advancing this emerging class of unprecedented zerovalent metal compounds.[5-7] However, subsequent progress with other metals was slow with fewer than ten new binary metal carbonyls over the next fifty years.[8]

Because of the highly toxic nature of $Ni(CO)_4$ and limited access to other metal carbonyls, most early studies in this field focused on $Fe(CO)_5$. For example, the photodecomposition of $Fe(CO)_5$ to $Fe_2(CO)_9$ was accurately described as early as 1905 along with other reactions including the synthesis of a highly air-sensitive compound in ethanolic potash that was later inferred to be the first metal carbonyl anion $K_2[Fe(CO)_4]$.[9,10] The industrial scale production of $Fe(CO)_5$ was later achieved in the 1920s by Alwin Mittasch of BASF.[9] A generous donation of this material to Walter Hieber spurred a tremendous expansion of academic research into metal

carbonyls leading to the first metal hydride $H_2Fe(CO)_4$ complex and direct evidence of metal carbonyl anions, the first compounds with metals in formally negative oxidation states.[2,10-12]

During this period, Hieber also discovered some of the earliest polynuclear metal carbonyl complexes and correctly formulated $Fe_3(CO)_{12}$ in 1930.[11,13] However, the field of metal atom cluster chemistry was slow to take off due to the limitations of using elemental analysis for structure determination. The widespread implementation of X-ray diffraction as an analytical method allowed the characterization of multinuclear systems to catch up with the impressive synthetic techniques developed over the previous half-century.[14] Indeed, hundreds of cluster compounds with CO ligands were structurally characterized over the following decades.[14,15]

It was noted that most clusters arranged themselves into polyhedral cores of metal atoms with all triangular faces, and the analogy was quickly drawn to metallic surfaces that have close-packed structures in heterogeneous catalysis.[16-18] This cluster-surface analogy was an attractive comparison to make given the monumental importance of heterogeneous processes such as nitrogen fixation (Haber-Bosch) and the difficulty of characterizing operative intermediates during catalysis.[16,18-22] Molecular clusters, the most common being metal carbonyl clusters, proved to be valuable model systems with regard to understanding the structure and bonding of chemisorbed species on metal surfaces. However, these clusters have had only limited success in mimicking the chemistry of heterogeneous reactions, namely hydrogenations and Fischer-Tropsch catalysis, with the diminished reactivity being ascribed to the coordinative saturation of metal sites with terminal and/or bridging ligands.[18,23-25]

As a result of the rich history of CO in transition-metal chemistry, this ligand has held a vital role in the extension of group theory to chemical systems establishing new methods to analyze the electronic structure of metal compounds and predict the geometries of unsaturated metal

fragments.[26-28] In these models, CO donates a carbon-centered lone pair to an empty metal-based orbital and accepts electron density from filled metal d-orbitals into a degenerate pair of π* orbitals, a synergistic bonding effect that has previously been described for olefin coordination to metals (Figure 1.1).[29,30] For CO, the electronegativity difference between carbon and oxygen renders these donor and accepter orbitals (HOMO and LUMO; highest occupied and lowest unoccupied molecular orbitals) energetically well-matched to interact with transition metals, leading to strong bonds between electron-rich metals and CO.[31,32] Thus, it is no coincidence that the first homoleptic metal carbonyls involved zerovalent nickel, iron, and cobalt with d-electron counts of 10, 8, and 9, respectively. However, the lack of steric protection afforded by CO often renders metal carbonyl complexes labile and vulnerable to undesired side reactions or aggregation processes.[15]

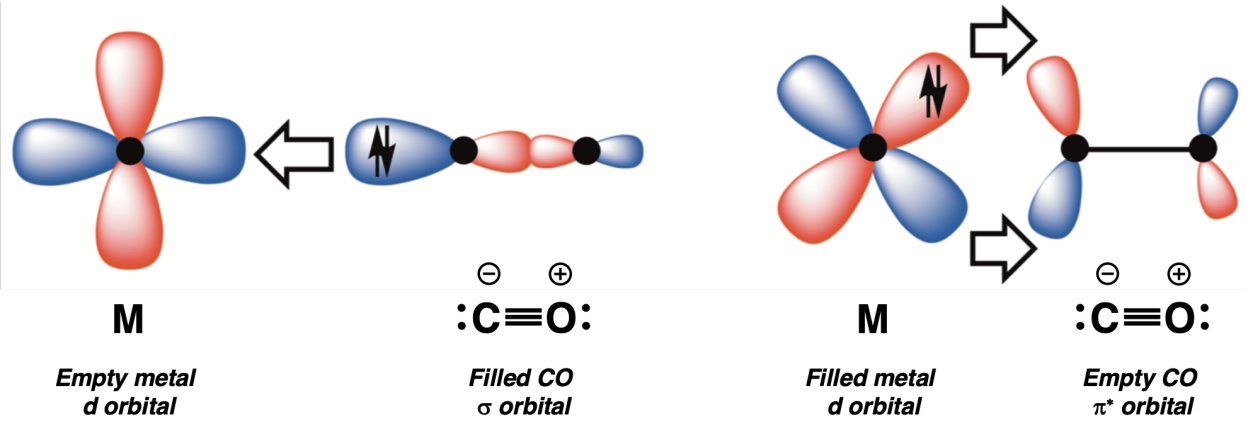


Figure 1.1. Cartoon representation of the Dewar-Chatt-Duncanson bonding model CO in the terminal coordination mode.

## 1.2 Transition-Metal Isocyanide Complexes

Another important class of ligand for the study of metals in low formal oxidation states is the isocyanide (C≡N–R).[33] Isolobal with CO, isocyanides possess a lone pair of electrons localized on carbon and a degenerate set of orthogonal π* orbitals capable of engaging in π-backdonation with a metal center. Yet, isocyanides are stronger σ-donors and weaker π-acceptors than CO owing to the lower electronegativity of the "N–R" unit relative to O.[33-35] A result of this increased σ-donor/π-acceptor ratio is that isocyanides impart greater stability on metal complexes in higher oxidation states than their carbonyl counterparts.[36] Despite this difference, isocyanides more effectively mimic the ligand field of CO than other π-acidic ligands such as trifluorophosphine,[37,38] phosphites,[39] or cyclic alkyl(amino)carbenes (CAACs),[40] As with early investigations of CO as a ligand, the first isocyanide complexes of a transition metal were four-coordinate Ni(0).[41,42] However, unlike CO, it took nearly 30 more years to discover an isocyano analogue of $Fe(CO)_5$,[43] and, homoleptic isocyanide complexes of metals in the 0 oxidation state remain comparatively rare.

An important benefit of organic isocyanides over CO is the ability to modulate their steric profile and, to some extent, electronic properties through the N-bound substituent.[35] Since 2008, our group has sought to use isocyanides in order to isolate mimics of classic unsaturated metal carbonyls that are not stable enough for systematic reactivity studies. These fleeting species result from the cleavage of a metal-metal bond or from the dissociation of one or more molecules of CO. They are often invoked as intermediates in catalytic cycles,[44-46] but they are typically only observed using gas-phase or cryogenic matrix-isolation studies[47] or ultrafast UV pump/IR probe spectroscopy.[48] Before our group's work expanding the encumbrance available to isocyanides, large variations in sterics of the substituent had not been thoroughly explored. Isocyanides

commonly considered to be "bulky", such as *tert*-butyl isocyanide, did not inhibit coordinative saturation, resulting in complexes with the same coordination numbers as their carbonyl relatives. Our group looked to implement the *m*-terphenyl framework, which has been widely used to provide kinetic stabilization as pure σ-aryl ligands[49,50] and as large ancillary groups for amido,[51,52] imido,[51,53] thiolate,[54] and carboxylate moieties,[55,56] among other classes of anionic ligands. Isocyanides with *m*-terphenyl substituents have been synthesized previously for use as supporting ligands in catalysis,[57,58] but their effect on coordination and electronic structure of the metal had not been deeply investigated.

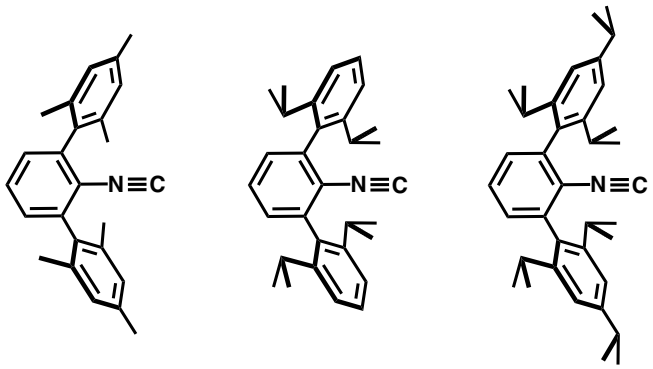


Figure 1.2. Sterically encumbering *m*-terphenyl isocyanides mentioned in this dissertation. (Left) $CNAr^{Mes2}$, (Middle) $CNAr^{Dipp2}$, (Right) $CNAr^{Tripp2}$.

In order to study isolobal analogs of the transient, unsaturated metal carbonyls, we have developed several *m*-terphenyl isocyanide ligands of varying size and subtle electronic differences.[35,59-61] This strategy quickly proved fruitful in the isolation of $Ni(CNAr^{Mes2})_3$ and $Ni(CNAr^{Dipp2})_3$ ($Ar^{Mes2}$ = 2,6-(2,4,6-$Me_3C_6H_2$)$_2C_6H_3$; $Ar^{Dipp2}$ = 2,6,-(2,6-(*i*-Pr)$_2C_6H_3$)$_2C_6H_3$).[62,63] These three-coordinate Ni(0) complexes served as important proofs of principle that sterically encumbering isocyanides can adequately stabilize unsaturated metal centers in low oxidation states. Importantly, the HOMO of both $Ni(CNAr^{Mes2})_3$ and $Ni(CNAr^{Dipp2})_3$ was shown to be

exclusively Ni $d_{z2}$ in character ($a_1'$ in $D_{3h}$ symmetry), faithfully reproducing the electronic structure of $Ni(CO)_3$. In contrast, the $d_{z2}$ orbital of threefold symmetric Ni-phosphine and Ni-olefin complexes lies below the $d_{x2-y2}$ and $d_{xy}$ orbitals ($e'$).[63]

Another success of this approach was the synthesis and thorough investigation of $Pd(CNAr^{Dipp2})_2$.[64] Curiously, stable binary carbonyl complexes of the heavier group 10 metals (i.e. Pd and Pt) are not known.[65] Additionally, only multinuclear isocyanide complexes of Pd(0) and Pt(0) had been reported with no previously known examples of a mononuclear binary palladium or platinum isocyanide.[33] Solid-state structural and solution spectroscopic data supported DFT calculations and matrix-isolation measurements of $Pd(CO)_2$ suggesting a bent instead of linear geometry.[66] A later communication containing the synthesis of $Pt(CNAr^{Dipp2})_2$ yielded similar results.[67]

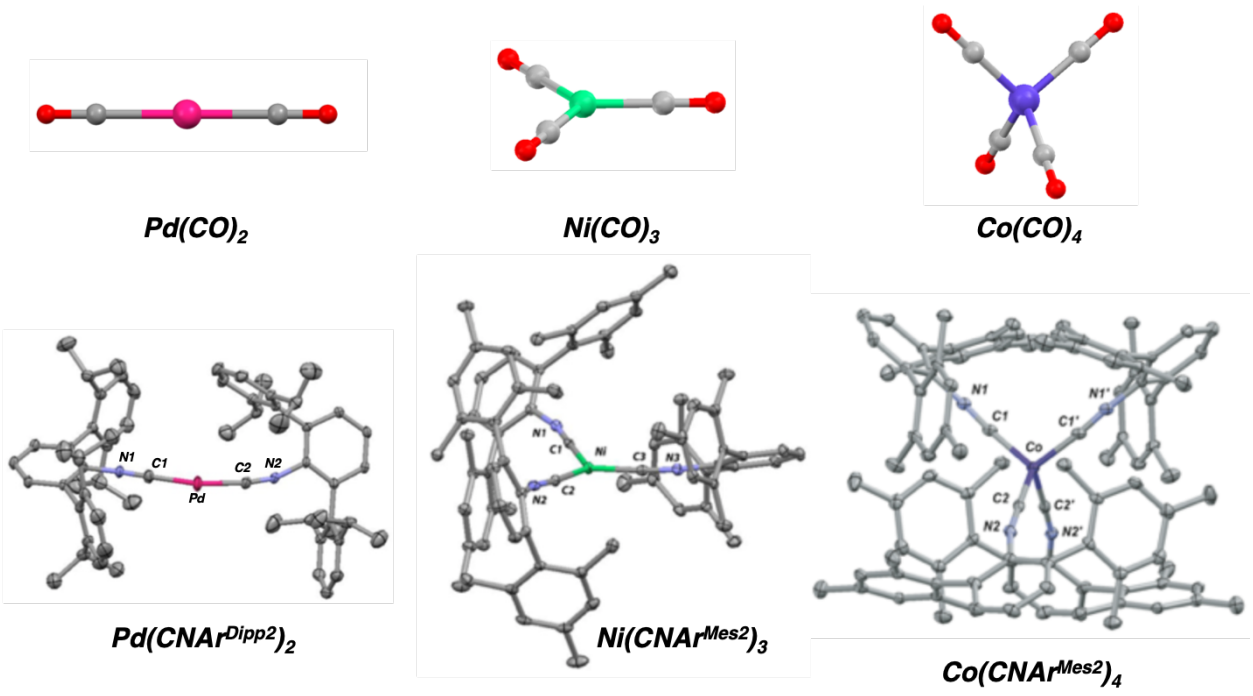


Figure 1.3. (Top) Representative classical unsaturated metal carbonyls. (Bottom) Respective homoleptic isocyanide analogues.

Other examples of our laboratory isolating analogues of catalytically relevant intermediates in metal-carbonyl chemistry include $Co(CNAr^{Mes2})_4$ and $Mn(CO)_3(CNAr^{Dipp2})_2$.[68,69] In some cases, we have also reported "masked" analogues of unsaturated photoproducts. These include $Cp^*Co(N_2)(CNAr^{Dipp2})$ ($Cp^* = [C_5Me_5]^-$]) and $Mo(HN(i\text{-}Pr)_2)(CO)_2(CNAr^{Dipp2})$ that display similar reactivity to $CpCo(CO)$ ($Cp = [C_5H_5]^-$) and *cis*-divacant $Mo(CO)_4$, respectively, but are further stabilized by weakly coordinating ligands.[68,69] The *m*-terphenyl periphery of these ligands has also aided in the stabilization of novel bonding motifs of small molecules, especially as seen with the unprecedented side-on coordination of nitrous oxide ($N_2O$).[70]

## 1.3 Metalates Bearing π-Acidic Ligands

A tremendously important consequence of the π-accepting nature of CO is the ability to stabilize transition metals in formally negative oxidation states.[12,71] The first anionic carbonyl complexes were $[HFe(CO)_4]^-$ and $[Fe(CO)_4]^{2-}$, synthesized by Hieber through the reaction of $Fe(CO)_5$ with hydroxide ($[OH]^-$).[10] In this reaction, $[OH]^-$ adds to a metal-bound carbonyl ligand forming a metallacarboxylic acid, which spontaneously ejects $CO_2$ along with a hydride transfer to generate $[HFe(CO)_4]^-$. This process is aptly named the Hieber base reaction and has been used to create $[Co(CO)_4]^-$ and $[Mn(CO)_5]^-$ and adapted to synthesize many more carbonyl metalates.[71]

These organometallic anions display varied nucleophilicity and are sometimes referred to as pseudohalides, pseudochalcogenides, or pseudopnictogenides, depending on their charge.[71,72] The reactivity of anionic metal carbonyls predominantly centers around nucleophilic displacement reactions in which the metalate reacts with an alkyl or aryl halide to form a metal-carbon bond and eliminate the corresponding halide salt. Analogous reactions using inorganic halides of many elements including silicon, boron, thallium, and other transition metals also proceed.[72,73] An

especially useful early application of this chemistry to organic synthesis was the conversion of alkyl bromides to aldehydes mediated by $[Fe(CO)_4]^{2-}$.[74] The extreme reactivity of this dianion was compared to that of a Grignard reagent by James Collman, and it is now widely known as Collman's reagent in recognition of his seminal work in the 1970s.[12,75]

Studies of homoleptic isocyanide metalates began much more recently with the synthesis of $[Co(CNXyl)_4]^-$ (Xyl = 2,6-$Me_2C_6H_3$) in 1989 and its structural characterization in 1994.[76,77] The delayed entry into this field is due largely to isocyanides being stronger σ-donors and weaker π-acceptors than CO such that they are less effective at stabilizing metals in low formal oxidation states.[78] Cooper and Ellis have made additional isocyanide metalates of Mn, Ru, V, Nb, Ta, and Fe, but the total number of examples remains very low.[36,79-82]

Through the use of *m*-terphenyl isocyanides, our group has synthesized several metal complexes with formal oxidation states less than 0. Similar to the results of Cooper and Ellis, we have reported the homoleptic metalates $[Co(CNAr^{Mes2})_4]^-$ and $[Fe(CNAr^{Mes2})_4]^{2-}$ in addition to a heteroleptic complex with both isocyanide and carbonyl ligation, $[Mn(CO)_3(CNAr^{Dipp2})_2]$,[83-85] and the heteroleptic ferrates $[Fe(CO)_2(CNAr^{Tripp2})_2]^{2-}$ and $[Fe(N_2)_2(CNAr^{Tripp2})_2]^{2-}$ ($Ar^{Tripp2}$ = 2,6-(2,4,6-(*i*-Pr)$_3C_6H_2$)$_2C_6H_3$) (Figure 1.4). We have also published a reactive source of $[Co(CNAr^{Mes2})_3]^-$ that is stabilized by $\eta^2$ coordination of the bis(triphenylphosphine)iminium cation,[86] and the exotic carbyne complex $[Cp^*Co{\equiv}CNAr^{Tripp2}]^{2-}$ derived from extreme π-backdonation to an isocyanide ligand.[87] Importantly, all of these metalates have shown significant metal-based nucleophilicity toward main-group electrophiles. We have also begun to explore anionic cluster compounds. Trinuclear $[Pt_3(\mu\text{-}CO)_3(CNAr^{Dipp2})_3]^{2-}$has charge spread evenly over three metal centers and six π-acidic ligands, but it retains metal-based reactivity.[88]

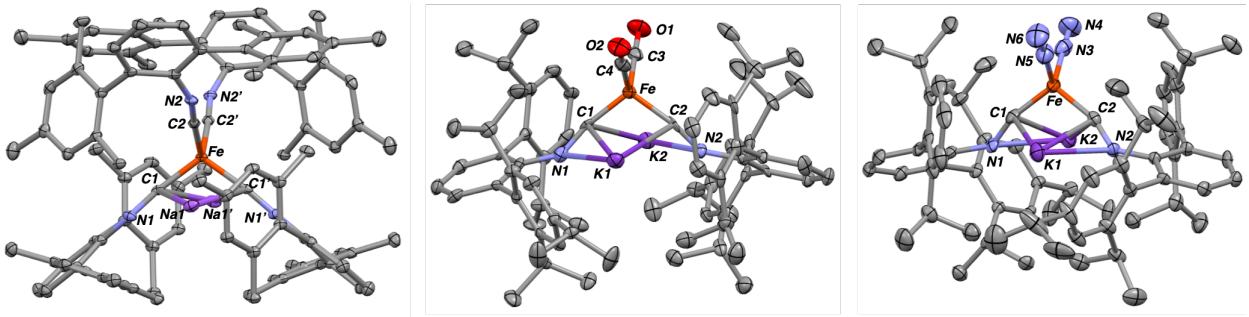


Figure 1.4. Dianionic ferrates with isocyanide and CO or $N_2$ ligation. $Na_2[Fe(CNAr^{Mes2})_4]$ (Left), $K_2[Fe(CO)_2(CNAr^{Tripp2})_2]$ (Middle), $K_2[Fe(N_2)_2(CNAr^{Tripp2})_2]$ (Right).

The results described in this dissertation draw inspiration from the themes outlined above. First, an anionic iron cluster is designed with both CO and *m*-terphenyl isocyanide ligands to achieve cluster growth via nucleophilic displacement reactions with metal salts. Second, a dianionic iron complex is developed with two *m*-terphenyl isocyanides and two carbonyls to discover new bonding motifs between main-group elements and transition metals. Third, this dianionic species serves as a precursor to a functional analogue of $Fe(CO)_4$. In contrast, the ferrate $[Fe(CNAr^{Mes2})_4]^{2-}$ proved to be too reducing and too sterically encumbered to observe desired reactivity, and the (bis)dinitrogen dianion was disregarded due to the high kinetic lability of reaction products.

## 1.4 References

(1) Mond, L.; Langer, C.; Quincke, F. *J. Chem. Soc., Trans.* **1890**, *57* (0), 749–753.

(2) Hermann, W. A. *Journal of Organometallic Chemistry* **1990**, *383* (1-3), 21–44.

(3) Schutzenberger, M. P. *Annales Chim. Physique (Paris)* **1868**, *15*, 100-106.

(4) Werner, H. *Angew. Chem. Int. Ed. Engl.* **1990**, *29* (10), 1077–1089.

(5) Mond, L.; Quincke, F. *J. Chem. Soc., Trans.* **1891**, *59* (0), 604–607.

(6) Mond, L.; Langer, C. *J. Chem. Soc., Trans.* **1891**, *59* (0), 1090–1093.

(7) Berthelot, M. *Compt. Rend.* **1891**, *112*, 1343.

(8) Abel, E. W.; Stone, F. G. A. *Q. Rev., Chem. Soc.* **1969**, *23* (3), 325–371.

(9) Mittasch, A. *Z. Angew. Chem.* **1928**, *41* (30), 827–833.

(10) Hieber, W.; Leutert, F. *Ber. dtsch. Chem. Ges. A/B* **1931**, *64* (11), 2832–2839.

(11) Hieber, W., in *Advances in Organometallic Chemistry*, **1970**, *8*, 1. Eds. Stone, F. G. A. and West, R., Academic Press, San Diego.

(12) Ellis, J. E. *Organometallics* **2003**, *22* (17), 3322–3338.

(13) Hieber, W.; Becker, E. *Ber. dtsch. Chem. Ges. A/B* **1930**, *63* (6), 1405–1417.

(14) Cotton, F. A. *Q. Rev., Chem. Soc.* **1966**, *20* (3), 389–401.

(15) Chini, P. *Large metal carbonyl clusters (LMCC)*; 1980; Vol. 200, pp 37–61.

(16) Ugo, R. *Catalysis Reviews* **1975**, *11* (1), 225–297.

(17) Muetterties, E. L. *Bull. Soc. Chim. Belges* **1975**, *84* (10), 959–986.

(18) Muetterties, E. L.; Rhodin, T. N.; Band, E.; Brucker, C. F.; Pretzer, W. R. *Chem. Rev.* **1979**, *79* (2), 91–137.

(19) Ertl, G. *Angew. Chem. Int. Ed.* **2008**, *47* (19), 3524–3535.

(20) Bozso, F. *Journal of Catalysis* **1977**, *49* (1), 18–41.

(21) Imbihl, R.; Behm, R. J.; Ertl, G.; Moritz, W. *Surface Science Letters* **1982**, *123* (1), A446.

(22) Tsai, M. C.; Seip, U.; Bassignana, I. C.; Küppers, J.; Ertl, G. *Surface Science Letters* **1985**, *155* (2-3), A269.

(23) Chisholm, M. H.; Hammond, C. E.; Johnston, V. J.; Streib, W. E.; Huffman, J. C. *J. Am. Chem. Soc.* **1992**, *114* (18), 7056–7065.

(24) Gates, B. C. *Angew. Chem. Int. Ed. Engl.* **1993**, *32* (2), 228–229.

(25) Dyson, P. J. *Coordination Chemistry Reviews* **2004**, *248* (21-24), 2443–2458.

(26) Burdett, J. K. *J. Chem. Soc., Faraday Trans. 2* **1974**, *70* (0), 1599–1613.

(27) Burdett, J. K. *Inorg. Chem.* **1975**, *14* (2), 375–382.

(28) Elian, M.; Hoffmann, R. *Inorg. Chem.* **1975**, *14* (5), 1058–1076.

(29) Dewar, M. J. S. *Bull. Soc. Chim. Fr.* **1951**, *18*, C79.

(30) Chatt, J.; Duncanson, L. A. *J. Chem. Soc.* **1953**, 2939-2947.

(31) Ehlers, A. W.; Dapprich, S.; Vyboishchikov, S. F.; Frenking, G. *Organometallics* **1996**, *15* (1), 105–117.

(32) Frenking, G.; Fröhlich, N. *Chem. Rev.* **2000**, *100* (2), 717–774.

(33) Yamamoto, Y. *Coordination Chemistry Reviews* **1980**, *32* (3), 193–233.

(34) Cotton, F. A.; Zingales, F. *J. Am. Chem. Soc.* **1961**, *83* (2), 351–355.

(35) Carpenter, A. E.; Mokhtarzadeh, C. C.; Ripatti, D. S.; Havrylyuk, I.; Kamezawa, R.; Moore, C. E.; Rheingold, A. L.; Figueroa, J. S. *Inorg. Chem.* **2015**, *54* (6), 2936–2944.

(36) Barybin, M. V.; Young, V. G.; Ellis, J. E. *J. Am. Chem. Soc.* **2000**, *122* (19), 4678–4691.

(37) Kruck, T. *Angew. Chem. Int. Ed. Engl.* **1967**, *6* (1), 53–67.

(38) Xiao, S.; Trogler, W. C.; Ellis, D. E.; Berkovitch-Yellin, Z. *J. Am. Chem. Soc.* **1983**, *105* (24), 7033–7037.

(39) Dias, P. B.; de Piedade, M. E. M.; Simões, J. A. M. *Coordination Chemistry Reviews* **1994**, *135-136*, 737–807.

(40) Soleilhavoup, M.; Bertrand, G. *Acc. Chem. Res.* **2015**, *48* (2), 256–266.

(41) Hieber, W.; Böckly, E. *Z. Anorg. Chem.* **1950**, *262* (6), 344–352.

(42) Klages, F.; Mönkemeyer, K. *Chem. Ber.* **1950**, *83* (6), 501–508.

(43) Bassett, J.-M.; Berry, D. E.; Barker, G. K.; Green, M.; Howard, J. A. K.; Stone, F. G. A. *J. Chem. Soc., Dalton Trans.* **1979**, No. 6, 1003–1011.

(44) Schroeder, M. A.; Wrighton, M. S. *J. Am. Chem. Soc.* **1976**, *98* (2), 551–558.

(45) Harmon, R. E.; Gupta, S. K.; Brown, D. J. *Chem. Rev.* **1973**, *73* (1), 21–52.

(46) Klingler, R. J.; Rathke, J. W. *J. Am. Chem. Soc.* **1994**, *116* (11), 4772–4785.

(47) Zhou, M.; Andrews, L.; Bauschlicher, C. W. *Chem. Rev.* **2001**, *101* (7), 1931–1962.

(48) Lomont, J. P.; Nguyen, S. C.; Harris, C. B. *Acc. Chem. Res.* **2014**, *47* (5), 1634–1642.

(49) Twamley, B.; Haubrich, S. T.; Power, P. P. In *Advances in Organometallic Chemistry Volume 44*; Advances in Organometallic Chemistry; Elsevier, 1999; Vol. 44, pp 1–65.

(50) Clyburne, J. A. C.; McMullen, N. *Coordination Chemistry Reviews* **2000**, *210* (1), 73–99.

(51) Gavenonis, J.; Tilley, T. D. *Organometallics* **2002**, *21* (25), 5549–5563.

(52) Wright, R. J.; Steiner, J.; Beaini, S.; Power, P. P. *Inorganica Chimica Acta* **2006**, *359* (6), 1939–1946.

(53) Gavenonis, J.; Tilley, T. D. *Organometallics* **2004**, *23* (1), 31–43.

(54) Ito, M.; Matsumoto, T.; Tatsumi, K. *Inorg. Chem.* **2009**, *48* (5), 2215–2223.

(55) Hagadorn, J. R.; Que, L.; Tolman, W. B.; Prisecaru, I.; Münck, E. *J. Am. Chem. Soc.* **1999**, *121* (41), 9760–9761.

(56) Yoon, S.; Lippard, S. J. *J. Am. Chem. Soc.* **2005**, *127* (23), 8386–8397.

(57) Tanabiki, M.; Tsuchiya, K.; Kumanomido, Y.; Matsubara, K.; Motoyama, Y.; Nagashima, H. *Organometallics* **2004**, *23* (16), 3976–3981.

(58) Ito, H.; Kato, T.; Sawamura, M. *Chem. Lett.* **2006**, *35* (9), 1038–1039.

(59) Fox, B. J.; Sun, Q. Y.; DiPasquale, A. G.; Fox, A. R.; Rheingold, A. L.; Figueroa, J. S. *Inorg. Chem.* **2008**, *47* (19), 9010–9020.

(60) Ditri, T. B.; Fox, B. J.; Moore, C. E.; Rheingold, A. L.; Figueroa, J. S. *Inorg. Chem.* **2009**, *48* (17), 8362–8375.

(61) Ditri, T. B.; Carpenter, A. E.; Ripatti, D. S.; Moore, C. E.; Rheingold, A. L.; Figueroa, J. S. *Inorg. Chem.* **2013**, *52* (22), 13216–13229.

(62) Fox, B. J.; Millard, M. D.; DiPasquale, A. G.; Rheingold, A. L.; Figueroa, J. S. *Angew. Chem. Int. Ed.* **2009**, *48* (19), 3473–3477.

(63) Emerich, B. M.; Moore, C. E.; Fox, B. J.; Rheingold, A. L.; Figueroa, J. S. *Organometallics* **2011**, *30* (9), 2598–2608.

(64) Labios, L. A.; Millard, M. D.; Rheingold, A. L.; Figueroa, J. S. *J. Am. Chem. Soc.* **2009**, *131* (32), 11318–11319.

(65) Kuendig, E. P.; McIntosh, D.; Moskovits, M.; Ozin, G. A. *J. Am. Chem. Soc.* **1973**, *95* (22), 7234–7241.

(66) Liang, B.; Zhou, M.; Andrews, L. *J. Phys. Chem. A* **2000**, *104* (17), 3905–3914.

(67) Barnett, B. R.; Moore, C. E.; Rheingold, A. L.; Figueroa, J. S. *J. Am. Chem. Soc.* **2014**, *136* (29), 10262–10265.

(68) Mokhtarzadeh, C. C.; Rheingold, A. L.; Figueroa, J. S. *Dalton Trans.* **2016**, *45* (37), 14561–14569.

(69) Mandla, K. A.; Moore, C. E.; Rheingold, A. L.; Figueroa, J. S. *Angew. Chem. Int. Ed.* **2018**, *57* (23), 6853–6857.

(70) Mokhtarzadeh, C. C.; Chan, C.; Moore, C. E.; Rheingold, A. L.; Figueroa, J. S. *J. Am. Chem. Soc.* **2019**, *141* (38), 15003–15007.

(71) Beck, W. *Angew. Chem. Int. Ed. Engl.* **1991**, *30* (2), 168–169.

(72) Ellis, J. E. *Journal of Organometallic Chemistry* **1975**, *86* (1), 1–56.

(73) King, R. B. *Acc. Chem. Res.* **1970**, *3* (12), 417–427.

(74) Cooke, M. P. *J. Am. Chem. Soc.* **1970**, *92* (20), 6080–6082.

(75) Collman, J. P. *Acc. Chem. Res.* **1975**, *8* (10), 342–347.

(76) Warnock, G. F.; Cooper, N. J. *Organometallics* **1989**, *8* (7), 1826–1827.

(77) Leach, P. A.; Geib, S. J.; Corella, J. A.; Warnock, G. F.; Cooper, N. J. *J. Am. Chem. Soc.* **1994**, *116* (19), 8566–8574.

(78) Weber, L. *Angew. Chem. Int. Ed.* **1998**, *37* (11), 1515–1517.

(79) Utz, T. L.; Leach, P. A.; Geib, S. J.; Cooper, N. J. *Chem. Commun. (Camb.)* **1997**, No. 9, 847–848.

(80) Corella, J. A.; Thompson, R. L.; Cooper, N. J. *Angew. Chem. Int. Ed. Engl.* **1992**, *31* (1), 83–84.

(81) Barybin, M. V.; Brennessel, W. W.; Kucera, B. E.; Minyaev, M. E.; Sussman, V. J.; Young, V. G.; Ellis, J. E. *J. Am. Chem. Soc.* **2007**, *129* (5), 1141–1150.

(82) Brennessel, W. W.; Ellis, J. E. *Angew. Chem. Int. Ed.* **2007**, *46* (4), 598–600.

(83) Margulieux, G. W.; Weidemann, N.; Lacy, D. C.; Moore, C. E.; Rheingold, A. L.; Figueroa, J. S. *J. Am. Chem. Soc.* **2010**, *132* (14), 5033–5035.

(84) Mokhtarzadeh, C. C.; Margulieux, G. W.; Carpenter, A. E.; Weidemann, N.; Moore, C. E.; Rheingold, A. L.; Figueroa, J. S. *Inorg. Chem.* **2015**, *54* (11), 5579–5587.

(85) Stewart, M. A.; Moore, C. E.; Ditri, T. B.; Labios, L. A.; Rheingold, A. L.; Figueroa, J. S. *Chem. Commun.* **2011**, *47* (1), 406–408.

(86) Carpenter, A. E.; Margulieux, G. W.; Millard, M. D.; Moore, C. E.; Weidemann, N.; Rheingold, A. L.; Figueroa, J. S. *Angew. Chem. Int. Ed.* **2012**, *51* (37), 9412–9416.

(87) Mokhtarzadeh, C. C.; Moore, C. E.; Rheingold, A. L.; Figueroa, J. S. *J. Am. Chem. Soc.* **2018**, *140* (26), 8100–8104.

(88) Barnett, B. R.; Rheingold, A. L.; Figueroa, J. S. *Angew. Chem. Int. Ed.* **2016**, *55*, 9253–9258.

Chapter 2

# Controlled Expansion of a Strong-Field Iron Nitride Cluster: Multi-Site Ligand Substitution as a Strategy for Activating Interstitial Nitride Nucleophilicity

## 2.1 Introduction

For many decades, investigations into the precise trajectories of multistep chemical processes at surfaces have been central to the field of heterogeneous catalysis.[1,2] Despite seminal advances in the understanding of substrate adsorption, substrate/surface dynamics, and reaction kinetics, characterizing key surface active sites with atomic-level resolution has remained difficult. These well-known challenges stem from the general complexity of surface sites, short- and long-range surface reconstruction processes during chemical reactions, and length-scale limitations of analytical techniques.[1–5]

To provide complementary insight, molecular transition-metal clusters have long been used, with varying success, as model systems for rationalizing the structural properties and chemisorption profiles of reactive surface sites.[6–8] To this end, the iron nitridocarbonyl cluster $[Fe_4(\mu_4\text{-}N)(CO)_{12}]^-$ was prepared over 30 years ago in an attempt to link this analogy to adsorbed nitrogen on iron surfaces in the Haber–Bosch process.[4,9,10] This system, however, does not effectively model ammonia production owing to preferential protonation at a bridging position between two iron centers, rather than at the interstitial nitrogen atom, and the fact that subsequent protonations with strong acids cannot be achieved.[9] Notably, the reactivity observed for $[Fe_4(\mu_4\text{-}N)(CO)_{12}]^-$ had been limited to monoprotonation and simple ligand exchange[11] until recently, when it was shown by Berben and co-workers that this species electrocatalytically reduces $H^+$ and

$CO_2$.[12–14] In contrast, the isoelectronic and isostructural species $[Fe_4(\mu_4\text{-}C)(CO)_{12}]^{2-}$ is susceptible to protonation at the interstitial carbon atom and displays chemistry pertinent to the metal cluster–surface analogy, specifically carbon monoxide activation and the cleavage of $H_2$ across the $\mu_4$-carbide.[15–18]

The greater nucleophilicity of $[Fe_4(\mu_4\text{-}C)(CO)_{12}]^{2-}$ relative to $[Fe_4(\mu_4\text{-}N)(CO)_{12}]^{-}$ has been rationalized qualitatively by two main factors, namely 1) the greater charge of the carbide cluster (–2 vs. –1) and 2) increased orbital energies, which are due to the more electropositive character of carbon compared to nitrogen.[11] One approach to augmenting the reactivity of $[Fe_4(\mu_4\text{-}N)(CO)_{12}]^{-}$ and other clusters has been to increase their electron density through the substitution of CO with more electron-donating ligands. Phosphine-substituted $[Fe_4(\mu_4\text{-}N)(CO)_{12-n}(L)_n]^{-}$ (n = 1, 2) clusters have been reported, but they have not exhibited reactivity patterns that differ from the all-carbonyl analogue.[11] Additionally, $[Fe_4(\mu_4\text{-}N)(CO)_{12-n}(L)_n]^{-}$ clusters with increasing levels of phosphine or other strong-donor substitution have remained elusive. These observations suggest that two ligand substitutions inhibit subsequent CO labilization prior to the onset of increased nucleophilicity at the interstitial nitrogen atom. Given this rationale, we postulated that organoisocyanides, which are strong donors, yet provide stabilizing π-acidity properties,[19,20] could yield the multiple substitutions necessary (n > 2) to meet the electronic threshold for activation of the interstitial nitride.

Accordingly, herein we report the use of *m*-terphenyl isocyanides[19–22] for the preparation of the heteroleptic cluster $Na[Fe_4(\mu_4\text{-}N)(CO)_8(CNAr^{Mes2})_4]$ (Na[**1**], $Ar^{Mes2}$ = 2,6-(2,4,6-$Me_3C_6H_2)_2C_6H_3$), where multiple isocyanide-for-carbonyl substitutions successfully activate the nucleophilic character of the interstitial nitride. This enhanced reactivity profile, coupled with the encumbering nature of the $CNAr^{Mes2}$ ligands, allows for controlled cluster growth with a variety

of electrophiles. Such cluster expansion reactions can be used for the systematic incorporation of coordinatively and electronically unsaturated transition-metal and main-group centers into the multi-metallic framework, thereby providing reactive sites in a molecular system that mimic some of the characteristics known for heterogeneous surfaces.[1]

## 2.2 Isocyanide-for-Carbonyl Ligand Substitution on a Tetranuclear Iron Cluster

In our initial attempts to prepare cluster **1**$^{-}$, we found that it cannot be directly obtained by simple thermolytic ligand exchange on $[Fe_4(\mu_4\text{-}N)(CO)_{12}]^{-}$. Prolonged heating of $[Na(diglyme)_2][Fe_4(\mu_4\text{-}N)(CO)_{12}]$ in the presence of excess $CNAr^{Mes2}$ led to intractable mixtures of products as assessed by $^1$H NMR spectroscopy. However, heating a benzene slurry of $[Na(diglyme)_2][Fe_4(\mu_4\text{-}N)(CO)_{12}]$ at reflux in the presence of 1.0 equivalent of benzoic acid and 4.2 equivalents of $CNAr^{Mes2}$ for 21 h generated the monohydride $HFe_4(\mu_4\text{-}N)(CO)_8(CNAr^{Mes2})_4$ (**1**-H; Scheme 2.1), as indicated by the consumption of free isocyanide and the appearance of an upfield singlet at –30.87 ppm in the $^1$H NMR spectrum of the reaction mixture. This resonance is consistent with bridging hydrides formed from Fe–Fe bond protonation in analogous butterfly clusters.[10] In addition, structural characterization of **1**-H (Figure 2.1) confirmed that the hydride bridges the Fe–Fe hinge bond (basal edge), as has been proposed for the all-carbonyl cluster, $HFe_4(\mu_4\text{-}N)(CO)_{12}$, based on low-resolution X-ray data.[9,14] Notably, the $CNAr^{Mes2}$ ligands are not evenly distributed on the four iron centers of **1**-H. Instead, two isocyanides add to a single wingtip iron (collinear with the nitride), and one of the basal iron atoms remains unsubstituted, most likely to reduce steric congestion from the ArMes2 groups. This ligand arrangement is configurationally stable in $C_6D_6$ solution, as the $^1$H NMR spectrum of **1**-H remains static up to 75 ˚C.

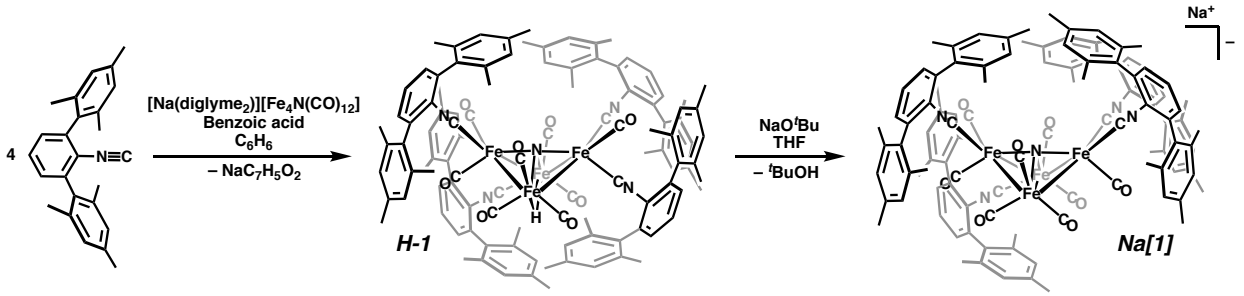


Scheme 2.1. Synthesis of $HFe_4(\mu_4\text{-}N)(CO)_8(CNAr^{Mes2})_4$ (**1**-H) and its deprotonation to $Na[Fe_4(\mu_4\text{-}N)(CO)_8(CNAr^{Mes2})_4]$ (Na[**1**]).

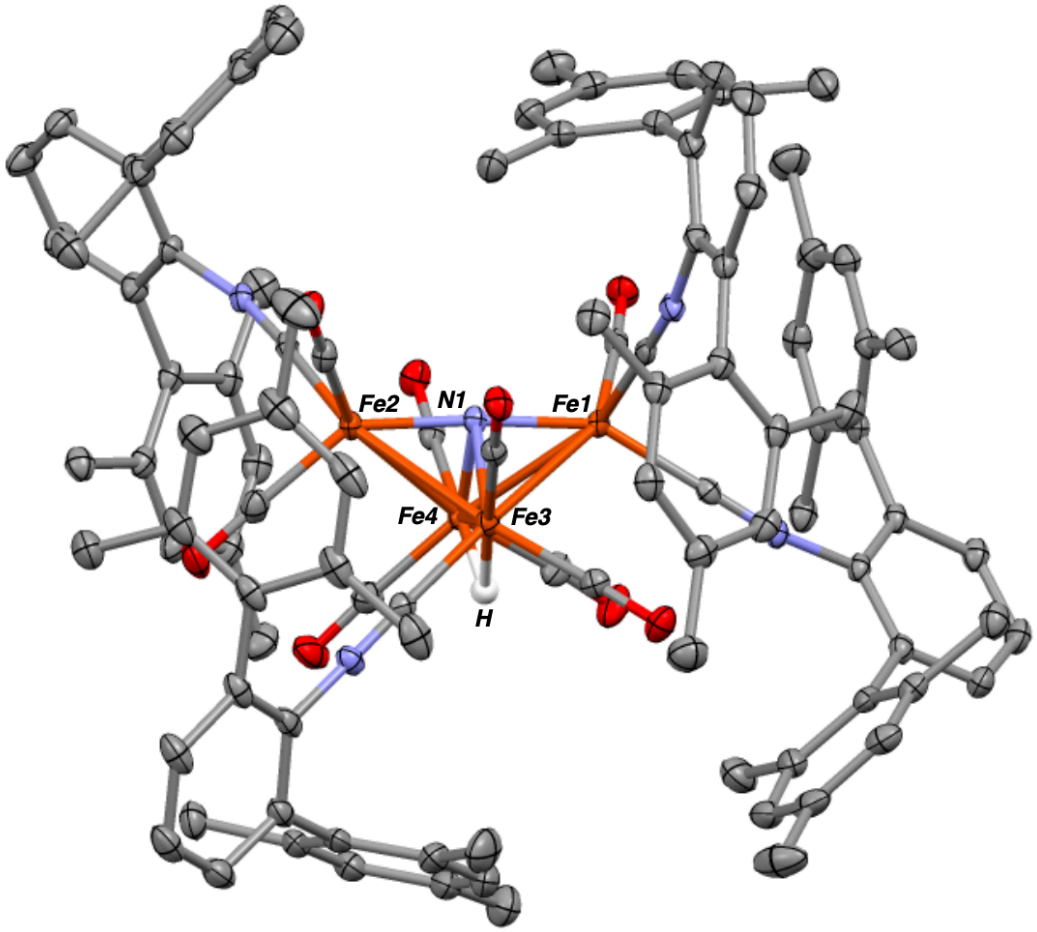


Figure 2.1. Solid-state structure of $HFe_4(\mu_4\text{-}N)(CO)_8(CNAr^{Mes2})_4$ (**1**-H). Selected bond distances (Å): Fe1-N1 = 1.776(2); Fe2-N1 = 1.795(2); Fe3-N1 = 1.908(2); Fe4-N1 = 1.928(2); Fe3-Fe4 = 2.5771(6). H-atoms except the hydride are omitted.

The hydride cluster **1**-H can subsequently be deprotonated with NaO*t*-Bu in THF solution to yield Na[$Fe_4(\mu_4\text{-}N)(CO)_8(CNAr^{Mes2})_4$] (Na[**1**]), as determined by X-ray diffraction (Figure 2.2). The solid-state structure of Na[**1**] reveals a contact-ion pair where the $Na^+$ counterion engages in several cation π(C≡N)/π(arene) interactions[20–22] and makes a long, but significant, contact with the interstitial nitride unit (2.580 Å (avg)). In addition, the uneven distribution of isocyanide ligands found in the solid state for **1**-H is retained in Na[**1**]. Notably, cluster Na[**1**] was isolated as an air- and moisture-sensitive brown solid. As a point of comparison, [$Na(diglyme)_2$][$Fe_4(\mu_4\text{-}N)(CO)_{12}$] is stable in air for hours and indefinitely in degassed water, a difference that we attribute to the more electron-rich nature of Na[**1**]. This energetic difference is also apparent in the FTIR spectrum of Na[**1**], which shows a 30 $cm^{-1}$ red-shift of the lowest-energy ν(CO) band relative to [$Na(diglyme)_2$][$Fe_4(\mu_4\text{-}N)(CO)_{12}$], which is indicative of greater Fe→π*(CO) back-donation when isocyanides are present.

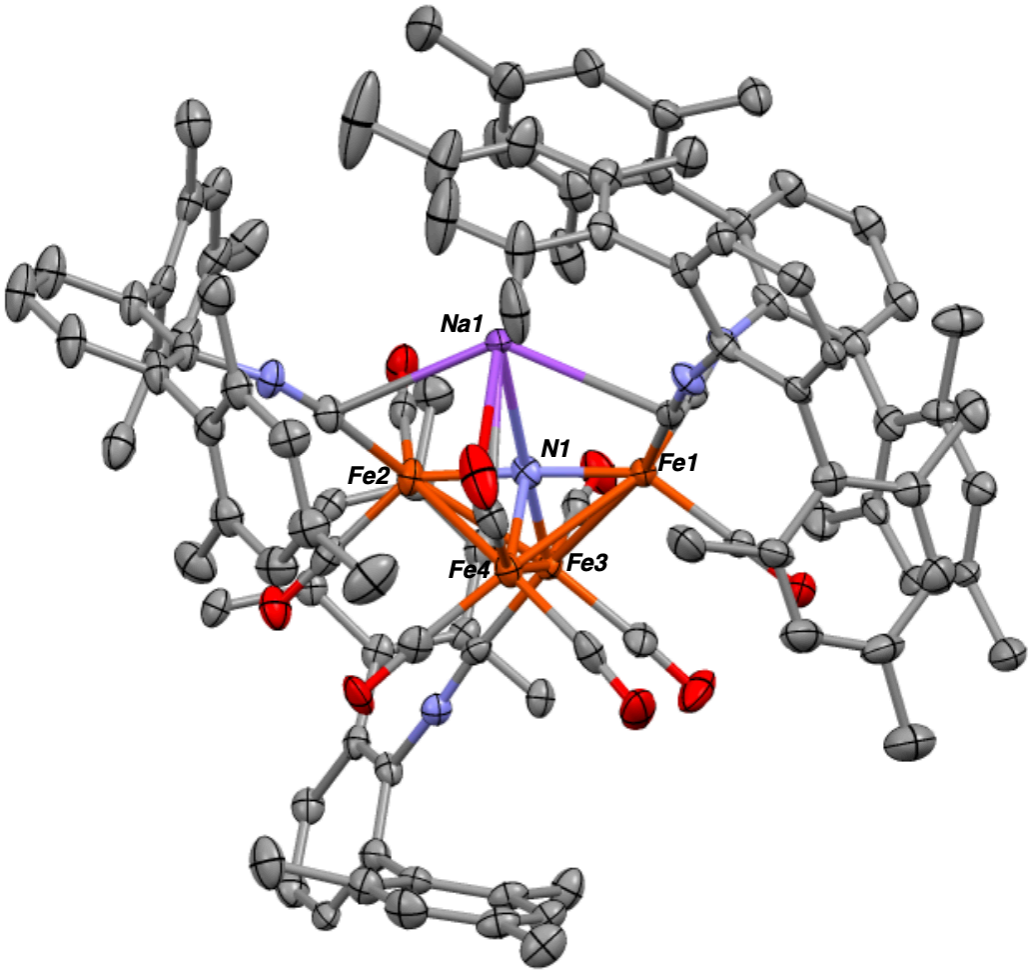


Figure 2.2. Solid-state structure of Na[$Fe_4(\mu_4\text{-}N)(CO)_8(CNAr^{Mes2})_4$] (Na[**1**]). One of two molecules in the asymmetric unit is displayed. Disorder of the sodium cation is omitted for clarity. Selected bond distances (Å): Fe1-N1 = 1.777(6); Fe2-N1 = 1.833(6); Fe3-N1 = 1.928(6); Fe4-N1 = 1.908(6); Fe3-Fe4 = 2.5040(14); N1-Na1 = 2.611(9).

## 2.3 Single-Electron Oxidation of Na[$Fe_4(\mu_4\text{-}N)(CO)_8(CNAr^{Mes2})_4$]

Additional evidence for the more electron-rich profile of cluster [**1**]$^-$ relative to [$Fe_4(\mu_4\text{-}N)(CO)_{12}$]$^-$ was obtained from cyclic voltammetry measurements. In THF solution, [$Fe_4(\mu_4\text{-}N)(CO)_{12}$]$^-$ has been well documented to undergo two reversible 1 e$^-$ reductions at –1.33 V and –1.78 V, as well as an irreversible 1 e$^-$ oxidation at + 0.78 V (all vs. SCE).[23] This latter redox process generates the unstable, neutral radical species $Fe_4(\mu_4\text{-}N)(CO)_{12}$,[23] which has also been implicated

as the key intermediate upon release of $H_2$ or formate in $H^+$ or $CO_2$ reduction, respectively, by this all-carbonyl system.[13,14] In contrast, the CV of Na[**1**] does not reveal reduction processes prior to –2.0 V vs. SCE, but shows a reversible oxidative event at –0.65 V, which was assigned to the 0/–1 couple of the cluster framework (Figure 2.4). These data indicate that the increased donor strength of the $CNAr^{Mes2}$ ligands creates a sufficiently electron-rich cluster as to discourage reduction events, while also allowing for the stabilization of electron-deficient cluster species. Indeed, as suggested by the reversibility of the –0.65 V event, chemical oxidation of Na[**1**] with trityl chloride ($ClCPh_3$) leads cleanly to the neutral, paramagnetic cluster $Fe_4N(CO)_8(CNAr^{Mes2})_4$ (**1**), as determined by X-ray diffraction (Scheme 2.2, Figure 2.3). EPR spectroscopic analysis of neutral **1** in toluene solution revealed a singlet ($g_{iso}$ = 2.034) with no discernible hyperfine coupling (Figure 2.5), while Evans method magnetic moment determination ($\mu_{eff}$ = 1.74(9) $\mu_B$; $C_6D_6$ , 20 ˚C) agrees well with the presence of an S = ½ metalloradical, as expected for a singly oxidized cluster in a strong ligand field.

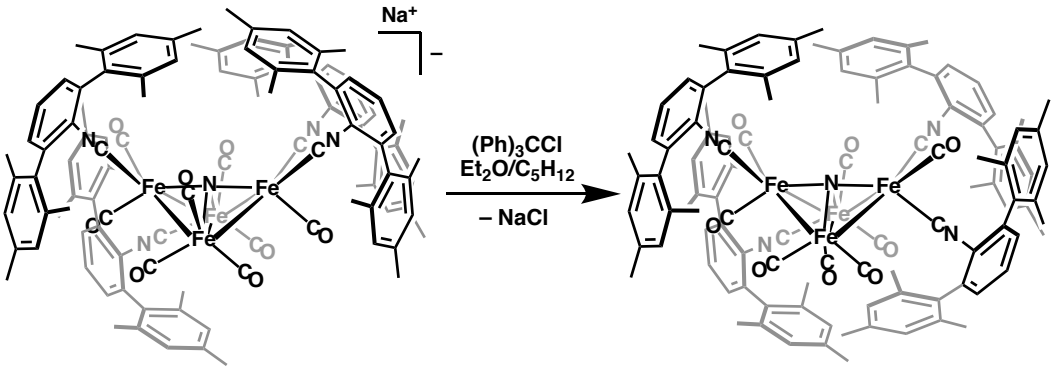


Scheme 2.2. Oxidation of Na[**1**] generating paramagnetic $Fe_4N(CO)_8(CNAr^{Mes2})_4$ (**1**).

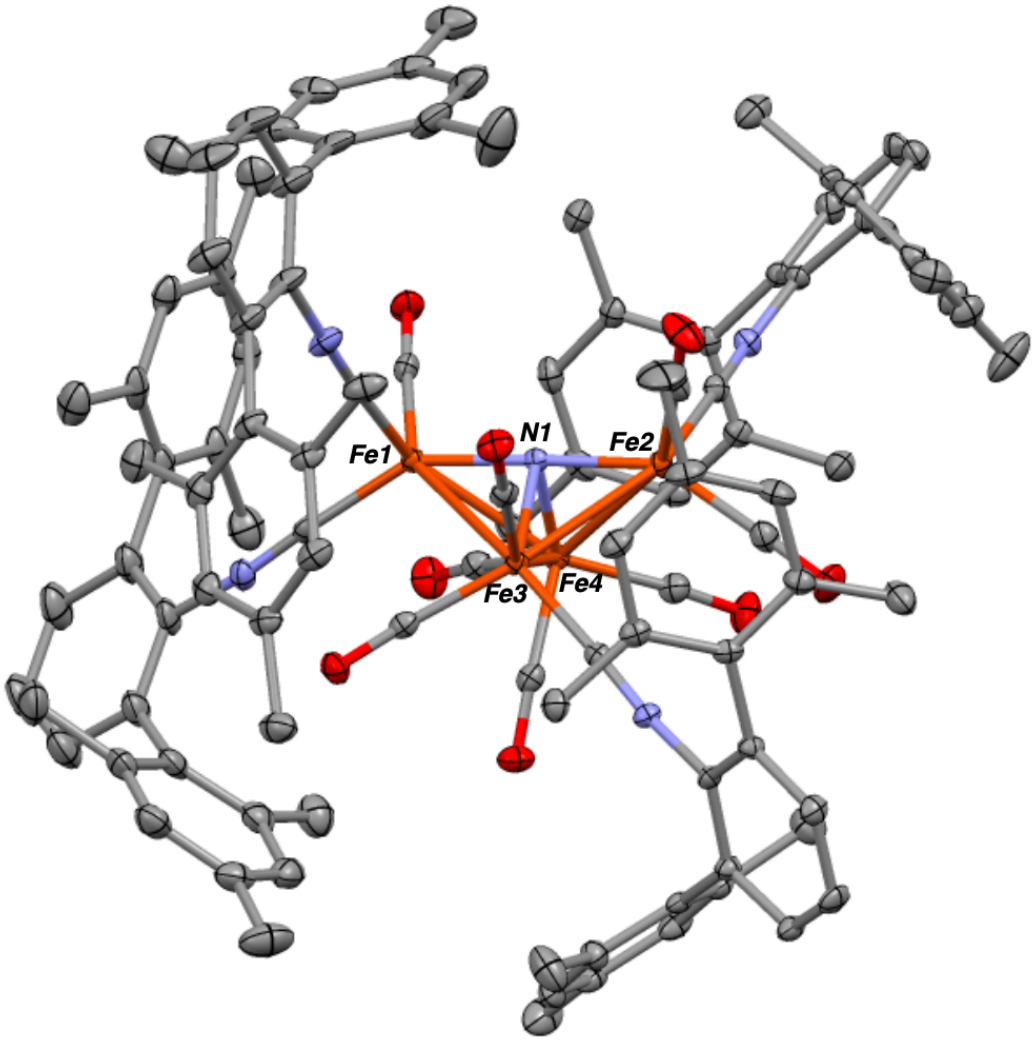


Figure 2.3. Solid-state structure of $Fe_4N(CO)_8(CNAr^{Mes2})_4$ (**1**). Selected bond distances (Å): Fe1-N1 = 1.7777(16); Fe2-N1 = 1.7863(16); Fe3-N1 = 1.8913(16); Fe4-N1 = 1.8960(16); Fe3-Fe4 = 2.5448(4).

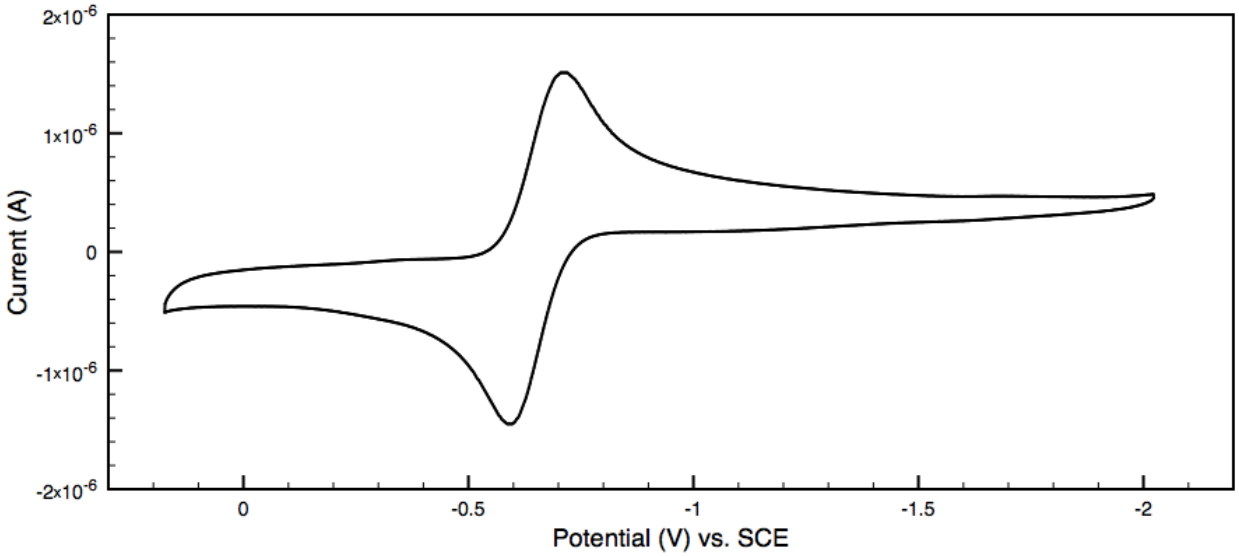


Figure 2.4. Cyclic voltammogram showing the reversible **1**/[**1**]$^{-}$ redox couple. See Ch. 2.8 for conditions.

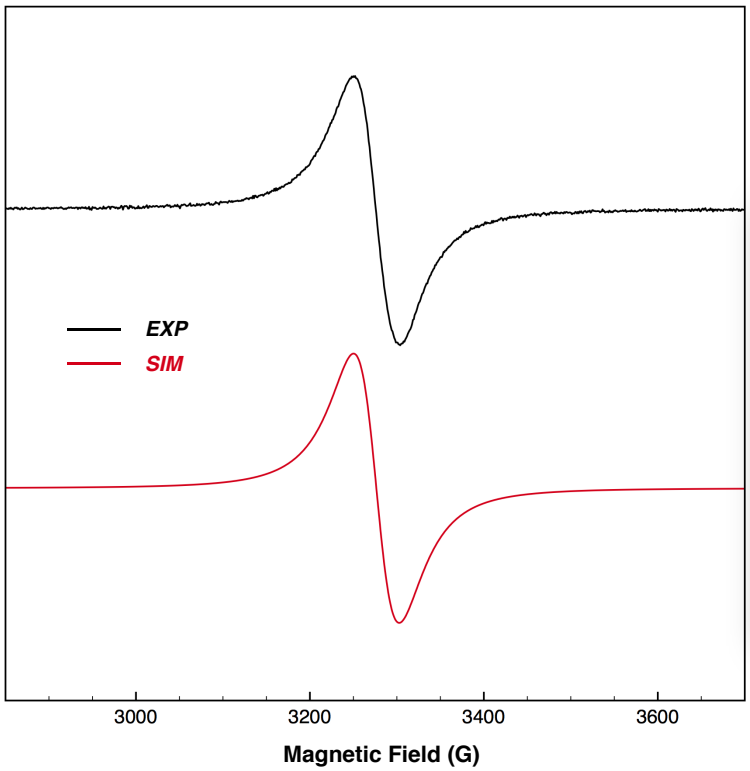


Figure 2.5. X-Band EPR spectrum of **1** at 295 K (top) and simulation (bottom).

## 2.4 Cluster Expansion of $[Fe_4(\mu_4\text{-}N)(CO)_8(CNAr^{Mes2})_4]^-$ via Salt Elimination

The most unique feature of [**1**]$^-$ relative to $[Fe_4(\mu_4\text{-}N)(CO)_{12}]^-$ is that its increased electron-rich character allows for nucleophilic reactivity of the interstitial nitride towards a variety of electrophilic substrates. For example, treatment of Na[**1**] with thallium triflate (TlOTf; OTf = $[O_3SCF_3]^-$) produces the adduct $Fe_4(Tl\text{-}(\mu_4\text{-}N))(CO)_8(CNAr^{Mes2})_4$ (**2**; Scheme 2.3, Figure 2.6). In contrast, $[Fe(\mu_4\text{-}N)(CO)_{12}]^-$ does not react with TlOTf even after the addition of multiple equivalents and several hours of heating in THF at 60 ˚C. In the solid-state structure of cluster **2**, the Tl atom occupies the void space proximal to the bridging nitride and features a N–Tl separation of 2.558(9) Å. Significantly, this separation is comparable to the N–Tl bond lengths found for many Tl(I) complexes featuring 2 e$^-$ nitrogen-donor ligands[24] and thereby indicates that a significant bonding interaction between the interstitial nitrogen atom and Tl is present in the cluster. Complex **2** also gives rise to ν(CN) and ν(CO) bands that are blue-shifted by approximately 25 cm$^{-1}$ relative to those of Na[**1**] (Figure 2.7). This shift to higher energies is reflective of decreased π back-donation from the iron centers to the π-acidic ligands upon binding of Tl to the cluster.[25] Accordingly, this electronic perturbation provides additional evidence that Tl interacts directly through the cluster nitride, rather than being associated with the $Fe_4N$ core by simple ion pairing.

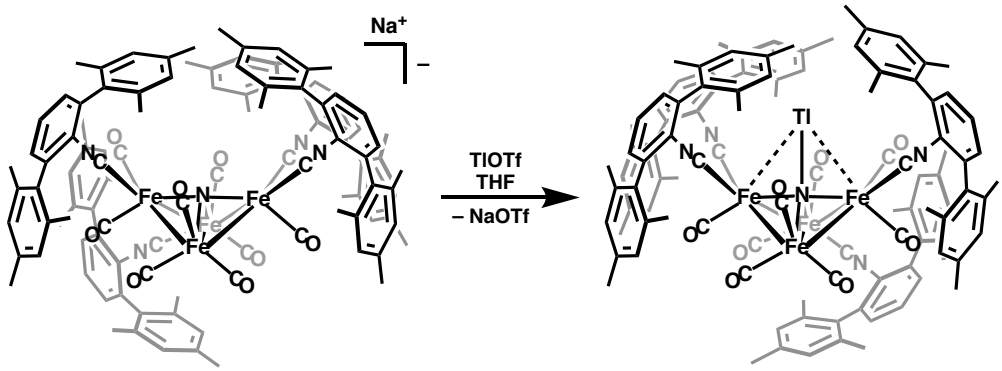


Scheme 2.3. Synthesis of $Fe_4(Tl\text{-}(\mu_4\text{-}N))(CO)_8(CNAr^{Mes2})_4$ (**2**) by reaction of $\mathbf{1}^-$ with $Tl^+$.

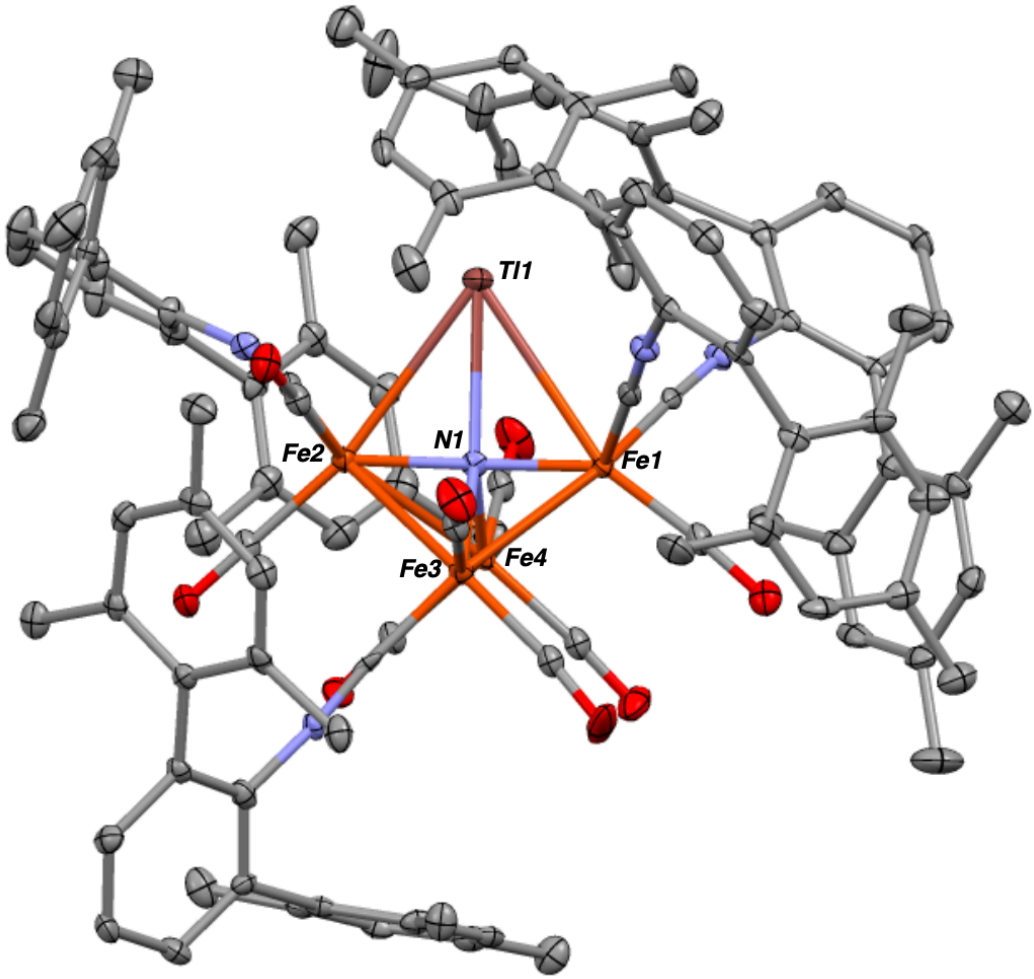


Figure 2.6. Solid-state structure of $Fe_4(Tl\text{-}(\mu_4\text{-}N))(CO)_8(CNAr^{Mes2})_4$ (**2**). One of two molecules in the asymmetric unit is displayed. Selected bond distances (Å) and angles (˚): Fe1-N1 = 1.800(6); Fe2-N1 = 1.819(6); Fe3-N1 = 1.892(5); Fe4-N1 = 1.871(6); Fe3-Fe4 = 2.5162(14); N1-Tl1 = 2.555(6); Fe1-Tl1 = 3.1314(11); Fe2-Tl1 = 3.1091(11); Fe1-Tl1-Fe2 = 70.87(3).

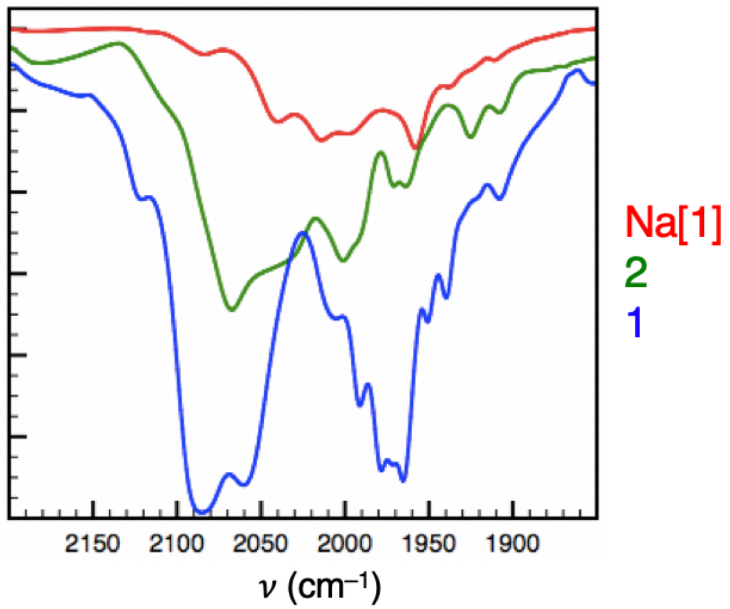


Figure 2.7. Comparison of the solution FTIR spectra of Na[**1**], **2**, **1** showing of progressive blueshift of the major νCN stretches correlating with level of cluster oxidation.

Extending this strategy to divalent metal salts, Na[**1**] readily reacts with $SnCl_2$ by elimination of NaCl to provide the nitrido chlorostannylene-substituted cluster, $Fe_4(ClSn\text{-}(\mu_4\text{-}N))(CO)_8(CNAr^{Mes2})_4$ (**3**; Scheme 2.4, Figure 2.8). Characterization of cluster **3** by both IR spectroscopy and X-ray crystallography revealed spectroscopic and structural features similar to those of thallium derivative **2**, including a close Sn–N contact indicative of a substantial bonding interaction between the Sn and N atoms (2.2045(97) Å). The isocyanide stretching bands of **3** lie at approximately 10 $cm^{-1}$ higher frequency than **2**. Evidently, tin binding withdraws more electron density from the cluster framework than thallium binding, consistent with the greater electronegativity of Sn versus Tl.

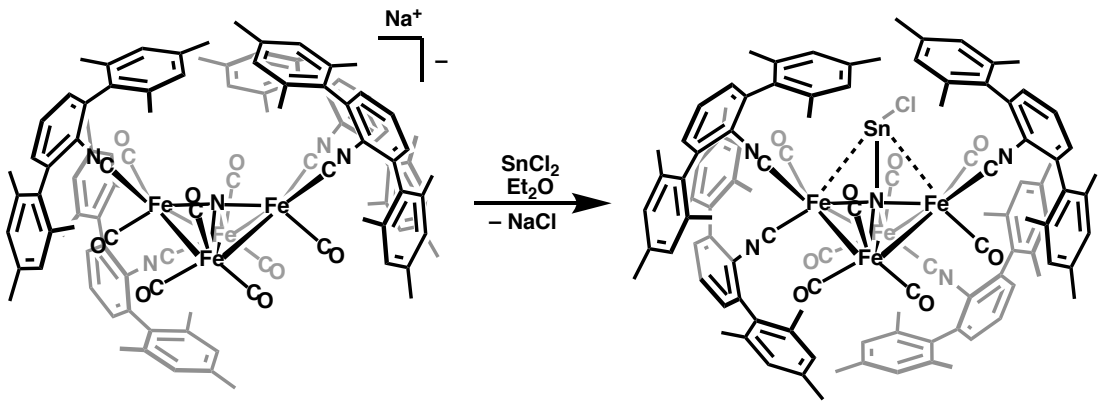


Scheme 2.4. Synthesis of stannylene-substituted cluster $Fe_4(ClSn\text{-}(\mu_4\text{-}N))(CO)_8(CNAr^{Mes2})_4$ (**3**).

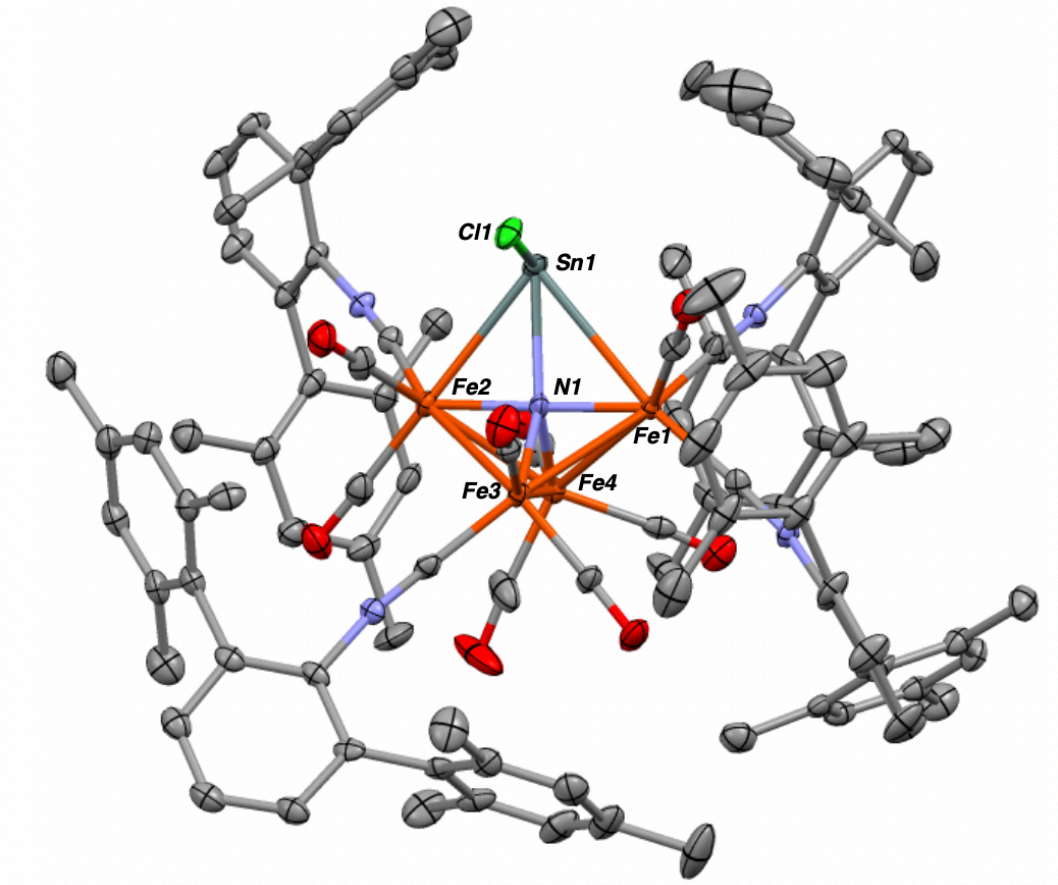


Figure 2.8. Solid-state structure of $Fe_4(ClSn\text{-}(\mu_4\text{-}N))(CO)_8(CNAr^{Mes2})_4$ (**3**). Positional disorder of the cluster metal atoms and chloride ligand has been omitted for clarity. Selected bond distances (Å) and angles (˚): Fe1-N1 = 1.824(6); Fe2-N1 = 1.837(6); Fe3-N1 = 1.848(5); Fe4-N1 = 1.882(7); Fe3-Fe4 = 2.5331(14); N1-Sn1 = 2.241(6); Fe1-Sn1 = 2.9541(11); Fe2-Sn1 = 2.8093(13); Sn1-Cl1 = 2.372(3); Fe1-Sn1-Fe2 = 78.78(3); N1-Sn1-Cl1 = 99.51(19).

The nucleophilicity of the interstitial nitride in Na[**1**] can also be used to incorporate high-spin transition-metal centers into an otherwise low-spin cluster framework. In addition, the inclusion of such high-spin centers allows for cooperative reactivity between electronically distinct portions of these expanded clusters. As shown in Scheme 2.5, treatment of Na[**1**] with $FeCl_2$ in THF solution produced the cluster $Fe_4(FeCl(THF)(\mu_4\text{-}N))(CO)_8(CNAr^{Mes2})_4$ (**5**), in which a [FeCl(THF)] fragment has been incorporated into the core proximal to the interstitial nitride (Figure 2.9). In solution, cluster **5** gave rise to an effective magnetic moment of 4.94(11) $\mu_B$, thereby indicating that the newly installed iron center possesses a high-spin, S = 2 ferrous ground state. The Fe–Fe separations from the wingtip iron centers to the [FeCl(THF)] unit are similar to those in the $Fe_4(\mu_4\text{-}N)$ portion derived from Na[**1**], suggesting that this high-spin unit has been incorporated into the cluster bonding framework.

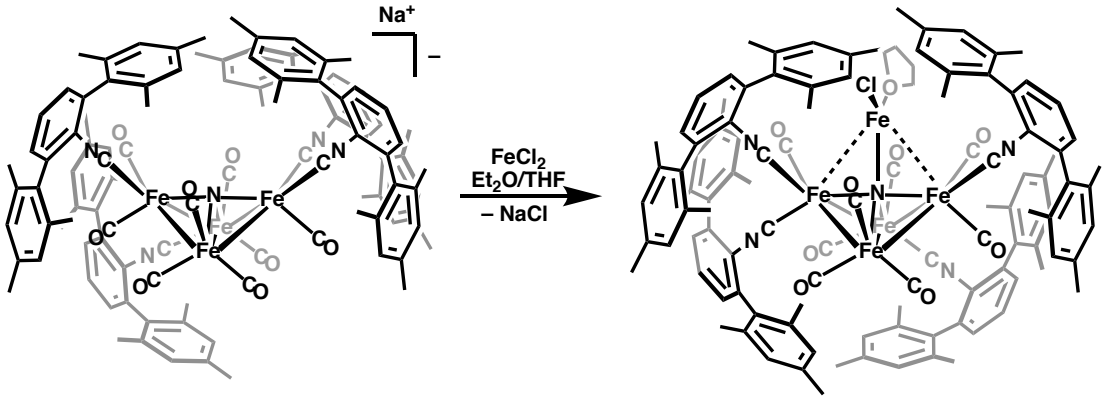


Scheme 2.5. Synthesis of a coordinatively and electronically unsaturated cluster, $Fe_4(FeCl(THF)(\mu_4\text{-}N))(CO)_8(CNAr^{Mes2})_4$ (**5**).

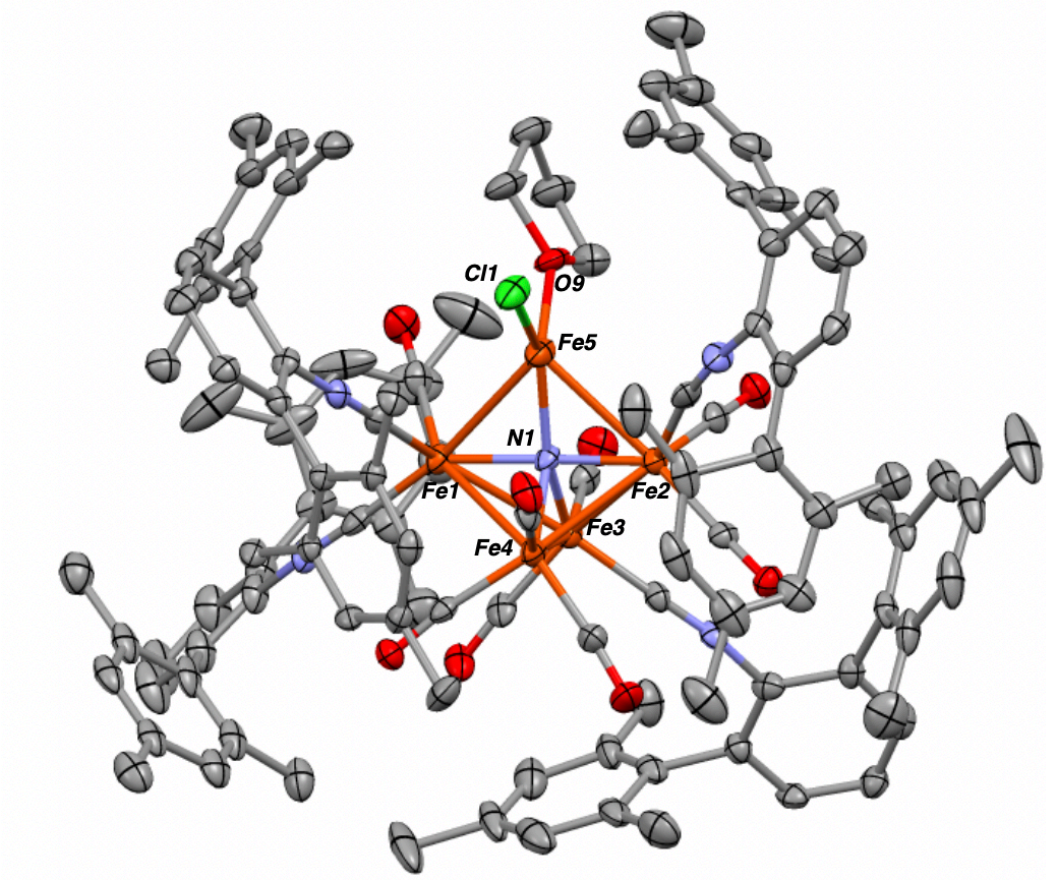


Figure 2.9. Solid-state structure of $Fe_4(FeCl(THF)(\mu_4\text{-}N))(CO)_8(CNAr^{Mes2})_4\cdot(C_6H_6)$ (**5**$\cdot(C_6H_6)$. Omitted items include one molecule of co-crystallized benzene, disorder of one of the *m*-terphenyl groups, and disorder of the bound THF molecule. Selected bond distances (Å) and angles (˚): Fe1-N1 = 1.847(5); Fe2-N1 = 1.843(5); Fe3-N1 = 1.884(5); Fe4-N1 = 1.899(5); Fe3-Fe4 = 2.5136(13); N1-Fe5 = 1.937(5); Fe1-Fe5 = 2.7068(13); Fe2-Fe5 = 2.6559(13); Fe5-Cl1 = 2.203(2); Fe5-O9 = 2.022(5); Fe1-Fe5-Fe2 = 86.93(4); N1-Fe5-Cl1 = 141.09(16).

## 2.5 Surface-Like Reactivity of Clusters with Open Coordination Sites

Whereas the addition of four $CNAr^{Mes2}$ ligands to the $Fe_4(\mu_4\text{-}N)$ core in this cluster class can activate the nitride unit towards reaction with electrophiles, it is most important that this strategy can be exploited to augment the topological, electrochemical, and reactivity properties of the cluster in a systematic manner. The dangling Sn–Cl group in **3** provides a site for additional synthetic elaboration and cluster-core expansion. Treatment of the chlorostannylene cluster **3** with

$Na[BAr^{F}{}_4]$ ($Ar^F$ = 3,5-$(CF_3)_2C_6H_3$) proceeded with loss of NaCl to afford the salt $[Fe_4Sn(\mu_5\text{-}N)(CO)_8(CNAr^{Mes2})_4][BAr^{F}{}_4]$ ([**4**]$BAr^{F}{}_4$), in which the divalent Sn center migrates into the core to become the fourth basal vertex of a pseudo-square-pyramidal cluster (Figure 1). Notably, [**4**]$^+$ is a cationic analogue to the classical carbide cluster $Fe_5(\mu_5\text{-}C)(CO)_{15}$ in which a $[Fe(CO)_3]$ fragment has been replaced by a Sn(II) cation.[26] The Fe–Fe distances in $Fe_5(\mu_5\text{-}C)(CO)_{15}$ and [**4**]$^+$ are comparable, but the larger Sn center of the latter significantly distorts the square base of the pyramid. Accordingly, this cluster rearrangement mimics the atomic scale restructuring of metal surfaces, which has been proposed to introduce structural strain in order to optimize coordination numbers with nearest-neighbor atoms.[5]

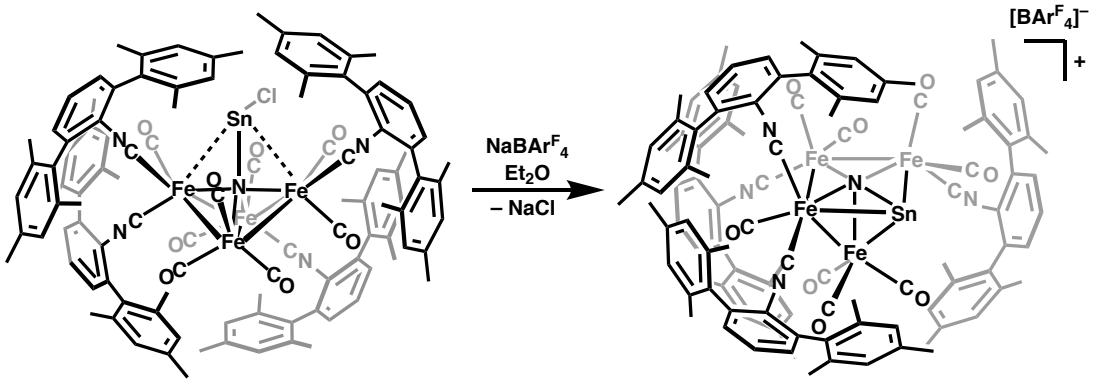


Scheme 2.6. Cluster reorganization resulting from halide abstraction to yield $[Fe_4Sn(\mu_5\text{-}N)(CO)_8(CNAr^{Mes2})_4][BAr^{F}{}_4]$ ([**4**]$BAr^{F}{}_4$).

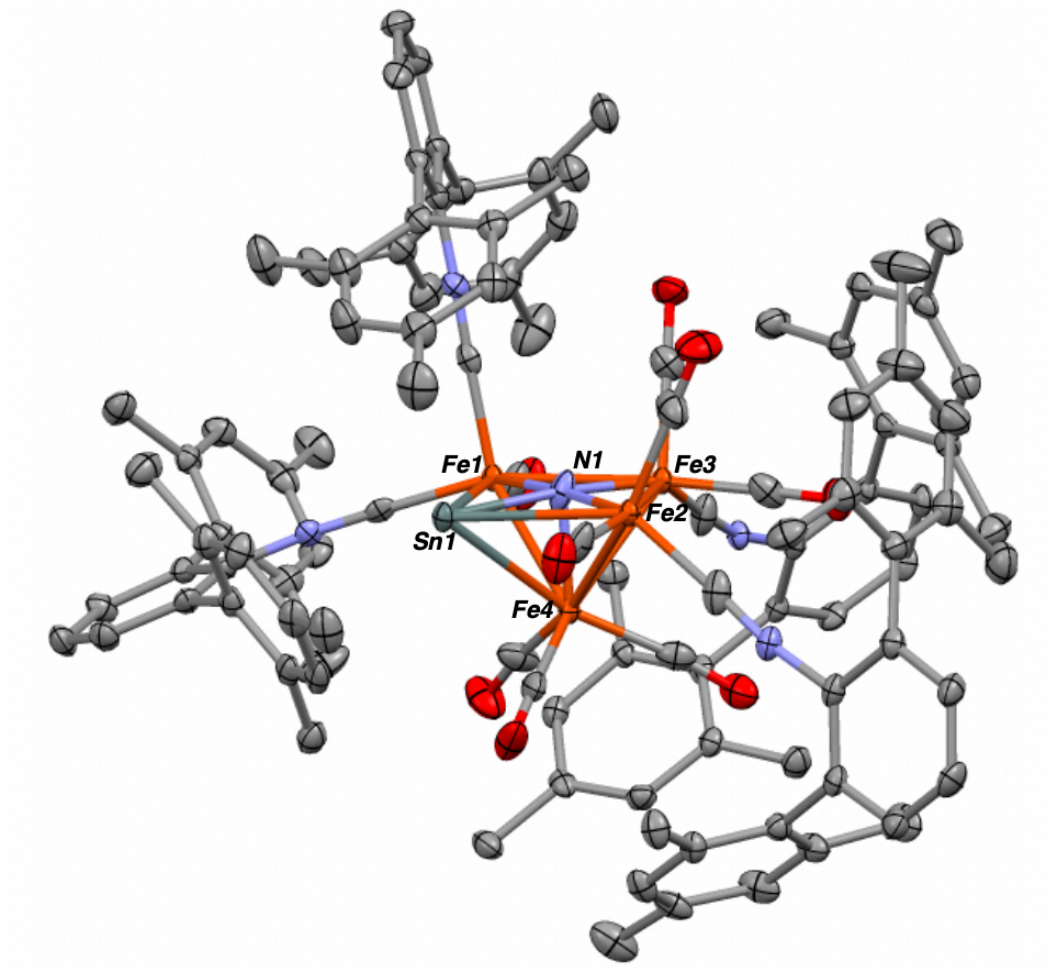


Figure 2.10. Solid-state structure of the cation of $[Fe_4Sn(\mu^5\text{-}N)(CO)_8(CNAr^{Mes2})_4][BAr^F{}_4]\cdot(Et_2O)$ (**4**·$(Et_2O)$). Omitted items include the $BAr^F{}_4$ counter ion, which contains disordered fluorine atoms, disorder of the cluster core, and one co-crystallized diethyl ether molecule. Selected bond distances (Å) and angles (˚): Fe1-N1 = 1.823(4); Fe2-N1 = 1.862(4); Fe3-N1 = 1.870(4); Fe4-N1 = 1.877(4); Fe3-Fe4 = 2.5583(10); N1-Sn1 = 2.181(4); Fe1-Sn1 = 2.736(19); Fe2-Sn1 = 2.9090(8); Fe4-Sn1 = 2.8243(8); Fe1-Sn1-Fe2 = 81.36(4); Sn1-N1-Fe3 = 173.5(2).

Cyclic voltammetry measurements on [**4**]$BAr^F{}_4$ also illustrate that cluster-expansion reactions with electropositive elements can significantly tune the electrochemical response of strong-field iron clusters. In THF solution, two reversible reduction events centered at –0.42 V and –0.65 V vs. SCE were observed for [**4**]$BAr^F{}_4$. Accordingly, the presence of the Sn center in $[\mathbf{4}]^+$, coupled with the unipositive charge, allows for the onset of two reductions at far less negative

potentials than for the all-carbonyl cluster $[Fe_4(\mu_4\text{-}N)(CO)_{12}]^-$. Importantly, this effect is reminiscent of the role played by $Ca^{2+}$ in tuning the redox potential of the $Mn_3Ca$ OEC cluster of photosystem II,[27,28] and demonstrates that the increased electron-rich character of isocyanide-containing strong-field clusters can be partially mitigated by judicious cluster-growth strategies.

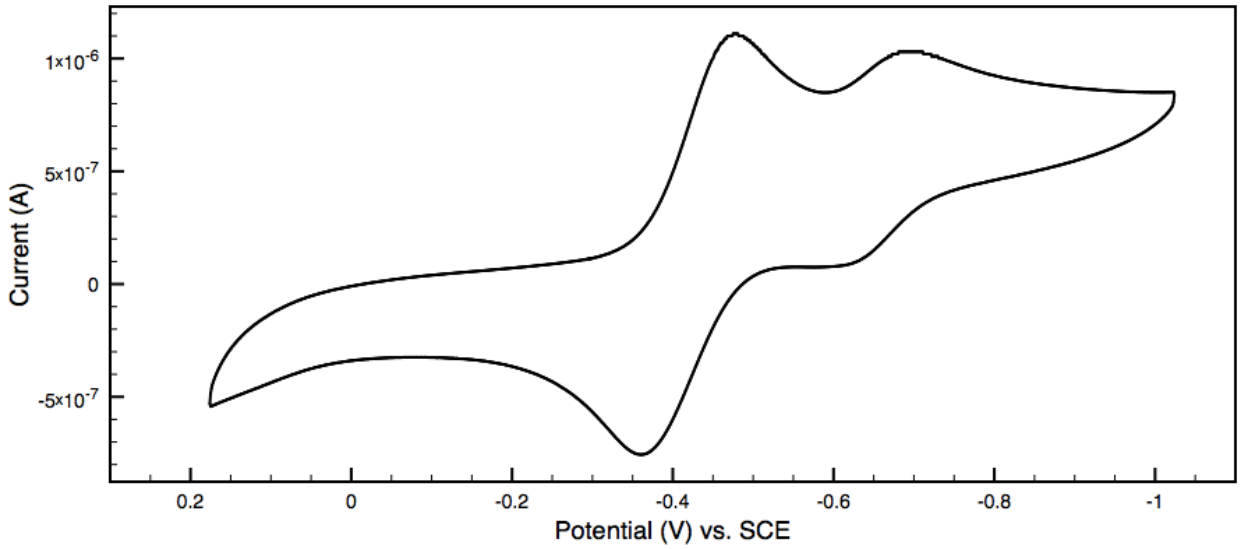


Figure 2.11. Cyclic voltammogram of [**4**]$BAr^F_4$. See Ch. 2.8 for conditions.

In **5**, it is also notable that the [FeCl(THF)] unit bares resemblance to mononuclear, S = 2 FeCl(THF)(dipyrromethene) complexes, which have been established by Betley to generate reactive iron nitrene species that effect C-H bond amination upon addition of organoazides.[29,30] In the case of cluster **5**, the $Fe_4(\mu_4\text{-}N)$ core can be viewed as a multimetallic ligand to the [FeCl(THF)] fragment and can potentially participate in substrate activation. Indeed, treatment of **5** with *p*-tolyl azide proceeded with loss of CO, $N_2$, and THF to the five-iron cluster $Fe_5Cl(\mu_5\text{-}N)(\mu_2\text{-}NTol)(CO)_7(CNAr^{Mes2})_4$ (**6**; Scheme 2.7, Figure 2.12), featuring both bridging nitrido and imido moieties (Figure 2). Most importantly, substrate activation by **5** induces cluster reorganization to the square-pyramidal cluster **6**. While the mechanistic sequence leading to **6** is not presently

known, the resultant iron imido unit further incorporates itself into the cluster framework by iron-centered oxidation of the unsubstituted [$Fe(CO)_3$] vertex and displacement of CO. This combination of metal-atom restructuring and formal 2 $e^-$ oxidation over two metal centers evokes the polynuclear hypothesis of substrate activation by both enzymatic cofactors and heterogeneous catalysts.[31]

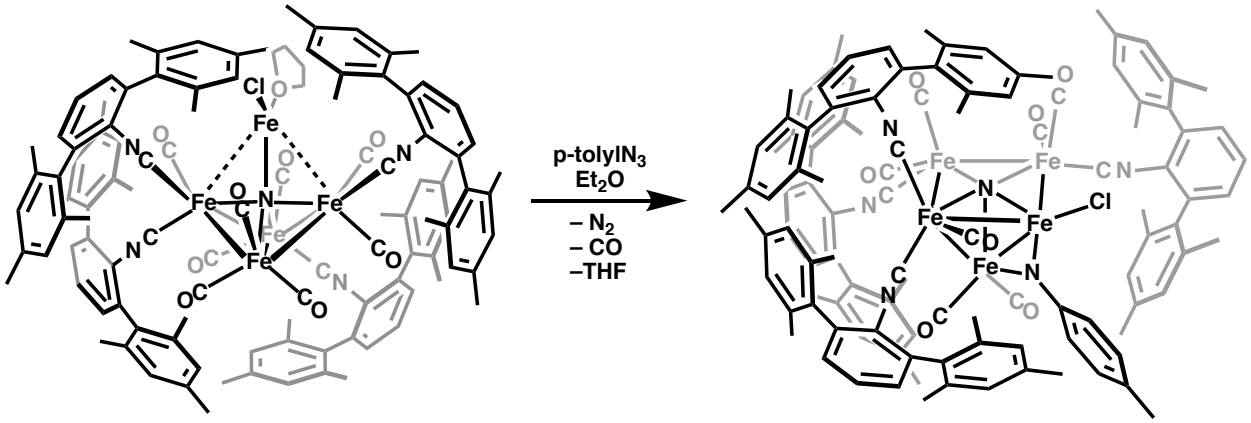


Scheme 2.7. Synthesis of $Fe_5Cl(\mu_5\text{-}N)(\mu_2\text{-}NTol)(CO)_7(CNAr^{Mes2})_4$ (**6**) by activation of *p*-tolyl azide.

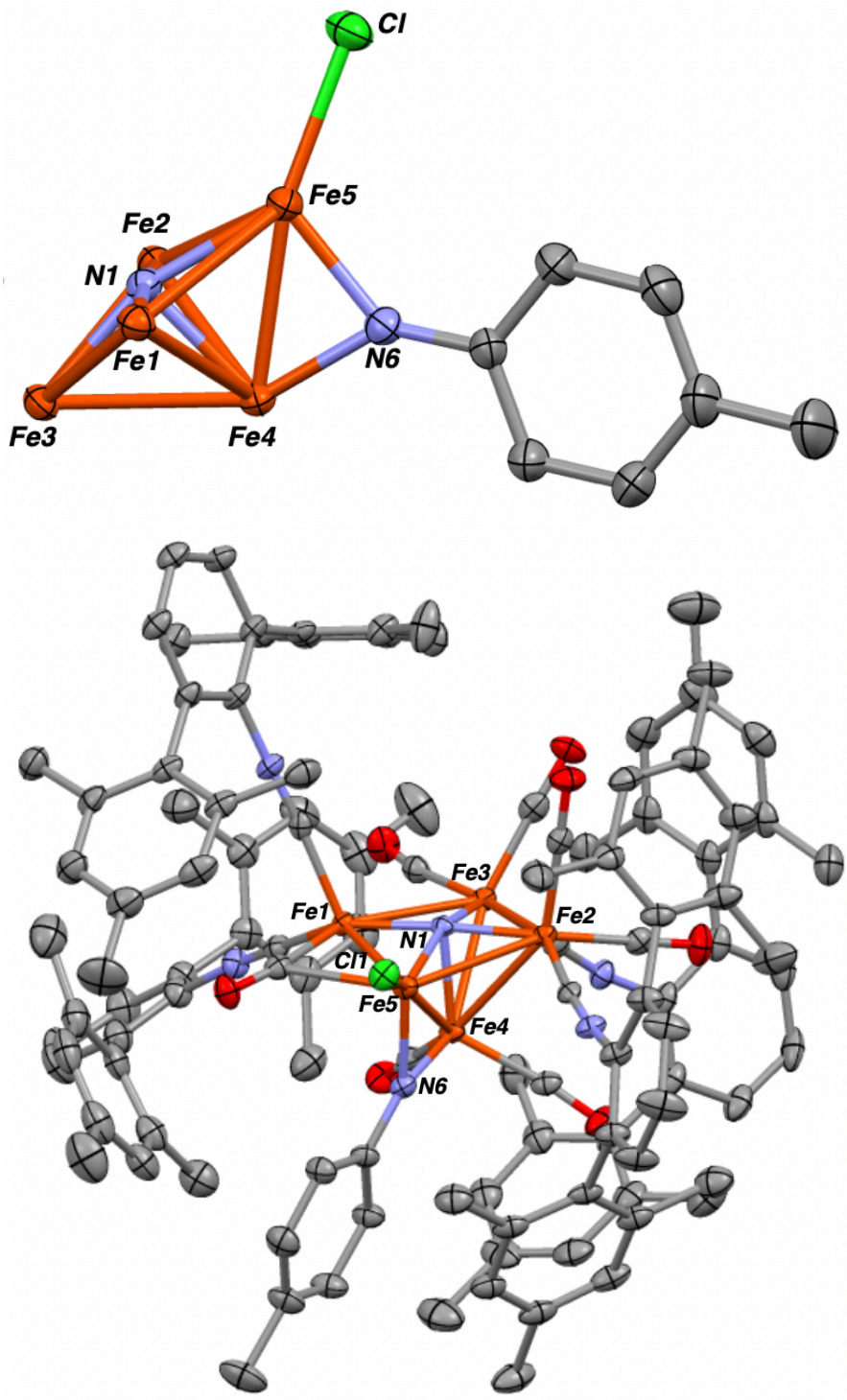


Figure 2.12. (Top) Solid-state cluster core of $Fe_5Cl(\mu^5\text{-}N)(\mu^2\text{-}NTol)(CO)_7(CNAr^{Mes2})_4$ (**6**). (Bottom) Full molecular structure of **6** with H-atoms omitted. Selected bond distances (Å) and angles (˚): Fe1-N1 = 1.851(2); Fe2-N1 = 1.841(2); Fe3-N1 = 1.898(2); Fe4-N1 = 1.918(2); Fe3-Fe4 = 2.5821(8); N1-Fe5 = 1.962(2); Fe1-Fe5 = 2.7087(7); Fe2-Fe5 = 2.7241(7); Fe5-Cl1 = 2.1972(9); Fe4-Fe5 = 2.4041(7); Fe5-N6 = 1.871(3); Fe4-N6 = 1.822(2); Fe1-Fe5-Fe2 = 85.51(2); N1-Fe5-Cl1 = 140.08(7); Fe4-N6-Fe5 = 81.22(10).

## 2.6 Concluding Remarks

In the present case, the enhanced electronic properties enabled by multiple ligand substitutions can impart strong-field molecular iron carbonyl clusters with multi-site reactivity by stepwise cluster expansion. Accordingly, we anticipate that this strategy will allow such clusters to mediate a range of multi-electron transformations in a general manner.

## 2.7 Synthetic Procedures and Characterization Data

**General Considerations.** All manipulations were carried out under an atmosphere of purified dinitrogen using standard Schlenk and glovebox techniques. Unless otherwise stated, reagent-grade starting materials were purchased from commercial sources and either used as received or purified by standard procedures.[32] Solvents were dried and deoxygenated according to standard procedures.[33] Benzene-$d_6$ (Cambridge Isotope Laboratories) was distilled from NaK alloy/benzophenone and stored over activated 3 Å molecular sieves for 2 d prior to use. Celite 405 (Fischer Scientific) was dried under vacuum (24 h) at a temperature above 250 ˚C and stored in a glovebox prior to use. Compounds $CNAr^{Mes2}$ and $[Na(diglyme)_2][Fe_4N(CO)_{12}]$ were prepared as previously reported.[34,13]

Solution $^1H$ and $^{13}C\{^1H\}$ NMR spectra were recorded on a Varian Mercury 400 or a Varian X-SENS 500 spectrometer. $^1H$ and $^{13}C\{^1H\}$ chemical shifts are reported in ppm relative to $SiMe_4$ ($^1H$ and $^{13}C$ $\delta$ = 0.0 ppm) with reference to residual solvent resonances of 7.16 ppm ($^1H$) and 128.06 ppm ($^{13}C$) for $C_6D_6$. FTIR spectra were recorded on a Thermo-Nicolet iS10 FTIR spectrometer. Samples were prepared as KBr pellets or $C_6D_6$ or THF solutions injected into a ThermoFisher solution cell equipped with KBr windows. Solvent peaks were digitally subtracted

from all solution FTIR spectra by comparison with an authentic solvent spectrum obtained prior to that of the sample. The following abbreviations were used for the intensities and characteristics of important IR absorption bands: vs = very strong, s = strong, m = medium, w = weak, vw = very weak; sh = shoulder. Combustion analyses were performed by Midwest Microlabs of Indianapolis, IN (USA) with the exception of $Fe_4(Tl\text{-}N)(CO)_8(CNAr^{Mes2})_4$, which was analyzed by Robertson Microlit Laboratories of Madison, New Jersey (USA).

**Preparation of $HFe_4N(CO)_8(CNAr^{Mes2})_4$ (1-H).** A Schlenk flask was loaded with $CNAr^{Mes2}$ (1.67 g, 4.93 mmol, 4.2 equiv.), benzoic acid (0.164 g, 1.17 mmol, 1 equiv.), and $[Na(diglyme)_2][Fe_4N(CO)_{12}]$ (1.01 g, 1.17 mmol, 1 equiv.). To this mixture was added 60 mL benzene. The resulting slurry was heated to reflux for 21 h and then evaporated to dryness *in vacuo*. The product was extracted in $Et_2O$ and filtered through Celite to remove the benzoate byproduct. Storage of a *n*-pentane solution of $HFe_4N(CO)_8(CNAr^{Mes2})_4$ at room temperature for 1 d provided analytically pure black/red crystals suitable for X-ray diffraction. Yield: 0.852 g, 0.468 mmol, 40%. $^1$H NMR (500.2 MHz, $C_6D_6$, 20 ˚C): δ = 7.06 (s, 5H), 7.04 (s, 4H), 6.98 – 6.82 (m, 19H), 2.39 (s, 12H), 2.36 (s, 9H), 2.34 (s, 6H), 2.26 (s, 9H), 2.24 (s, 6H), 2.22 (s, 9H), 2.14 (m, 12H), 2.13 (s, 9H), –30.88 (s, 1H) ppm. $^{13}C\{^1H\}$ NMR (125.7 MHz, $C_6D_6$, 20 ˚C): δ = 213.8$_{(CO)}$, 212.7$_{(CO)}$, 212.5$_{(CO)}$, 207.0$_{(CO)}$, 182.7$_{(CN)}$, 176.4$_{(CN)}$, 174.5$_{(CN)}$, 173.1$_{(CN)}$, 139.19, 139.14, 138.9, 137.7, 137.44, 137.42, 137.2, 136.1, 135.79, 135.75, 135.72, 135.67, 135.62, 135.45, 135.0, 134.58, 134.52, 129.8, 129.7, 129.5, 129.38, 129.36, 129.30, 129.20, 129.17, 129.13, 128.9, 128.6, 127.7, 127.53, 127.47, 127.2, 21.53, 21.50, 21.39, 21.37, 21.28, 20.9, 20.8, 20.6, 20.5, 20.4 ppm. FTIR (KBr windows, THF, 25 ˚C): υ(C≡N) = 2124 (vw), 2090 (vs), 2073 (vs), 2044 (s) cm$^{-1}$, υ(C≡O) = 2019 (m), 1999 (m), 1979 (s), 1931 (vw) cm$^{-1}$, also 1615, 1464, 1416, 1377, 1252, 1033,

849, 805, 756, 652, 603 $cm^{-1}$. Anal. Calcd for $C_{108}H_{101}Fe_4N_5O_8$: C, 71.26; H, 5.59; N, 3.85. Found: C, 71.20; H, 5.63; N, 3.85.

**Preparation of Na[$Fe_4N(CO)_8(CNAr^{Mes2})_4$] (Na[1]).** To a resealable ampoule charged with NaO*t*-Bu (0.0651 g, 0.676 mmol, 1.1 equiv.) was added a THF solution of **1**-H (1.12 g, 0.615 mmol, 1 equiv.). The solution was stirred at 60 ˚C for 5 h, and all volatiles were then removed *in vacuo*. The product was extracted in 3:1 *n*-pentane/$Et_2O$, filtered through fiberglass filter paper to separate from unreacted NaO*t*-Bu, and evaporated to dryness. Analytically pure material was obtained from a saturated *n*-pentane solution stored at –35 ˚C over 1 day. Yield: 1.04 g, 0.566 mmol, 92%. Crystals suitable for X-ray diffraction were grown from a saturated *n*-pentane solution (~0.75 mL) combined with 10 drops of $Et_2O$ and 3 drops of benzene and storing the resulting solution at –35 ˚C for 2 days. $^1$H NMR (500.2 MHz, $C_6D_6$, 20 ˚C): δ = 7.10 (s, 2H), 7.09 (s, 1H), 7.07 (s, 2H), 7.05 (s, 2H), 7.02 (s, 4H), 6.99 – 6.85 (m, 13H), 6.77 (m, 4H), 2.41 (s, 6H), 2.39 (s, 6H), 2.34 (s, 6H), 2.31 (s, 6H), 2.29 (s, 6H), 2.28 (s, 6H), 2.26 (s, 6H), 2.10 (br s, 9H), 2.09 (s, 9H), 2.06 (s, 6H) ppm. $^{13}C\{^1H\}$ NMR (125.7 MHz, $C_6D_6$, 20 ˚C): δ = 218.0$_{(CO)}$, 216.7$_{(CO)}$, 216.3$_{(CO)}$, 215.4$_{(CO)}$, 184.3$_{(CN)}$, 180.5$_{(CN)}$, 177.7$_{(CN)}$, 139.4, 139.2, 137.73, 137.70, 137.2, 136.9, 136.5, 136.1, 135.92, 135.90, 135.88, 135.8, 135.6, 135.5, 135.4, 130.4, 129.9, 129.8, 129.54, 129.47, 129.4, 129.3, 129.2, 129.1, 129.0, 128.9, 127.3, 126.92, 126.86, 126.81, 25.8, 21.63, 21.57, 21.0, 20.9, 20.8, 20.6, 20.3 ppm. FTIR (KBr windows, THF, 25 ˚C): υ(C≡N) 2083 (w), 2040 (s), 2014 (vs) $cm^{-1}$, υ(C≡O) = 1998 (vs), 1958 (vs), 1938 (sh), 1909 (sh) $cm^{-1}$, also 1615, 1578, 1560, 1416, 1035, 846, 802, 755, 632, 592, 565 $cm^{-1}$. Anal. Calcd for $C_{108}H_{100}Fe_4N_5NaO_8$: C, 70.41; H, 5.47; N, 3.80. Found: C, 69.92; H, 5.59; N, 3.69.

**Preparation of $Fe_4N(CO)_8(CNAr^{Mes2})_4$ (1).** A colorless *n*-pentane solution of trityl chloride (0.223 g, 0.800 mmol, 1.1 equiv.) was added to a stirring $Et_2O$ solution of red/brown $Na[Fe_4N(CO)_8(CNAr^{Mes2})_4]$ (1.34 g, 0.727 mmol, 1 equiv.) in a scintillation vial, and the resulting mixture was stirred for 30 minutes. The solution gradually lightened as a white film deposited on the vial walls and dark precipitate formed. The solution was decanted off, and the remaining black solid was washed five times with $Et_2O$. The product was dissolved in THF, filtered through Celite to remove NaCl, and evaporated to dryness to yield analytically pure $Fe_4N(CO)_8(CNAr^{Mes2})_4$. Yield: 0.981 g, 0.539 mmol, 74%. X-ray diffraction quality crystals were grown from a 1:5 THF/*n*-pentane solution stored at room temperature overnight. $\mu_{eff}$ (Evans Method; 400 MHz, $C_6D_6$ with $(Me_3Si)_2O$ reference, 20 ˚C, 4 runs): 1.74(±0.09) $\mu_B$ FTIR (KBr windows, $C_6D_6$, 25 ˚C): υ(C≡N) = 2120 (sh), 2085 (vs), 2060 (vs) $cm^{-1}$, υ(C≡O) = 2007 (m), 1991 (s), 1978 (vs), 1971 (vs), 1965 (vs), 1951 (m), 1939 (m), 1908 (w) $cm^{-1}$, also 2956 (m), 2921 (m), 1581 (w), 1415 (w), 1377 (w), 1036 (w), 849 (w), 756 (w) $cm^{-1}$. Anal. Calcd for $C_{108}H_{100}Fe_4N_5O_8 \bullet C_5H_{12}$: C, 71.75; H, 6.13; N, 3.70. Found: C, 71.44; H, 6.04; N, 3.67.

**Preparation of $Fe_4(Tl\text{-}N)(CO)_8(CNAr^{Mes2})_4$ (2).** THF (5 mL) was added to solid TlOTf (0.0234 g, 0.066 mmol, 1.05 equiv.) and $Na[Fe_4N(CO)_8(CNAr^{Mes2})_4]$ (0.116 g, 0.063 mmol, 1 equiv.), and the solution was stirred for 30 minutes. The reaction mixture was evaporated *in vacuo* revealing a brown solid and a white precipitate coating the vial. The solid was dissolved in a 2:1 *n*-pentane/$Et_2O$ mixture, stirred for two minutes, and evaporated to dryness. This process was repeated 3 times before filtering through Celite to ensure the removal of NaOTf and unreacted TlOTf. Analytically pure X-ray diffraction quality crystals were grown from 5:1 *n*-pentane/$Et_2O$ solution stored at room temperature overnight. Yield: 0.119 g, 0.059 mmol, 93%. $^1H$ NMR (500.2

MHz, $C_6D_6$, 20 ˚C): δ = 7.12 (s, 2H), 7.10 (s, 1H), 7.07 (s, 2H), 7.04 (s, 2H), 7.02 (s, 4H), 7.00 – 6.92 (m, 8H), 6.89 – 6.84 (m, 5H), 6.76 (br s, 4H), 2.46 (s, 6H), 2,44 (s, 6H), 2.38 (s, 6H), 2.34 (s, 6H), 2.32 (s, 6H), 2.31 (s, 6H), 2.27 (s, 6H), 2.26 (s, 6H), 2.12 (s, 6H), 2.11 (s, 6H), 2.02 (br s, 12H) ppm. $^{13}C\{^1H\}$ NMR (125.7 MHz, $C_6D_6$, 20 ˚C): δ = 216.4$_{(CO)}$, 216.3$_{(CO)}$, 215.9$_{(CO)}$, 215.6$_{(CO)}$, 213.9$_{(CO)}$, 181.3$_{(CN)}$, 180.4$_{(CN)}$, 176.9$_{(CN)}$, 176.8$_{(CN)}$, 139.5, 139.3, 137.6, 137.4, 137.0, 136.0, 135.9, 135.8, 135.66, 135.63, 135.22, 135.20, 130.2, 130.0, 129.8, 129.46, 129.37, 129.23, 129.21, 129.18, 129.14, 129.09, 129.02, 128.96, 128.4, 127.6, 127.5, 127.3, 127.2, 21.8, 21.57, 21.54, 21.51, 21.00, 20.98, 20.94, 20.88, 20.85, 20.80, 20.76, 20.73, 20.69, 20.65, 20.63 ppm. FTIR (KBr pellet, 25 ˚C): υ(C≡N) = 2157 (vw), 2068 (vs), 2032 (vs) $cm^{-1}$, υ(C≡O) = 1992 (vs), 1962 (s), 1933 (m), 1924 (m), 1910 (m) $cm^{-1}$, also 2970 (m), 2917 (m), 2862 (m), 1617 (w), 1577 (w), 1414 (m), 1375 (m), 848 (w), 803 (w), 755 (w) $cm^{-1}$. Anal. Calcd for $C_{108}H_{100}Fe_4N_5O_8Tl$: C, 64.10; H, 4.98; N, 3.46. Found: C, 63.96; H, 5.08; N, 3.38.

**Preparation of $Fe_4(ClSn\text{-}N)(CO)_8(CNAr^{Mes2})_4$ (3).** $SnCl_2$ (0.0204 g, 0.108 mmol, 1.5 equiv.) was slurried in 3 mL $Et_2O$ for 5 minutes before being combined with a thawing solution of $Na[Fe_4N(CO)_8(CNAr^{Mes2})_4]$ (0.132 g, 0.0716 mmol, 1 equiv.) in $Et_2O$. The mixture was stirred for 30 minutes as it warmed to room temperature, at which time solvent was removed *in vacuo*. The resulting solid was slurried in 5 mL *n*-pentane for 5 minutes to fully precipitate NaCl and unreacted $SnCl_2$. The product was extracted by adding 2 mL $Et_2O$ to this solution and filtering through Celite. Analytically pure crystals were grown from a 5:1 *n*-pentane/$Et_2O$ solution at –35 ˚C for 1 day. Yield: 0.124 g, 0.063 mmol, 88%. $^1H$ NMR (500.2 MHz, $C_6D_6$, 20 ˚C): δ = 7.10 (s, 3H), 7.06 (m, 3H), 7.02 (s, 4H), 6.99 (s, 3H), 6.94 (s, 3H), 6.93 – 6.81 (m, 12H), 2.46 (s, 9H), 2.45 (s, 9H), 2.32 (br s, 3H), 2.30 (s, 6H), 2.28 (s, 3H), 2.27 (s, 6H), 2.25 (s, 9H), 2.22 (br s, 18H), 2.15 (s, 6H), 2.12

– 2.09 (m, 3H) ppm. $^{13}C\{^{1}H\}$ NMR (125.7 MHz, $C_6D_6$, 20 ˚C): δ = 218.2$_{(CO)}$, 216.5$_{(CO)}$, 213.5$_{(CO)}$, 206.4$_{(CO)}$, 177.4$_{(CN)}$, 168.9$_{(CN)}$, 167.8$_{(CN)}$, 165.9$_{(CN)}$, 139.7, 139.5, 138.0, 137.8, 137.6, 137.4, 135.9, 135.8, 135.73, 135.66, 135.63, 135.55, 135.4, 135.1, 134.75, 134.72, 134.6, 130.3, 130.16, 130.07, 129.7, 129.5, 129.4, 129.3, 129.2, 129.1, 129.0, 128.9, 128.6, 127.75, 127.72, 127.6, 21.7, 21.4, 21.1, 20.74, 20.70, 20.61, 20.55 FTIR (KBr windows, $C_6D_6$, 25 ˚C): υ(C≡N) = 2165 (vw), 2081 (vs), 2055 (sh) cm$^{-1}$, υ(C≡O) = 1998 (s), 1983 (s), 1962 (m), 1943 (w) cm$^{-1}$, also 2978 (m), 2867 (m), 1540 (w), 1416 (w), 1379 (w), 1118 (m), 1045 (w), 850 (w), 756 (w), 680 (w), 669 (w) cm$^{-1}$. Anal. Calcd for $C_{108}H_{100}ClFe_4N_5O_8Sn$: C, 65.73; H, 5.11; N, 3.55. Found: C, 66.01; H, 5.38; N, 3.22.

**Preparation of [$Fe_4Sn(\mu^5$-N)$(CO)_8(CNAr^{Mes2})_4$][$BAr^F_4$] (4).** A $Et_2O$ solution of $NaBAr^F_4$ (0.042 g, 0.048 mmol, 1 equiv.) was added to Fe4(ClSn-N)$(CO)_8(CNAr^{Mes2})_4$] (0.094 g, 0.048 mmol, 1 equiv.), and the solution was stirred for 15 minutes. Solvent was removed *in vacuo*, and benzene was added to the resulting solid to separate the product from NaCl and unreacted $NaBAr^F_4$. This solution was filtered through Celite and evaporated to dryness. The solid was dissolved in $Et_2O$, and *n*-pentane was slowly added until an oily precipitate began to form. This saturated solution was then filtered through a fiberglass filter paper pipet and allowed to sit at room temperature overnight producing large, analytically pure crystals of [$Fe_4Sn(\mu^5$-N)$(CO)_8(CNAr^{Mes2})_4$][$BAr^F_4$]. Yield: 0.126 g, 0.045, 94%. $^{1}H$ NMR (500.2 MHz, $C_6D_6$, 20 ˚C): δ = 8.45 (s, 8H, *o*-$Ar^{F24}$), 7.68 (s, 4H, *p*-$Ar^{F24}$), 7.08 (t, 1H, *J* = 7.7 Hz, *p*-Ph), 7.04 – 6.82 (m, 21H), 6.82 – 6.46 (br m, 6H), 2.50 (br s, 4H), 2.44 (s, 6H), 2.30 (s, 9H), 2.13 (s, 10H), 2.11 (s, 19H), 2.08 (s, 6H), 2.03 (s, 6H), 1.81 (s, 12H) ppm. $^{13}C\{^{1}H\}$ NMR (125.7 MHz, $C_6D_6$, 20 ˚C): δ = 215.8$_{(CO)}$, 213.2$_{(CO)}$, 212.2$_{(CO)}$, 211.2$_{(CO)}$, 203.6$_{(CO)}$, 202.2$_{(CO)}$, 166.4$_{(CN)}$, 166.2$_{(CN)}$, 163.7$_{(CN)}$, 162.4

(q, $^{1}J_{B\text{-}C}$ = 49.8 Hz), 156.9$_{(CN)}$, 135.78, 135.69, 135.5, 135.2, 134.2, 130.64, 130.56, 130.2, 129.9 (q, $^{2}J_{C\text{-}F}$ = 31.5 Hz) 129.89, 129.2, 127.6, 127.4, 127.2, 126.5, 125.3 (q, $^{1}J_{C\text{-}F}$ = 272.5 Hz), 118.0, 21.30, 21.29, 21.0, 20.48, 20.44, 20.3, 20.2 ppm. FTIR (KBr pellet, 25 ˚C): υ(C≡N) = 2168 (vw), 2124 (vs), 2085 (s) cm$^{-1}$, υ(C≡O) = 2028 (s), 2009 (vs), 1992 (vs), 1973 (s), 1954 (s) cm$^{-1}$, υ(C–F) 1356 (vs), 1280 (vs), 1128 (s) cm$^{-1}$, also 2964, 2924, 2862, 1612, 1452, 804, 756, 714, 683, 674 cm$^{-1}$. Anal. Calcd for $C_{140}H_{112}BF_{24}Fe_4N_5O_8Sn$: C, 60.03; H, 4.03; N, 2.50. Found: C, 60.24; H, 4.09; N, 2.57.

**Preparation of $Fe_4(FeCl(THF)\text{-}N)(CO)_8(CNAr^{Mes2})_4$ (5).** THF (3 mL) was added to $FeCl_2$ (0.021 g, 0.167 mmol, 1.5 equiv.), and the resulting suspension was stirred for 30 minutes. A thawing $Et_2O$ solution of $Na[Fe_4N(CO)_8(CNAr^{Mes2})_4]$ (0.205 g, 0.111 mmol, 1 equiv, 3 mL) was added to the $FeCl_2$ suspension, and the mixture was stirred for 30 minutes. All volatiles were removed *in vacuo*. The solid was twice slurried in *n*-pentane and dried, and the resulting product was extracted in $Et_2O$ and filtered through Celite. Yield: 0.201 g, 0.104 mmol, 91%. Crystals suitable for X-ray diffraction were grown from a saturated *n*-pentane/$Et_2O$ solution (5:1) combined with 3 drops of benzene and storing the resulting solution at –35 ˚C for 2 days. $\mu_{eff}$ (Evans Method; 400 MHz, $C_6D_6$ with $(Me_3Si)_2O$ reference, 20 ˚C, 3 runs): 4.94(±0.11) $\mu_B$. FTIR (KBr windows, $C_6D_6$, 25 ˚C): υ(C≡N) = 2119 (sh), 2072 (vs) cm$^{-1}$, υ(C≡O) = 2012 (sh), 1986 (s), 1952 (m), 1927 (sh) cm$^{-1}$, also 2959 (m), 2931 (m), 1614 (w), 1574 (w), 1463 (w), 1415 (w), 1377 (w), 1119 (w), 1045 (w), 1014 (w), 850 (w), 756 (w), 566 (w) cm$^{-1}$. Despite multiple attempts, satisfactory combustion analysis on compound **5** could not be obtained.

**Preparation of $Fe_5Cl(\mu^5\text{-}N)(\mu^2\text{-}NTol)(CO)_7(CNAr^{Mes2})_4$ (6).** To a thawing $Et_2O$ solution of $Fe_4(FeCl(THF)\text{-}N)(CO)_8(CNAr^{Mes2})_4$ (0.154 g, 0.078 mmol, 1 equiv.) was added a 0.5 M 4-azidotoluene solution in MTBE (0.187 mL, 0.094 mmol, 1.2 equiv.). The mixture was stirred for 10 mintues before evaporating to dryness. Storage of a *n*-pentane solution of the resulting solid overnight at –35 ˚C deposited $Fe_5Cl(\mu^5\text{-}N)(\mu^2\text{-}NTol)(CO)_8(CNAr^{Mes2})_4$ as a black, microcrystalline powder. Yield: 0.143 g, 0.072 mmol, 92%. X-ray diffraction quality crystals were grown by dissolving 0.080 g of the powder in 1 mL of toluene, reducing the volume to ¼, adding 0.25 mL *n*-pentane, and storing the solution at –35 ˚C for 3 days. $\mu_{eff}$ (Evans Method; 400 MHz, $C_6D_6$ with $(Me_3Si)_2O$ reference, 20 ˚C, 4 runs): 3.36(±0.04) $\mu_B$. FTIR (KBr windows, $C_6D_6$, 25 ˚C): υ(C≡N) = 2113 (sh), 2082 (vs) $cm^{-1}$, υ(C≡O) = 1993 (s), 1971 (s), 1948 (s) $cm^{-1}$, also 2960 (m), 2861 (m), 1614 (w), 1569 (w), 1540 (w), 1415 (w), 1377 (w), 1161 (w), 1045 (w), 850 (w), 756 (w) $cm^{-1}$. Despite multiple attempts, satisfactory combustion analysis on compound **6** could not be obtained.

## 2.8 Electrochemical Studies

**Experimental details.** Cyclic voltammetry measurements were carried out using a EG&G potentiostat (PAR-model 263A) and an electrochemical cell with a Pt disk working electrode, Pt wire counter-electrode, and Ag as a (pseudo) reference electrode. Measurements were performed in an argon-filled glovebox using a room temperature THF solution of $Fe_4N(CO)_8(CNAr^{Mes2})_4$ (**1**) or $[Fe_4Sn(\mu^5\text{-}N)(CO)_8(CNAr^{Mes2})_4][BAr^F{}_4]$ (**4**) containing $[(n\text{-}Bu)_4N][PF_6]$ (0.1 M) using decamethylferrocene as an external standard ($Cp^*{}_2Fe/Cp^*{}_2Fe^+$ = +0.102 V vs. SCE in THF)[5] at a scan rate of 0.1 V/s. For compound **1**, one reversible redox wave was observed centered at –0.65 V vs. SCE. The peak-to-peak separation (118 mV) is fairly large for a one-electron process but

can be explained by the semi-bridging carbonyl rearrangement that takes place in reduction of **1** to $\mathbf{1}^{-}$. For compound **4**, two quasi-reversible waves were observed at –0.42 and –0.65 V with peak-to-peak separations of 117 and 95 mV, respectively, also consistent with one-electron processes. For clusters **1** and **4**, scanning to both more negative and more positive potentials resulted in the appearance of unidentified irreversible redox events and decreased reversibility of the existing waves presumably due to cluster degradation.

## 2.9 Results of EPR Measurements and Simulations

**X-Band EPR Measurements.** The X-Band continuous wave (CW) EPR spectrum of $Fe_4N(CO)_8(CNAr^{Mes2})_4$ (**1**) was measured on a Bruker E500 spectrometer equipped with a Bruker ER 041 X Microwave Bridge and a liquid nitrogen cooling system. The spectrum was recorded in a 4 mm quartz tube at 295 K, and the magnetic field was calibrated with DPPH. The sample was prepared in a nitrogen-filled glovebox using dry toluene as the solvent.

**Input file for Easyspin EPR simulation.**

```
Sys.g=[2.0335]
Sys.lwpp=[1.0205, 5.0531]
Sys.HStrain=[10.2316, 4.1607, 17.9942]
Exp.mwFreq=[9.3949]
Exp.CenterSweep=[325, 40]
garlic(Sys,Exp);
```

## 2.10 Details of Crystallographic Structure Determinations

**General.** Single X-ray structure determinations were performed at 100 K on Bruker Kappa diffractometers equipped with a Mo radiation source and an APEX-II CCD area detector. All structures were solved via direct methods with SHELXS[35] and refined by full-matrix least-squares procedures using SHELXL[36] within the Olex2[37] software. The Platon routine SQUEEZE[38] was used to account for residual electron density in solvent accessible voids in all structures except compound **5**. All hydrogen atoms were omitted for clarity except the hydride in H-**1**. Crystallographic data collection and refinement information is listed in Tables 2.1–3.

Table 2.1. Crystallographic Data Collection and Refinement Information.

| Name | $HFe_4N(CO)_8(CNAr^{Mes2})_4$ (**1**-H) | $Na[Fe_4N(CO)_8(CNAr^{Mes2})_4]$ (Na[**1**]) | $Fe_4N(CO)_8(CNAr^{Mes2})_4$ (**1**) |
|---|---|---|---|
| Formula | $C_{108}H_{101}Fe_4N_5O_8$ | $C_{108}H_{101}Fe_4N_5NaO_8$ | $C_{108}H_{100}Fe_4N_5O_8$ |
| Crystal System | Monoclinic | Orthorhombic | Triclinic |
| Space Group | $P2_1/c$ | $Pna2_1$ | $P\bar{1}$ |
| $a$, Å | 26.2689(13) | 25.2307(5) | 15.3902(7) |
| $b$, Å | 14.8266(8) | 47.9356(10) | 15.4068(7) |
| $c$, Å | 28.5060(16) | 16.2220(3) | 24.9702(10) |
| α, deg | 90 | 90 | 78.7400(10) |
| β, deg | 105.0720(10) | 90 | 79.4810(10) |
| γ, deg | 90 | 90 | 63.6120(10) |
| V, Å$^3$ | 10720.5(10) | 19619.7(7) | 5170.8(4) |
| $Z$ | 4 | 8 | 2 |
| Radiation (λ, Å) | Mo-Kα, 0.71073 | Mo-Kα, 0.71073 | Mo-Kα, 0.71073 |
| ρ (calcd.), Mg/m$^3$ | 1.128 | 1.247 | 1.169 |
| μ (Mo Kα), mm$^{-1}$ | 0.583 | 0.642 | 0.604 |
| Temp, K | 100 | 100 | 100 |
| θ max, deg | 25.414 | 25.391 | 27.106 |
| data/ parameters | 19727/1154 | 35952/2354 | 22662/1150 |
| $R_1$ | 0.0487 | 0.0592 | 0.0409 |
| $wR_2$ | 0.1277 | 0.1362 | 0.1084 |
| GOF | 1.031 | 1.017 | 1.048 |

Table 2.2. Crystallographic Data Collection and Refinement Information.

| Name | $Fe_4(Tl\text{-}N)(CO)_8(CNAr^{Mes2})_4$ (**2**) | $Fe_4(ClSn\text{-}N)(CO)_8(CNAr^{Mes2})_4]$ (**3**) | $Fe_4Sn(\mu^5\text{-}N)(CO)_8(CNAr^{Mes2})_4\cdot(Et_2O)$ (**4**)$\cdot(Et_2O)$ |
|---|---|---|---|
| Formula | $C_{108}H_{101}Fe_4N_5O_8Tl$ | $C_{108}H_{101}ClFe_4N_5NaO_8Sn$ | $C_{144}H_{122}BF_{24}Fe_4N_5O_9Sn$ |
| Crystal System | Orthorhomic | Monoclinic | Triclinic |
| Space Group | $Pna2_1/c$ | $P2_1$ | $P\text{–}1$ |
| $a$, Å | 25.412(4) | 16.322(3) | 17.5467(7) |
| $b$, Å | 48.035(7) | 16.712(3) | 19.5121(7) |
| $c$, Å | 15.994(3) | 20.200(4) | 21.9968(9) |
| α, deg | 90 | 90 | 82.630(2) |
| β, deg | 90 | 104.703(6) | 69.560(2) |
| γ, deg | 90 | 90 | 78.008(2) |
| V, Å$^3$ | 19524(5) | 5329.9(18) | 6890.2(5) |
| $Z$ | 8 | 2 | 2 |
| Radiation (λ, Å) | Mo-Kα, 0.71073 | Mo-Kα, 0.71073 | Mo-Kα, 0.71073 |
| ρ (calcd.), Mg/m$^3$ | 1.377 | 1.230 | 1.386 |
| μ (Mo Kα), mm$^{-1}$ | 2.283 | 0.844 | 0.680 |
| Temp, K | 100 | 100 | 100 |
| θ max, deg | 25.039 | 25.455 | 25.401 |
| data/ parameters | 30180/2215 | 19602/1198 | 25219/1663 |
| $R_1$ | 0.0385 | 0.0495 | 0.0594 |
| $wR_2$ | 0.0756 | 0.1140 | 0.1308 |
| GOF | 0.902 | 1.001 | 1.030 |

Table 2.3. Crystallographic Data Collection and Refinement Information.

| Name | $Fe_4(FeCl(THF)\text{-}N)(CO)_8(CNAr^{Mes2})_4\cdot(C_6H_6)$ (**5**·$C_6H_6$) | $Fe_5Cl(\mu^5\text{-}N)(\mu^2\text{-}NTol)(CO)_7(CNAr^{Mes2})_4$ (**6**) |
|---|---|---|
| Formula | $C_{118}H_{114}ClFe_5N_5O_9$ | $C_{114}H_{107}ClFe_5N_6O_7$ |
| Crystal System | Monoclinic | Triclinic |
| Space Group | $P2_1/c$ | $P\text{–}1$ |
| *a*, Å | 13.5164(4) | 14.997(2) |
| *b*, Å | 24.9908(8) | 16.035(3) |
| *c,* Å | 31.2760(13) | 24.198(4) |
| α, deg | 90 | 92.419(5) |
| β, deg | 99.990(2) | 99.610(6) |
| γ, deg | 90 | 114.610(5) |
| V, $Å^3$ | 10404.4(6) | 5329.9(18) |
| *Z* | 4 | 2 |
| Radiation (λ, Å) | Mo-Kα, 0.71073 | Mo-Kα, 0.71073 |
| ρ (calcd.), $Mg/m^3$ | 1.316 | 1.276 |
| μ (Mo Kα), $mm^{-1}$ | 0.767 | 0.767 |
| Temp, K | 100 | 100 |
| θ max, deg | 21.935 | 25.393 |
| data/ parameters | 12616/1328 | 18949/1223 |
| $R_1$ | 0.0587 | 0.0449 |
| $wR_2$ | 0.1141 | 0.1041 |
| GOF | 1.024 | 1.017 |

## 2.11 Acknowledgments

Chapter 2 is adapted from **Drance, M. J.**; Mokhtarzadeh, C. C.; Melaimi, M.; Agnew, D. W.; Moore, C. E.; Rheingold, A. L.; Figueroa, J. S. "Controlled Expansion of a Strong-Field Iron-Nitride Cluster: Multi-Site Ligand Substitution as a Strategy for Activating Interstitial Nitride Nucleophilicity" *Angewandte Chemie, International Edition* **2018**, *57*, 13057–13061. DOI: 10.1002/anie.201801206. Copyright 2018 Wiley-VCH, Weinheim. Permission to include published material in this dissertation has been obtained from all coauthors. The dissertation author is the first author of this paper. Prof. Michael J. Tauber is also acknowledged for assistance with EPR measurements.

## 2.12 References

(1) Ertl, G. *Angew. Chem. Int. Ed.* **2008**, *47*, 3524.

(2) Hellman, A.; Baerends, E. J.; Biczysko, M.; Bligaard, T.; Christensen, C. H.; Clary, D. C.; Dahl, S.; van Harrevelt, R.; Honkala, K.; Jonsson, H.; Kroes, G. J.; Luppi, M.; Manthe, U.; Nørskov, J. K.; Olsen, R. A.; Rossmeisl, J.; Skfflason, E.; Tautermann, C. S.; Varandas, A. J. C.; Vincent, J. K. *J. Phys. Chem. B* **2006**, *110*, 17719.

(3) Bozso, F.; Ertl, G.; Grunze, M.; Weiss, M. *J. Catal.* **1977**, *49*, 18.

(4) Imbihl, R.; Behm, R. J.; Ertl, G.; Moritz, W. *Surf. Sci.* **1982**, *123*, 129.

(5) Somorjai, G. A. *Langmuir* **1991**, *7*, 3176.

(6) Muetterties, E. L. *Science* **1977**, *196*, 839.

(7) Muetterties, E. L.; Rhodin, T. N.; Band, E.; Brucker, C. F.; Pretzer, W. R. *Chem. Rev.* **1979**, *79*, 91.

(8) Dyson, P. J. *Coord. Chem. Rev.* **2004**, *248*, 2443.

(9) Tachikawa, M.; Stein, J.; Muetterties, E. L.; Teller, R. G.; Beno, M. A.; Gerbert, E.; Williams, J. M. *J. Am. Chem. Soc.* **1980**, *102*, 6648.

(10) Fjare, D. E.; Gladfelter, W. L. *Inorg. Chem.* **1981**, *20*, 3533.

(11) Gourdon, A.; Jeannin, Y. *J. Organomet. Chem.* **1992**, *440*, 353.

(12) Rail, M. D.; Berben, L. A.; *J. Am. Chem. Soc.* **2011**, *133*, 18577.

(13) Nguyen, A. D.; Rail, M. D.; Shanmugam, M.; Fettinger, J. C.; Berben, L. A. *Inorg. Chem.* **2013**, *52*, 12847.

(14) Taheri, A.; Thompson, E. J.; Fettinger, J. C.; Berben, L. A. *ACS Catal.* **2015**, *5*, 7140.

(15) Beno, M. A.; Williams, J. M.; Tachikawa, M.; Muetterties, E. L. *J. Am. Chem. Soc.* **1980,** *102*, 4542.

(16) Tachikawa, M.; Muetterties, E. L. *J. Am. Chem. Soc.* **1980**, *102*, 4541.

(17) Davis, J. H.; Beno, M. A.; Williams, J. M.; Zimmie, J.; Tachikawa, M.; Muetterties, E. L. *Proc. Natl. Acad. Sci. USA* **1981**, *78*, 668.

(18) Holt, E. M.; Whitmire, K. H.; Shriver, D. F. *J. Am. Chem. Soc.* **1982**, *104*, 5621.

(19) Carpenter, A. E.; Mokhtarzadeh, C. C.; Ripatti, D. S.; Havrylyuk, I.; Kamezawa, R.; Moore, C. E.; Rheingold, A. L.; Figueroa, J. S. *Inorg. Chem.* **2015**, *54*, 2936.

(20) Carpenter, A. E.; Chan, C.; Rheingold, A. L.; Figueroa, J. S. *Organometallics* **2016**, *35*, 2319.

(21) Margulieux, G. W.; Weidemann, N.; Lacy, D. C.; Moore, C. E.; Rheingold, A. L.; Figueroa, J. S. *J. Am. Chem. Soc.* **2010**, *132*, 5033.

(22) Mokhtarzadeh, C. C.; Margulieux, G. W.; Carpenter, A. E.; Weidemann, N.; Moore, C. E.; Rheingold, A. L.; Figueroa, J. S. *Inorg. Chem.* **2015**, *54*, 5579.

(23) Zanello, P.; Laschi, F.; Cinquantini, A.; Della Pergola, R.; Garlaschelli, L.; Cucco, M.; Demartin, F.; Spalding, T. R. *Inorg. Chim. Acta* **1994**, *226*, 1.

(24) Cambridge Structural Database, V 5.38 (November 2017).

(25) Barnett, B. R.; Figueroa, J. S. *Chem. Commun.* **2016**, *52*, 13829.

(26) Braye, E. H.; Dahl, L. F.; Hubel, W.; Wampler, D. L. *J. Am. Chem. Soc.* **1962**, *84*, 4633.

(27) Kanady, J. S.; Tsui, E. Y.; Day, M. W.; Agapie, T. *Science* **2011**, *333*, 733.

(28) Tsui, E. Y.; Tran, R.; Yano, J.; Agapie, T. *Nat. Chem.* **2013**, *5*, 293.

(29) King, E. R.; Hennessy, E. T.; Betley, T. A. *J. Am. Chem. Soc.* **2011**, *133*, 4917.

(30) Hennessy, E. T.; Betley, T. A. *Science* **2013**, *340*, 591.

(31) Powers, T. M.; Betley, T. A. *J. Am. Chem. Soc.* **2013**, *135*, 12289.

(32) Armarego, W. L. F.; Chai, C. L. L. *Purification of Laboratory Chemicals*, 5th Ed.; *Elsevier*, **2003**.

(33) Pangborn, A. B.; Giardello, M. A.; Grubbs, R. H.; Rosen, R. K.; Timmers, F. J. *Organometallics*, **1996**, *15*, 1518–1520.

(34) Fox, B. J.; Sun, Q. Y.; DiPasquale, A. G.; Fox, A. R.; Rheingold, A. L.; Figueroa, J. S. *Inorg. Chem.* **2008**, *47*, 9010–9020.

(35) Aranzaes, J. R.; Daniel, M.-C.; Astruc, D. *Can. J. Chem.* **2006**, *84*, 288–299.

(36) Sheldrick. G. M. *Acta Crystallogr. A.* **2008**, *64*, 112.

(37) Dolomanov, O. V.; Bourhis, L. J.; Gildea, R. J.; Howard, J. A. K.; Puschmann, H. *J. Appl. Cryst.* **2009**, *42*, 339.

(38) van der Sluis, P.; Spek. A. L. *Acta Crystallogr.* **1990**, *A46*, 194-201.

# Chapter 3

# Terminal Coordination of Diatomic Boron Monofluoride to Iron

## 3.1 Introduction

Carbon monoxide (CO) is among the most widely studied ligands in organometallic chemistry. Since the original report of a CO coordination compound 150 years ago[1] and the discovery of the first homoleptic metal carbonyl $Ni(CO)_4$ in 1890,[2] the coordination chemistry of CO has occupied a central role in the development of the reactivity and electronic structure theory of transition-metal complexes.[3,4] The binding of CO to transition metals has been described classically by the Dewar-Chatt-Duncanson bonding model.[5,6] In the terminal coordination mode, σ-donation from the carbon-centered lone pair of CO to an empty, acceptor orbital on the metal provides a primary bonding interaction. However, this metal-CO linkage is fortified by π-backdonation interactions from filled metal-based d-orbitals to the π* orbitals of CO.[7] The success of CO as a ligand is derived from the polarized nature of the C–O triple bond, which renders both its σ-donor and π-acceptor functionalities energetically well matched for interaction with a transition metal.[8] Diatomic molecules and ions that are isoelectronic and isolobal to CO— such as $N_2$, $CN^-$, and $NO^+$—are also widely known to bind transition metals.[9] However, the less polarized nature of these diatomics substantially alters their properties as ligands. Indeed, $N_2$ has comparatively lower-energy σ-donor orbitals and higher-energy π* orbitals than those of CO, which limits its binding ability.[8,9] In addition, the π* orbitals of $CN^-$ are too high in energy for

effective π-backdonation, and although $NO^+$ is a strong π-acid, it is a relatively weak π-donor ligand.[8,9]

It has long been recognized that the quintessential neutral, yet highly polarized, isoelectronic analog to CO is boron monofluoride (BF).[10–15] Diatomic BF has been predicted to bind even more favorably to transition metals owing to a decreased HOMO/LUMO gap (HOMO, highest occupied molecular orbital; LUMO, lowest unoccupied molecular orbital) relative to that of CO, leading to both more potent σ-donor and π-acceptor abilities.[16–19] However, this electronic feature also renders the free BF molecule far more reactive than CO. As such, BF is not a stable molecule at room temperature. It must be prepared under low pressure between 1800° to 2000°C, and it quickly oligomerizes upon cooling.[11,12,14] Whereas coordination to transition metals is often used as a strategy for the stabilization of highly reactive species, fluoroborylene complexes, in which BF serves as a terminal ligand, have remained long-sought synthetic targets that have eluded isolation.[14,20–24] Here, we report the preparation and X-ray crystal structure of a terminal fluoroborylene complex of iron that possesses sufficient kinetic stability for isolation at room temperature. In addition, the iron-based molecular platform presented here allows for the direct comparison of the structural and electronic consequences of BF coordination relative to those of the neutral isoelectronic diatomic molecules CO and $N_2$.

To prepare a terminal fluoroborylene complex amenable to isolation, we chose to construct the BF unit directly within the coordination sphere of a kinetically stabilizing metal center. Previously, Vidovic and Aldridge reported that two equivalents of the ruthenium-based nucleophile $Na[CpRu(CO)_2]$ (Cp, cyclopentadienyl; $[C_5H_5]^-$) reacts with boron trifluoride diethyl etherate ($BF_3{\cdot}Et_2O$) with the formal loss of two equivalents of sodium fluoride (NaF) to produce the bridging BF complex $(\mu_2\text{-BF})[CpRu(CO)_2]_2$.[20] The latter is the only crystallographically

characterized compound in which BF functions as a ligand to metal centers. We reasoned that a mononuclear terminal BF complex could be similarly obtained through salt elimination, if a sterically encumbered, dianionic metal-based nucleophile were used to prevent the addition of two metals to a single boron atom. Accordingly, the formally Fe(-II) species, $K_2[Fe(CO)_2(CNAr^{Tripp2})_2]$ ($K_2$[**1**]; ArTripp2 = 2,6-(2,4,6-(*i*-Pr)$_3C_6H_2$)$_2C_6H_3$; Scheme 3.1, Figure 3.1), was developed for this purpose because of the presence of two encumbering *meta*-terphenyl isocyanide ligands[25] and its overall isolobal relationship to Collman's reagent, the well-known dianionic, iron-based nucleophile $[Fe(CO)_4]^{2-}$.[26]

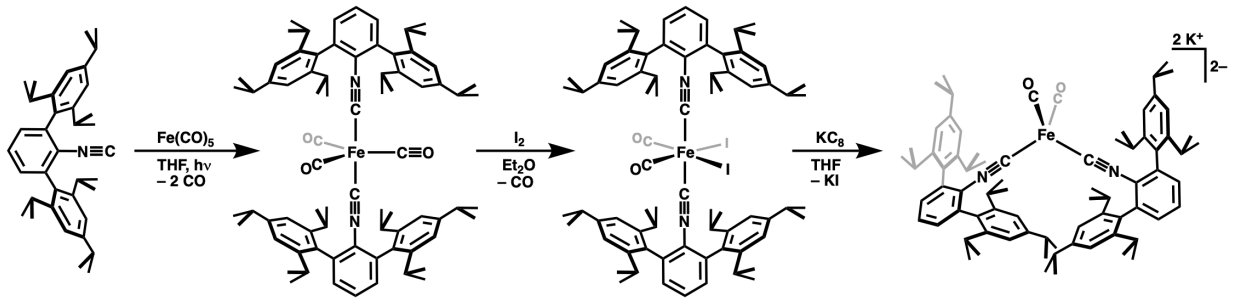


Scheme 3.1. Synthesis of $K_2[Fe(CO)_2(CNAr^{Tripp2})_2]$ ($K_2$[**1**]) and complexes $Fe(CO)_3(CNAr^{Tripp2})_2$ (**4**) and $FeI_2(CO)_2(CNAr^{Tripp2})_2$ (**5**) starting from $Fe(CO)_5$ and $CNAr^{Tripp2}$.

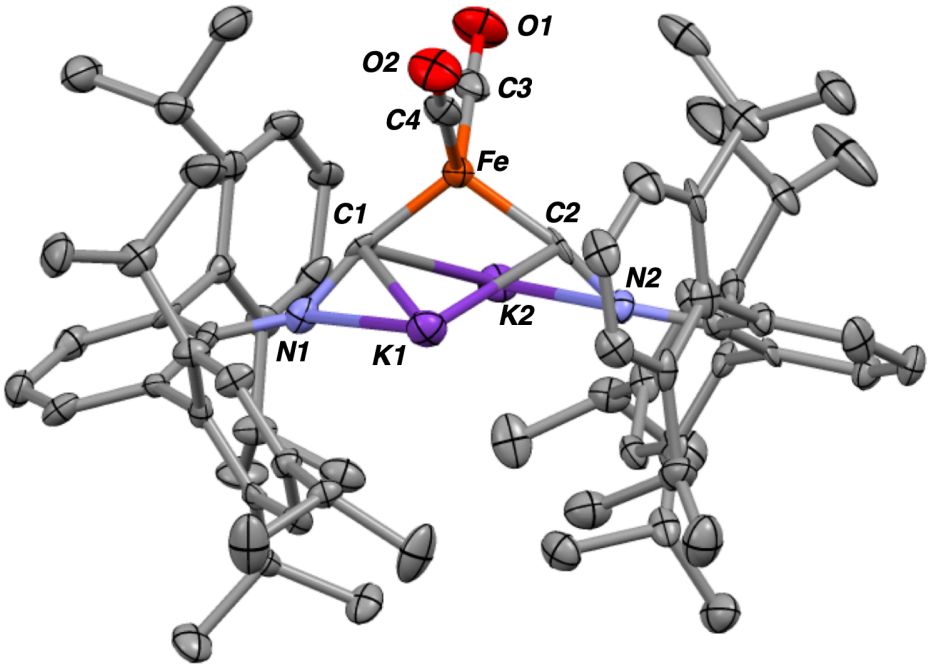


Figure 3.1. Solid-state structure of one of two molecules of $K_2[Fe(CO)_2(CNAr^{Tripp2})_2]$ ($K_2$[**1**]) in the asymmetric unit. One fully occupied and two 80% occupied molecules of co-crystallized toluene are omitted for clarity.

## 3.2 Synthesis and Characterization of a Terminal Fluoroborylene Complex

Treatment of $K_2$[**1**] with 1.0 equivalent of $BF_3 \cdot Et_2O$ in a cold diethyl ether/*n*-hexane mixture (9:1; –100°C), followed by the removal of salts and analysis by $^1$H nuclear magnetic resonance (NMR) spectroscopy, revealed the presence of unreacted $K_2$[**1**] and a new diamagnetic product. However, treatment of $K_2$[**1**] with 2.5 equivalents of $BF_3 \cdot Et_2O$ under the same conditions resulted in a distinct color change to yellow-brown from red, with $^1$H NMR spectroscopy indicating ~90% conversion to this new product. Crystallization of the reaction mixture from *n*-hexane produced yellow single crystals, which were determined by means of X-ray crystallography to be the five-coordinate complex $Fe(BF)(CO)_2(CNAr^{Tripp2})_2$ (**2**), featuring a terminally bound fluoroborylene ligand (Scheme 3.2, Figure 3.2).

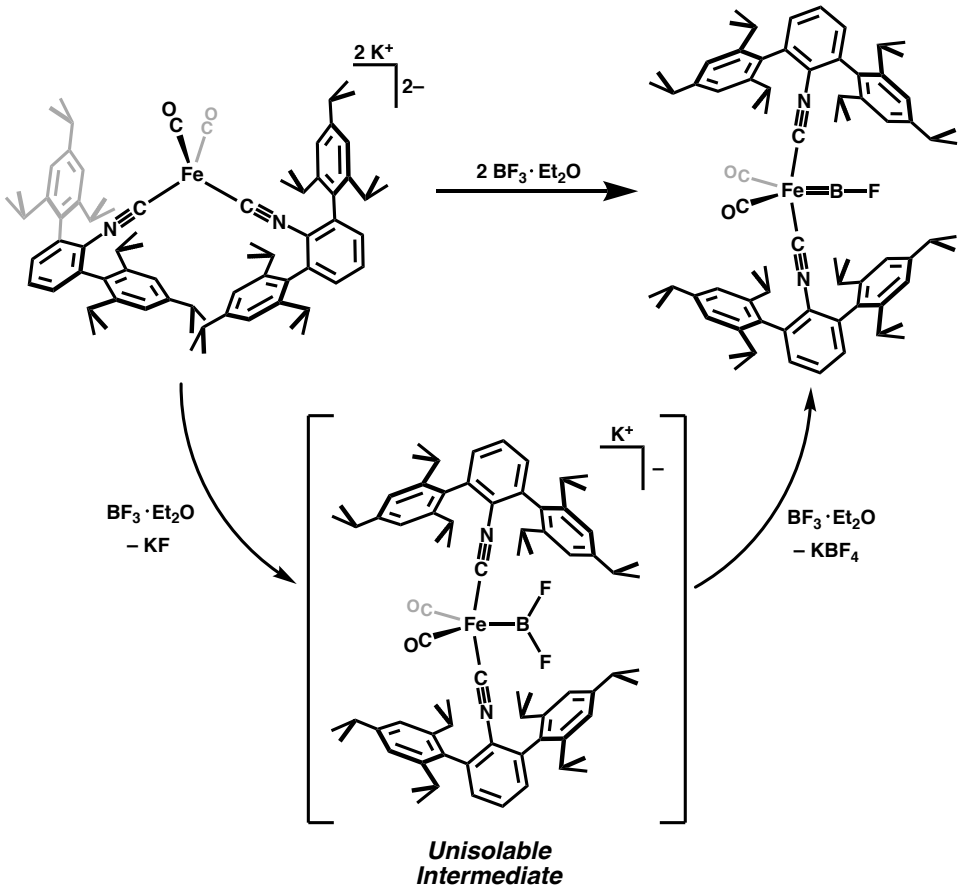


Scheme 3.2. Synthesis of $Fe(BF)(CO)_2(CNAr^{Tripp2})_2$ (**2**) via a proposed difluoroboryl intermediate.

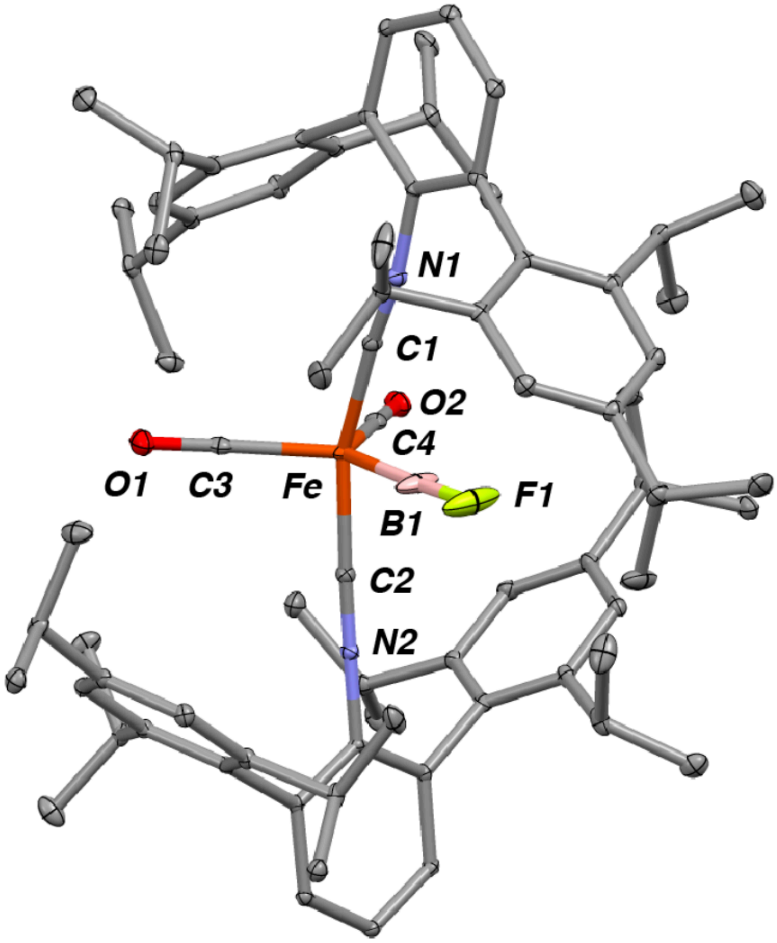


Figure 3.2. Solid-state structure of $Fe(BF)(CO)_2(CNAr^{Tripp2})_2$ (**2**).

Analysis by means of $^{19}F$ NMR spectroscopy of the salts produced from the reaction revealed tetrafluoroborate ($[BF_4]^-$) ion as a by-product (Figure 3.3–Figure 3.6), suggesting that a second equivalent of $BF_3$ promotes fluoride loss during the formation of **2**. A reasonable mechanism for the formation of **2** is one that proceeds through an unobserved iron difluoroboryl intermediate (Scheme 3.2), the formation or fragmentation of which through fluoride ion elimination is aided by a second equivalent of $BF_3$. Accordingly, this inference allowed the synthesis to be optimized by using 2.8 equivalents of $BF_3{\cdot}Et_2O$, which resulted in the complete

conversion to **2** and allowed for its isolation as a room-temperature stable, yellow crystalline material in 82% yield.

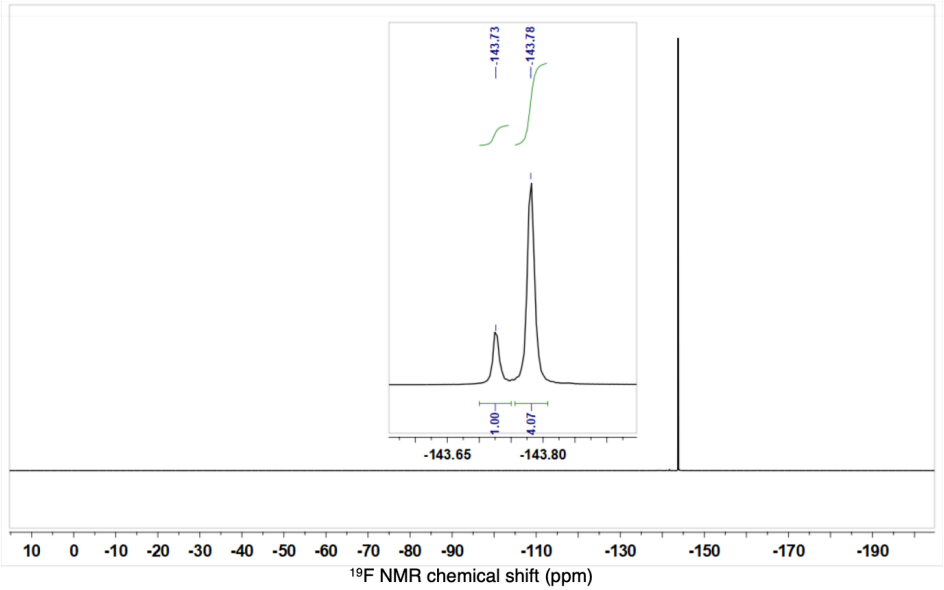


Figure 3.3. $^{19}$F NMR spectrum (470.6 MHz, 20 ˚C) of the KF and $KBF_4$ precipitate from the reaction producing $Fe(BF)(CO)_2(CNAr^{Tripp2})_2$ (**2**) dissolved in DMSO-$d_6$.

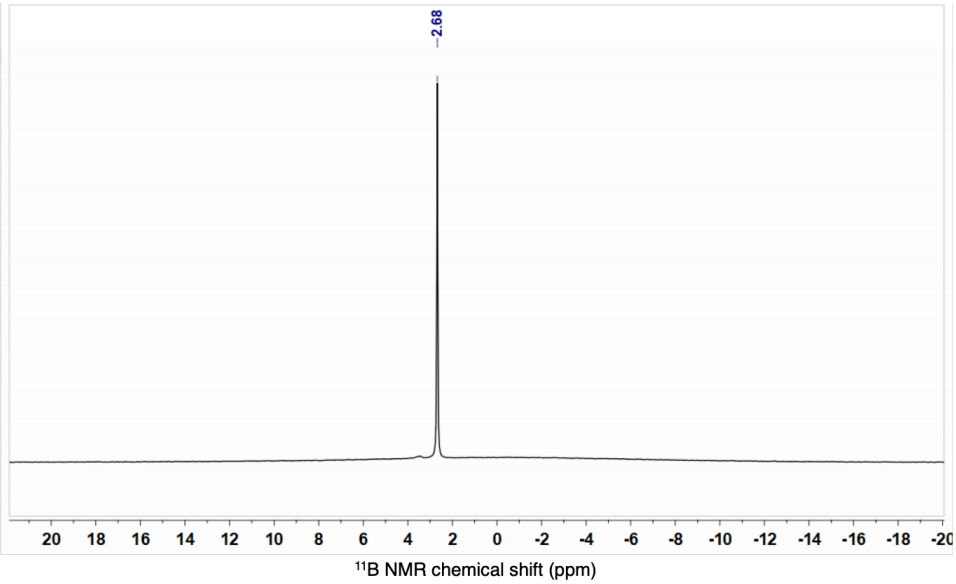


Figure 3.4. $^{11}$B NMR spectrum (160.5 MHz, 20 ˚C) of the KF and $KBF_4$ precipitate from the reaction producing $Fe(BF)(CO)_2(CNAr^{Tripp2})_2$ (**2**) dissolved in DMSO-$d_6$.

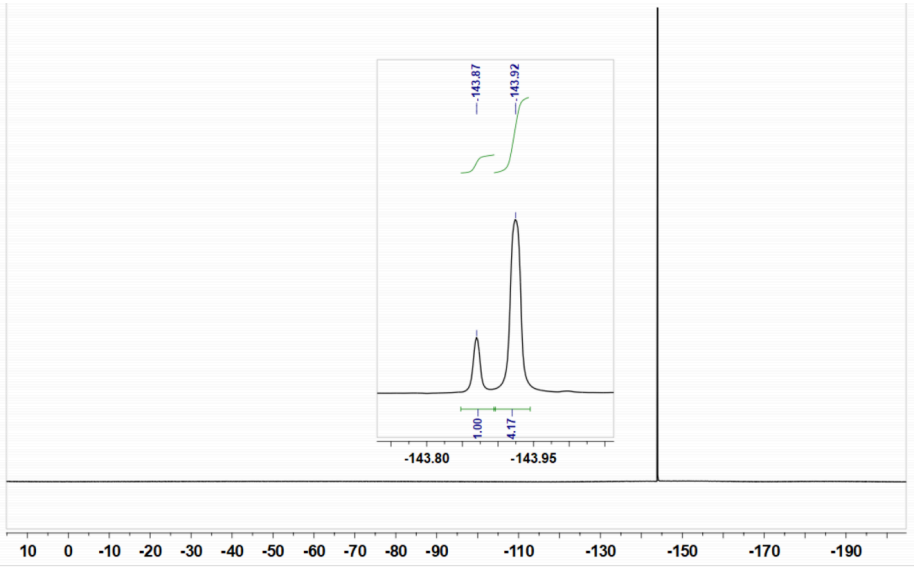


Figure 3.5. $^{19}F$ NMR spectrum (470.6 MHz, 20 ˚C) of a 1:1 molar mixture of NaF and $NaBF_4$ dissolved in DMSO-$d_6$. This control mixture gives rise to nearly identical spectroscopic signatures as the precipitate produced during the formation of $Fe(BF)(CO)_2(CNAr^{Tripp2})_2$ (**2**).

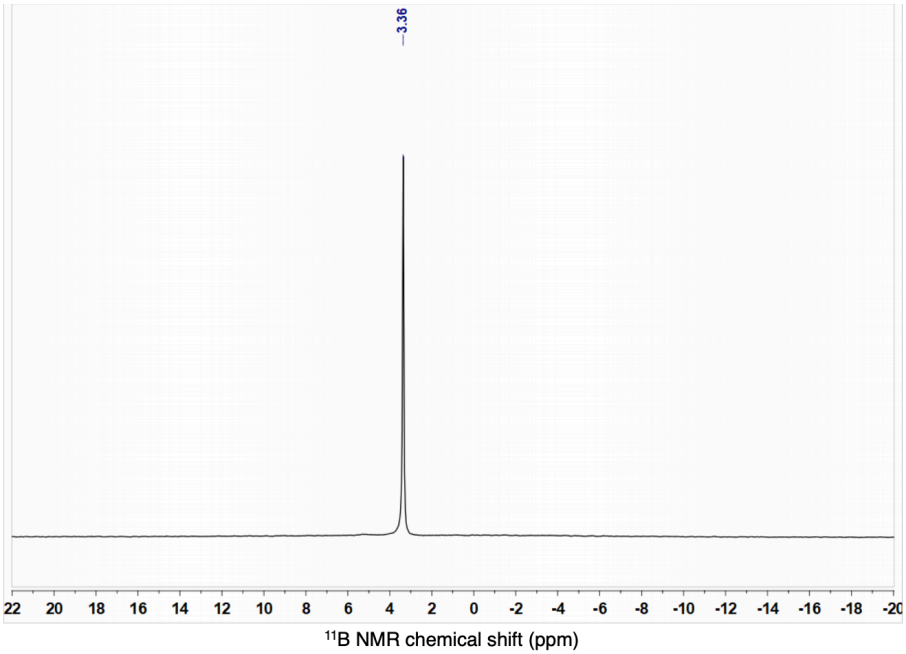


Figure 3.6. $^{11}B$ NMR spectrum (160.5 MHz, 20 ˚C) of a 1:1 molar mixture of NaF and $NaBF_4$ dissolved in DMSO-$d_6$. This control mixture gives rise to nearly identical spectroscopic signatures as the precipitate produced during the formation of $Fe(BF)(CO)_2(CNAr^{Tripp2})_2$ (**2**).

Complex **2** is an isolobal analog to the simple, yet hypothetical, molecular species $Fe(BF)(CO)_4$, which is the most well-considered theoretical and computational model of a fluoroborylene complex.[16–19] In line with this analogy, the axial ∠C1–Fe–C2 bond angle in **2** (160.38(7)˚ is in excellent agreement with the $\angle C_{ax}$–Fe–$C_{ax}$ (163.4˚; ax, axial) bond angle previously predicted for $Fe(BF)(CO)_4$, as are the equatorial $C_{eq}$–Fe–B angles (124.6˚(average) for **2** versus 123.4˚ for $Fe(BF)(CO)_4$; eq, equatorial).[17,19] This pronounced distortion from an ideal trigonal bipyramidal geometry likely results from the strong σ-donor properties of the BF ligand, which, owing to orbital mixing in $C_{2v}$ symmetry, imparts substantial antibonding character on an otherwise nonbonding orbital directed toward the axial isocyanide ligands.[17,19] In addition, the Fe–B bond distance in **2** (1.7703(25) Å) is the shortest reported for a transition metal–boron bond (Figure 3.22). Accordingly, this metrical parameter reflects substantial π-interactions between the BF unit and the iron center, which are in accord with the ligand's predicted strong π-acceptor properties.[17] However, the B–F bond distance in **2** (1.2769(29) Å) is the shortest known for any structurally characterized boron-fluorine compound (Figure 3.23 and Figure 3.24) and compares well with the equilibrium internuclear separation of free BF in the gas phase (1.262672(7) Å).[14]

The diamagnetism of **2** allows for an assessment of the BF unit with NMR spectroscopy. In benzene-$d_6$ solution, **2** gives rise to a broad $^{11}B$ NMR signal centered at $\delta_B$ = +56.5 parts per million (ppm) (full width at half maximum = 1820 Hz). This chemical shift is most similar to those of transition-metal aminoborylene complexes ($\delta_B$ = +60 to 90 ppm)[27] and is downfield of that for the formally platinum(II) oxoboryl complex *trans*-$Pt(BO)Br(PCy_3)_2$ (δB = +17 ppm) that features a B–O triple bond akin to the cyanide ion ([CN]– ).[28] This difference in chemical shift signifies that π-donation from fluorine to boron in **2** is substantially diminished relative to B–O π-bonding in the oxoboryl group and is reflective of the greater electronegativity of the fluorine atom in the

BF unit. Complex **2** also gives rise to a $^{19}F$ NMR resonance at $\delta_F = +1.6$ ppm, which is significantly downfield relative to that found in the dinuclear bridging BF complex $(\mu_2\text{-BF})[CpRu(CO)_2]_2$ ($\delta_F = -185.0$ ppm)[20] and $BF_3 \cdot Et_2O$ ($\delta_F = -153$ ppm). Rapid quadrupolar relaxation of the $I = 3/2$ $^{11}B$ nucleus prevented a determination of the $^1J_{BF}$ coupling constant in both the one-dimensional (1D) $^{11}B$ and $^{19}F$ NMR spectra of **2**. However, 2D $^{19}F$–$^{11}B$ heteronuclear multiple-quantum coherence (HMQC) NMR experiments (Figure 3.7)[29,30] showed maximum cross-peak signal intensity in the measurement optimized for $^1J_{BF} = 650$ Hz. This extremely large implied coupling constant is consistent with the very short B–F bond distance observed in the X-ray structure of complex **2**. It also indicates that a high degree of boron s-orbital character is a major component of the bonding within the B–F ligand.

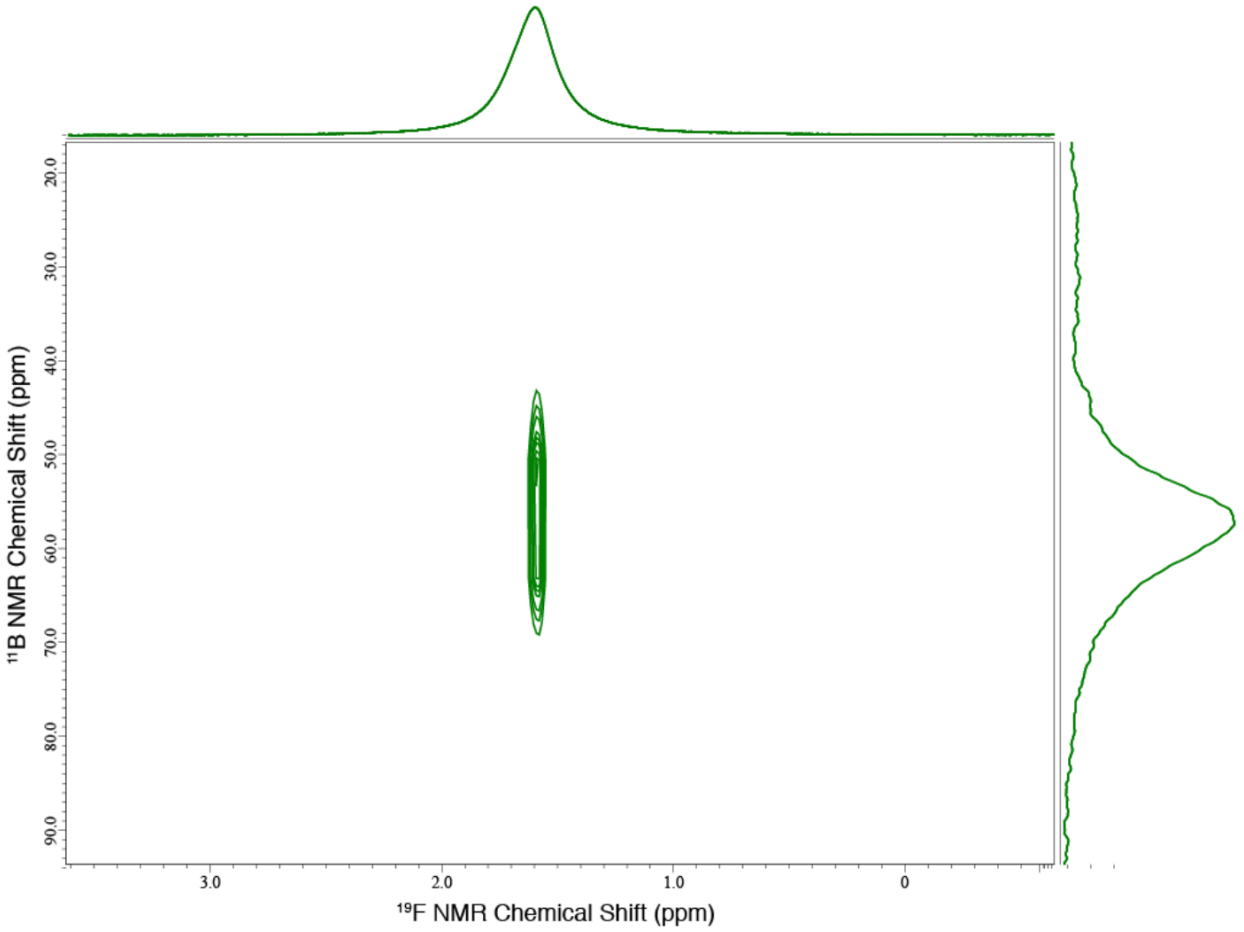


Figure 3.7. $^{19}$F–$^{11}$B HMQC spectrum ($C_6D_6$, 20 ˚C) of $Fe(BF)(CO)_2(CNAr^{Tripp2})_2$ (2) acquired using X-band decoupling and a BIRD pulse element with the experiment optimized for $^1J_{BF}$ = 650 Hz.

## 3.3 Comparing the Neutral, 10 Valence-Electron Diatomic Molecules of Period 2

To further evaluate the structural and electronic effects of terminal BF coordination, the isoelectronic $N_2$ and CO complexes $Fe(N_2)(CO)_2(CNAr^{Tripp2})_2$ (**3**) and $Fe(CO)_3(CNAr^{Tripp2})_2$ (**4**) were prepared and characterized by means of X-ray crystallography (Fig. 2A). Complexes **3** and **4** both adopt undistorted trigonal bipyramidal coordination geometries, as indicated by near-linear

axial isocyanide ∠C1–Fe–C2 angles (179.05(14)˚ for **3**; 178.61(22)˚ for **4**). These metrical parameters contrast with the significantly bent ∠C1–Fe–C2 angle of complex **2** and support the notion that both CO and $N_2$ are weaker σ-donors than the BF ligand.[17] Similarly, the infrared (IR) spectroscopic data of the complexes show a clear redshift of the asymmetric νCN stretch in the order **4** > **3** > **2** (Fig. 2A), further illustrating that the σ-donor ability of BF is greatest relative to CO and $N_2$. Accordingly, when coupled with the short Fe–B bond length in **2**, the structural and spectroscopic comparison provided by complexes **3** and **4** offers complementary support to the conclusion that BF possesses simultaneously strong σ-donor and π-acceptor characteristics.

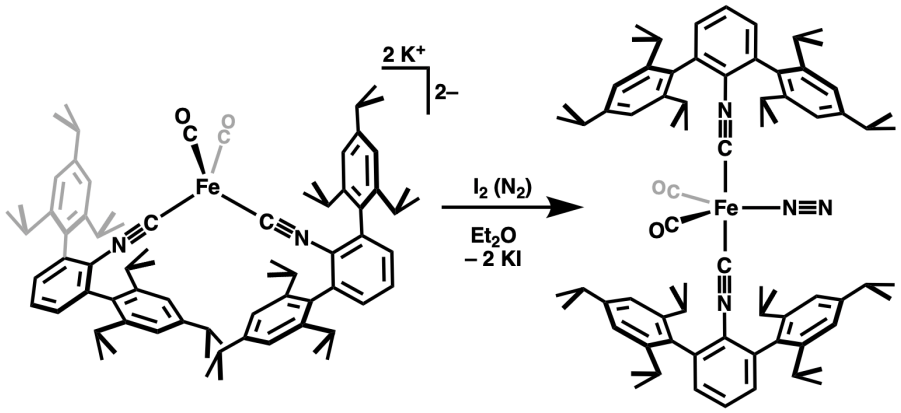


Scheme 3.3. Synthesis of $Fe(N_2)(CO)_2(CNAr^{Tripp2})_2$ (**3**) by two-electron oxidation of $K_2[Fe(CO)_2(CNAr^{Tripp2})_2$ ($K_2$[**1**]) with $I_2$.

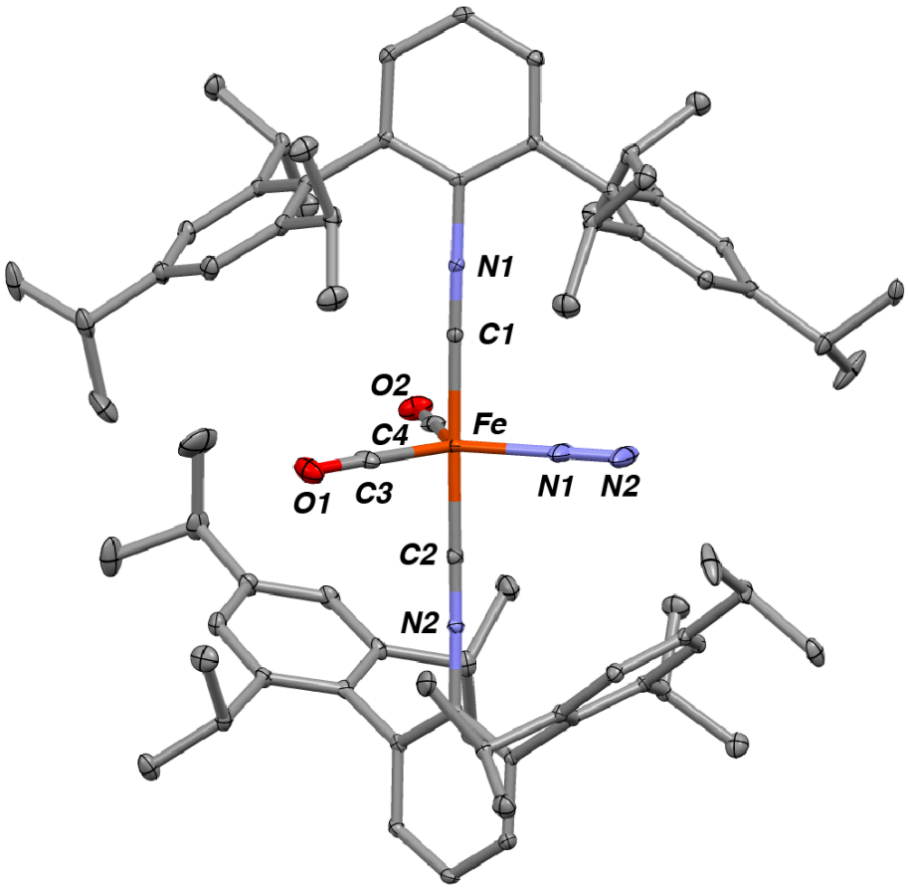


Figure 3.8. Solid-state structure of $Fe(N_2)(CO)_2(CNAr^{Tripp2})_2$ (**3**). Four molecules of co-crystallized benzene have been omitted.

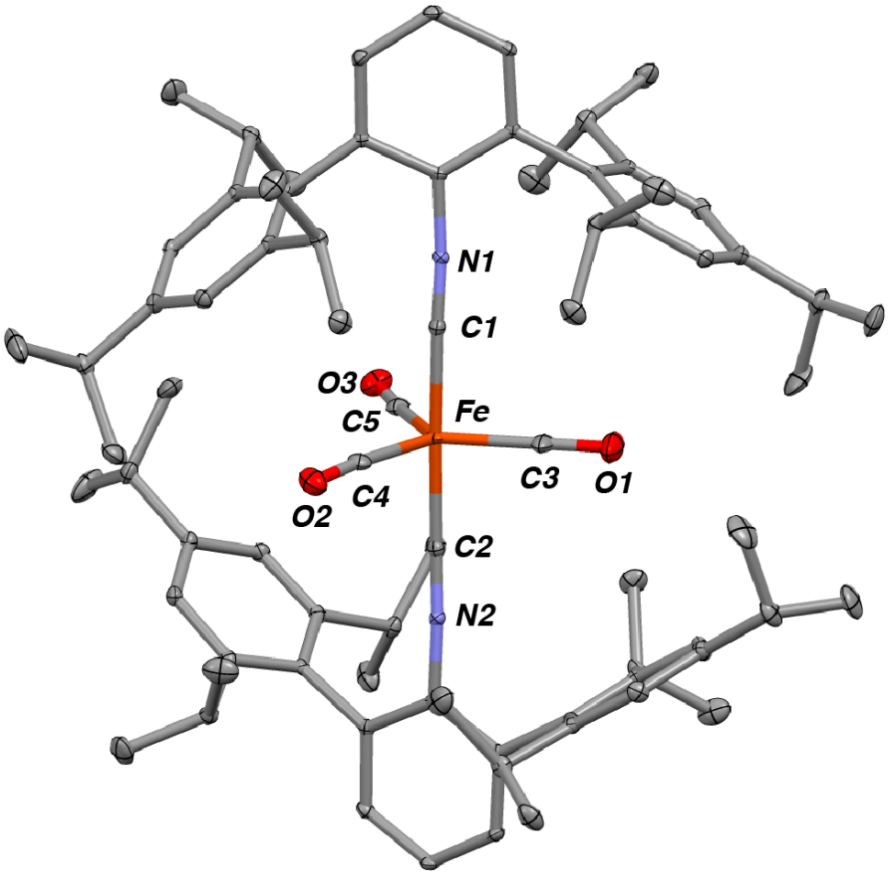


Figure 3.9. Solid-state structure of $Fe(CO)_3(CNAr^{Tripp2})_2$ (**4**). Three molecules of co-crystallized benzene have been omitted.

This distinct electronic character of the BF ligand is further confirmed by the Mössbauer spectroscopic data of **2**, **3**, and **4** (figs. S13 to S15). Of the series, complex **2** gives rise to the most negative isomer shift ($\delta$ = –0.15 $mms^{-1}$), followed by **4** then **3** ($\delta$ = –0.08 and +0.08 $mms^{-1}$ , respectively). This trend indicates that the total bonding interactions [31] to the iron center are greatest for complex **2** and diminish predictably as both the σ-donor and π-acceptor abilities of CO and $N_2$ weaken. Furthermore, the Mössbauer quadrupolar-splitting values ($\Delta E_Q$), which are sensitive to the iron structural environment,[31] are nearly identical for complexes **3** and **4** ($\Delta E_Q$ =

1.94 and 2.02 $mms^{-1}$, respectively), whereas that of **2** varies significantly ($\Delta E_Q$ = 1.27 $mms^{-1}$) in a manner consistent with the solid-state structural data for the series.

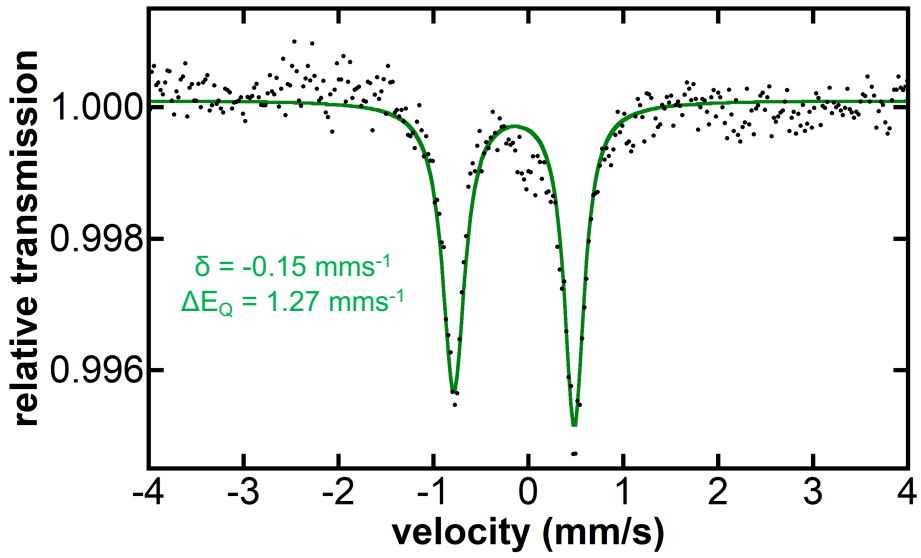


Figure 3.10. $^{57}$Fe Mössbauer spectrum of compound $Fe(BF)(CO)_2(CNAr^{Tripp2})_2$ (**2**).

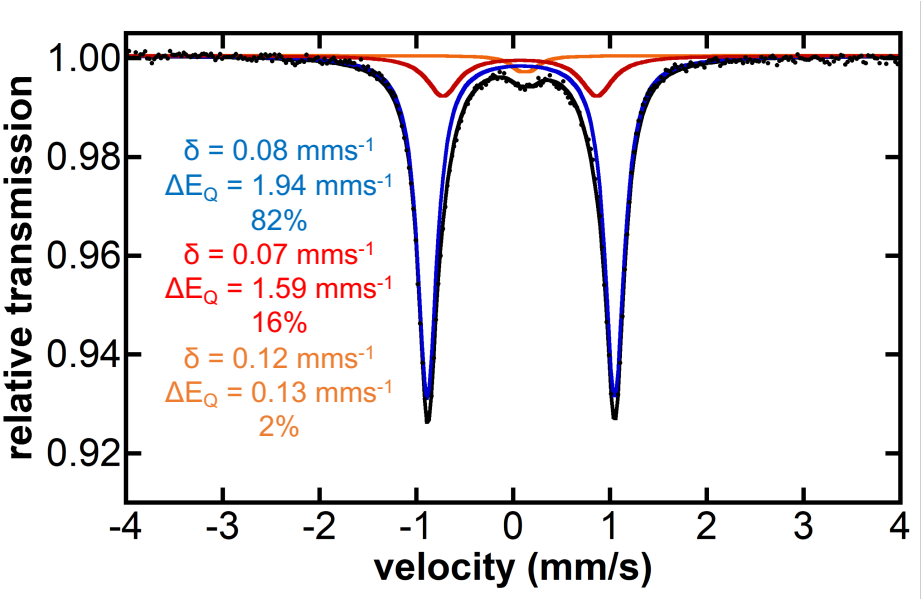


Figure 3.11. $^{57}$Fe Mössbauer spectrum of compound $Fe(N_2)(CO)_2(CNAr^{Tripp2})_2$ (**3**) (blue). The red trace has been tentatively assigned as $Fe(CO)_2(CNAr^{Tripp2})_2$ resulting from loss of $N_2$ during sample sealing. The orange trace represents an unknown iron containing impurity in 2% relative abundance.

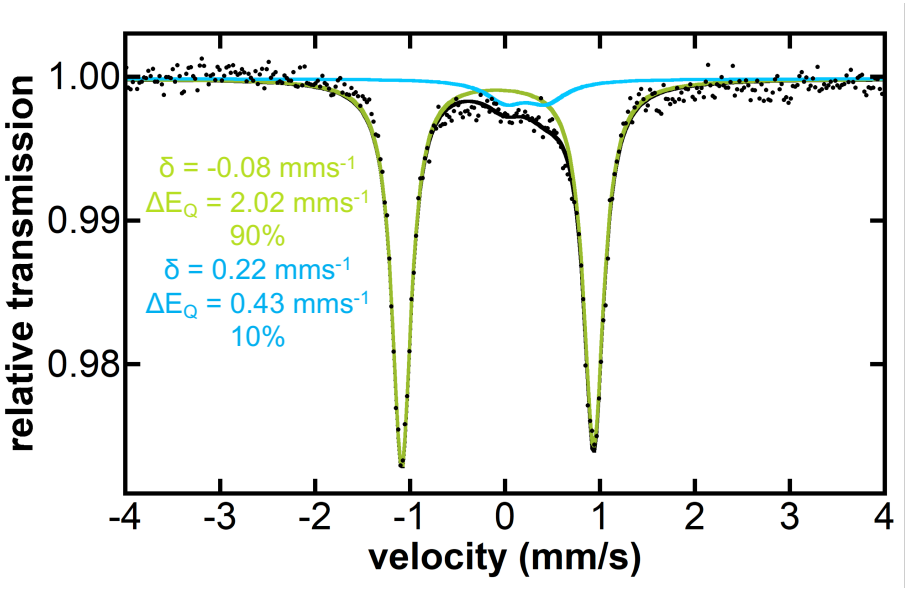


Figure 3.12. $^{57}$Fe Mössbauer spectrum of compound $Fe(CO)_3(CNAr^{Tripp2})_2$ (**4**) (chartreuse). The light blue trace represents an unknown iron containing impurity in 10% relative abundance.

With respect to the bonding interactions within the BF ligand, the IR spectrum of complex **2** shows a moderately intense band centered at 1407 $cm^{-1}$ assignable to the $\nu^{11}$BF stretch (Figure 3.13). Unfortunately, the IR stretch from the $^{10}$B isotopologue, expected at *ca.* 1451 $cm^{-1}$ by a reduced mass calculation, is masked by a band of moderate intensity at 1456 $cm^{-1}$ stemming from an aromatic C-C stretch of the *meta*-terphenyl ligands. The band of **2** is higher in energy than that of free BF ($\nu$BF = 1374 $cm^{-1}$)[32] and the matrix-produced terminal fluoroborylene complexes $Zr(BF)F_2$ and $Hf(BF)F_2$ ($\nu$BF = 1373 and 1378 $cm^{-1}$, respectively).[21] However, it agrees well with those calculated with density functional theory methods for $Fe(BF)(CO)_4$ ($\nu$BF = 1465 $cm^{-1}$)[19] and the model complex $Fe(BF)(CO)_2(CNAr^{Ph2})_2$ (**2m**, $\nu$BF = 1416 $cm^{-1}$; ArPh2 = 2,6-$(C_6H_5)_2C_6H_3$), as well as that for the titanium terminal fluoroborylene species $Ti(BF)F_2$ ($\nu$BF = 1404 $cm^{-1}$) observed under matrix conditions.[21] Accordingly, the low energy nature of these experimental and

calculated νBF bands provides strong indication that B–F multiple bonding is not significant in terminal fluoroborylene complexes.

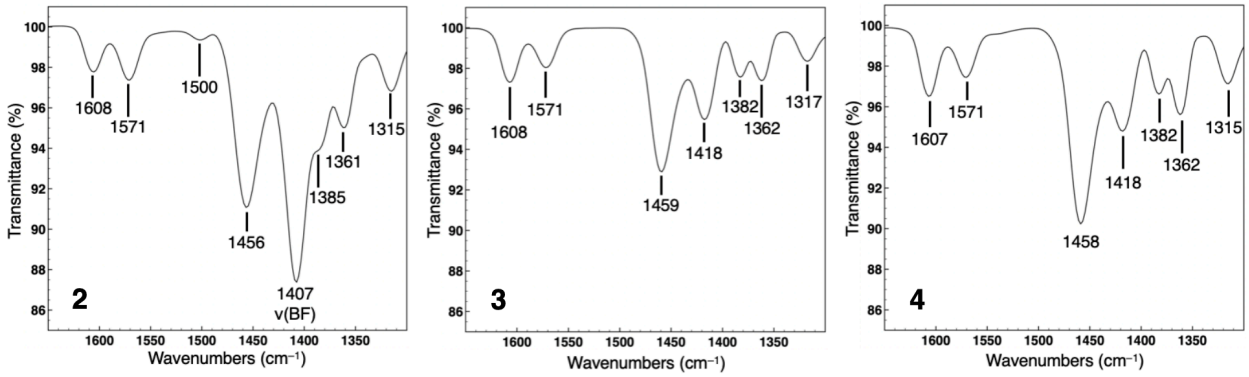


Figure 3.13. Room-temperature solid-state FTIR spectra of compounds $Fe(BF)(CO)_2(CNAr^{Tripp2})_2$ (**2**, left), $Fe(N_2)(CO)_2(CNAr^{Tripp2})_2$ (**3**, middle), and $Fe(CO)_3(CNAr^{Tripp2})_2$ (**4**, right) in the region 1650 – 1300 $cm^{-1}$. The band of moderate intensity at 1407 $cm^{-1}$ in the spectrum of **2** is attributed to the ν(B-F) stretch of the $^{11}B$ isotopomer. The ν(B-F) stretch of the $^{10}B$ isotopomer of **2**, calculated at *ca*. 1451 $cm^{-1}$ from a reduced mass calculation, is masked by a band of moderate intensity at 1456 $cm^{-1}$ . This band is assigned to a ν(C=C) stretch of the $CNAr^{Tripp2}$ ligand and is also present in the spectra of **3** (1459 $cm^{-1}$) and **4** (1458 $cm^{-1}$).

## 3.4 Electronic Structure Insights by Density Functional Theory (DFT) and Quantum Theory of Atoms in Molecules (QTAIM) Computational Methods

Density functional theory calculations on model **2m** support the electronic structure description of negligible B-F multiple bond character. Analysis of the molecular orbitals calculated for **2m** reveal that the ostensible π-bonding orbitals between the fluorine and boron atoms in the molecular y and z directions (fig. S21) are exceedingly low-lying (HOMO-63 and HOMO-64) and possess predominantly fluorine π-orbital character. As such, these components of the electronic structure of **2m** are best described as fluorine p-orbital lone pairs, rather than B–F π-bonding interactions, and indicate a nominal single bond between the boron and fluorine atoms. Natural

bond orbital (NBO) analysis also indicates the presence of a B-F single bond in **2m**, yielding a Wiberg bond index (WBI) of 0.8646.[33] Separately, the WBI of the Fe-B bond is nearly double that of the B–F bond, suggesting double bond character (Table 3.1).

Table 3.1. Natural Bond Orbital (NBO)-derived Wiberg Bond Indices (WBI) of selected bonds in $Fe(BF)(CO)_2(CNAr^{Ph2})_2$ (**2m**) at the B3LYP/6-31G(d,p) level of theory.

| Selected Bond | Wiberg Bond Index (WBI) |
|---|---|
| Fe-B | 1.4295 |
| Fe-C1 | 1.0993 |
| Fe-C3 | 1.2435 |
| B-F | 0.8646 |
| C1-N1 | 2.1127 |
| C3-O3 | 2.0508 |

Note: The WBI for the B-F bond of 0.8646 can be compared to the C1-N1 bond of the $CNAr^{Ph2}$ isocyanide ligand. This C1-N1 bond is reduced from a nominal bond order of 3.0 (i.e. WBI = 2.4 – 2.6 (34)) due to π-backdonation from the iron center. However, multiple bonding character in this bond is still present as indicated by a WBI of 2.1127. In comparison, the WBI for the BF bond indicates that only a single bond is present.

Electron density topology calculations[34] on **2m**, and the model complexes $Fe(N_2)(CO)_2(CNAr^{Ph2})_2$ (**3m**) and $Fe(CO)_3(CNAr^{Ph2})_2$ (**4m**), most clearly illustrate the electronic differences between coordinated BF, $N_2$, and CO ligands (Figure 3.14). A contour plot of the Laplacian of the electron density ($\nabla^2\rho$) for **2m** shows a significant depletion of electron density at the BF bond critical point, which is reflective of a highly polarized bonding interaction.[34] By contrast, the Laplacian contour plots for the $N_2$ and CO complexes **3m** and **4m** reveal far greater concentrations of electron density in the regions between N–N and C–O atoms, respectively, with **3m** displaying a highly symmetric electron-density distribution fully consistent with the presence of nonpolarized, multiple-bonding character.[34]

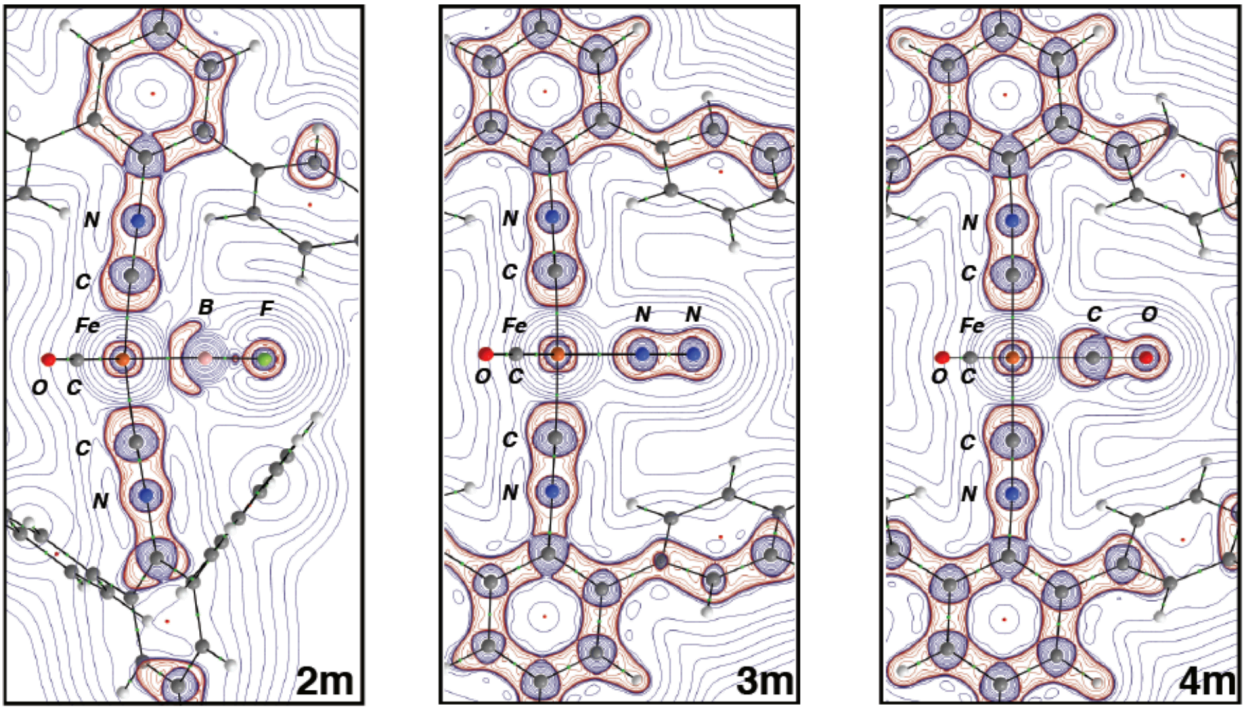


Figure 3.14. Plot of the Laplacian of charge density ($\nabla^2(\rho)$) for $Fe(BF)(CO)_2(CNAr^{Ph2})_2$ (**2m**, Left), $Fe(N_2)(CO)_2(CNAr^{Ph2})_2$ (**3m**, middle) and $Fe(CO)_3(CNAr^{Ph2})_2$ (**4m**, right). Areas of charge depletion are depicted with blue curves and areas of charge concentration are depicted with red curves. Bond and ring critical points are denoted by small green and red spheres, respectively.

Table 3.2 Topological analysis of electron density at selected bond critical points of **2m**, **4m**, and **3m**.

| Bond Critical Point | Rho (ρ) | Laplacian of Rho ($\nabla^2(\rho)$) | Ellipticity (ε) |
|---|---|---|---|
| B-F (**2m**) | 0.211040 | +1.527447 | 0.040162 |
| C5-O3 (**4m**) | 0.451280 | +0.904596 | 0.007718 |
| N3-N4 (**3m**) | 0.630285 | –1.991719 | 0.001504 |
| Fe-B (**2m**) | 0.141310 | +0.128643 | 0.153743 |
| Fe-C5 (**4m**) | 0.144650 | +0.575484 | 0.012004 |
| Fe-N3 (**3m**) | 0.107816 | +0.658798 | 0.063049 |

## 3.5 Concluding Remarks

In conclusion, although BF is isoelectronic to the 10-electron diatomics CO and $N_2$, it lacks multiple bonding character between the boron and fluorine atoms and therefore does not possess a similar electronic structure to these ligands when complexed to a transition metal. Moreover, the totality of spectroscopic and computational results suggest that the short B–F bond distance observed for complex **2** manifests simply from a high degree of sp-hybridization of the two-coordinate boron atom, in which the diminished radial extension of the boron 2s orbital relative to its 2p orbitals results in a short BF bond.[35] The molecular design principles and synthetic strategy presented here outline a possible blueprint for the formation and stabilization of terminal BF ligands on transition metals. Given the particular electronic characteristics of terminally coordinated BF, it is anticipated that this diatomic ligand can be exploited in a general fashion to modulate the physical and chemical properties of transition-metal complexes for specific applications.

## 3.6 Synthetic Procedures and Characterization Data

**General Considerations.** All manipulations were carried out under an atmosphere of purified dinitrogen using standard Schlenk and glovebox techniques. Unless otherwise stated, reagent-grade starting materials were purchased from commercial sources and either used as received or purified by standard procedures.[36] Solvents were dried and deoxygenated according to standard procedures.[37] Benzene-$d_6$ (Cambridge Isotope Laboratories) was distilled from NaK alloy/benzophenone and stored over activated 3 Å molecular sieves for 2 d prior to use. Celite 405 (Fischer Scientific) was dried under vacuum at a temperature above 250 ˚C for 24 h and stored in a glovebox prior to use. $CNAr^{Tripp2}$ was synthesized as previously reported.[25] The compounds

$Fe(CO)_3(CNAr^{Tripp2})_2$ and $FeI_2(CO)_2(CNAr^{Tripp2})_2$ were prepared through modified procedures for the syntheses of $Fe(CO)_3(CNAr^{Mes2})_2$ and $FeI_2(CO)_2(CNAr^{Mes2})_2$.[38]

Solution $^1H$, $^{13}C\{^1H\}$, $^{11}B$, and $^{19}F$ NMR spectra were recorded on a Varian 500 MHz spectrometer equipped with a 5mm X-Sens cold probe or a JEOL ECA 500 spectrometer equipped with a two-channel, broadband, inverse-detect 5 mm probe. $^1H$ and $^{13}C\{^1H\}$ chemical shifts are reported in ppm relative to $SiMe_4$ ($^1H$ and $^{13}C$ $\delta$ = 0.0 ppm) with reference to residual solvent resonances of 7.16 ppm ($^1H$) and 128.06 ppm ($^{13}C$) for $C_6D_6$.[39] $^{11}B$ NMR chemical shifts were referenced externally to $BF_3{\cdot}Et_2O$ ($\delta$ = 0.0 ppm). $^{19}F$ NMR chemical shifts were referenced externally to $C_6H_5F$ ($\delta$ = –113.11 ppm in $C_6D_6$).[40] Solid state FTIR spectra were recorded using a Bruker Alpha II Platinum ATR spectrometer in a nitrogen filled glovebox. Data were acquired on solid samples mounted on a diamond ATR module. The following abbreviations were used for the intensities and characteristics of important IR absorption bands: vs = very strong, s = strong, m = medium, w = weak, vw = very weak, sh = shoulder. Photolysis experiments were performed with a 254 nm model UVGL-25 Hg lamp (UVP, Inc., Upland, CA).

**Preparation of $Fe(CO)_3(CNAr^{Tripp2})_2$ (4).** To a 100 mL ampoule was added a THF solution of $CNAr^{Tripp2}$ (1.500 g, 2.954 mmol, 20 mL) followed by $Fe(CO)_5$ (0.2630 g, 1.343 mmol). The ampoule was sealed and irradiated (254 nm; Hg lamp) for 20 min, followed by a freeze-pump-thaw cycle (25 mTorr) to degas the headspace of the reaction mixture. This process was repeated 4 times, followed by continuous irradiation for 6 h, and two more freeze-pump-thaw-irradiation cycles, by which time IR spectroscopy revealed only one isocyanide stretching band. The reaction mixture was then concentrated to a solid *in vacuo*, and the resulting solid was then extracted with $Et_2O$ (15 mL), filtered, and evaporated to dryness to afford $Fe(CO)_3(CNAr^{Tripp2})_2$ as a yellow solid.

The material was purified by crystallization in *n*-pentane/benzene solutions at –35 ˚C over 2 d. Yield: 1.133 g, 0.980 mmol, 73%. $^{1}$H NMR (499.8 MHz, $C_6D_6$, 20 ˚C): d = 7.22 (s, 8H, *m*-Tripp), 7.02 (d, *J* = 7.5 Hz, 4H, *m*-Ph), 6.89 (t, *J* = 7.6 Hz, 2H, *p*-Ph), 2.96 (sept, *J* = 6.9 Hz, 4H, C*H*$(CH_3)_2$), 2.70 (sept, *J* = 6.9 Hz, 8H, C*H*$(CH_3)_2$), 1.41 (d, *J* = 7.0 Hz, 24H, CH(C*H*$_3)_2$), 1.32 (d, *J* = 6.9 Hz, 24H, CH(C*H*$_3)_2$), 1.14 (d, *J* = 6.9 Hz, 24H, CH(C*H*$_3)_2$) ppm. $^{13}$C{$^{1}$H} NMR (125.7 MHz, $C_6D_6$, 20 ˚C): δ = 212.3 (*C*O), 178.1 (*C*NR), 149.5, 146.4, 138.6, 132.4, 129.7, 129.6, 127.4, 121.4, 35.2, 31.4, 24.9, 24.4, 24.0 ppm. FTIR (solid state): ν(C≡N) = 2146 (vw), 2092 (vs) cm$^{-1}$, ν(C≡O) = 1940 (vs) cm$^{-1}$, also 3056 (vw), 2958 (s), 2930 (m), 2868 (m), 1607 (w), 1571 (vw), 1458 (m), 1418 (w), 1382 (w), 1362 (w), 1315 (w), 1254 (vw), 1243 (vw), 1171 (vw), 1102 (w), 1066 (vw), 943 (w), 876 (m), 849 (vw), 803 (m), 756 (m), 720 (vw), 646 (m), 603 (s), 554 (vw), 475 (w), and 434 (vw) cm$^{-1}$.

**Preparation of *cis*,*cis*,*trans*-$FeI_2(CO)_2(CNAr^{Tripp2})_2$ (5).** To a thawing $Et_2O$ solution of $Fe(CO)_3(CNAr^{Tripp2})_2$ (1.150 g, 0.9954 mmol, 10 mL) was added an equally cold $Et_2O$ solution of $I_2$ (0.253 g, 0.9954 mmol, 2 mL). The resulting solution was stirred to room temperature for 25 min, whereupon it was concentrated to 1/3 volume under reduced pressure. The slurry was then washed with cold 1:1 diethyl ether/*n*-pentane (4 × 3 mL) and filtered leaving a spectroscopically pure red/brown *cis*,*cis*,*trans*-$FeI_2(CO)_2(CNAr^{Tripp2})_2$ (1.020 g, 74%). X-ray diffraction quality crystals were grown from a saturated THF/*n*-hexane solution (1:5) overnight at –35 ˚C to yield as large red/brown crystals. *Note: Compound **2** isomerizes over time in solution and only crystallizes as the *trans*,*trans*,*trans* isomer. $^{1}$H NMR (499.8 MHz, $C_6D_6$, 20 ˚C): δ = 7.24 (s, 8H, *m*-Tripp), 7.00 (d, *J* = 7.7 Hz, 4H, *m*-Ph), 6.84 (t, *J* = 7.6 Hz, 2H, *p*-Ph), 2.94 (sept, *J* = 6.9 Hz, 4H, C*H*$(CH_3)_2$), 2.69 (sept, *J* = 6.9 Hz, 8H, C*H*$(CH_3)_2$), 1.48 (d, *J* = 6.9 Hz, 24H, CH(C*H*$_3)_2$), 1.40

(d, $J$ = 6.9 Hz, 24H, CH(C$H_3$)$_2$), 1.10 (d, $J$ = 6.8 Hz, 24H, CH(C$H_3$)$_2$) ppm. $^{13}$C{$^1$H} NMR (125.7 MHz, $C_6D_6$, 20 ˚C): δ = 211.7 (*C*O), 157.7 (*C*NR), 149.8, 146.3, 140.6, 132.0, 130.4, 129.0, 121.8, 35.1, 31.5, 25.1, 24.6, 24.3 ppm. FTIR (KBr windows, $C_6D_6$, 25 ˚C): ν(C≡N) = 2156 (vs) cm$^{-1}$, ν(C≡O) = 2057 (s), 2019 (s) cm$^{-1}$, also 3056 (vw), 2958 (s), 2930 (m), 2868 (m), 1608 (w), 1570 (vw), 1458 (m), 1418 (w), 1382 (w), 1362 (w), 1351 (w), 1315 (w), 1254 (vw), 1243 (vw), 1171 (vw), 1102 (w), 1066 (vw), 943 (w), 876 (m), 849 (vw), 803 (m), 756 (m), 720 (vw), 646 (m), 603 (vs), 554 (vw), 475 (w), and 434 (vw) cm$^{-1}$.

**Preparation of $K_2[Fe(CO)_2(CNAr^{Tripp2})_2]$ ($K_2$[1])**. A 20 mL scintillation vial was charged with $KC_8$ (0.185 g, 1.368 mmol) and placed in a liquid nitrogen cooled cold well. To this solid was added a thawing THF solution of *cis*,*cis*,*trans*-$FeI_2(CO)_2(CNAr^{Tripp2})_2$ (0.420 g, 0.304 mmol, 8 mL), and the resulting mixture was stirred with a glass stir bar for 40 minutes at –35 ˚C. The product mixture was filtered through Celite and evaporated to dryness. This deep red/brown solid was stirred in 3:1 *n*-pentane/diethyl ether and evaporated under reduced pressure twice to separate the desired product from solvated KI. The solid was washed 4 times with 2 mL of *n*-pentane to remove soluble byproducts. Pure $K_2[Fe(CO)_2(CNAr^{Tripp2})_2]$ was dissolved in $C_6H_6$, filtered through fiberglass filter paper, and lyophilized to a dark red, fluffy solid. Yield: 0.285 g, 0.237 mmol, 78%. Crystals suitable for diffraction were grown over 2 d from *n*-pentane/toluene. $^1$H NMR (499.8 MHz, $C_6D_6$, 20 ˚C): δ = 7.19 (s, 8H, *m*-Tripp), 6.95 (d, $J$ = 7.4 Hz, 4H, *m*-Ph), 6.83 (t, $J$ = 7.4 Hz, 2H, *p*-Ph), 3.06 (sept, $J$ = 6.9 Hz, 8H, C*H*(CH$_3$)$_2$), 2.91 (sept, $J$ = 6.9 Hz, 4H, C*H*(CH$_3$)$_2$), 1.40 (d, $J$ = 7.0 Hz, 24H, CH(C$H_3$)$_2$), 1.340 (d, $J$ = 6.9 Hz, 24H, CH(C$H_3$)$_2$), 1.15 (d, $J$ = 6.9 Hz, 24H, CH(C$H_3$)$_2$) ppm. $^{13}$C{$^1$H} NMR (125.7 MHz, $C_6D_6$, 20 ˚C): δ = 279.0 (*C*O), 231.9 (*C*NR), 148.6, 148.0, 138.9, 133.5, 129.7, 128.6, 120.5, 35.1, 31.5, 25.1, 24.6, 24.3 ppm.

FTIR (KBr windows, $C_6D_6$, 25 ˚C): ν(C≡N) = 1599 (vw), 1562 (s) $cm^{-1}$, ν(C≡O) = 1878 (w), 1793 (m) $cm^{-1}$, also 3056 (vw), 2961 (vs), 2927 (s), 2868 (s), 1458 (m), 1418 (w), 1382 (w), 1362 (w), 1351 (w), 1315 (w), 1254 (vw), 1243 (vw), 1171 (vw), 1102 (w), 1066 (vw), 943 (w), 876 (m), 849 (vw), 803 (m), 756 (m), 720 (vw), 646 (m), 603 (vs), 554 (vw), 475 (w), and 434 (vw) $cm^{-1}$.

**Preparation of Fe(BF)(CO)$_2$(CNAr$^{Tripp2}$)$_2$ (2)**. A thawing $Et_2O$/*n*-hexane (9:1) solution of $K_2[Fe(CO)_2(CNAr^{Tripp2})_2]$ (0.180 g, 0.149 mmol, 8 mL) was treated with an equally cold solution of $BF_3{\cdot}OEt_2$ in $Et_2O$ (0.0594 g, 0.418 mmol, 1 mL) in a liquid nitrogen cooled cold well. This solution was stirred at room temperature for 30 s, then re-chilled for 1 min, and this process was repeated five times before allowing the solution to stir at room temperature for 10 min, during which time, the solution changed from red to yellow/brown. All volatiles were removed *in vacuo*, and the resulting yellow solid was subjected to three cycles of stirring in *n*-pentane and evaporating solvent before being filtered through Celite to remove the KF and $KBF_4$ byproducts. The solid was re-dissolved in *n*-hexane with 2 drops of benzene and set at –35 ˚C overnight revealing pale yellow blocks suitable for X-ray diffraction. Yield: 0.141 g, 0.122 mmol, 82%. $^1$H NMR (499.8 MHz, $C_6D_6$, 20 ˚C): δ = 7.22 (s, 8H, *m*-Tripp), 7.00 (d, *J* = 7.5 Hz, 4H, *m*-Ph), 6.88 (t, *J* = 7.6 Hz, 2H, *p*-Ph), 2.96 (sept, *J* = 6.9 Hz, 4H, C*H*$(CH_3)_2$), 2.76 (sept, *J* = 6.9 Hz, 8H, C*H*$(CH_3)_2$), 1.41 (d, *J* = 6.9 Hz, 24H, CH(C*H*$_3)_2$), 1.31 (d, *J* = 6.9 Hz, 24H, CH(C*H*$_3)_2$), 1.16 (d, *J* = 6.8 Hz, 24H, CH(C*H*$_3)_2$) ppm. $^{13}$C{$^1$H} NMR (125.7 MHz, $C_6D_6$, 20 ˚C): δ = 213.7 (*C*O), 178.4 (*C*NR), 149.3, 146.6, 138.2, 133.0, 130.6, 129.7, 126.5, 121.3, 35.1, 31.3, 24.8, 24.4, 24.0 ppm. $^{11}$B NMR (160.4 MHz, $C_6D_6$, 20 ˚C): δ = 56.5 ppm (br s, fwhm = 1820 Hz). $^{19}$F NMR (470.4 MHz, $C_6D_6$, 20 ˚C): δ = 1.64 ppm (br s, fwhm = 187 Hz). $^{19}$F{$^{11}$B} NMR (470.4 MHz, $C_6D_6$, 20 ˚C): δ = 1.68 ppm (s, fwhm = 113 Hz). FTIR (solid state): ν(C≡N) = 2126 (sh), 2056 (s) $cm^{-1}$, ν(C≡O) = 1980 (s), 1942 (vs) $cm^{-1}$,

ν(B–F) = 1407 (s) $cm^{-1}$, also 3053 (vw), 2958 (s), 2930 (m), 2865 (m), 1608 (w), 1571 (w), 1500 (vw), 1456 (m), 1385 (sh), 1361 (w), 1315 (w), 1239 (vw), 1167 (vw), 1101 (w), 1068 (w), 943 (w), 876 (m), 845 (vw), 800 (m), 754 (m), 648 (s), 597 (vs), 479 (m), and 420 (vw) $cm^{-1}$.

**Preparation of $Fe(N_2)(CO)_2(CNAr^{Tripp2})_2$ (3)**. To a thawing $Et_2O$ solution of $K_2[Fe(CO)_2(CNAr^{Tripp2})_2]$ (0.150 g, 0.124 mmol, 6 mL) was added an equally cold $Et_2O$ solution of $I_2$ (0.030 g, 0.118 mmol, 2 mL). This mixture was stirred at –35 ˚C for 15 min, filtered through pre-cooled Celite into a vial in a liquid nitrogen cooled cold well, and evaporated to dryness under reduced pressure. The golden yellow solid was extracted with cold *n*-pentane and filtered once more to separate from residual KI. Crystals suitable for X-ray diffraction were grown from a concentrated *n*-pentane/benzene solution stored at –35 ˚C over 2 d. Yield: 0.122 g, 0.105 mmol, 85%. Workup and characterization of compound **5** must be performed quickly and at low temperature as partial decomposition becomes apparent within 10 minutes in solution at room temperature. $^1$H NMR (499.8 MHz, $C_6D_6$, 20 ˚C): δ = 7.22 (s, 8H, *m*-Tripp), 7.02 (d, *J* = 7.5 Hz, 4H, *m*-Ph), 6.89 (t, *J* = 7.4 Hz, 2H, *p*-Ph), 2.95 (sept, *J* = 6.8 Hz, 4H, C*H*$(CH_3)_2$), 2.73 (sept, *J* = 6.8 Hz, 8H, C*H*$(CH_3)_2$), 1.40 (d, *J* = 6.9 Hz, 24H, CH(C*H*$_3)_2$), 1.33 (d, *J* = 6.8 Hz, 24H, CH(C*H*$_3)_2$), 1.15 (d, *J* = 6.8 Hz, 24H, CH(C*H*$_3)_2$) ppm. $^{13}$C{$^1$H} NMR (125.7 MHz, $C_6D_6$, 20 ˚C): δ = 212.6 (*C*O), 181.0 (*C*NR), 149.4, 146.5, 138.3, 132.6, 129.7, 127.2, 121.4, 35.7, 31.4, 24.9, 24.4, 24.0 ppm. FTIR (solid state): ν(N≡N) = 2194 $cm^{-1}$, ν(C≡N) = 2122 (vw), 2075 (vs) $cm^{-1}$, ν(C≡O) = 1953 (m), 1918 (s) $cm^{-1}$, also 3055 (vw), 2958 (s), 2930 (m), 2869 (m), 1608 (w), 1571 (w), 1459 (m), 1418 (w), 1382 (vw) 1362 (vw), 1317 (vw), 1243 (vw), 1170 (vw), 1103 (w), 1064 (w), 942 (w), 875 (w), 847 (vw), 804 (w), 756 (w), 639 (w), 594 (s), 473 (w), and 420 (vw) $cm^{-1}$.

## 3.7 Nuclear Magnetic Resonance (NMR) Spectroscopic Measurements

**Experimental Details for One-Dimensional $^{19}F$ and $^{11}B$ NMR Spectra of $Fe(BF)(CO)_2(CNAr^{Tripp2})_2$ (2).** Samples were prepared by using ~40 mg of compound 2 dissolved in ~700 μL of benzene-$d_6$. Room temperature $^{19}F$ NMR data were acquired using both single pulse experiments and separately with $^{11}B$ decoupling (i.e. $^{19}F\{^{11}B\}$). The $^{19}F$ $\pi/2$ pulse time was measured as 9.4 μs and a 1 s pulse delay was used for all experiments. An exponential line broadening of 2.0 Hz was applied to both $^{19}F$ and $^{19}F\{^{11}B\}$ NMR spectra. Room temperature $^{11}B$ NMR data were acquired with a single-pulse experiment using a pulse delay of 1 s and a 30˚ pulse tip angle (the $^{11}B$ $\pi/2$ pulse time was measured to be 20.4 μs). An exponential line broadening of 50.0 Hz was applied to the $^{11}B$ NMR spectrum. $^{11}B$-detected, $^{19}F$-decoupled NMR experiments were acquired, but the single $^{11}B$ transition observed for **2** did not show a notable linewidth change under $^{19}F$ decoupling from that observed in the single-pulse experiment. $T_1$ measurements were performed at room temperature on samples using an inversion-recovery pulse sequence and using JEOL's native processing algorithms. $T_1$ values were found to be 0.10(1) s and 0.20(1) ms on **2** for $^{19}F$ and $^{11}B$, respectively. Variable temperature NMR experiments were performed in toluene-$d_8$ over the range of –60 to +80 ˚C but did not result in any significant changes in chemical shift or linewidth as compared to the $^{19}F$ or $^{11}B$ NMR transitions of **2** observed at room temperature. The inability to directly observe $^1J_{BF}$ coupling constants in one-dimensional spectra is a longstanding challenge in NMR spectroscopic studies of boron-fluoride compounds and is attributed to rapid quadrupolar relaxation of the I = 3/2 $^{11}B$ nucleus.[41–44] One-dimensional $^1H$, $^{13}C\{^1H\}$, $^{19}F$, $^{19}F\{^{11}B\}$ and $^{11}B$ NMR spectra for **2** are shown in Figs. S6-S9.

**Experimental Details for Two-Dimensional $^{19}F–^{11}B$ NMR Spectra of $Fe(BF)(CO)_2(CNAr^{Tripp2})_2$ (2).** Two-dimensional $^{19}F–^{11}B$ HMQC spectra were collected with 1024 points in $t_2$ and 64 $t_1$ increments.[29,30] Each $t_1$ increment represents a total of 128 scans. Owing to the fact that the magnitude of the $^{11}B–^{19}F$ coupling constant of **2** could not be directly measured, several data sets incrementally optimized for various $^1J_{BF}$ values were acquired, with the highest signal-to-noise found in the experiment optimized for a $^1J_{BF}$ of 650 Hz (Fig. S10). The absolute value HMQC experiments were acquired using X-band decoupling, a BIRD pulse element,[45] and without pulsed field gradients. The data were processed by using phase-shifted sine bell multiplication followed by exponential line broadening (5 Hz and 100 Hz for $^{19}F$ and $^{11}B$, respectively) on the time domain data. The data were then zero-filled in both $t_2$ and $t_1$ to yield a final 2048×256 real matrix.

**Experimental Details for NMR Analysis of the Salt Byproducts Produced During the Synthesis of $Fe(BF)(CO)_2(CNAr^{Tripp2})_2$ (2).** Separately, the salt byproducts from the reaction generating **2** were analyzed. The reaction vial, pipet, and filter were thoroughly washed with *n*-pentane (8 x 1.5 mL) leaving behind a white precipitate. This precipitate was brought outside the glovebox and dissolved in DMSO-$d_6$. $^{19}F$ NMR spectroscopy of this precipitate revealed two sharp singlets located at 143.73 ppm and 143.78 in a 1:4 ratio (Fig. S11), respectively, while analysis by $^{11}B$ NMR spectroscopy revealed a singlet centered at –2.68 ppm (Fig. S12). These spectroscopic signatures are indicative of the tetrafluoroborate ($[BF_4]^–$) ion, with the 1:4 resonances in the $^{19}F$ spectrum corresponding to the $^{10}B$ and $^{11}B$ isotopomers, respectively. These $^{19}F$ and $^{11}B$ spectra were compared to those of a 1:1 mixture of NaF and $NaBF_4$ in DMSO-$d_6$ (Figs. S13-S14), which were identical in character. The resonance for fluoride ($[F]^–$) ion as its potassium salt ($[K]^+$) are

not observed in either $^{19}F$ spectrum due to the low solubility of both KF and NaF in DMSO-$d_6$ and known difficulty of observing the $^{19}F$ NMR signal of fluoride ion in wet solvent.[46,47]

## 3.8 Results of $^{57}Fe$ Mössbauer Spectroscopic Studies

**Experimental Details.** All solid samples for $^{57}Fe$ Mössbauer spectroscopy were run on non-enriched samples of isolated complexes. All samples were prepared in Delrin Mössbauer sample cups in a nitrogen-filled glovebox equipped with a liquid nitrogen fill port to enable sample freezing to 77 K within the glovebox. Samples were fitted with a fitted inner Delrin cup prior to freezing. Low temperature $^{57}Fe$ Mössbauer measurements were performed using a See Co. MS4 Mössbauer spectrometer integrated with a Janis SVT400T He/$N_2$ cryostat for measurements at 80 K. Isomer shifts were determined relative to α-Fe at 298 K. All Mössbauer spectra were fit using the program WMoss (SeeCo). All Mössbauer spectra display the raw data (black dots) and where applicable, the total fit (black line) and individual components represented by colored doublets. Errors of the fit analyses are $\delta \pm 0.02$ mm/s and $\Delta E_Q \pm 3\%$. For multicomponent fits, the quantitation errors of individual components were ±3%.

Special preparative measures were taken for temperature sensitive samples. The solid samples were rapidly transferred from a liquid $N_2$ storage dewar to a dog bowl dewar inside of a glovebox. Samples were subsequently ground in a mortar chilled to cryogenic temperatures and transferred to a prechilled Delrin sample cup where they were sealed and submerged in liquid $N_2$ for data collection.

## 3.9 Results of Computational Studies

**Computational Details.** Density Functional Theory (DFT) calculations were carried out on the truncated model complexes $Fe(BF)(CO)_2(CNAr^{Ph2})_2$ (**2m**), $Fe(N_2)(CO)_2(CNAr^{Ph2})_2$ (**3m**) and $Fe(CO)_3(CNAr^{Ph2})_2$ (**4m**) (ArPh2 = 2,6-$(C_6H_5)_2C_6H_3$) using the ORCA computational suite 4.0.0.[48] Geometry optimizations and infrared frequency calculations were performed using the BP86 functional,[49–52] along with the all-electron Ahlrichs triple-zeta basis sets def2-TZVP (standard)[53] and def2-TZVP/J (auxiliary).[54] The resolution of identity (RI) approximation[55] and tight SCF criteria were employed. Input geometries for **2m**, **4m**, and **3m** were based on the crystallographically determined atomic coordinates of compounds **2**, **4**, and **3**, respectively. Visualization of optimized structures and rendering of molecular orbitals was performed using the program Chemcraft.[56] The absolute, isotropic shielding for the $^{11}B$ and $^{19}F$ nuclei in **2m** were calculated using the "NMR" keyword in ORCA employing B3LYP/def2TZVPP. The $^1J_{BF}$ coupling constant was calculated with the Gaussian package[57] using the input nmr=(giao,spinspin) B3LYP/6-31G(d,p).[49,58,59] Wiberg bond indices were determined using NBO 3.1[60] also using the B3LYP functional and 6-31G(d,p) basis set. QTAIM measurements were performed with AIMAll[61] employing the Proaim integration approach with .wfn files generated in Gaussian (B3LYP/6-31G(d,p)).

**Input for Geometry Optimization of $Fe(BF)(CO)_2(CNAr^{Ph2})_2$ (2m)**. The input for the optimization of **2m** is listed below. Inputs for **4m** and **3m** optimizations are identical except for the input coordinates.

```
#UKS OPT of  FeL4BF
%pal nprocs 8 end
! UKS Opt freq BP86 RIJCOSX def2-TZVP def2/J VerySlowConv TightSCF
%basis
end
%output
```

```
Print[ P_Basis ] 2
Print[ P_MOs ] 1
end

* xyz 0 1
  Fe     0.291838    0.113220   -0.030551
  N      1.111582   -0.129003    2.855742
  C      0.765286   -0.029643    1.721206
  C     -0.491557    1.726679    0.144747
  C      1.487846   -0.293984    4.166106
  C      1.532382    0.835986    5.027500
  C      1.912322    0.633752    6.362251
  H      1.959178    1.499019    7.024992
  C      2.260068   -0.630096    6.835163
  H      2.562482   -0.760555    7.874942
  C      2.222675   -1.726607    5.975695
  H      2.477618   -2.720971    6.344407
  C      1.830044   -1.591998    4.636164
  N      0.487894    0.234585   -3.032994
  C      0.403508    0.196197   -1.848408
  C     -0.910980   -1.226773   -0.021795
  C      0.598837    0.274555   -4.401957
  C      1.726028   -0.326234   -5.025720
  C      1.830006   -0.248768   -6.421908
  H      2.690079   -0.714165   -6.905333
  C      0.845610    0.372253   -7.188387
  H      0.942657    0.413429   -8.274441
  C     -0.265810    0.936193   -6.564313
  H     -1.034537    1.432687   -7.158301
  C     -0.413158    0.912627   -5.169888
  B      2.060362   -0.164637   -0.118234
  F      3.344980   -0.328904   -0.113928
  O     -0.958008    2.782410    0.259769
  O     -1.661067   -2.112229   -0.020831
  C      1.197132    2.208783    4.569753
  C      1.814695    2.787535    3.447059
  C      0.276356    2.981423    5.300233
  C      1.519173    4.097781    3.068447
  C     -0.023180    4.289655    4.916650
  C      0.597673    4.852605    3.798941
  H      2.545491    2.213866    2.876269
  H     -0.223228    2.540663    6.164950
  H      2.010182    4.529613    2.195379
  H     -0.750020    4.867935    5.489696
```

| | | | |
|---|---|---|---|
| H | 0.361914 | 5.873509 | 3.495899 |
| C | 1.788019 | -2.798665 | 3.769910 |
| C | 2.905926 | -3.649729 | 3.706305 |
| C | 0.635338 | -3.151401 | 3.046561 |
| C | 2.873573 | -4.816522 | 2.940720 |
| C | 0.601602 | -4.320775 | 2.285595 |
| C | 1.720356 | -5.156576 | 2.228315 |
| H | 3.812981 | -3.381511 | 4.251055 |
| H | -0.250091 | -2.516695 | 3.096248 |
| H | 3.754518 | -5.459669 | 2.897998 |
| H | -0.304746 | -4.576714 | 1.735588 |
| H | 1.692724 | -6.070102 | 1.632303 |
| C | 2.780115 | -1.040848 | -4.260283 |
| C | 4.134218 | -0.719093 | -4.463057 |
| C | 2.465388 | -2.088179 | -3.375914 |
| C | 5.143297 | -1.420208 | -3.800604 |
| C | 3.475675 | -2.793973 | -2.720782 |
| C | 4.817438 | -2.462091 | -2.928707 |
| H | 4.392442 | 0.101086 | -5.136042 |
| H | 1.423056 | -2.367575 | -3.218385 |
| H | 6.187500 | -1.148255 | -3.964047 |
| H | 3.211041 | -3.609163 | -2.045662 |
| H | 5.604872 | -3.012680 | -2.412376 |
| C | -1.611225 | 1.542129 | -4.556713 |
| C | -1.504853 | 2.507952 | -3.541567 |
| C | -2.892210 | 1.204192 | -5.029164 |
| C | -2.645125 | 3.116509 | -3.015804 |
| C | -4.032598 | 1.809263 | -4.499005 |
| C | -3.912533 | 2.768333 | -3.490395 |
| H | -0.521227 | 2.797975 | -3.171699 |
| H | -2.991635 | 0.442959 | -5.805723 |
| H | -2.539904 | 3.862261 | -2.226865 |
| H | -5.017888 | 1.524468 | -4.871141 |
| H | -4.802752 | 3.240466 | -3.072742 |

*

**Optimized coordinates for $Fe(BF)(CO)_2(CNAr^{Ph2})_2$ (2m).**

| | | | |
|---|---|---|---|
| Fe | 0.291876 | 0.113977 | -0.030556 |
| N | 1.111516 | -0.128454 | 2.855759 |
| C | 0.765249 | -0.029069 | 1.721207 |
| C | -0.490062 | 1.728219 | 0.144569 |
| C | 1.487950 | -0.293712 | 4.166118 |
| C | 1.531925 | 0.835994 | 5.027845 |

| | | | |
|---|---|---|---|
| C | 1.912530 | 0.633649 | 6.362360 |
| H | 1.958944 | 1.498734 | 7.025385 |
| C | 2.261504 | -0.630127 | 6.834744 |
| H | 2.564510 | -0.760715 | 7.874335 |
| C | 2.224520 | -1.726372 | 5.974918 |
| H | 2.480374 | -2.720680 | 6.343178 |
| C | 1.831177 | -1.591602 | 4.635590 |
| N | 0.488027 | 0.234528 | -3.033080 |
| C | 0.403733 | 0.196409 | -1.848469 |
| C | -0.911978 | -1.225121 | -0.021320 |
| C | 0.598925 | 0.274121 | -4.402135 |
| C | 1.725501 | -0.327835 | -5.025795 |
| C | 1.829203 | -0.251282 | -6.422057 |
| H | 2.688777 | -0.717665 | -6.905437 |
| C | 0.845125 | 0.370174 | -7.188686 |
| H | 0.941924 | 0.410693 | -8.274790 |
| C | -0.265649 | 0.935385 | -6.564583 |
| H | -1.034128 | 1.432201 | -7.158640 |
| C | -0.412701 | 0.912568 | -5.170086 |
| B | 2.060179 | -0.165508 | -0.118111 |
| F | 3.344584 | -0.331089 | -0.113873 |
| O | -0.955533 | 2.784431 | 0.259214 |
| O | -1.662641 | -2.110099 | -0.020320 |
| C | 1.195440 | 2.208696 | 4.570623 |
| C | 1.812190 | 2.788459 | 3.448036 |
| C | 0.274108 | 2.980266 | 5.301585 |
| C | 1.515465 | 4.098612 | 3.070011 |
| C | -0.026677 | 4.288389 | 4.918620 |
| C | 0.593474 | 4.852377 | 3.801002 |
| H | 2.543216 | 2.215618 | 2.876677 |
| H | -0.224887 | 2.538690 | 6.166240 |
| H | 2.005914 | 4.531202 | 2.196998 |
| H | -0.753944 | 4.865761 | 5.492048 |
| H | 0.356774 | 5.873206 | 3.498430 |
| C | 1.789474 | -2.798021 | 3.768919 |
| C | 2.908048 | -3.648255 | 3.704645 |
| C | 0.636799 | -3.151587 | 3.046066 |
| C | 2.876308 | -4.814943 | 2.938882 |
| C | 0.603631 | -4.320896 | 2.284931 |
| C | 1.722998 | -5.155829 | 2.226954 |
| H | 3.815147 | -3.379452 | 4.249046 |
| H | -0.249143 | -2.517610 | 3.096128 |
| H | 3.757805 | -5.457306 | 2.895636 |
| H | -0.302827 | -4.577452 | 1.735380 |

| | | | |
|---|---|---|---|
| H | 1.695740 | -6.069303 | 1.630838 |
| C | 2.779302 | -1.042739 | -4.260213 |
| C | 4.133567 | -0.721873 | -4.463329 |
| C | 2.464189 | -2.089347 | -3.375130 |
| C | 5.142386 | -1.423153 | -3.800649 |
| C | 3.474180 | -2.795326 | -2.719728 |
| C | 4.816120 | -2.464363 | -2.928069 |
| H | 4.392178 | 0.097765 | -5.136846 |
| H | 1.421723 | -2.368054 | -3.217149 |
| H | 6.186708 | -1.151859 | -3.964469 |
| H | 3.209137 | -3.609929 | -2.044047 |
| H | 5.603337 | -3.015078 | -2.411533 |
| C | -1.610215 | 1.543235 | -4.556961 |
| C | -1.503133 | 2.509659 | -3.542509 |
| C | -2.891548 | 1.205686 | -5.028834 |
| C | -2.642959 | 3.119192 | -3.016848 |
| C | -4.031498 | 1.811688 | -4.498812 |
| C | -3.910693 | 2.771399 | -3.490850 |
| H | -0.519296 | 2.799425 | -3.172964 |
| H | -2.991613 | 0.444012 | -5.804893 |
| H | -2.537057 | 3.865425 | -2.228446 |
| H | -5.017027 | 1.527119 | -4.870506 |
| H | -4.800557 | 3.244303 | -3.073300 |

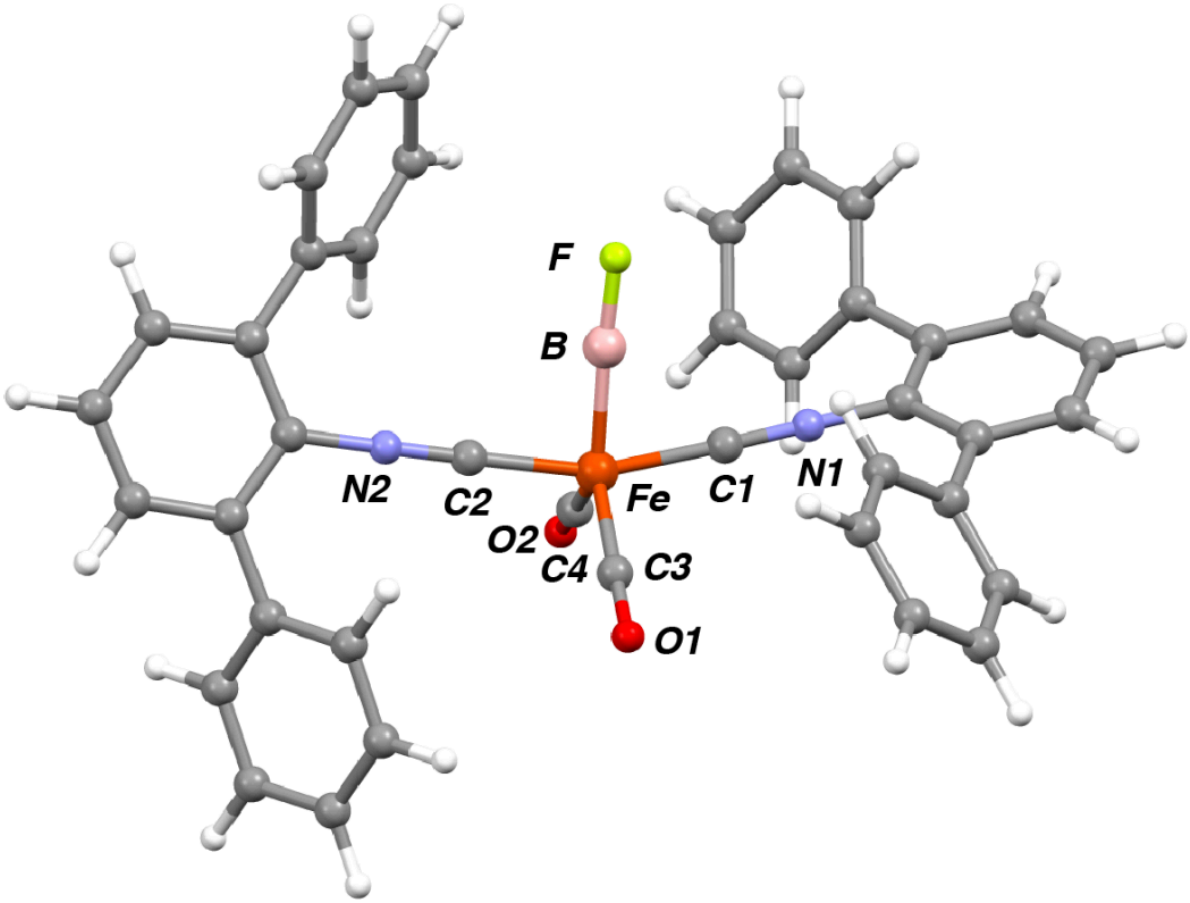


Figure 3.15. Geometry optimized structure of $Fe(BF)(CO)_2(CNAr^{Ph2})_2$ (**2m**) (BP86/def2TZVP/J).

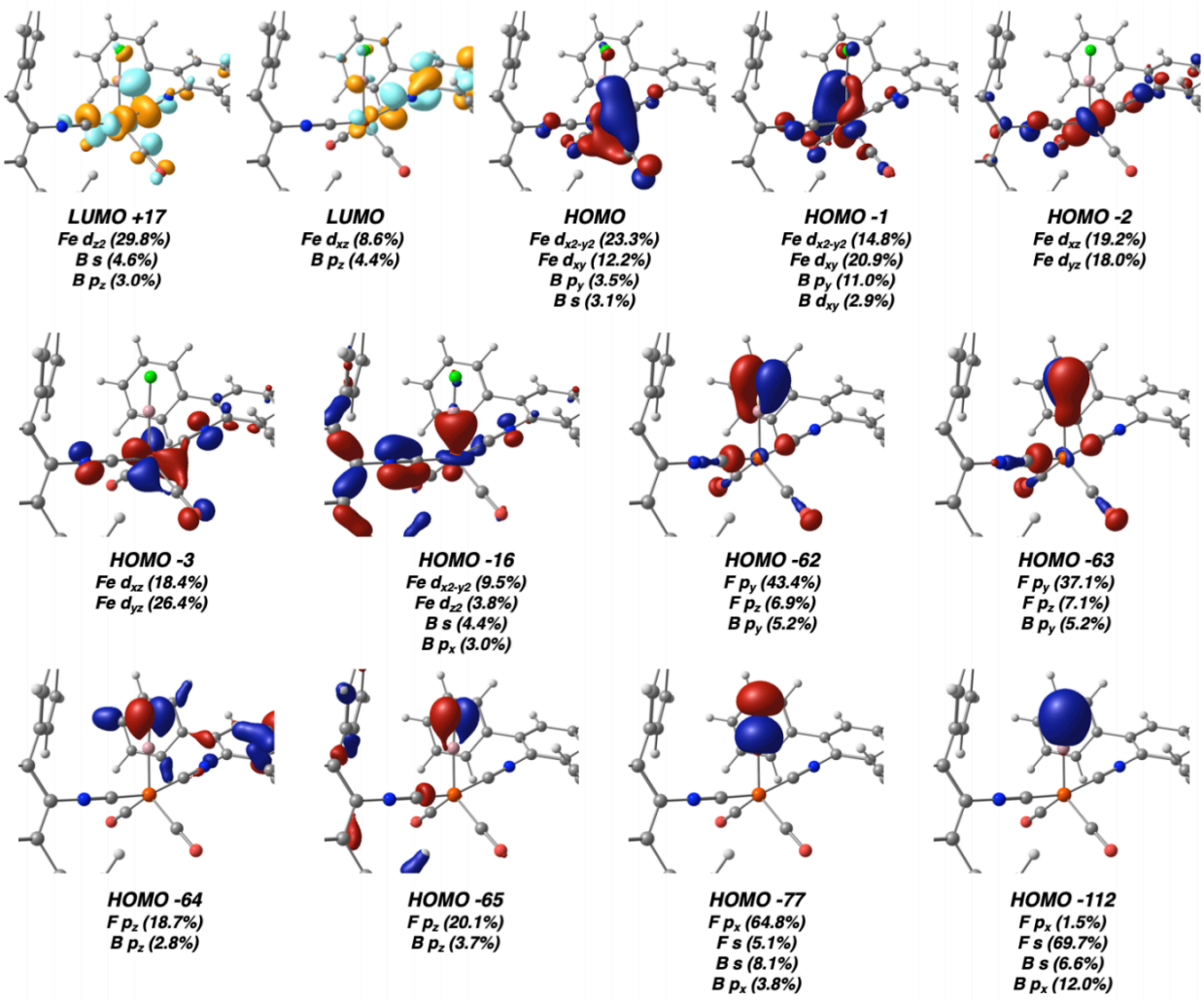


Figure 3.16. Selected molecular orbitals (MOs) of $Fe(BF)(CO)_2(CNAr^{Ph2})_2$ (**2m**) with predominantly iron d-orbital character in addition to MOs primarily involving boron and fluorine. Atomic orbital contributions (AO%) to the molecular orbitals are listed. The HOMO and HOMO-1 are indicative of significant Fe-B π-bonding. HOMO-62 through HOMO-65 represent MOs with ostensible π-bonding character between the boron and fluorine atoms. The atomic orbital contribution to these MOs reveal substantial electronic localization on the fluorine atom, with little contribution from boron in the molecular z- and y-axis directions. These features are indicative of fluorine lone pair character, with little B-F π-bonding character.

Table 3.3. Comparison of structural parameters calculated and experimentally determined for compounds **2m** and **2**, respectively.

| Parameter | Calculated | Experimental | % Difference |
|---|---|---|---|
| d(Fe-B) (Å) | 1.79239 | 1.7703(25) | 1.24% |
| d(B-F) (Å) | 1.29504 | 1.2769(29) | 1.41% |
| d(Fe-C1) (Å) | 1.82022 | 1.8243(16) | 0.22% |
| ∠(C1-Fe-C2) (˚) | 161.296 | 160.38(7) | 0.57% |
| ∠(C3-Fe-C4) (˚) | 112.057 | 110.74(8) | 1.18% |
| ∠(Fe-B-F) (˚) | 176.594 | 177.39(24) | 0.45% |

Table 3.4 Comparison of spectroscopic parameters calculated and experimentally determined for compounds **4m** and **4**, respectively.

| Parameter | Calculated | Experimental | % Difference |
|---|---|---|---|
| ν(C≡N) ($cm^{-1}$) | 2121.80 | 2126 | 0.20% |
| ν(C≡N) ($cm^{-1}$) | 2062.69 | 2056 | 0.32% |
| ν(C≡O) ($cm^{-1}$) | 1978.37 | 1980 | 0.08% |
| ν(C≡O) ($cm^{-1}$) | 1953.92 | 1942 | 0.61% |
| ν(B–F) ($cm^{-1}$) | 1415.73 | 1407 | 0.62% |

Table 3.5. Experimental and calculated $^{19}F$ and $^{11}B$ chemical shifts and coupling constant for **2**/**2m**. (B3LYP/6-31G(d,p))

| Parameter | δ $^{19}$**F** | δ $^{11}$**B** | $^{1}J_{B-F}$ |
|---|---|---|---|
| Experimental | 1.6 ppm | 56.5 ppm | Not observable |
| Calculated | –32.8 ppm | 55.9 ppm | –444.5 Hz |

**Optimized coordinates for $Fe(CO)_3(CNAr^{Ph2})_2$ (4m).**

| | | | |
|---|---|---|---|
| N | -0.008316 | 0.032676 | 3.021703 |
| C | -5.032546 | 0.949328 | 2.918683 |
| C | -1.340967 | 0.273791 | 5.022131 |
| C | -0.084834 | 0.049152 | 4.396886 |
| C | 0.014577 | 0.027185 | 1.838287 |
| C | -2.596246 | 0.497427 | 4.259178 |
| C | -3.735935 | -0.271660 | 4.557075 |
| C | -2.700247 | 1.497679 | 3.277822 |
| C | -3.908253 | 1.721848 | 2.615406 |
| H | -3.966314 | 2.503659 | 1.856829 |
| C | -4.942501 | -0.049414 | 3.891464 |
| H | -5.812802 | -0.662725 | 4.130999 |
| C | -1.385002 | 0.279391 | 6.424129 |
| H | -2.343583 | 0.461640 | 6.911842 |
| C | -0.234747 | 0.091865 | 7.188210 |
| H | -0.293488 | 0.110182 | 8.277637 |
| C | -0.888746 | 1.543201 | -0.040460 |
| O | -1.474764 | 2.544988 | -0.079286 |
| Fe | 0.026053 | -0.000019 | 0.000264 |
| C | 4.969401 | -0.995803 | 3.490251 |
| C | 1.094025 | -0.162217 | 5.160280 |
| C | 2.417146 | -0.434164 | 4.541438 |
| C | 3.536102 | 0.328176 | 4.921858 |
| C | 2.600288 | -1.483827 | 3.624526 |
| C | 3.865938 | -1.762538 | 3.107291 |
| H | 3.989580 | -2.583298 | 2.399233 |
| C | 4.800361 | 0.052145 | 4.398389 |
| H | 5.654361 | 0.661673 | 4.698128 |
| C | 0.989815 | -0.121905 | 6.558354 |
| H | 1.889726 | -0.292194 | 7.150932 |
| N | -0.014719 | -0.029653 | -3.021147 |
| C | -5.027948 | -1.005510 | -2.913379 |
| C | -1.346621 | -0.286311 | -5.020214 |
| C | -0.092554 | -0.046941 | -4.396254 |
| C | 0.010803 | -0.026237 | -1.837779 |
| C | -2.598408 | -0.524864 | -4.256038 |
| C | -3.747196 | 0.231159 | -4.552418 |
| C | -2.689896 | -1.526780 | -3.275183 |
| C | -3.894553 | -1.765231 | -2.611698 |
| H | -3.942872 | -2.548097 | -1.853535 |
| C | -4.950422 | -0.005291 | -3.885700 |
| H | -5.827946 | 0.598099 | -4.123983 |

| | | | |
|---|---|---|---|
| C | -1.392171 | -0.291688 | -6.422175 |
| H | -2.349037 | -0.485131 | -6.908929 |
| C | -0.245108 | -0.089891 | -7.187433 |
| H | -0.304840 | -0.108295 | -8.276802 |
| C | -0.875730 | -1.550810 | 0.043172 |
| O | -1.452884 | -2.557670 | 0.083511 |
| C | 4.949324 | 1.060332 | -3.494784 |
| C | 1.082807 | 0.179280 | -5.160845 |
| C | 2.403157 | 0.467321 | -4.543382 |
| C | 3.531485 | -0.279396 | -4.927066 |
| C | 2.573819 | 1.517319 | -3.624462 |
| C | 3.836434 | 1.811611 | -3.108520 |
| H | 3.950270 | 2.632421 | -2.398867 |
| C | 4.792768 | 0.012201 | -4.404919 |
| H | 5.654243 | -0.585441 | -4.707112 |
| C | 0.977471 | 0.138431 | -6.558824 |
| H | 1.874539 | 0.320068 | -7.152338 |
| H | -3.665037 | -1.062371 | 5.306636 |
| H | -5.974493 | 1.124365 | 2.396907 |
| H | -1.836608 | 2.120781 | 3.043992 |
| H | 1.750342 | -2.100529 | 3.330463 |
| H | 3.405419 | 1.156046 | 5.621769 |
| H | 5.955993 | -1.211925 | 3.078388 |
| H | 3.410614 | -1.107470 | -5.628495 |
| H | 5.933592 | 1.288570 | -3.083923 |
| H | 1.716260 | 2.122186 | -3.327910 |
| H | -1.818869 | -2.140053 | -3.042765 |
| H | -3.686153 | 1.022911 | -5.301750 |
| H | -5.967258 | -1.191640 | -2.390702 |
| C | 1.827045 | 0.006588 | -0.001889 |
| O | 2.986092 | 0.010433 | -0.003441 |

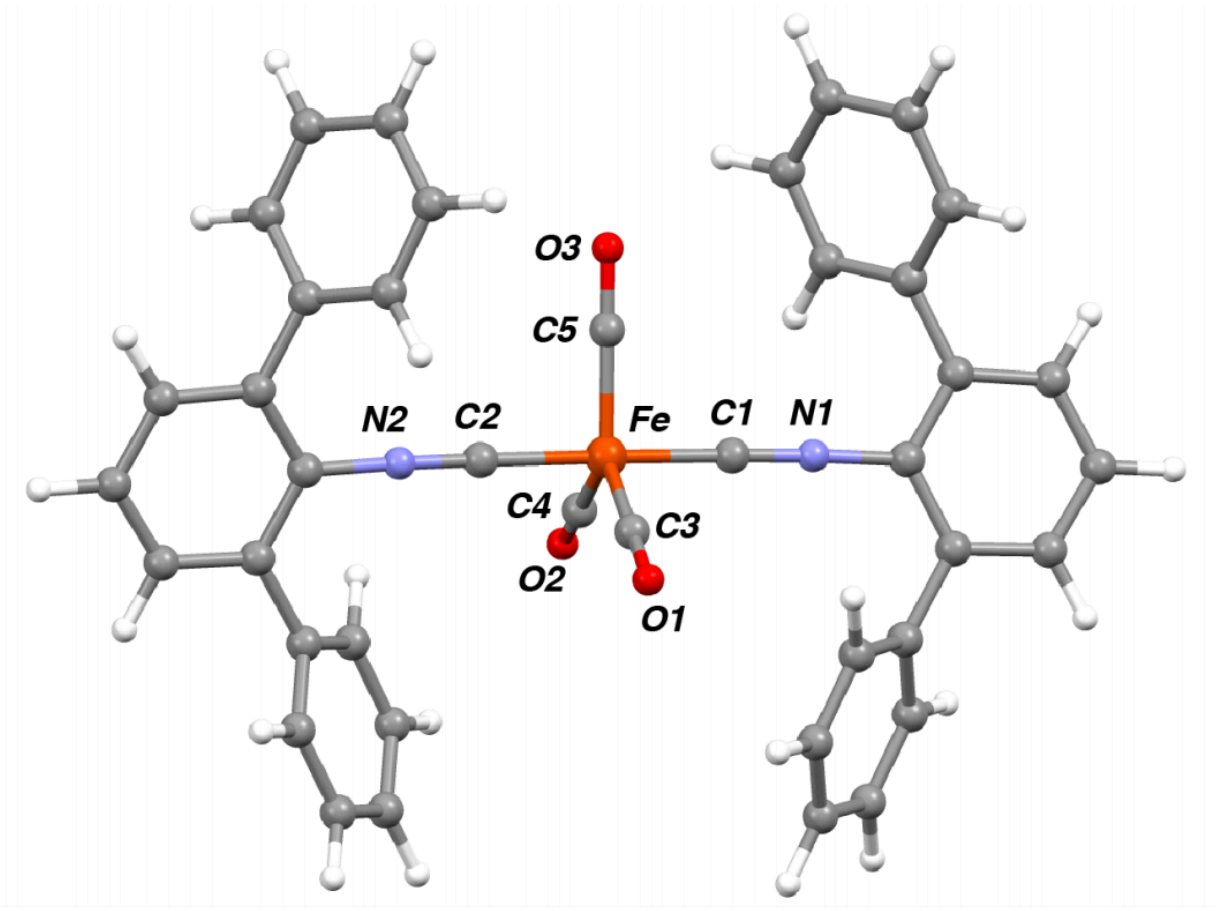


Figure 3.17. Geometry optimized structure of $Fe(CO)_3(CNAr^{Ph2})_2$ (**4m**) (BP86/def2TZVP/J).

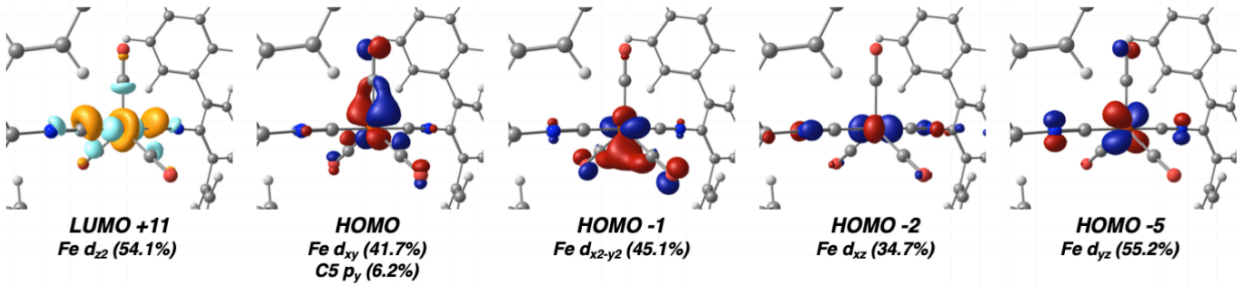


Figure 3.18. Selected molecular orbitals (MOs) of $Fe(CO)_3(CNAr^{Ph2})_2$ (**4m**) with predominantly iron d-orbital character. Atomic orbital contributions (AO%) to the molecular orbitals are listed.

Table 3.6. Comparison of structural parameters calculated and experimentally determined for compounds **4m** and **4**, respectively.

| Parameter | Calculated | Experimental | % Difference |
|---|---|---|---|
| d(Fe-C5) (Å) | 1.80101 | 1.7822(34) | 1.05% |
| d(C5-O3) (Å) | 1.15905 | 1.1472(38) | 1.03% |
| d(Fe-C1) (Å) | 1.83829 | 1.8500(19) | 0.63% |
| ∠(C1-Fe-C2) (˚) | 179.166 | 178.61(12) | 0.31% |
| ∠(C3-Fe-C4) (˚) | 119.181 | 117.34(13) | 1.56% |
| ∠(Fe-C5-O3) (˚) | 179.978 | 180.00* | 0.01% |

*Perfect 180˚ angle imposed crystallographically

Table 3.7 Comparison of spectroscopic parameters calculated and experimentally determined for compounds **4m** and **4**, respectively.

| Parameter | Calculated | Experimental | % Difference |
|---|---|---|---|
| ν(C≡N) ($cm^{-1}$) | 2153.73 | 2146 | 0.36% |
| ν(C≡N) ($cm^{-1}$) | 2096.63 | 2092 | 0.22% |
| ν(C≡O) ($cm^{-1}$) | 1992.50 | N/A | N/A |
| ν(C≡O) ($cm^{-1}$) | 1955.90 | 1940 | 0.82% |
| ν(C≡O) ($cm^{-1}$) | 1948.24 | 1940 | 0.42% |

**Optimized coordinates for $Fe(N_2)(CO)_2(CNAr^{Ph2})_2$ (3m).**

| | | | |
|---|---|---|---|
| N | -0.205830 | -0.132404 | -3.020589 |
| C | -4.810617 | -2.340169 | -3.191201 |
| C | -1.318883 | -0.695141 | -5.090097 |
| C | -0.205731 | -0.148453 | -4.397486 |
| C | -0.135835 | -0.092125 | -1.839217 |
| C | -2.510221 | -1.250242 | -4.397283 |
| C | -3.794751 | -0.817713 | -4.773905 |
| C | -2.400127 | -2.239307 | -3.405542 |
| C | -3.540457 | -2.780623 | -2.810637 |
| H | -3.432007 | -3.546612 | -2.041880 |
| C | -4.934262 | -1.355305 | -4.174444 |
| H | -5.921108 | -0.998010 | -4.472531 |
| C | -1.281639 | -0.699329 | -6.492302 |
| H | -2.127788 | -1.127038 | -7.031764 |
| C | -0.183154 | -0.203440 | -7.191907 |

| | | | |
|---|---|---|---|
| H | -0.173092 | -0.228851 | -8.282746 |
| C | -0.927938 | -1.554587 | 0.112107 |
| O | -1.538888 | -2.540465 | 0.204547 |
| Fe | -0.067159 | 0.001403 | 0.000918 |
| C | 4.306502 | 2.239266 | -3.213707 |
| C | 0.911559 | 0.384948 | -5.094834 |
| C | 2.071954 | 1.005145 | -4.404713 |
| C | 3.377070 | 0.580693 | -4.711240 |
| C | 1.906637 | 2.059925 | -3.490193 |
| C | 3.014592 | 2.672886 | -2.904261 |
| H | 2.865632 | 3.494629 | -2.202195 |
| C | 4.484086 | 1.189221 | -4.117852 |
| H | 5.488279 | 0.837510 | -4.359281 |
| C | 0.900421 | 0.329498 | -6.495891 |
| H | 1.752314 | 0.742252 | -7.037978 |
| N | -0.183334 | 0.132677 | 3.023420 |
| C | -4.755706 | 2.396255 | 3.269589 |
| C | -1.257693 | 0.700958 | 5.111758 |
| C | -0.161812 | 0.143967 | 4.400223 |
| C | -0.123534 | 0.094269 | 1.841394 |
| C | -2.452052 | 1.273605 | 4.438816 |
| C | -3.736327 | 0.855874 | 4.832552 |
| C | -2.343868 | 2.264697 | 3.448888 |
| C | -3.485735 | 2.822139 | 2.872189 |
| H | -3.378857 | 3.589222 | 2.104327 |
| C | -4.877525 | 1.409685 | 4.251329 |
| H | -5.864381 | 1.063801 | 4.562537 |
| C | -1.199325 | 0.698822 | 6.513230 |
| H | -2.032156 | 1.134110 | 7.067154 |
| C | -0.096314 | 0.187161 | 7.194131 |
| H | -0.069589 | 0.207671 | 8.284801 |
| C | -0.963506 | 1.537860 | -0.104866 |
| O | -1.596982 | 2.509543 | -0.194632 |
| C | 4.307253 | -2.284048 | 3.137367 |
| C | 0.959907 | -0.404725 | 5.078387 |
| C | 2.103271 | -1.033894 | 4.368199 |
| C | 3.416980 | -0.622291 | 4.655122 |
| C | 1.913834 | -2.084168 | 3.453109 |
| C | 3.006663 | -2.705074 | 2.847379 |
| H | 2.838806 | -3.522934 | 2.145058 |
| C | 4.508788 | -1.238741 | 4.042049 |
| H | 5.519890 | -0.896849 | 4.268385 |
| C | 0.970562 | -0.354971 | 6.479664 |
| H | 1.825871 | -0.779446 | 7.007138 |

| | | | |
|---|---|---|---|
| H | -3.895759 | -0.036911 | -5.530590 |
| H | -5.700132 | -2.760648 | -2.720283 |
| H | -1.415969 | -2.603736 | -3.110675 |
| H | 0.904377 | 2.417580 | -3.252314 |
| H | 3.520015 | -0.247738 | -5.408196 |
| H | 5.170724 | 2.715756 | -2.749349 |
| H | 3.578492 | 0.202431 | 5.352422 |
| H | 5.159609 | -2.766643 | 2.657633 |
| H | 0.904735 | -2.432117 | 3.230266 |
| H | -1.359474 | 2.617400 | 3.140713 |
| H | -3.836131 | 0.073683 | 5.587972 |
| H | -5.646534 | 2.829402 | 2.812862 |
| N | 1.813212 | 0.019792 | -0.004536 |
| N | 2.932540 | 0.030987 | -0.006220 |

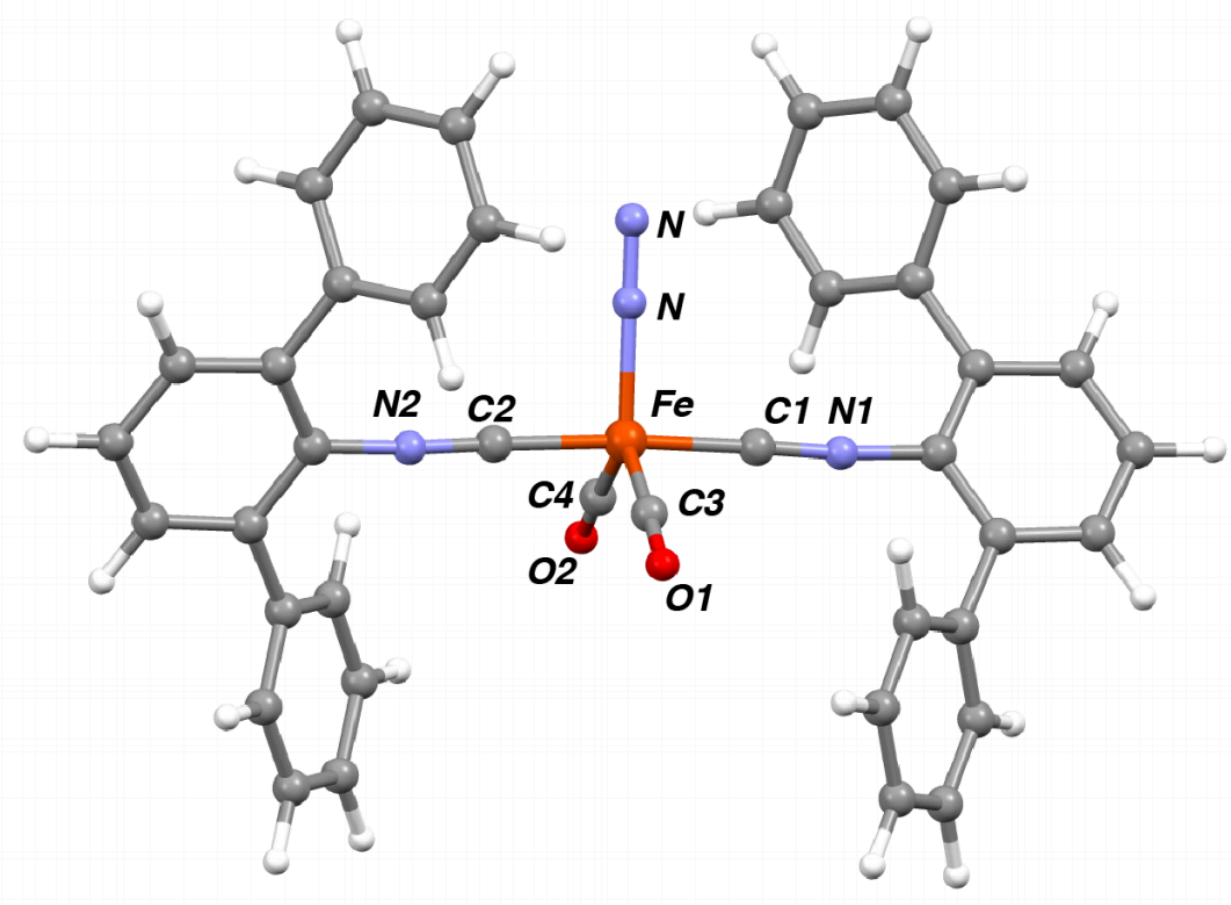


Figure 3.19. Geometry optimized structure of $Fe(N_2)(CO)_2(CNAr^{Ph2})_2$ **3m** (BP86/def2TZVP/J).

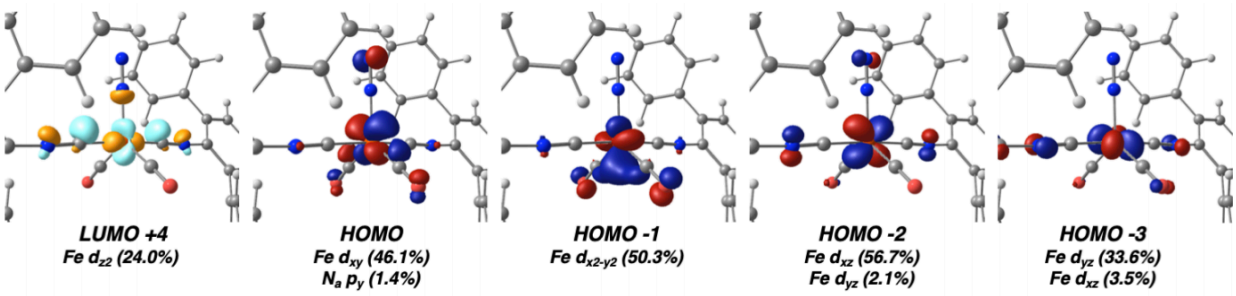


Figure 3.20. Selected molecular orbitals (MOs) of $Fe(N_2)(CO)_2(CNAr^{Ph2})_2$ (**3m**) with predominantly iron d-orbital character. Atomic orbital contributions (AO%) to the molecular orbitals are listed.

Table 3.8. Comparison of structural parameters calculated and experimentally determined for compounds **3m** and **3**, respectively.

| Parameter | Calculated | Experimental | % Difference |
|---|---|---|---|
| d(Fe-N3) (Å) | 1.88047 | 1.8850(33) | 0.24% |
| d(N3-N4) (Å) | 1.11939 | 1.1059(41) | 1.21% |
| d(Fe-C1) (Å) | 1.84368 | 1.8587(20) | 0.81% |
| ∠(C1-Fe-C2) (˚) | 176.113 | 179.04(12) | 1.65% |
| ∠(C3-Fe-C4) (˚) | 120.910 | 115.82(15) | 4.30% |
| ∠(Fe-N3-N4) (˚) | 179.919 | 180.00* | 0.04% |

*Perfect 180˚ angle imposed crystallographically

Table 3.9 Comparison of spectroscopic parameters calculated and experimentally determined for compounds **3m** and **3**, respectively.

| Parameter | Calculated | Experimental | % Difference |
|---|---|---|---|
| ν(C≡N) ($cm^{-1}$) | 2125.02 | 2122 | 0.14% |
| ν(C≡N) ($cm^{-1}$) | 2089.27 | 2075 | 0.68% |
| ν(C≡O) ($cm^{-1}$) | 1964.29 | 1953 | 0.58% |
| ν(C≡O) ($cm^{-1}$) | 1937.32 | 1918 | 1.00% |
| ν(N≡N) ($cm^{-1}$) | 2188.75 | 2194 | 0.22% |

## 3.10 Details of Crystallographic Structure Determinations

**General.** Single X-ray structure determinations were performed at 100 K on Bruker Kappa diffractometers equipped with a Mo radiation source and an APEX-II CCD area detector. All structures were solved via direct methods with SHELXS[62] and refined by full-matrix least-squares procedures using SHELXL[62] within the Olex2[63] software. All hydrogen atoms have been removed for clarity.

Disordered components and co-crystallized solvent molecules are not shown for clarity. Nonetheless, the following molecules contained positional disorder that was successfully modeled and refined anisotropically. They are listed along with their respective disordered components:

**$Fe(CNAr^{Tripp2})_2(CO)_2(N_2)$; (3)** contains one positionally disordered *iso*-propyl group.

**$FeI_2(CNAr^{Tripp2})_2(CO)_2$; (5)** exhibits wagging positional disorder of a flanking phenyl ring. Residual electron density in the unit cell was modeled as 1.4% of molecular iodine ($I_2$).

**CCDC Deposition.** All crystal structures reported herein have been deposited with the Cambridge Crystallographic Data Center (CCDC) and have been assigned the following CCDC deposition numbers:

CCDC-1887069: $Fe(BF)(CO)_2(CNAr^{Tripp2})_2$ (**2**)

CCDC-1887070: $Fe(N_2)(CO)_2(CNAr^{Tripp2})_2$ (**3**)

CCDC-1887071: $Fe(CO)_3(CNAr^{Tripp2})_2$ (**4**)

CCDC-1887072: $K_2[Fe(CO)_2(CNAr^{Tripp2})_2]$ ($K_2$[**1**])

CCDC-1887072: *trans*,*trans*,*trans*-$FeI_2(CO)_2(CNAr^{Tripp2})_2$ (**5**)

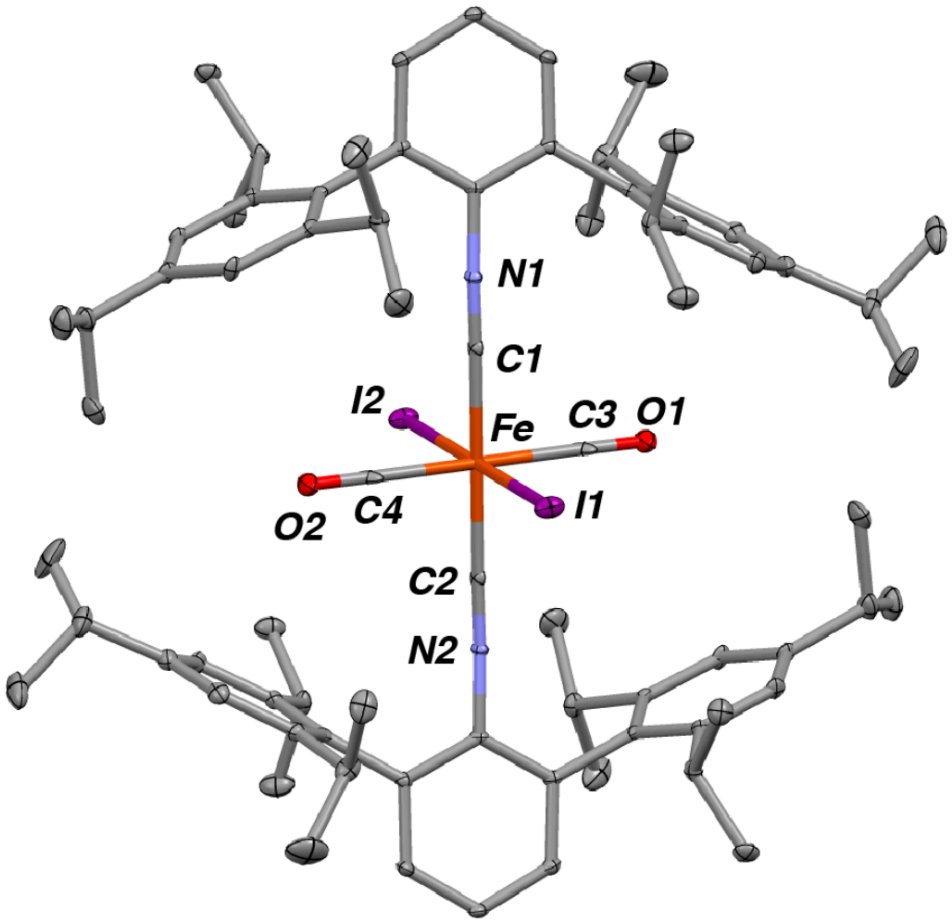


Figure 3.21. Solid-state structure of $FeI_2(CO)_2(CNAr^{Tripp2})_2$ (**5**).

Table 3.10. Crystallographic Data Collection and Refinement Information.

| Name | $K_2$[**1**] · 1.3 ($C_7H_8$) | **2** | **3** · 4 ($C_6H_6$) |
|---|---|---|---|
| Formula | $C_{85.1}H_{106.9}FeK_2N_2O_2$ | $C_{76}H_{98}BFFeN_2O_2$ | $C_{100}H_{122}FeN_4O_2$ |
| Crystal System | Monoclinic | Monoclinic | Monoclinic |
| Space Group | $P2_1$ | $P2_1/n$ | $C2/c$ |
| *a*, Å | 13.2224(8) | 17.0537(4) | 23.7567(15) |
| *b*, Å | 24.0957(14) | 18.1712(4) | 14.7179(8) |
| *c,* Å | 24.0527(14) | 22.4475(5) | 25.8145(17) |
| α, deg | 90 | 90 | 90 |
| β, deg | 90.185(2) | 97.0690(10) | 100.934(4) |
| γ, deg | 90 | 90 | 90 |
| V, Å$^3$ | 7663.2(8) | 6903.3(3) | 8862.2(9) |
| *Z* | 2 | 4 | 4 |
| Radiation (λ, Å) | Mo-Kα, 0.71073 | Mo-Kα, 0.71073 | Mo-Kα, 0.71073 |
| ρ (calcd.), Mg/m$^3$ | 1.147 | 1.113 | 1.100 |
| μ (Mo-Kα), mm$^{-1}$ | 0.352 | 0.266 | 0.219 |
| Temp, K | 100 | 100 | 100 |
| θ max, deg | 23.865 | 27.161 | 25.716 |
| data/restraints/ parameters | 23626 / 193 / 1699 | 15205 / 0 / 772 | 8420 / 22 / 516 |
| $R_1$ | 0.0604 | 0.0431 | 0.0458 |
| $wR_2$ | 0.1376 | 0.1113 | 0.0965 |
| GOF | 1.031 | 1.052 | 1.023 |

Table 3.11. Crystallographic Data Collection and Refinement Information.

| Name | **4** · 3 ($C_6H_6$) | **5** |
|---|---|---|
| Formula | $C_{95}H_{116}FeN_2O_3$ | $C_{76}H_{98}FeI_{2.03}N_2O_2$ |
| Crystal System | Monoclinic | Monoclinic |
| Space Group | *C*2/c | *P*2$_1$/c |
| *a*, Å | 22.996(3) | 12.5641(3) |
| *b*, Å | 15.525(2) | 17.8044(5) |
| *c,* Å | 24.572(3) | 17.0544(5) |
| α, deg | 90 | 90 |
| β, deg | 109.973 | 107.1260(10) |
| γ, deg | 90 | 90 |
| V, Å$^3$ | 8244.9(19) | 3645.85(17) |
| *Z* | 4 | 2 |
| Radiation (λ, Å) | Mo-Kα, 0.71073 | Mo-Kα, 0.71073 |
| ρ (calcd.), Mg/m$^3$ | 1.120 | 1.262 |
| μ (Mo-Kα), mm$^{-1}$ | 0.232 | 0.266 |
| Temp, K | 100 | 100 |
| θ max, deg | 25.428 | 25.706 |
| data/restraints/ parameters | 7587 / 0 / 469 | 6942 / 315 / 541 |
| $R_1$ | 0.0428 | 0.0294 |
| $wR_2$ | 0.0926 | 0.0693 |
| GOF | 1.018 | 1.038 |

## 3.11 Cambridge Structural Database Search Results

The Cambridge Structural Database[64,65] was searched using ConQuest[66] for all crystallographically characterized compounds containing a B-F bond between 0.5 Å and 2.5 Å. A total of 85308 data points were obtained and plotted in the histogram shown in Figure S14. The data set resulted in a mean B-F bond distance of 1.364 Å with a standard deviation of 0.052 Å. To exclude four-coordinate borates, the atom connectivity of boron was set to 3. This gave 146 data points with an average B-F distance of 1.345 Å and a standard deviation of 0.061 Å. Five reported compounds display B-F bond distances less than 1.29 Å, but these values are artificially shortened due to crystallographic disorder (CCDC refcodes HAXNID, HAXNID10, QACJIQ, XIJJOQ, XIJJUW, YIMCAY). No previously reported compounds contain a two-coordinate boron center bound to fluorine.

Additionally, transition metal (TM) complexes containing a TM-B bond within the range of 0 to 5 Å were searched. The query yielded 4720 hits with a mean TM-B distance of 2.223 Å and a standard deviation of 0.160 Å. The three shortest TM-B bond lengths were 1.780 Å (CCDC – WOJGIM,[67]), 1.792 Å (CCDC – EJIRUK,[68]) and 1.793 Å (CCDC – TAMMIF,[69]), all of which are longer than the Fe-B bond distance in $Fe(BF)(CO)_2(CNAr^{Tripp2})_2$ (**2**, d(Fe-B) = 1.7703(25) Å).

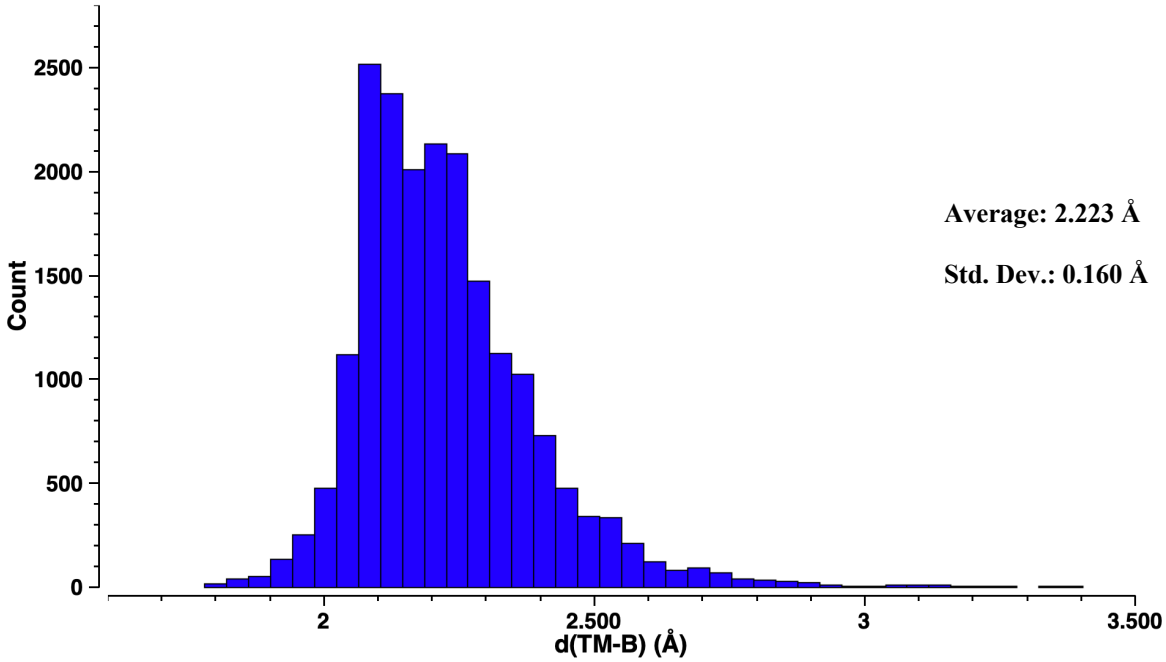


Figure 3.22. CSD search results for all transition metal (TM)-B bonds in structurally characterized molecules.

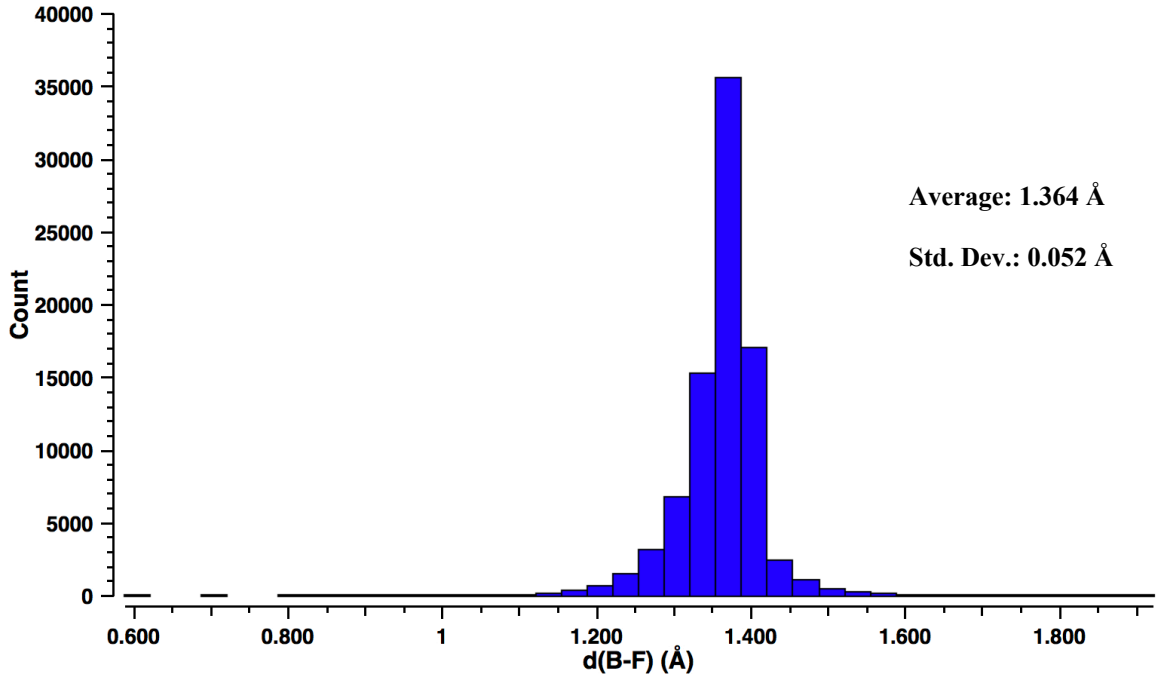


Figure 3.23. CSD search results for all B-F bonds in structurally characterized molecules.

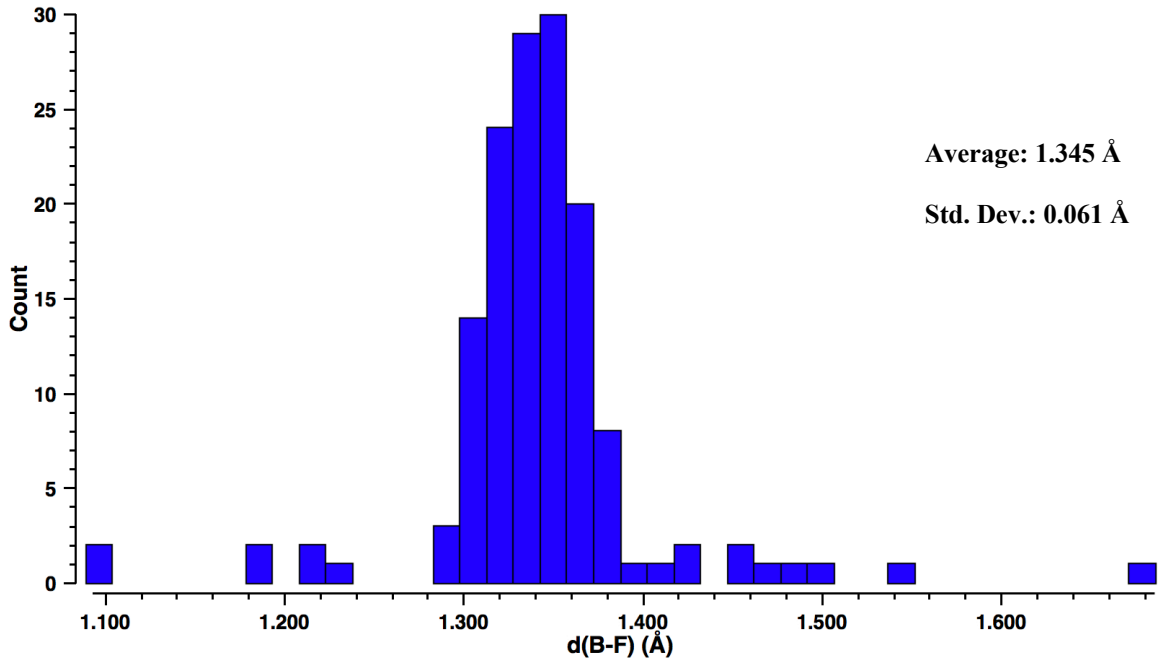


Figure 3.24. CSD search results for all B-F bonds in structurally characterized molecules excluding four-coordinate borates.

## 3.12 Acknowledgments

**Chapter 3**: This chapter is adapted with permission from Drance, M. J.; Sears, J. D.; Mrse, A. M.; Moore, C. E.; Rheingold, A. L.; Neidig, M. L.; Figueroa, J. S. "Terminal Coordination of Diatomic Boron Monofluoride to Iron" *Science*, **2019**, *363*, 1203–1205. Copyright 2019 The Authors. Permission to include published material in this dissertation has been obtained from all coauthors. The dissertation author is the first author of this paper. Prof. C. C. Cummins, Prof. G. Debelouchina, and Dr. B. R. Barnett are also thanked for helpful discussions.

## 3.13 References


(1) Schutzenberger, M. P. *Annales Chim. Physique (Paris)* **1868**, *15*, 100-106.

(2) Mond, L.; Langer, C.; Quincke, F. *J. Chem. Soc., Trans.* **1890**, *57*, 749-753.

(3) Elian, M.; Hoffmann, R. *Inorg. Chem.* **1975**,*14*, 1058-1076.

(4) Herrmann, W. A. *J. Organomet. Chem.* **1990**, *383*, 21-44.

(5) Dewar, M. J. S. *Bull. Soc. Chim. Fr.* **1951**, *18*, C79.

(6) Chatt, J.; Duncanson, L. A. *J. Chem. Soc.* **1953**, 2939-2947.

(7) Cotton, F. A.; Kraihanzel, C. S. *J. Am. Chem. Soc.* **1962**, *84*, 4432-4438.

(8) Ehlers, A. W.; Dapprich, S.; Vyboishchikov, S. F.; Frenking, G. *Organometallics* **1996**, *5*, 105-117.

(9) Werner, H. *Angew. Chem. Int. Ed.* **1990**, *29*, 1077-1089.

(10) Nesbet, R. K. *J. Chem. Phys.* **1964**, *40*, 3619-3633.

(11) Timms, P. L. *J. Am. Chem. Soc.* **1967**, *89*, 1629-1632.

(12) Timms, P. L. *J. Am. Chem. Soc.* **1968**, *90*, 4585-4589.

(13) Lovas, F. J.; Johnson, D. R. *J. Chem. Phys.* **1971**, *55*, 41-44.

(14) Timms, P. L. *Acc. Chem. Res.* **1973**, *6*, 118-123.

(15) Esterhuysen, C.; Frenking, G. *Theor. Chem. Acc.* **2004**, *111,* 381-389.

(16) Ehlers, A. W.; Baerends, E. J.; Bickelhaupt, F. M.; Radius, U. *Chem. Eur. J.* **1998**, *4*, 210-221.

(17) Udo, R.; Bickelhaupt, F. M.; Ehlers, A. W.; Goldberg, N.; Hoffmann, R. *Inorg. Chem.* **1998**, *37*, 1080-1090.

(18) Bickelhaupt, F. M.; Radius, U.; Ehlers, A. W.; Hoffmann, R.; Baerends, E. J. *New J. Chem.* **1998**, *22*, 1-3.

(19) Xu, L.; Li, Q.-S.; Xie, Y.; King, R. B.; Schaefer, H. F. III *Inorg. Chem.* **2010**, *49*, 1046-1055.

(20) Vidovic, D.; Aldridge, S. *Angew. Chem. Int. Ed.* **2009**, *48*, 3669-3672.

(21) Wang, X.; Roos, B. O.; Andrews, L. *Angew. Chem. Int. Ed.* **2009**, *49*, 157-160.

(22) Wang, X.; Roos, B. O.; Andrews, L. *Chem. Commun.* **2010**, *46*, 1646-1648.

(23) Braunschweig, H.; Kraft, K.; Kupfer, T.; Radacki, K.; Seeler, F. *Angew. Chem. Int. Ed.* **2008**, *47*, 4931-4933.

(24) Braunschweig, H.; Dewhurst, R. D. *Angew. Chem. Int. Ed.* **2010**, *49*, 3412-3414.

(25) Carpenter, A. E.; Mokhtarzadeh, C. C.; Rippati, D. S.; Havrylyuk, I.; Kamezawa, R.; Moore, C. E.; Rheingold, A. L.; Figueroa, J. S. *Inorg. Chem.* **2015**, *54*, 2936-2944.

(26) Collman, J. P. *Acc. Chem. Res.* **1975**, *8*, 342-347.

(27) Braunschweig, H.; Dewhurst, R. D.; Gessner, V. H. *Chem. Soc. Rev.* **2013**, *42*, 3197-3208.

(28) Braunschweig, H.; Radacki, K.; Schneider, A. *Science* **2010**, *328*, 345-347.

(29) Mueller, L. *J. Am. Chem. Soc.* **1979**, *101*, 4481-4484.

(30) Bax, A.; Subramanian, S. *J. of Mag. Res.* **1986**, *67*, 565-569.

(31) Gütlich, P.; Bill, E.; Trautwein, A. X. *Springer: Berlin* (2011).

(32) Hassanzadeh, P.; Andrews, L. *J. Phys. Chem.* **1993**, *97*, 4910-4915.

(33) Foster, J. P.; Weinhold, F. *J. Am. Chem. Soc.* **1980**, *102*, 7211-7218.

(34) Bader, R. F. W. *Chem. Rev.* **1991**, *91*, 893-928.

(35) Gillespie, R. J.; Robinson, E. A. *J. Comp. Chem.* **2007**, *28*, 87-97.

(36) Armarego, W. L. F.; Chai, C. L. L. *Purification of Laboratory Chemicals*, 5th Ed.; *Elsevier* (2003).

(37) Pangborn, A. B.; Giardello, M. A.; Grubbs, R. H.; Rosen, R. K.; Timmers, F. J. *Organometallics* **1996**, *15*, 1518–1520.

(38) Mokhtarzadeh, C. C.; Margulieux, G. W.; Carpenter, A. E.; Weidemann, N.; Moore, C. E.;. Rheingold, A. L; Figueroa, J. S. *Inorg. Chem.* **2015**, *54*, 5579–5587.

(39) Fulmer, G. R.; Miller, A. J. M.; Sherden, N. H.; Gottlieb, H. E.; Nudelman, A;. Stoltz, B. M.; Bercaw, J. E.; Goldberg, K. I. *Organometallics* **2010**, *29*, 2176.

(40) Rosenau, C. P.; Jelier, B. J.; Gossert, A. D.; Togni, A. *Angew. Chem. Int. Ed.* **2018**, *57*, 9528–9533.

(41) Pople. J. A. *Mol. Phys.* **1958**, *1*, 168–174.

(42) Bacon, J.; Gillespie, R. J.; Quail. J. W. *Can. J. Chem.* **1963**, *41*, 3063–3069.

(43) Bacon, J.; Gillespie, R. J.; Hartman, J. S.; Rao U. R. K. *Mol. Phys.* **1970**, *18*, 561–570.

(44) Kofod, P. *J. Magn. Res. A.* **1996**, *119*, 212–224.

(45) Garbow, J. R.; Weitekamp, D. P.; Pines, A. *Chem. Phys. Lett.* **1982**, *93*, 504–509.

(46) Christe, K. O.; Wilson, W. W. *J. Fluorine Chem.* **1990**, *46*, 339–342.

(47) Christe, K. O.; Wilson, W. W.; Wilson, R. D.; Bau, R.; Feng, J. A. *J. Am. Chem. Soc.* **1990**, *112*, 7619–7625.

(48) Neese, F. *ORCA-an Ab Inito, Density Functional Theory and Semiemperical SCFMO Program Package*, Version 4.0.0. Max Planck Institute for Chemical Energy Conversion D-45470 Muelheim/Ruhr, Germany (2013).

(49) Becke, A. D. *J. Chem. Phys.* **1986**, *84*, 4524.

(50) Becke, A. D. *J. Chem. Phys.* **1993**, *98*, 5648.

(51) Perdew, J. P. *Phys. Rev. B* **1986**, *33*, 8822.

(52) Perdew, J. P. *Phys. Rev. B* **1986**, *34*, 7406 (Erratum).

(53) Schaefer, A.; Horn, H.; Ahlrichs, R. *J. Chem. Phys.* **1992**, *97*, 2571.

(54) Weigend, F.; Ahlrichs, R. *Phys. Chem. Chem. Phys.* **2005**, *7*, 3297.

(55) Werner, H.-J.; Manby, F. R.;. Knowles, P. J *Chem. Phys.* **2003**, *118*, 8149.

(56) ChemCraft. Zhurko, G. A.; Zhurko, D. A. (2014). www.chemcraftprog.com

(57) Gaussian 09, Revision D.01, Frisch, M. J.; Trucks, G. W.; Schlegel, H. B.; Scuseria, G. E.; Robb, M. A.; Cheeseman, J. R.; Scalmani, G.; Barone, V.; Mennucci, B.; Petersson, G. A.; Nakatsuji, H.; Caricato, M.; Li, X.; Hratchian, H. P.; Izmaylov, A. F.; Bloino, J.; Zheng, G.; Sonnenberg, J. L.; Hada, M.; Ehara, M.; Toyota, K.; Fukuda, R.; Hasegawa, J.; Ishida, M.; Nakajima, T.; Honda, Y.; Kitao, O.; Nakai, H.; Vreven, T.; Montgomery Jr., J. A.; Peralta, J. E.; Ogliaro, F.; Bearpark, M.; Heyd, J. J.; Brothers, E.; Kudin, K. N.; Staroverov, V. N.; Keith, T.; Kobayashi, R.; Normand, J.; Raghavachari, K.; Rendell, A.; Burant, J. C.; Iyengar, S. S.; Tomasi, J.; Cossi, M.; Rega, N.; Millam, J. M.; Klene, M.; Knox, J. E.;

Cross, J. B.; Bakken, V.; Adamo, C.; Jaramillo, J.; Gomperts, R.; Stratmann, R. E.; Yazyev, O.;. Austin, A. J; Cammi, R.; Pomelli, C.; Ochterski, J. W.; Martin, R. L.; Morokuma, K.; Zakrzewski, V. G.; Voth, G. A.; Salvador, P.; Dannenberg, J. J.; Dapprich, S.; Daniels, A. D.; Farkas, O.; Foresman, J. B.; Ortiz, J. V.; Cioslowski, J.; Fox, D. J.; Gaussian, Inc., Wallingford CT, (2013).

(58) Vosko, S. H.; Wilk, L.; Nusair, M. *Can. J. Phys.* **1980**, *58*, 1200.

(59) Lee, C.; Yang, W.; Parr, R. G. *Phys. Rev.* **1988**, *B37*, 785.

(60) NBO Version 3.1, Glendening, E. D.; Reed, J, E.; Carpenter, J. E.; Weinhold, F.Theoretical Chemistry Institute, University of Wisconsin, Madison (2013).

(61) AIMAll (Version 17.11.14), Keith, T. A. TK Gristmill Software, Overland Park KS, USA, 2017 (aim.tkgristmill.com)

(62) Sheldrick, G. M. *Acta Cryst.* **2008**, *A64*, 112.

(63) Dolomanov, O. V.; Bourhis, L. J.; Gildea, R. J.; Howard, J. A. K.; Puschmann, H. *J. Appl. Cryst.* **2009**, *42*, 339.

(64) Cambridge Structural Database (CSD), version 5.39 (November 2017)

(65) Groom, C. R.; Bruno, I. J.; Lightfoot, M. P.; Ward, S. C. *Acta Cryst.* **2016**, *B72*, 171-179.

(66) Bruno, I. J.; Cole, J. C.; Edgington, P. R.; Kessler, M.; Macrae, C. F.; McCabe, P.; Pearson, J.;. Taylor, R *Acta Cryst.* **2002**, *B58*, 389-397.

(67) Alcaraz, G.; Helmstedt, U.; Clot, E.; Vendier, L.; Sabo-Etienne, S. *J. Am. Chem. Soc.* **2008**, *130*, 12878-12879.

(68) Coombs, D. L.; Aldridge, A.; Jones, C.; Willcok, D. J. *J. Am. Chem. Soc.* **2003**, *125*, 6356-6357.

(69) Braunschweig, H.; Ye, Q.; Radacki, K. *Chem. Commun.* **2012**, *48*, 2701-2703.

# Chapter 4

# Reactivity Studies of a Terminal Fluoroborylene Complex

## 4.1 Introduction

Carbon monoxide (CO) is ubiquitous in inorganic chemistry, and its use as a ligand to transition metals dates back more than 150 years.[1] The 1890 discovery of $Ni(CO)_4$, the first binary metal carbonyl,[2] marked the beginning of a very important chapter in organometallic chemistry, which led to what has been called a "renaissance of inorganic chemistry" in the mid- to late-20$^{th}$ century.[3] Accordingly, CO has played a central role in developing the reactivity of transition-metal complexes as well as in devising models of their electronic structure.[4-6] A relatively high energy σ-donor orbital and two low energy π-acceptor orbitals stemming from the polarized triple bond of CO provide it with a high binding affinity for electron-rich transition-metal ions.[6,7] Because of the widespread success of CO as a ligand, much effort has gone into the preparation of metal complexes containing other isolobal, 10 valence-electron diatomic molecules and ions.[3] Longstanding examples involve the readily available species dinitrogen ($N_2$), cyanide ($[CN]^-$), and nitrosonium ($[NO]^+$), and more recent cases have used transition metals to stabilize previously unisolable fragments such as $[CF]^+$ [8-10] and $[BO]^-$.[11]

Theoretical methods have predicted boron monofluoride (BF), a more polarized, neutral analog of CO, to be both a stronger σ-donor and π-acceptor due to a higher energy HOMO (highest occupied molecular orbital) and lower energy LUMO (lowest unoccupied molecular orbital), respectively.[19-21] However, this decreased HOMO/LUMO gap renders the diatomic fluoroborylene molecule unstable at standard temperature and pressure, and although BF can be generated under

high vacuum at ~2000 ˚C, it rapidly oligomerizes under more synthetically relevant conditions.[22,23] Borylenes constitute a general class of molecule isolobal to CO with particularly strong σ-donor capabilities that result in strong metal-boron bonds. However, the buildup of positive charge at boron upon complexation to a metal imparts high kinetic lability to these ligands.[12] This instability was first overcome by Cowley[13] and Braunschweig[14] utilizing substituents with large steric profiles and/or π-donating capabilities (i.e. $[C_5Me_5]^-$ and $[N(SiMe_3)_2]^-$, respectively). While transition-metal-borylene chemistry is now a mature field, stable examples are still limited by the steric and electronic properties of the substituents on boron.[15-18]

Matrix isolation infrared (IR) spectroscopy has identified numerous terminal fluoroborylene complexes of the formulation $M(BF)F_2$, but their fleeting nature has precluded detailed investigations of their structure and reactivity.[24-27] To circumvent the challenges associated with handling BF, Vidovic and Aldridge first constructed the BF molecule in a bridging mode between two ruthenium centers by treating $Na[CpRu(CO)_2]$ with $BF_3{\cdot}Et_2O$.[28] Extending this strategy, we recently reported a dianionic iron complex bearing the encumbering *m*-terphenyl isocyanide $CNAr^{Tripp2}$ ($Ar^{Tripp2}$ = 2,6-(2,4,6-(*i*-Pr)$_3C_6H_2$]$_2C_6H_3$)[29] to kinetically stabilize $Fe(BF)(CO)_2(CNAr^{Tripp2})_2$ (**1**), the first structurally characterized compound possessing a linear fluoroborylene ligand.[30] Herein, we revisit the synthesis of **1** and differentiate fluoroborylene versus bis(difluoro)boryl complex formation from the dianionic iron starting material. We also report the reactivity of ligated BF with various nucleophiles. The small fluoride substituent with negligible π-donating capabilities yields an electrophilic boron center that displays more diverse reactivity compared with other borylene ligands.

## 4.2 Validating the Proposed Mechanism of Formation

It was previously noted in Chapter 3 of this dissertation that 2.8 equivalents of $BF_3{\cdot}Et_2O$ were required in the optimized synthesis of fluoroborylene complex **1** from $K_2[Fe(CO)_2(CNAr^{Tripp2})_2$. Additionally, tetrafluoroborate ($[BF_4]^-$) ion was identified in the reaction precipitate by $^{19}F$ and $^{11}B$ NMR spectroscopy. Because of these observations, we hypothesized that the formation of **1** proceeds via an unobserved monoanionic difluoroboryl intermediate, and the second fluoride elimination is facilitated by another equivalent of $BF_3{\cdot}Et_2O$.[30] In order to test this, we sought to isolate an analogue of the postulated anionic intermediate. Stirring **1** in a dimethoxyethane (DME) suspension of CsF for 3 hours resulted in its clean conversion to a single product, as assessed by $^1H$, $^{19}F$, and $^{11}B\{^1H\}$ NMR spectroscopy. Analysis of single crystals by X-ray diffraction confirmed the product to be $Cs[Fe(BF_2)(CO)_2(CNAr^{Tripp2})_2]$ (**2**), in which boron binds exogenous fluoride, and the resulting anionic $BF_2$ moiety occupies an apical site of a trigonal bipyramid (Scheme 4.1, Figure 4.1). The measured B-F bond distances (1.364 Å, av.) and $^{19}F$ and $^{11}B$ NMR chemical shifts ($\delta_F$ = –8.3 ppm; $\delta_B$ = 46.8 ppm) of **2** match well with the previously reported and structurally characterized difluoroboryl complexes.[31-33] Notably, the conversion of **1** to **2** changes the bond hybridization of boron from sp to $sp^2$, respectively, resulting in significantly longer Fe-B and B-F bonds (Table 1). Most importantly, when **2** is treated with $BF_3{\cdot}Et_2O$ in a thawing $Et_2O$ solution, complex **1** is returned demonstrating the viability of the previously reported mechanism of formation.

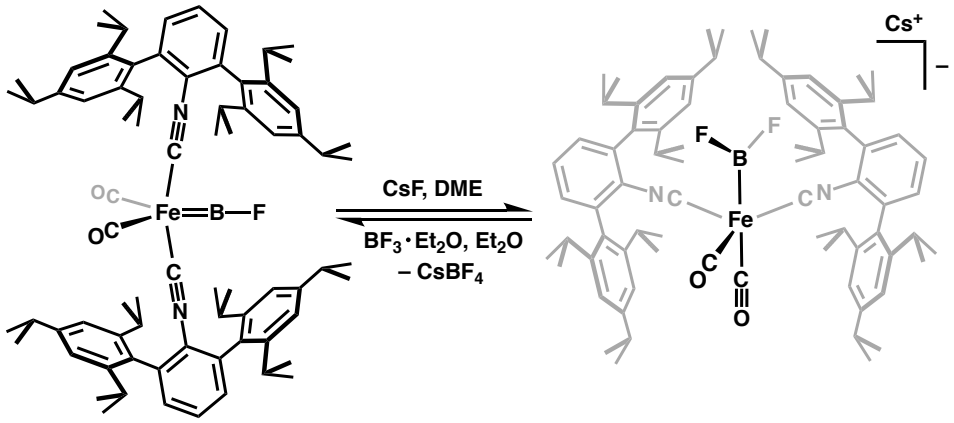


Scheme 4.1. Synthesis of difluoroboryl complex $Cs[Fe(BF_2)(CO)_2(CNAr^{Tripp2})_2]$ (**2**), and the regeneration of $Fe(BF)(CO)_2(CNAr^{Tripp2})_2$ (**1**) by fluoride abstraction using $BF_3{\cdot}Et_2O$.

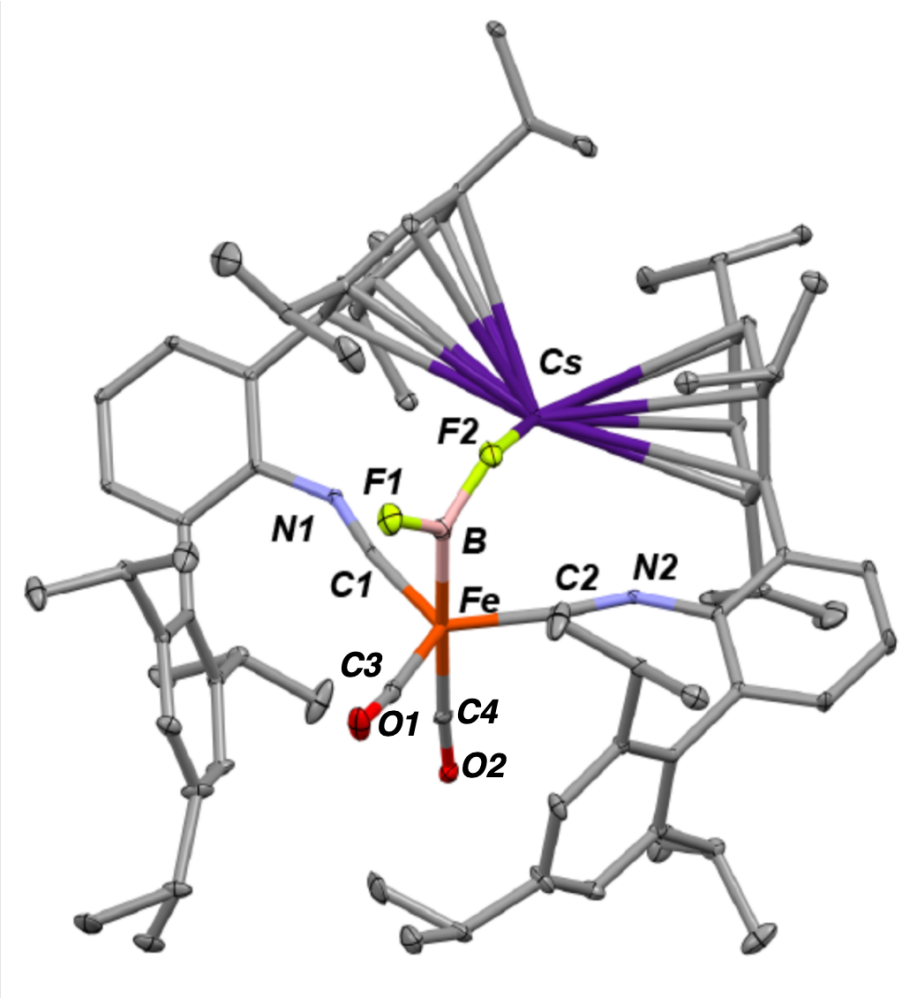


Figure 4.1. Solid-state structure of $Cs[Fe(BF_2)(CO)_2(CNAr^{Tripp2})_2]$ (**2**).

The synthesis of **1** from either $K_2[Fe(CO)_2(CNAr^{Tripp2})_2]$ or **2** must be performed at low temperatures (< –50 ˚C) in order to avoid the appearance of a second diamagnetic product that displays a partially collapsed quartet in the $^{19}F$ NMR spectrum centered at $\delta_F$ = 2.56 ppm and a broad singlet at $\delta_B$ = 44.2 ppm in the $^{11}B\{^1H\}$ spectrum. This other species can be generated as the major product by using toluene as the reaction solvent, which allowed for its crystallization and identification as the bis(difluoro)boryl complex $Fe(BF_2)_2(CO)_2(CNAr^{Tripp2})_2$ (**3**; Scheme 2, Figure 4.2). A similar solvent effect was also observed by Aldridge in the reactivity of $Na[CpRu(CO)_2]$ with $BF_3{\cdot}Et_2O$, which favored a bridging fluoroborylene product in $Et_2O$ and a mononuclear difluoroboryl complex in toluene.[28] Presumably, the coordinating O-atom of $Et_2O$ can donate electron density into the vacant p-orbital of boron, which increases the basicity of fluorine and leads to double fluoride loss for both us and Aldridge. Compound **3** exhibits similar infrared spectra with asymmetric C≡N stretches blueshifted by *ca*. 40 $cm^{-1}$ and C≡O stretches differing by *ca*. 10 $cm^{-1}$ despite formal iron oxidation states of 0 and +2 in **1** and **3**, respectively. This can be attributed to the large σ-donor/π-acceptor ratio of difluoroboryl ligands[34] that make **3** a comparatively electron-rich divalent iron center that engages in a high degree of π backbonding to the isocyanide and carbonyl ligands. Positional disorder of the equatorial ligands (i.e. CO and $BF_2$) precludes a detailed structural comparison of the Fe-B and B-F bond distances, but they appear roughly consistent with the values found in anionic difluoroboryl complex **2**.

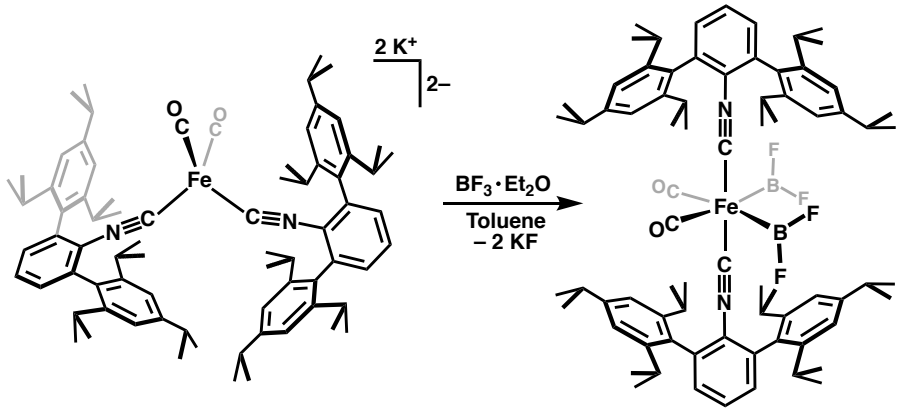


Scheme 4.2. Selective synthesis of $Fe(BF_2)_2(CO)_2(CNAr^{Tripp2})_2$ (**3**) in toluene.

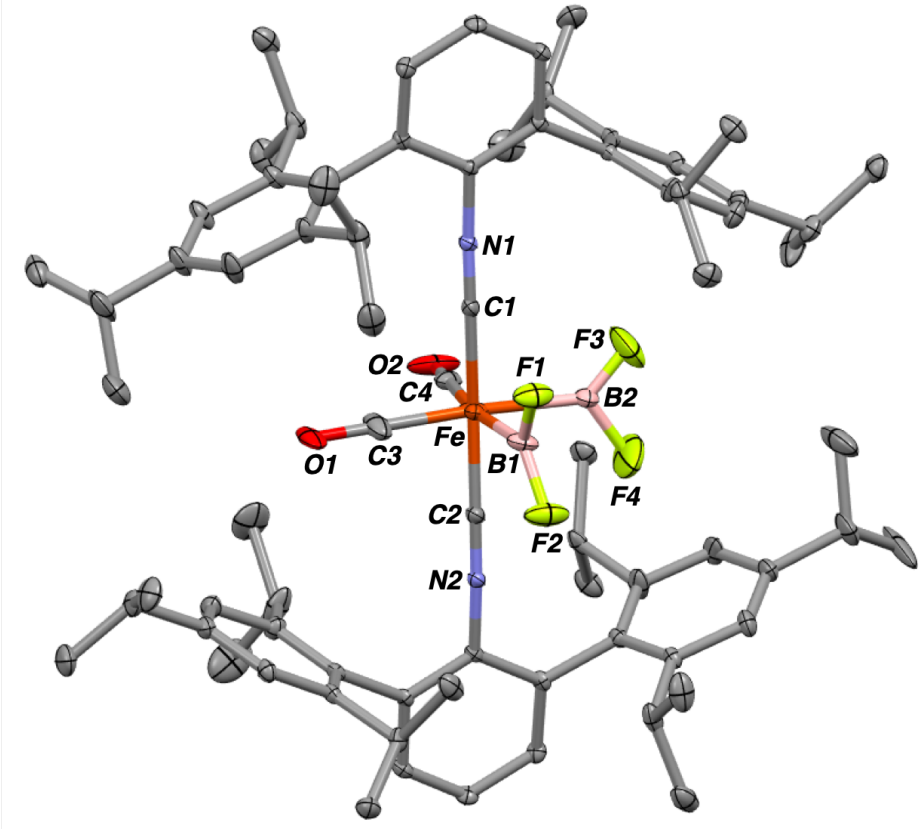


Figure 4.2. Solid-state structure of $Fe(BF_2)_2(CO)_2(CNAr^{Tripp2})_2$ (**3**).

## 4.3 Reactivity of Coordinated BF with Nitrogen-Based Nucleophiles

The ability of **1** to bind a weak base such as fluoride led us to investigate the reactivity of coordinated BF with more potent nucleophiles. Treating a thawing $Et_2O$ solution of **1** with 4-dimethylaminopyridine (DMAP) resulted in an immediate color change from yellow to brown and gave a single new $^{19}F$ resonance at $\delta_F$ = –6.2 ppm. X-ray diffraction of dark yellow crystals deposited from a *n*-pentane solution revealed the product to be the Lewis adduct $Fe(B(F)(DMAP))(CO)_2(CNAr^{Tripp2})_2$ (**4**; Scheme 4.3, Figure 4.3). As in compound **2**, the Fe-B and B-F bond lengths in **4** elongate as the geometry at boron changes from linear to trigonal planar and boron migrates to an axial coordination site. The pyridine ring retains aromaticity, and the B-N distance of 1.554 Å is consistent with a single bond, suggesting that DMAP does not engage in π bonding with boron. Surprisingly, the $^{11}B$ resonance of **4** shifts to slightly lower field than **1**. This effect runs opposite of the typical upfield shift observed when borylene coordination number changes from 2 to 3 and electron density around the $^{11}B$ nucleus increases.[35,36] However, in **1**, significant double bond character between iron and boron gives a $^{11}B$ resonance at unusually high field for transition-metal borylene complexes.[18] Coordination of DMAP in **4** disrupts π bonding between iron and boron, which results in an unexpected downfield shift of the $^{11}B$ nucleus. This electronic effect is further borne out by a *ca*. 80–100 $cm^{-1}$ redshift of the isocyanide and carbonyl stretching bands relative to **1**. As Fe→B π backbonding is eliminated through a break in symmetry, the excess electron density at iron from the strongly donating base-stabilized borylene is accommodated by C≡N and C≡O $\pi^*$ orbitals, weakening these bonds and leading to lower frequency vibrations.

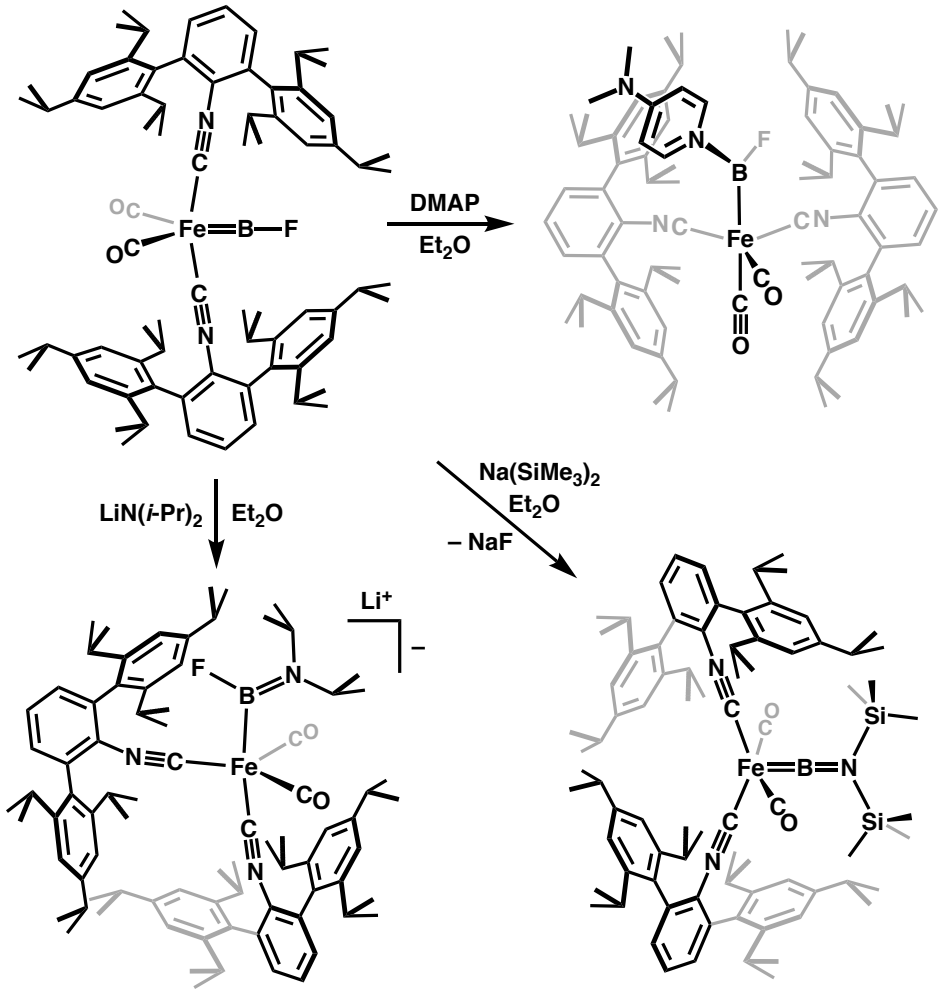


Scheme 4.3. Derivatization of **1** with neutral and anionic nucleophiles forming, in clockwise order, $Fe(B(F)(DMAP))(CO)_2(CNAr^{Tripp2})_2$ (**4**), $Fe(BN(SiMe_3)_2)(CO)_2(CNAr^{Tripp2})_2$ (**5**), and $[Fe(B(F)N(i\text{-}Pr)_2)(CO)_2(CNAr^{Tripp2})_2]^-$ ($[\mathbf{6}]^-$).

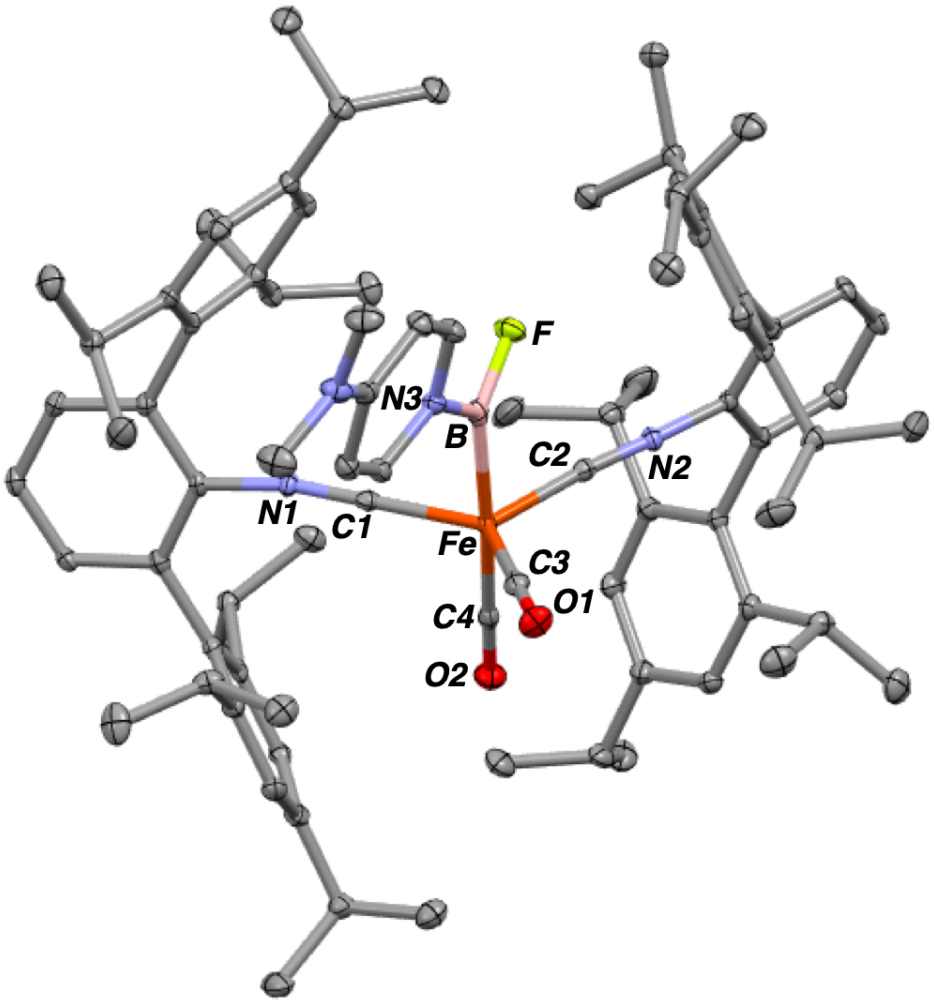


Figure 4.3. Solid-state structure of Fe(B(F)(DMAP))$(CO)_2(CNAr^{Tripp2})_2$ (**4**).

In an attempt to generate an aminoborylene complex analogous to the first linear borylenes reported,[14] **1** was treated with a $Et_2O$ solution of sodium bis(trimethylsilyl)amide ($NaN(SiMe_3)_2$). After 3 hours, the starting material had been fully consumed, and no new resonances were observed in the $^{19}F$ NMR spectrum. Additionally, the $^{11}B\{^1H\}$ NMR spectrum displayed a very broad, downfield resonance at $\delta_B$ = 88.5 ppm, which lies in the typical range for aminoborylene complexes[18] and 1 ppm away from a spectroscopically observed species assigned as $Fe(BN(SiMe_3)_2)(CO)_4$.[14] Indeed, X-ray diffraction confirmed the product to be

$Fe(BN(SiMe_3)_2)(CO)_2(CNAr^{Tripp2})_2$ (**5**; Scheme 4.3, Figure 4.4), an isolobal analogue of that previously observed species. Contrasting with **1**, this new borylene complex features axial carbonyl ligands and an equatorial plane containing the two isocyanides and borylene, likely as a result of steric pressures between the encumbering $Ar^{Tripp2}$ and trimethylsilyl substituents. Notably, the B-N distance (1.376 Å) and planar geometry about nitrogen suggest double bond character, as seen in other aminoborylene complexes.[9-14] Consequently, the degree of π bonding between iron and boron in **5** is diminished relative to **1**, as evidenced by a *ca*. 0.05 Å Fe-B bond elongation.

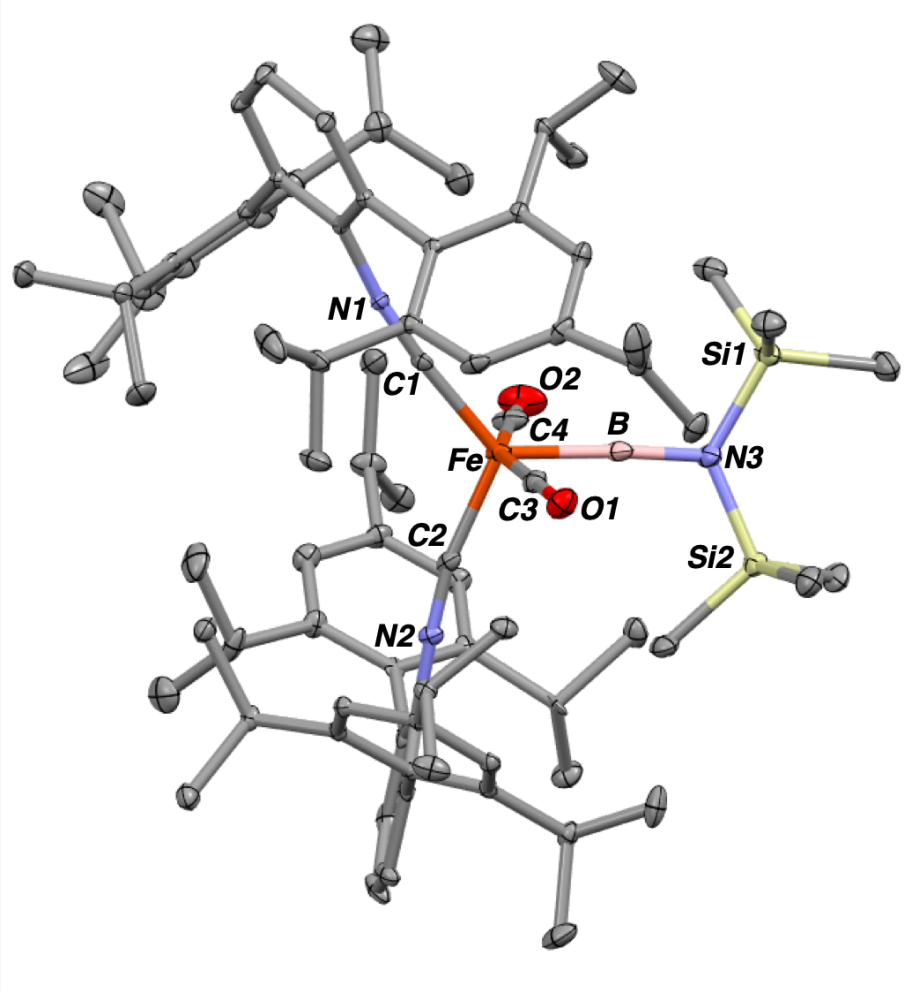


Figure 4.4. Solid-state structure of $Fe(BN(SiMe_3)_2)(CO)_2(CNAr^{Tripp2})_2$ (**5**)

A parallel reaction using lithium diisopropylamide (LiN(*i*-Pr)$_2$) as the nucleophile produced a new singlet in the $^{19}$F NMR spectrum at $\delta_F$ = –41.6 ppm, indicating that fluoride elimination did not occur. This species was identified by X-ray analysis as the anionic boryl complex [Li(Et$_2$O)][Fe(B(F)N(*i*-Pr)$_2$)(CO)$_2$(CNAr$^{Tripp2}$)$_2$] (**6**; Scheme 4.3, Figure 4.5). As in **2** and **4**, the geometry about iron is trigonal bipyramidal with boron bound axially. However, in **6**, CNAr$^{Tripp2}$ is coordinated *trans* to boron, but this difference is likely a steric effect rather than an electronic preference considering the strongly donating nature of both isocyanides and boryl ligands. Importantly, **6** serves as an analogue of the intermediate in the formation of **5** before fluoride elimination. The crystal structure of **6** also represents an intermediate geometry in the ancillary ligand isomerization between axial isocyanides in **1** and equatorial isocyanides in **5**. The B-N distance in **6** is similar to **5**, which is significantly shorter than in **4**, due to π donation from amido substituents and a lack thereof from DMAP. The differentiation between nucleophilic substitution in **5** and addition in **6** is not fully understood and is under further investigation. Using LiN(SiMe$_3$)$_2$ in place of NaN(SiMe$_3$)$_2$ produces aminoborylene **5** in comparable yield with no detectable boryl formation. Accordingly, cation identity is not the dominant factor at play.

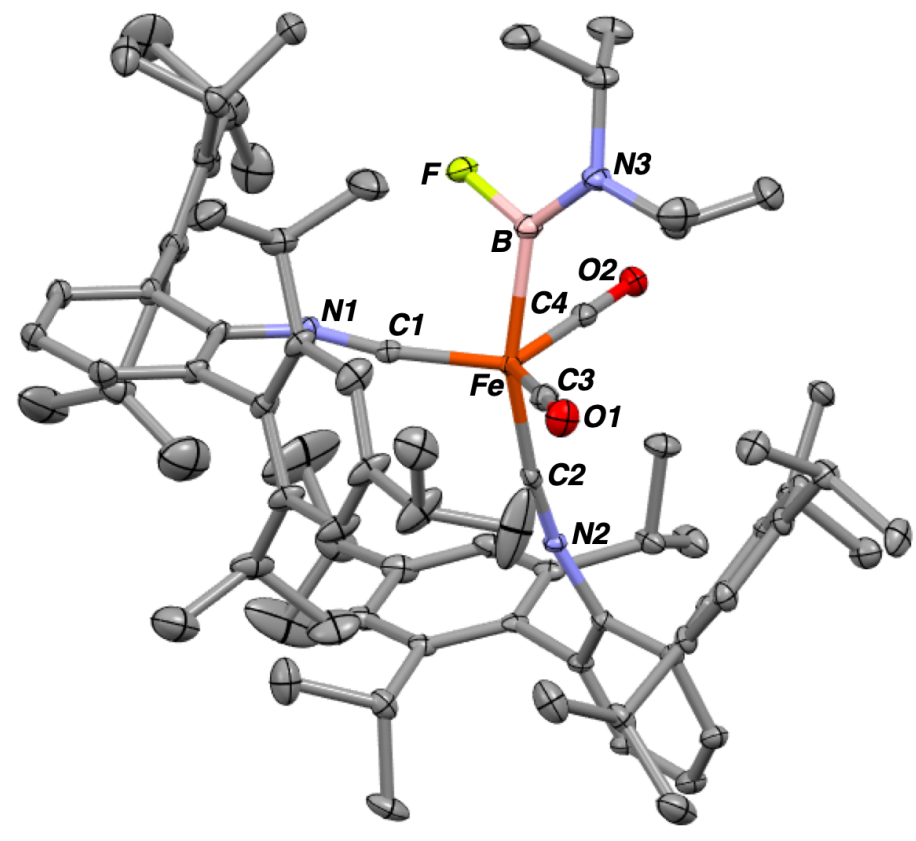


Figure 4.5. Solid-state structure of $[Fe(B(F)N(i\text{-}Pr)_2)(CO)_2(CNAr^{Tripp2})_2]^-$ ([**6**]$^-$). Lithium cation with coordinated $Et_2O$ omitted for clarity.

## 4.4 B≡E Triple Bonds (E = N and O)

Braunschweig and co-workers isolated the first imino- and oxoboryl complexes via Pt-centered oxidative addition of $Br_2BN(SiMe_3)_2$ or $Br_2BOSiMe_3$, respectively, followed by intramolecular elimination of bromotrimethylsilane, and this remains the only strategy for generating these ligands.[11,37] While, the addition of $NaN(SiMe_3)_2$ to fluoroborylene **1** furnished **5** with no observed generation of an anionic iminoboryl complex, we believed that a trimethylsilyl group could be removed by exploiting the high affinity of silicon for fluorine. Stirring complex **5** in a DME suspension of CsF overnight resulted in broad, redshifted IR bands characteristic of an anionic species, and $^1$H NMR revealed the formation of a single product with one $CNAr^{Tripp2}$

environment and a singlet at $\delta_H$ = 0.10 ppm integrating to 9 protons. Crystals readily deposited from *n*-pentane/$Et_2O$ at –35 ˚C, which upon X-ray diffraction were shown to be the desired $Cs[Fe\{BN(SiMe_3)\}(CO)_2(CNAr^{Tripp2})_2]$ (**7**; Scheme 4.4, Figure 4.6). Similarly to the aforementioned boryl complexes, the iminoboryl ligand of **7** binds at an apical site of five-coordinate iron that deviates slightly from idealized trigonal bipyramidal geometry ($\tau_5$ = 0.78).[38] The $[BN(SiMe_3)]^-$ ligand features a short B-N internuclear distance of 1.277 Å that is slightly longer than other structurally characterized examples of B-N triple bonds supported by transition metals (1.245 – 1.266 Å).[37,39,40] The Cs cation is encapsulated by several cation-pi interactions with the isocyanide triple bonds, the flanking arenes of the *m*-terphenyl substituents, and the BN triple bond. This contact with $Cs^+$ and π backdonation from the electron rich, formally Fe(0) center likely are the origin of the slightly longer B-N bond as well as a relatively downfield $^{11}B$ resonance ($\delta_B$ = 56.0 ppm). In comparison, previously reported iminoboryl complexes display $^{11}B$ resonances between 16.9 and 33.6 ppm.[41] Furthermore, the $^{11}B{\equiv}N$ stretch was located at 1712 $cm^{-1}$, redshifted by *ca.* 90 $cm^{-1}$ from previously reported examples,[37,39,40] consistent with the moderately activated triple bond of **7**. Attempts to displace the second trimethylsilyl group in search of the nitridoboryl moiety ($[BN]^{2-}$) using excess fluoride or more potent nucleophiles (e.g. NaH, $LiHBEt_3$, $NaNH_2$) have thus far been unsuccessful.

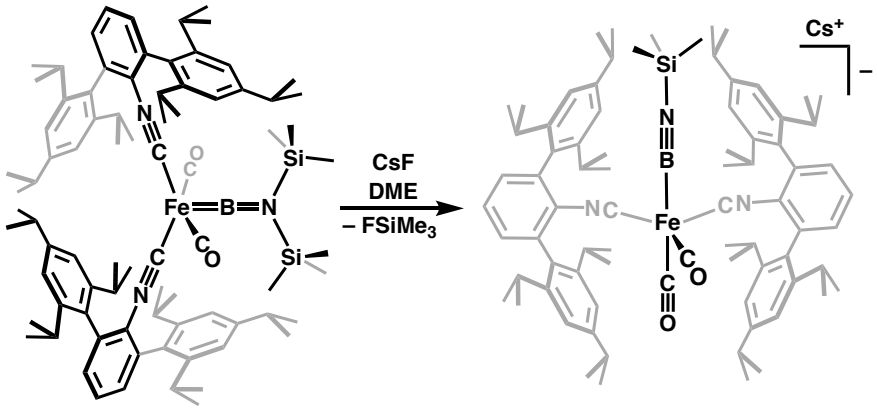


Scheme 4.4. Synthesis of iminoboryl complex Cs[Fe{BN(SiMe$_3$)}(CO)$_2$(CNAr$^{Tripp2}$)$_2$] (**7**) via de-silylation of **6** with CsF.

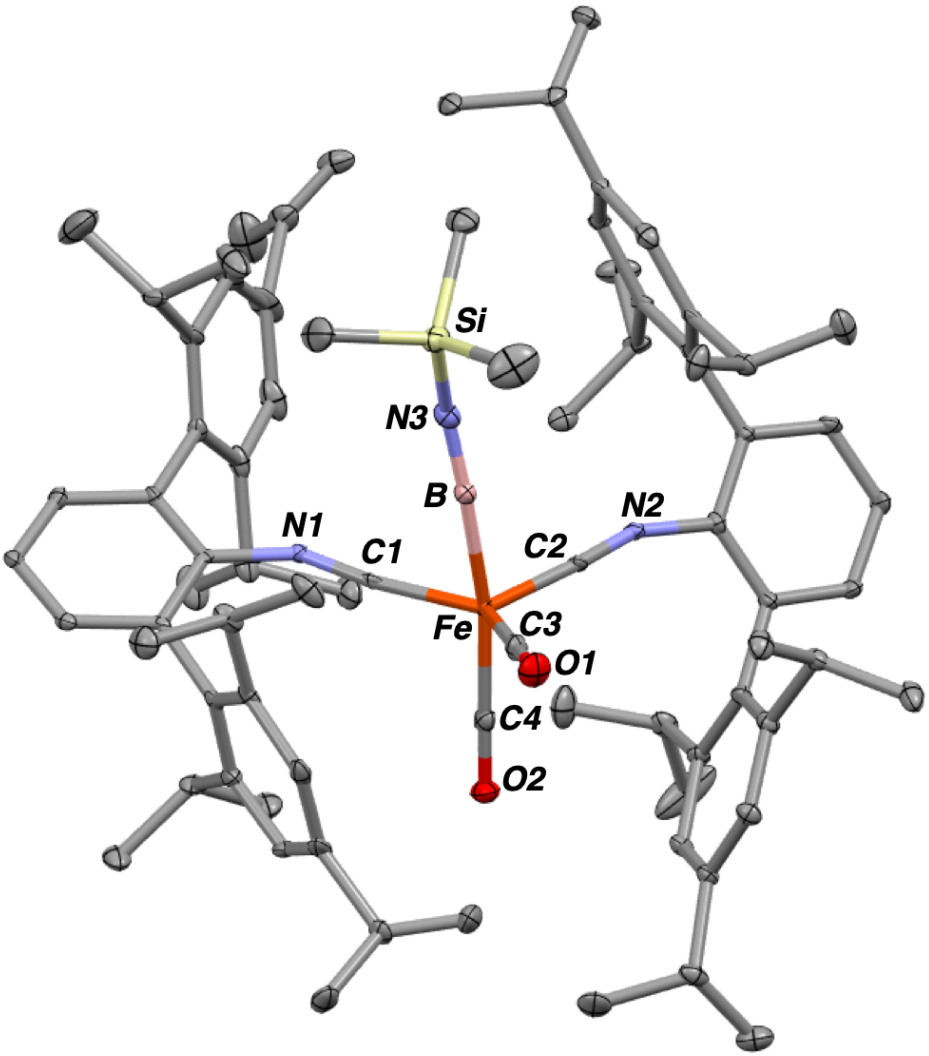


Figure 4.6. Solid-state structure of Cs[Fe{BN(SiMe$_3$)}(CO)$_2$(CNAr$^{Tripp2}$)$_2$] (**7**).

This novel synthetic route to an Fe-bound iminoboryl ligand encouraged the pursuit of an oxoboryl complex derived from the fluoroborylene moiety. To this end, lithium trimethylsilanolate ($LiOSiMe_3$) was deemed a to **1** in a 1:2 DME/$Et_2O$ mixture at room temperature led to the full consumption of starting material, as determined by the disappearance of the $^{19}F$ resonance associated with **1**. X-ray analysis of yellow crystals grown from 9:1 *n*-pentane/DME revealed the dimeric structure $\{[Li(DME)][Fe(BO)(CO)_2(CNAr^{Tripp2})_2]\}_2$ (**8**; Scheme 4.5, Figure 4.7), in which two lithium cations coordinated by DME form a bridge between two inward facing oxoboryl O atoms. The solid-state geometry of **8** resembles aminoborylene complex **5** with axial carbonyl ligands and equatorial isocyanides in a distorted trigonal bipyramidal geometry. The Fe-B distance in **8** (1.852 Å) is longer than in borylene complexes **1** and **5** but shorter than in boryl complexes **2**, **6**, and **7**, and the short B-O distance of 1.255 Å suggests multiple bond character for the BO moiety. However, coordination of $Li^+$ lowers the $\pi^*$ orbital energy of the ostensible triple bond allowing for increased Fe→B π backdonation. This results in a B-O internuclear distance that is longer than the two reported values of terminal oxoboryl ligands (1.197, 1.210 Å)[11,42] and comparable to borane-capped oxoboryl complexes (1.233, 1.245 Å).[42] While the $^{11}B$ NMR resonance could not be located, likely as a result of a short T2 relaxation time from slower molecular tumbling,[ref] the solution FTIR spectrum of **8** in $C_6D_6$ or *n*-pentane displays a band of moderate intensity at 1609 $cm^{-1}$ along with a very weak band at 1660 $cm^{-1}$, assignable to highly activated B≡O stretches from both $^{11}B$ and $^{10}B$ isotopologues, respectively (Figure 4.8). For comparison, the oxoboryl-borane adducts exhibit $^{11}B{\equiv}O$ stretches at 1732 and 1721 $cm^{-1}$, further indicating the highly activated nature of the B-O bond in **8**.

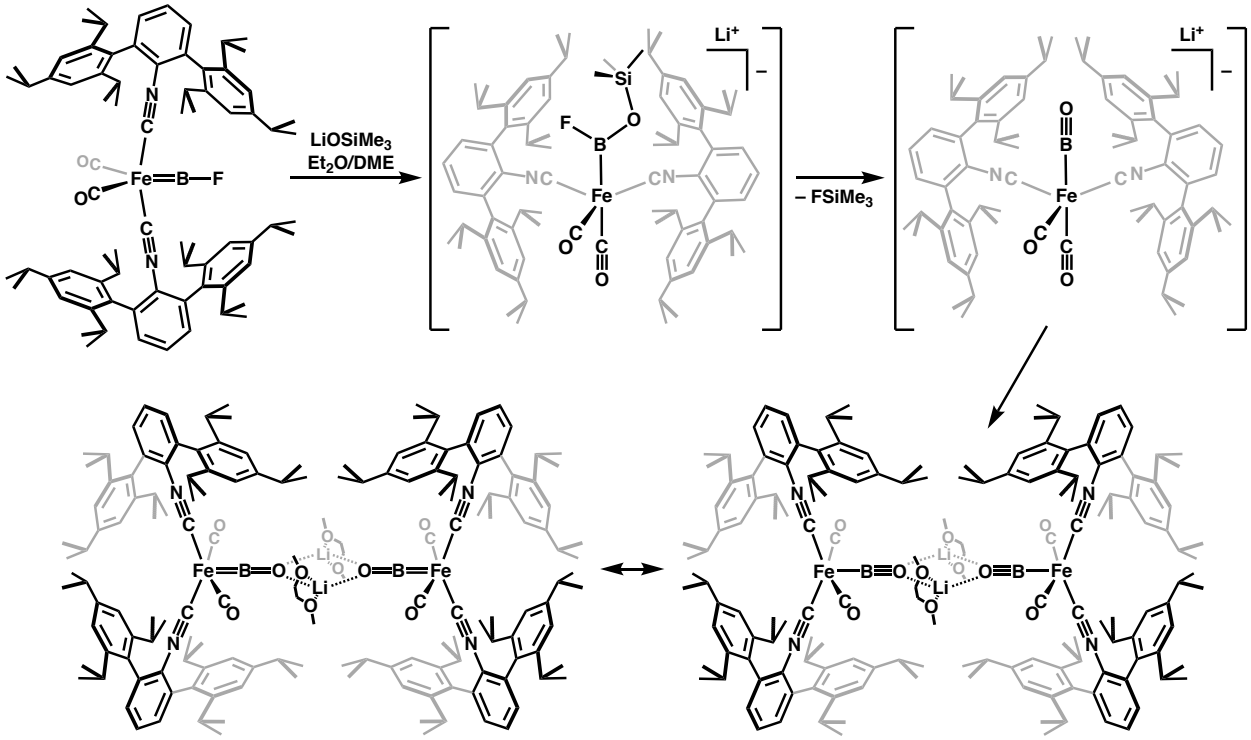


Scheme 4.5. Formation of dimeric oxoboryl complex $\{[Li(DME)][Fe(BO)(CO)_2(CNAr^{Tripp2})_2]\}_2$ (**8**) from $LiOSiMe_3$ and **1**. Boryl and borylene resonance forms are drawn.

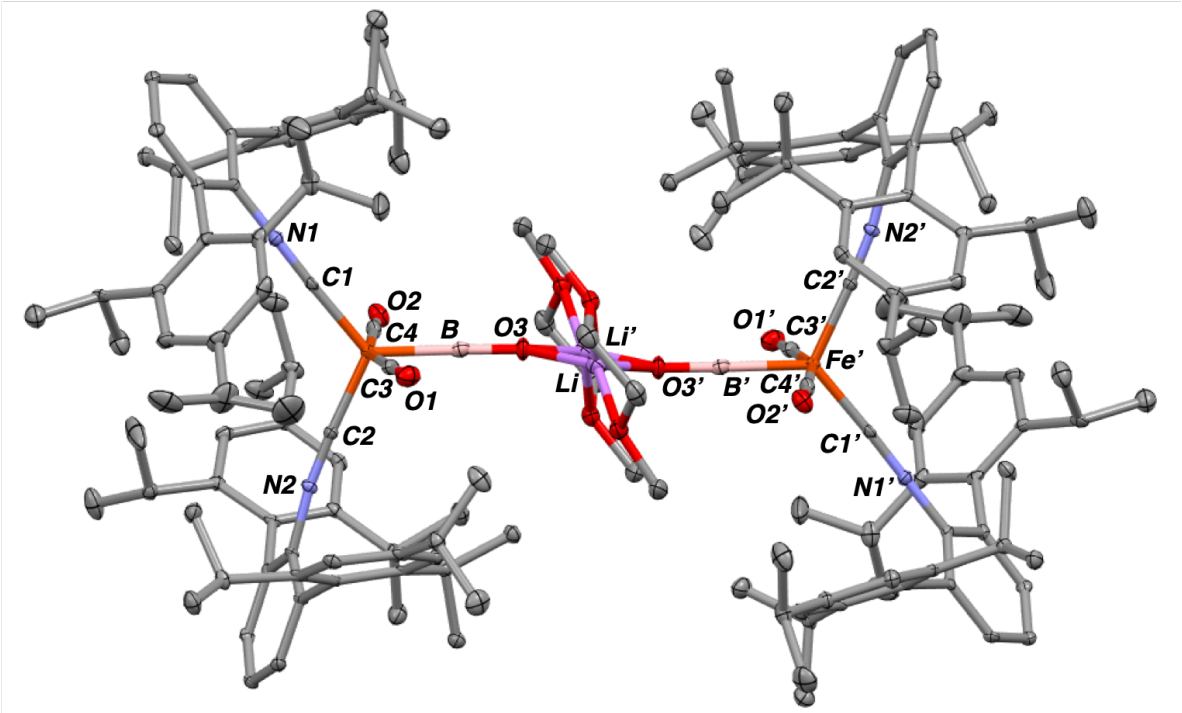


Figure 4.7. Solid-state structure of $\{[Li(DME)][Fe(BO)(CO)_2(CNAr^{Tripp2})_2]\}_2$ (**8**).

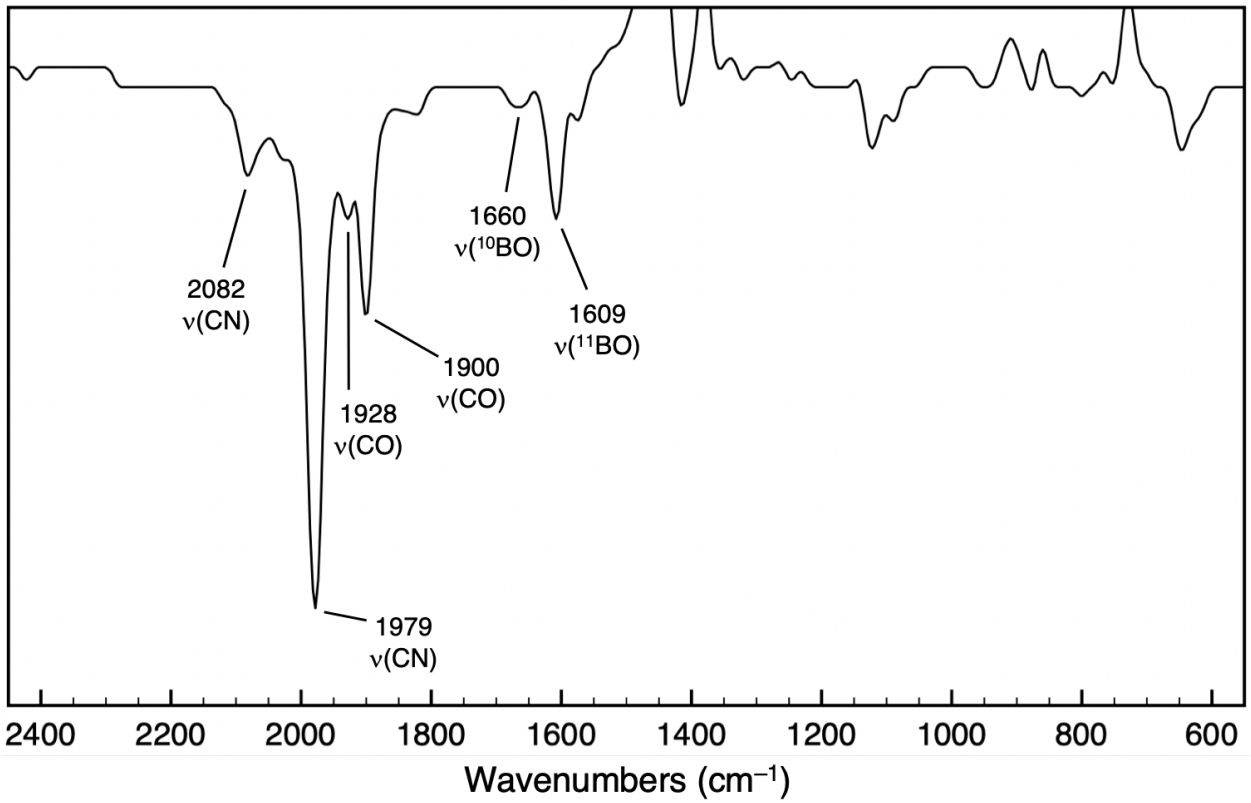


Figure 4.8. Solution FTIR spectrum of **8** recorded in *n*-pentane at 25 ˚C with KBr windows. Selected stretching bands are labeled.

It was observed that dissolution of **8** in coordinating solvents (e.g. THF, DME) produces a different IR spectrum with broadened and slightly redshifted isocyanide and carbonyl stretches in addition to more intense B≡O bands at 1744 and 1692 $cm^{-1}$ in a 1:4 integrated ratio, respectively, due to the natural abundances of $^{10}B$ and $^{11}B$ (Figure 4.9). Importantly, the $^{11}B$ NMR spectrum of **8** dissolved in THF or DME exhibits an identifiable broad resonance centered at $\delta_B$ = 44.3 ppm. Consistent with the $^{11}B$ resonance of **7**, this signal is roughly 30 ppm downfield of Pt-based systems.[41] These data suggest that the dimeric structure of **8** can be broken up in solution by lithium cation encapsulation. However, recrystallization from 100% DME or THF returned crystals of dimeric **8** with no evidence for a monomer in the solid state. We tentatively assign the solution-

phase geometry as analogous to **7** based on FTIR analysis. The more intense B≡O stretches seen in THF likely arise from a greater change in dipole moment associated with axial versus equatorial coordination, and nearly equal intensity symmetric and asymmetric C≡O stretches implies a ~90˚ arrangement of the two carbonyl ligands.[43,44]

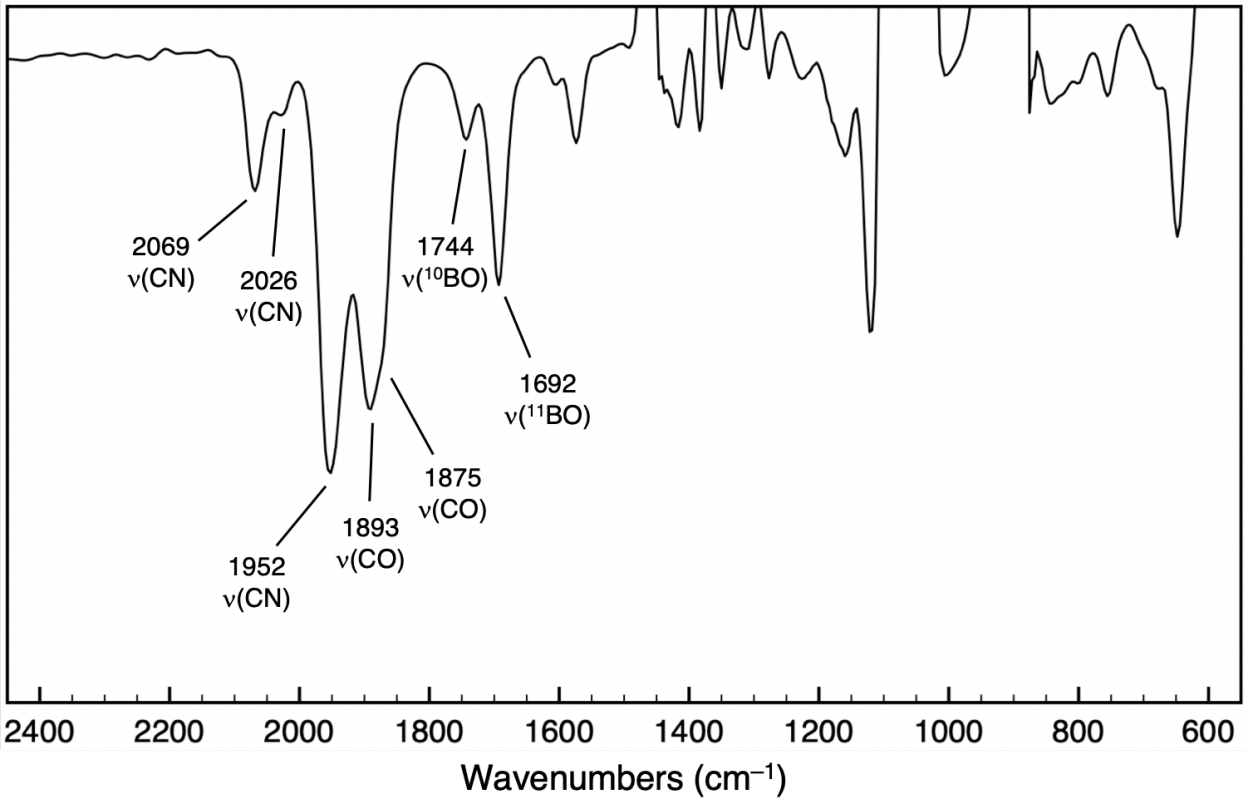


Figure 4.9. Solution FTIR spectrum of **8** recorded in THF at 25 ˚C with KBr windows. Selected stretching bands are labeled.

In order to isolate an oxoboryl complex of iron with a bona fide triple bond both in solution and in the solid state, **8** was stirred in a THF solution of tetra-*n*-butylammonium chloride ($NBu_4Cl$) to exchange the cation prevent dimerization. A white precipitate formed within minutes, and NMR spectroscopy exhibited $^{1}H$ resonances belonging to a single new product, and a $^{11}B$ signal observable in $C_6D_6$ at $\delta_B$ = 42.9 ppm. X-ray diffraction of yellow single crystals grown from *n*-

pentane/benzene showed the discrete ion pair $NBu_4[Fe(BO)(CO)_2(CNAr^{Tripp2})_2]$ ($NBu_4$[**9**]; Scheme 4.6, Figure 4.10). Separation of the cation away from the oxoboryl ligand in **8** resulted in a significant change in geometry closer in likeness to a square pyramid than a trigonal bipyramid ($\tau_5$ = 0.30). The distorted solid-state geometry may be partially influenced by the $NBu_4$ cation, which approaches the $[BO]^-$ ligand placing two α C-H protons within the range of non-classical hydrogen bonding, less than 2.6 Å away from the oxoboryl O atom.[45] However, the structure of $[\mathbf{9}]^-$ bears resemblance to $Fe(CN\textit{t}\text{-}Bu)_5$, an electron-rich analog of $Fe(CO)_5$.[46] Accordingly, the distortion in $[\mathbf{9}]^-$ is likely due primarily to the extreme σ-donor/π-acceptor ratio of $[BO]^-$.[19] Importantly, cation exchange also leads to an elongation of the Fe-B distance to 1.925 Å and a contraction of the B-O bond to 1.224 Å, along with a new $^{11}B{\equiv}O$ IR absorbance at 1720 $cm^{-1}$ indicating a stronger bond than in **8** (Figure 4.11). Both the B-O distance and $^{11}B{\equiv}O$ IR stretch for $[\mathbf{9}]^-$ deviate slightly from the previously reported neutral species *trans*-$[(Cy_3P)_2(SPh)Pt(BO)]$ (Cy = cyclohexyl; Ph = phenyl) (1.210(3) Å; 1793 $cm^{-1}$, respectively)[11] implying a triple bond that is activated by π backbonding from iron instead of Lewis acid coordination as in **8** or previously reported oxoboryl-borane adducts.[42]

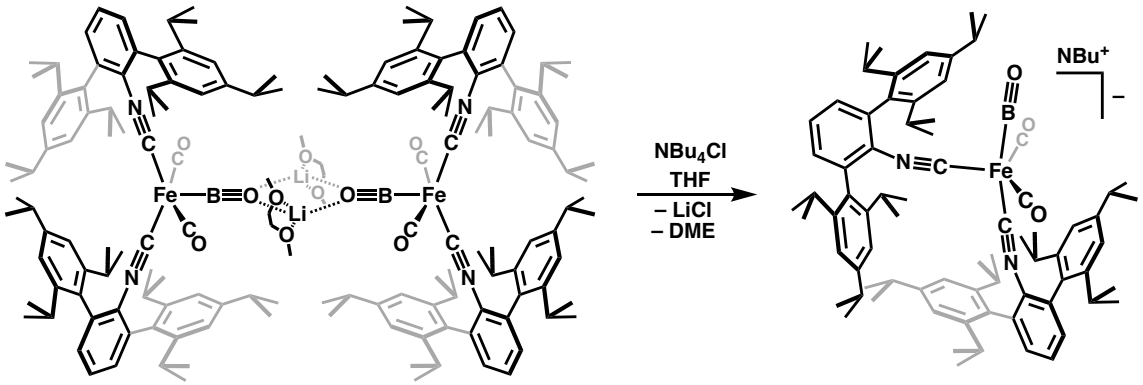


Scheme 4.6. $Li^+$ for $NBu_4^+$ cation exchange of **8** to generate $NBu_4[Fe(BO)(CO)_2(CNAr^{Tripp2})_2]$ ($NBu_4$[**9**]).

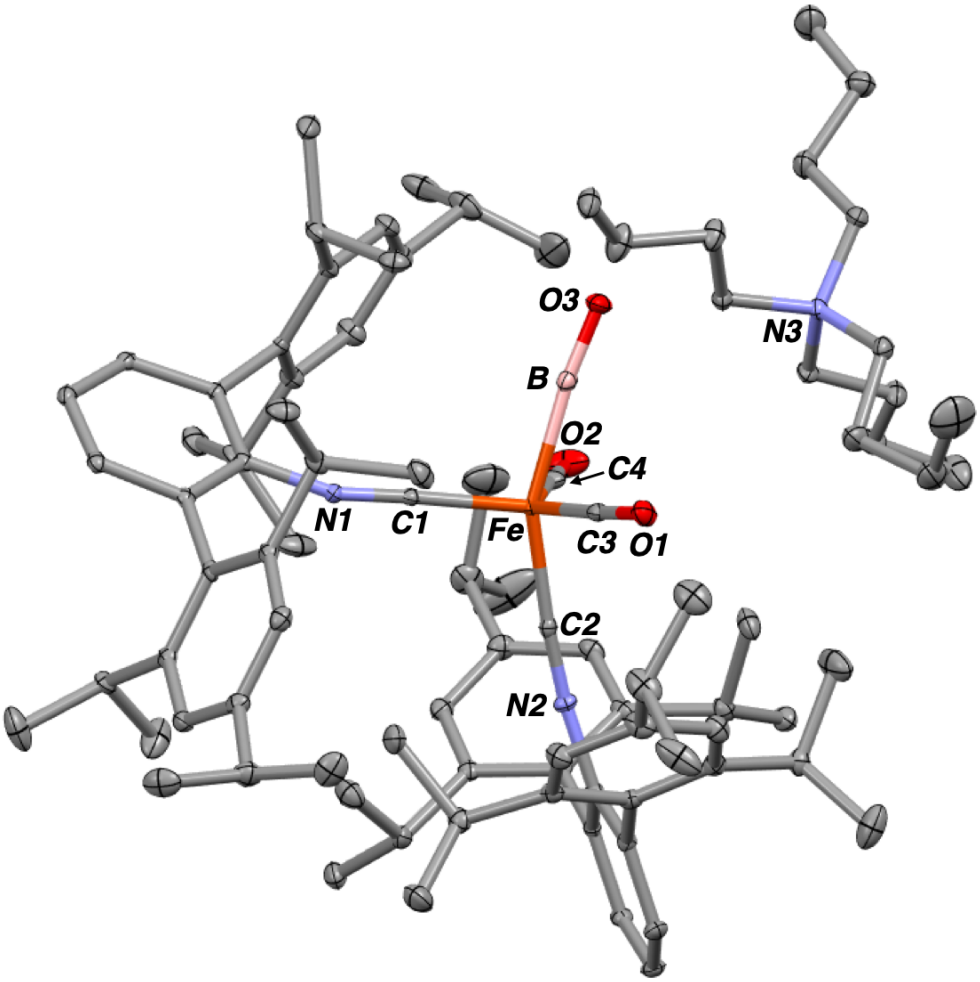


Figure 4.10. Solid-state structure of $NBu_4[Fe(BO)(CO)_2(CNAr^{Tripp2})_2]$ ($NBu_4$[**9**]).

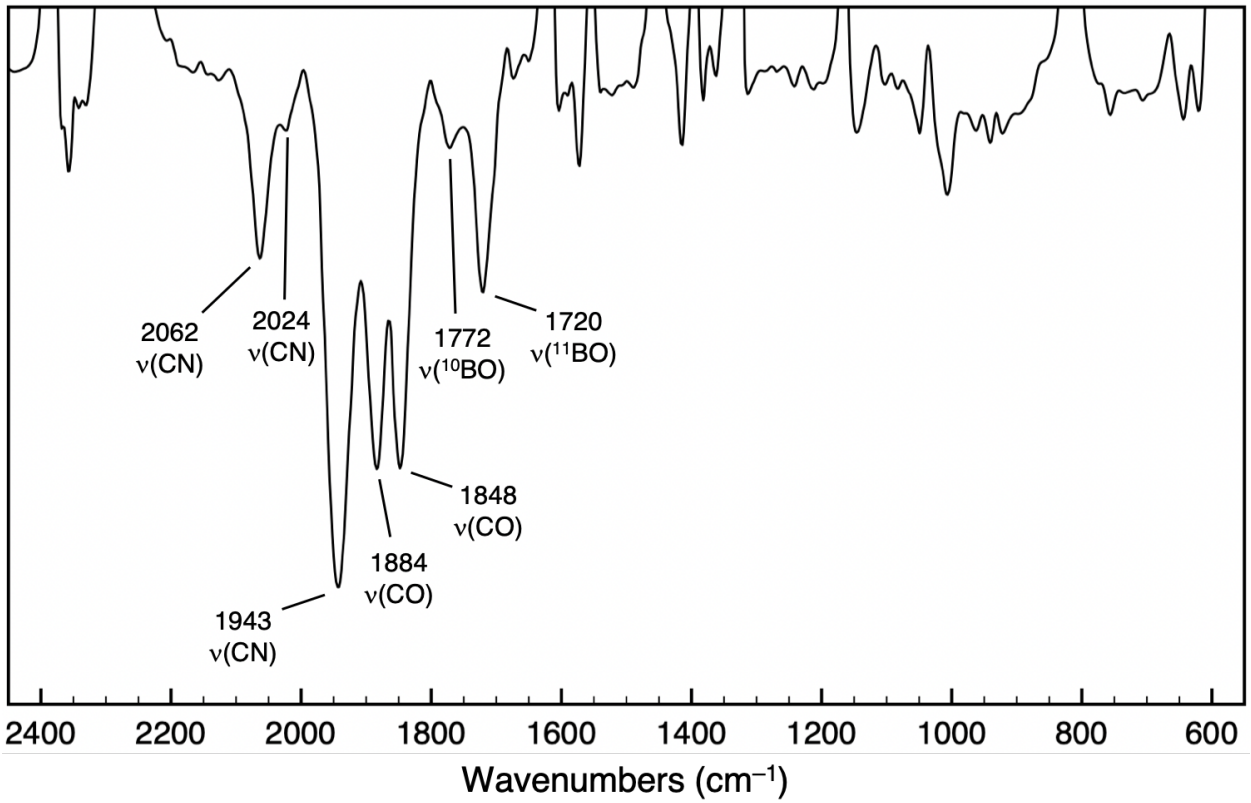


Figure 4.11. Solution FTIR spectrum of **9** recorded in $C_6D_6$ at 25 ˚C with KBr windows. Selected stretching bands are labeled.

Over the course of these investigations, it was observed that the solution FTIR spectrum of **1** often displays four CO stretches instead of two, but $^{1}H$, $^{19}F$, and $^{11}B$ NMR spectroscopy show only one compound. This suggests that compound **1** isomerizes between at least two geometries faster than the NMR timescale but slow enough to be detected by IR spectroscopy. Fortuitously, in a couple isolated incidents, $Fe(BF)(CO)_2(CNAr^{Tripp2})_2$ crystallized into a new distorted square pyramidal geometry ($\tau_5 = 0.23$) that is somewhat similar to $[\mathbf{9}]^-$ (**1'**; Figure 4.12). The B-F distance in **1'** is even shorter than in **1** (1.245 vs. 1.277 Å), but we still refrain from invoking any significant π donation from fluorine to boron. In an attempt to determine the energy difference between **1** and **1'**, variable temperature IR (VT-IR) measurements were performed. However, the ratio of the two

pairs of CO stretches appeared unchanged between the temperature range –60˚ C – 50 ˚C. Additionally, two-dimensional IR experiments failed to elucidate any information as a result of low intensity bands from **1'** and decomposition occurring before a cross-peak could be identified. These two geometries evidently are very close in energy, and the only known factor to favor one geometry over the other is crystal packing; the crystal structure of **1'** contains co-crystallized benzene.

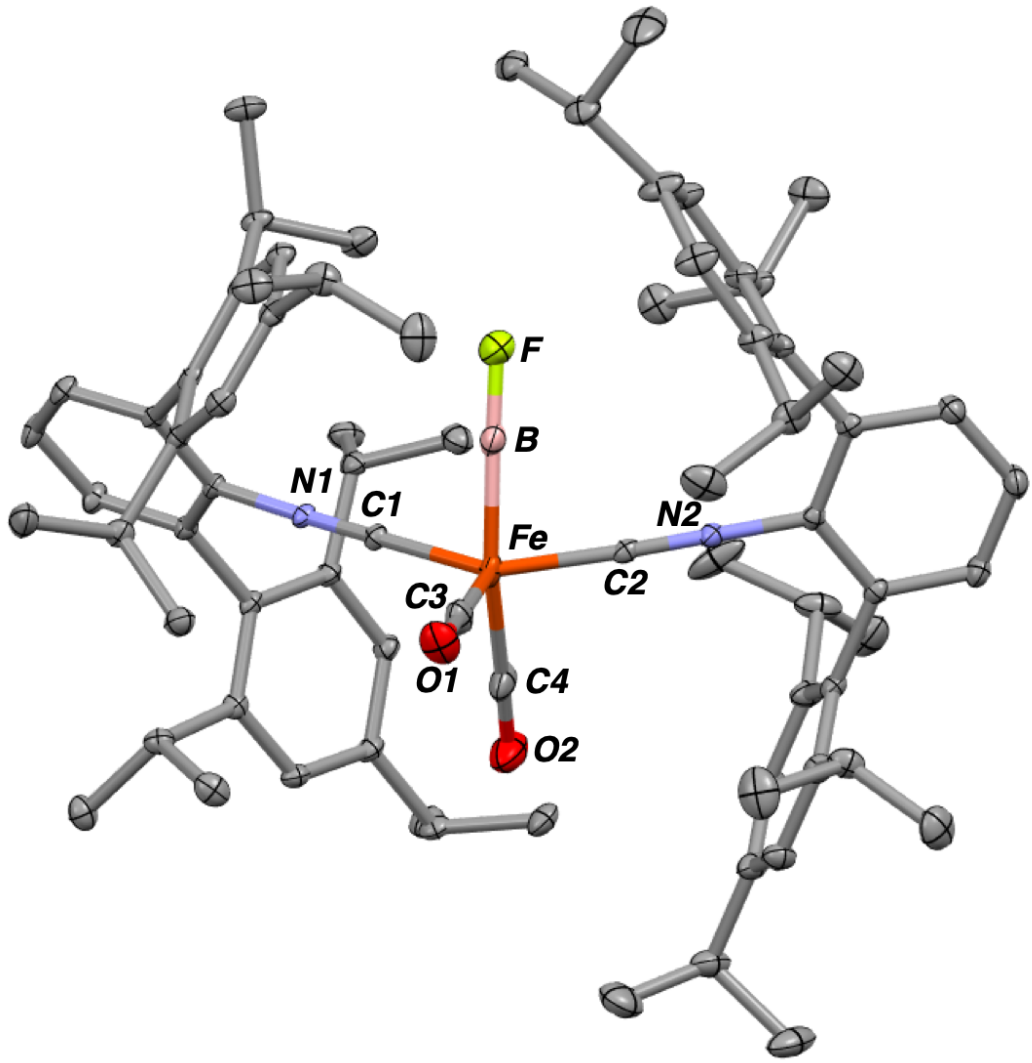


Figure 4.12. Solid-state structure of pseudo-square pyramidal $Fe(BF)(CO)_2(CNAr^{Tripp2})_2$ (**1'**).

## 4.5 Concluding Remarks

In summary, we have shown that boron monofluoride coordinated to iron is susceptible to nucleophilic attack at boron. We have provided experimental evidence to suggest that the fluoroborylene ligand of **1** is formed by fluoride abstraction from an anionic difluoroboryl intermediate. Reaction with other nucleophiles resulted in novel boryl, base-stabilized borylene, and aminoborylene functionalities. We have shown that a bis(trimethylsilyl)aminoborylene can be directly converted to the first anionic iminoboryl complex. While early aminoborylene and iminoboryl complexes both possessed trimethylsilyl substituents,[14,37] interconversion between these ligand types has never been reported. Separately, direct conversion of **1** to the first anionic oxoboryl complex can be achieved in a manner functionally similar to yet operationally distinct from the synthesis of other oxoboryl species. To the best of our knowledge, this is the only case where the same metal center has been shown to support all of these ligand types.

## 4.6 Synthetic Procedures and Characterization Data

**General Considerations.** All manipulations were carried out under an atmosphere of purified dinitrogen using standard Schlenk and glovebox techniques. Unless otherwise stated, reagent-grade starting materials were purchased from commercial sources and either used as received or purified by standard procedures.[46] Solvents were dried and deoxygenated according to standard procedures.[47] Benzene-$d_6$ (Cambridge Isotope Laboratories) was distilled from NaK alloy/benzophenone and stored over activated 3 Å molecular sieves for 2 d prior to use. Celite 405 (Fischer Scientific) was dried under vacuum at a temperature above 250 ˚C for 24 h and stored in a glovebox prior to use. $Fe(BF)(CO)_2(CNAr^{Tripp2})_2$ was synthesized as previously reported.[30]

Solution $^{1}H$, $^{13}C\{^{1}H\}$, $^{11}B$, and $^{19}F$ NMR spectra were recorded on a Varian X-SENS 500 or a JEOL ECA 500 spectrometer equipped with a two-channel, broadband, inverse-detect 5 mm probe. $^{1}H$ and $^{13}C\{^{1}H\}$ chemical shifts are reported in ppm relative to $SiMe_4$ ($^{1}H$ and $^{13}C$ $\delta = 0.0$ ppm) with reference to residual solvent resonances of 7.16 ppm ($^{1}H$) and 128.06 ppm ($^{13}C$) for $C_6D_6$.[48] $^{11}B$ NMR chemical shifts were referenced externally to $BF_3 \cdot OEt_2$ ($\delta = 0.0$ ppm). $^{19}F$ NMR chemical shifts were referenced externally to $C_6H_5F$ ($\delta = -113.11$ ppm in $C_6D_6$.[49] Solution FTIR spectra were recorded on a Thermo-Nicolet iS10 FTIR spectrometer using a ThermoFisher solution cell equipped with KBr windows. Solvent peaks were digitally subtracted from all solution FTIR spectra by comparison with an authentic solvent spectrum obtained prior to that of the sample. The following abbreviations were used for the intensities and characteristics of important IR absorption bands: vs = very strong, s = strong, m = medium, w = weak, vw = very weak; sh = shoulder.

**Preparation of $Cs[Fe(BF_2)(CO)_2(CNAr^{Tripp2})_2]$ (2).** To a 20 mL scintillation vial charged with CsF (10 equiv.) was added a DME solution of **1** (5 mL). The resulting suspension was stirred at room temperature for 4 hours, after which time the red solution was filtered through Celite into a clean vial. The solvent was removed *in vacuo*, and the solid was stirred in *n*-pentane (~2 mL) for 5 minutes before evaporating to dryness. This process was repeated three times to ensure the removal of solubilized CsF. The golden yellow $Cs[Fe(BF_2)(CO)_2(CNAr^{Tripp2})_2]$ powder was extracted in $Et_2O$, filtered through a fiberglass filter pipet, and evaporated once more. The material was purified by recrystallization from *n*-pentane/$Et_2O$ (9:1) overnight at –35 ˚C giving diffraction quality crystals. $^{1}H$ NMR (499.8 MHz, $C_6D_6$, 20 ˚C): $\delta = 7.21$ (s, 8H, *m*-Tripp), 6.94 (d, $J = 7.1$ Hz, 4H, *m*-Ph), 6.85 (t, $J = 7.6$ Hz, 2H, *p*-Ph), 2.95 (sept, $J = 6.9$ Hz, 4H, C*H*$(CH_3)_2$), 2.87 (sept, *J*

= 6.9 Hz, 8H, C*H*($CH_3$)$_2$), 1.39 (d, *J* = 7.0 Hz, 24H, CH(C*H*$_3$)$_2$), 1.38 (d, *J* = 6.9 Hz, 24H, CH(C*H*$_3$)$_2$), 1.11 (d, *J* = 6.9 Hz, 24H, CH(C*H*$_3$)$_2$) ppm. $^{13}C\{^1H\}$ NMR (125.7 MHz, $C_6D_6$, 20 ˚C): δ = 212.9, 212.6, 148.7, 147.4, 136.49, 136.46, 136.35, 130.4, 123.8, 121.4, 34.8, 31.2, 24.9, 24.5, 23.6 ppm. $^{11}B$ NMR (160.4 MHz, $C_6D_6$, 20 ˚C): δ = 46.8 ppm (br s). $^{19}F$ NMR (470.4 MHz, $C_6D_6$, 20 ˚C): δ = –8.29 ppm (br s).

**Synthesis of Fe(BF)(CO)$_2$(CNAr$^{Tripp2}$)$_2$ (1) from Cs[Fe(BF$_2$)(CO)$_2$(CNAr$^{Tripp2}$)$_2$] (2).** A thawing $Et_2O$ solution of **2** (5 mL) was treated with an equally cold solution of $BF_3{\cdot}Et_2O$ in $Et_2O$ (1.9 equiv.) in a liquid nitrogen cooled cold well. This solution was stirred at room temperature for 30 s, then re-chilled for 1 min, and this process was repeated five times before allowing the solution to stir at room temperature for 10 min, during which time, the solution changed from red to yellow/brown. Analysis of the crude reaction mixture by $^1H$ and $^{19}F$ NMR revealed **1** to be the major product.

**Preparation of Fe(BF$_2$)$_2$(CO)$_2$(CNAr$^{Tripp2}$)$_2$ (3).** $K_2$[Fe(CO)$_2$(CNAr$^{Tripp2}$)$_2$] was dissolved in 4 mL toluene and frozen in a liquid nitrogen-cooled cold well. $BF_3{\cdot}Et_2O$ (3.0 equiv.) was dissolved in a separate vial of toluene (2 mL), which was also frozen. The two solutions were combined upon thawing and allowed to stir at room temperature for 1 min, then re-chilled for 2 minutes. The vial that contained the $BF_3{\cdot}Et_2O$ was rinsed with another 1 mL toluene, cooled, and added to the reaction vial. The cooling and stirring process was repeated five times before allowing the solution to stir at room temperature for 10 min, during which time, the solution changed from red to yellow/brown. All volatiles were removed *in vacuo*, and the resulting yellow solid was subjected to three cycles of stirring in *n*-pentane and evaporating solvent before being filtered

through Celite to remove the salt byproducts. The solid was re-dissolved in *n*-hexane/$Et_2O$ (9:1) with 2 drops of benzene and set at –35 ˚C overnight revealing pale yellow blocks suitable for X-ray diffraction. $^1$H NMR (300 MHz, $C_6D_6$, 20 ˚C): δ = 7.22 (s, 8H, *m*-Tripp), 6.94 (d, *J* = 7.1 Hz, 4H, *m*-Ph), 6.87 (t, *J* = 7.0 Hz, 2H, *p*-Ph), 2.95 (sept, *J* = 6.4 Hz, 4H, C*H*$(CH_3)_2$), 2.68 (sept, *J* = 6.5 Hz, 8H, C*H*$(CH_3)_2$), 1.40 (d, *J* = 6.7 Hz, 24H, CH(C*H*$_3)_2$), 1.36 (d, *J* = 6.7 Hz, 24H, CH(C*H*$_3)_2$), 1.10 (d, *J* = 6.4 Hz, 24H, CH(C*H*$_3)_2$) ppm. $^{11}$B NMR (96 MHz, $C_6D_6$, 20 ˚C): δ = 44.2 ppm (br s). $^{19}$F NMR (282 MHz, $C_6D_6$, 20 ˚C): δ = 2.58 ppm (partially collapsed quartet, *J* = 181 Hz). FT-IR ($C_6D_6$, KBr Windows, 25 ˚C): ν(C≡N) = 2100 (vs) cm$^{-1}$, ν(C≡O) = 1992 (s), 1944 (s) cm$^{-1}$, also 1608 (m), 1542 (w), 1469 (vw), 1442 (vw), 1384 (w), 1362 (vw), 1319 (w), 1271 (vw), 1218 (w), 1149 (w), 1007 (vw), 960 (vw), 917 (w), 879 (vw), 760 (w), 706 (vw), and 609 (m) cm$^{-1}$.

**Preparation of Fe(B(F)(DMAP))$(CO)_2$$(CNAr^{Tripp2})_2$ (4).** Compound **1** and 4-dimethylaminopyridine (0.95 equiv.) were separately dissolved in 3 mL $Et_2O$ and frozen in a liquid nitrogen-cooled cold well. Upon thawing, the solution of DMAP was added to **1** over the course of 2 minutes, and the solution quickly turned from yellow to dark brown. The reactions was stirred at room temperature for 25 minutes before evaporating the solvent. The dark yellow solid was dissolved in *n*-pentane/$Et_2O$ (1:1) and stored overnight at –35 ˚C depositing blackish-yellow crystals of mostly pure Fe(B(F)(DMAP))$(CO)_2$$(CNAr^{Tripp2})_2$. Crystals suitable for X-ray diffraction were grown from the first crystal harvest in $Et_2O$/toluene (20:1) over two days at –35 ˚C. $^1$H NMR (499.8 MHz, $C_6D_6$, 20 ˚C): δ = 8.20 (d, *J* = 7.3 Hz, 2H), 7.21 (s, 8H, *m*-Tripp), 6.96 (d, *J* = 7.5 Hz, 4H, *m*-Ph), 6.82 (dd, *J* = 7.9, 7.0 Hz, 2H, *p*-Ph), 5.82 (d, *J* = 7.3 Hz, 2H), 2.98 (m, 12H, C*H*$(CH_3)_2$), 2.04 (s, 6H, N(C*H*$_3)_2$), 1.45 (d, *J* = 6.9 Hz, 24H, CH(C*H*$_3)_2$), 1.39 (d, *J* = 6.9 Hz, 24H, CH(C*H*$_3)_2$), 1.23 (d, *J* = 6.7 Hz, 24H, CH(C*H*$_3)_2$) ppm. $^{11}$B NMR (160.4 MHz, $C_6D_6$, 20 ˚C):

δ = 74.0 ppm (br s) *tentative. $^{19}$F NMR (470.4 MHz, $C_6D_6$, 20 ˚C): δ = –6.19 ppm (br s). FT-IR ($Et_2O$, KBr Windows, 25 ˚C): ν(C≡N) = 2052 (m), 1946 (s), 1915 (s) $cm^{-1}$, ν(C≡O) = 1903 (s), 1862 (s) $cm^{-1}$, also 1640 (m), 1612, (vw), 1571 (vw), 1559 (vw), 1265 (vw), 927 (w), 873 (w), 841 (vw), 816 (m), 752 (w), 723 (w), 679 (w), 668 (w), 647 (w), 598 (w), 514 (vw), and 490 (w) $cm^{-1}$.

**Preparation of Fe(BN(SiMe$_3$)$_2$)(CO)$_2$(CNAr$^{Tripp2}$)$_2$ (5).** To a thawing $Et_2O$ solution of **1** (5 mL) was added a room temperature solution of NaN(SiMe$_3$)$_2$ in $Et_2O$ (1.05 equiv., 1 mL) over 1 minute. The reaction was stirred at room temperature for 30 minutes, and volatiles were removed *in vacuo*. The resulting brown solid was stirred in *n*-pentane for 3 minutes and dried three times to liberate solvated NaF. Successive washes with *n*-pentane left behind pure Fe(BN(SiMe$_3$)$_2$)(CO)$_2$(CNAr$^{Tripp2}$)$_2$ as an orange solid in moderate yield, and yield was maximized by recrystallizing from the wash. Diffraction quality crystals were grown from *n*-pentane/benzene (9:1) at –35˚ C overnight. $^1$H NMR (499.8 MHz, $C_6D_6$, 20 ˚C): δ = 7.25 (s, 8H, *m*-Tripp), 6.95 (d, *J* = 7.5 Hz, 4H, *m*-Ph), 6.83 (t, *J* = 7.5 Hz, 2H, *p*-Ph), 3.02 (sept, *J* = 6.8 Hz, 4H, C*H*(CH$_3$)$_2$), 2.89 (sept, *J* = 6.6 Hz, 8H, C*H*(CH$_3$)$_2$), 1.43 (d, *J* = 6.8 Hz, 24H, CH(C*H*$_3$)$_2$), 1.40 (d, *J* = 6.8 Hz, 24H, CH(C*H*$_3$)$_2$), 1.20 (d, *J* = 6.7 Hz, 24H, CH(C*H*$_3$)$_2$), 0.10 (s, 18 H, Si(C*H*$_3$)$_2$) ppm. $^{13}$C{$^1$H} NMR (125.7 MHz, $C_6D_6$, 20 ˚C): δ = 219.5 (*C*O), 188.5 (*C*NR), 148.6, 146.5, 137.5, 134.2, 131.1, 130.9, 125.1, 121.5, 35.0, 31.3, 24.9, 24.8, 24.5, 3.1 ppm. $^{11}$B NMR (160.4 MHz, $C_6D_6$, 20 ˚C): δ = 88.5 ppm (br s). FT-IR ($C_6D_6$, KBr Windows, 25 ˚C): ν(C≡N) = 2084 (s), 2060 (m), 2021 (vs), $cm^{-1}$, ν(C≡O) = 1990 (vs), 1954 (m), 1924 (vs) $cm^{-1}$, also 3046 (vw), 2959 (vs), 2930 (s), 2904 (m), 2870 (s), 1607 (w), 1570 (w), 1542 (vw), 1461 (w), 1428 (w), 1384 (vw), 1365 (w), 1253 (m),

1243 (vw), 1153 (vw), 1104 (vw), 1053 (w), 941 (w), 868 (m), 756 (w), 735 (vw), 702 (vw), 646 (m) $cm^{-1}$.

**Preparation of [Li($Et_2O$)][Fe(B(F)N(*i*-Pr)$_2$)(CO)$_2$($CNAr^{Tripp2}$)$_2$] (6).** **1** was frozen in $Et_2O$ (5 mL), and while thawing, a room temperature $Et_2O$/DME (9:1) solution of LiN(*i*-Pr)$_2$ (1.0 equiv., 3 mL) was slowly added over the course of 3 minutes. The mixture was chilled in the cold well for another 4 minutes before stirring at room temperature for 25 minutes. Volatiles were removed, and [Li($Et_2O$)][Fe(B(F)N(*i*-Pr)$_2$)(CO)$_2$($CNAr^{Tripp2}$)$_2$] was extracted in *n*-pentane. The volume of this solution was reduced to ~1 mL, and 5 drops of $Et_2O$ were added. Storage of this solution at –35 ˚C for two days produced diffraction quality crystals. $^1$H NMR (300 MHz, $C_6D_6$, 20 ˚C): δ = 7.29 (s, 8H, *m*-Tripp), 6.95 (d, *J* = 7.1 Hz, 4H, *m*-Ph), 6.84 (t, *J* = 7.9 Hz, 2H, *p*-Ph), 2.98 (sept, *J* = 6.9 Hz, 4H, C*H*($CH_3$)$_2$), 2.92 (sept, *J* = 6.8 Hz, 8H, C*H*($CH_3$)$_2$), 1.40 (d, *J* = 6.8 Hz, 24H, CH(C*H*$_3$)$_2$), 1.34 (d, *J* = 6.6 Hz, 24H, CH(C*H*$_3$)$_2$), 1.18 (d, *J* = 6.6 Hz, 24H, CH(C*H*$_3$)$_2$) ppm. $^{11}$B NMR (160.4 MHz, $C_6D_6$, 20 ˚C): δ = 46.2 ppm (br s) *tentative. $^{19}$F NMR (470.4 MHz, $C_6D_6$, 20 ˚C): δ = –41.65 ppm (br s).

**Preparation of Cs[Fe{B(N($SiMe_3$)}(CO)$_2$($CNAr^{Tripp2}$)$_2$] (7).** To a vial charged with CsF (15 equiv.) was added a DME/THF (1:1) solution of **5**, and the mixture was stirred for 6 hours. All volatiles were then removed by vacuum evaporation, and the solid was stirred in *n*-pentane (~2 mL) for 5 minutes before evaporating to dryness. This process was repeated three times to ensure the full precipitation of solvated CsF. Gently washing the product with 5 x 1 mL *n*-pentane left behind spectroscopically pure Cs[Fe{B(N($SiMe_3$)}(CO)$_2$($CNAr^{Tripp2}$)$_2$]. Single crystals suitable for X-ray diffraction were grown from *n*-pentane/$Et_2O$ (5:1) with a drop of benzene. $^1$H NMR

(499.8 MHz, $C_6D_6$, 20 ˚C): δ = 7.24 (s, 8H, *m*-Tripp), 6.88 (d, *J* = 7.3 Hz, 4H, *m*-Ph), 6.82 (t, *J* = 7.3 Hz, 2H, *p*-Ph), 2.99 (sept, *J* = 6.8 Hz, 4H, C*H*($CH_3$)$_2$), 2.90 (sept, *J* = 6.9 Hz, 8H, C*H*($CH_3$)$_2$), 1.43 (d, *J* = 6.7 Hz, 24H, CH(C*H*$_3$)$_2$), 1.40 (d, *J* = 6.9 Hz, 24H, CH(C*H*$_3$)$_2$), 1.15 (d, *J* = 6.6 Hz, 24H, CH(C*H*$_3$)$_2$), 0.31 (s, 9H, Si(C*H*$_3$)$_3$) ppm. $^{13}C\{^1H\}$ NMR (125.7 MHz, $C_6D_6$, 20 ˚C): δ = 206.8, 206.6, 148.6, 147.5, 136.1, 135.1, 130.3, 124.1, 121.6, 121.4, 34.7, 31.3, 24.7, 24.53, 24.48, 4.4 ppm. $^{11}B$ NMR (160.4 MHz, $C_6D_6$, 20 ˚C): δ = 55.4 ppm (br s). FT-IR ($C_6D_6$, KBr Windows, 25 ˚C): ν(C≡N) = 2072 (m), 1924 (s) cm$^{-1}$, ν(C≡O) = 1894 (s), 1813 (s) cm$^{-1}$, ν($^{11}$B≡N) = 1712 cm$^{-1}$, also 3047 (vw), 2962 (vs), 2934 (m), 2904 (w), 2869 (m), 1608 (w), 1573 (w), 1472 (vw), 1415 (w), 1384 (vw), 1361 (vw), 1240 (vw), 1243 (vw), 1149 (w), 1103 (vw), 1049 (w), 1006 (w), 941 (vw), 883 (m), 756 (m), 651 (w), 617 (w) cm$^{-1}$. *ν($^{10}$B≡N) not observable due to overlap with the lowest energy ν(C≡O).

**Preparation of {[Li(DME)][Fe(BO)(CO)$_2$(CNAr$^{Tripp2}$)$_2$]}$_2$ (8).** A solution of LiOTMS in $Et_2O$/DME (2:1; 4.2 equiv., 4 mL) was slowly added to a solution of **1** in $Et_2O$ (5 mL) at room temperature over 8 minutes, gradually darkening to orange-brown. After 40 minutes, all volatile components were removed *in vacuo*. The solid was stirred in *n*-pentane, and the volatiles were again removed. Subsequent washing with *n*-pentane revealed a spectroscopically pure bright yellow powder that showed relatively low solubility in alkane and arene solvents but very good solubility in ethereal solvents accompanied by a color change from yellow to orange. Diffraction quality crystals could be grown from $Et_2O$/DME (1:1) stored at –35 ˚C over two days. $^1H$ NMR (499.8 MHz, $C_6D_6$, 20 ˚C): δ = 7.26 (s, 8H, *m*-Tripp), 6.99 (d, *J* = 7.6 Hz, 4H, *m*-Ph), 6.86 (dd, *J* = 7.8, 7.2 Hz, 2H, *p*-Ph), 3.46 (br s, 4H, DME C*H*$_2$), 3.36 (s, 6H, DME C*H*$_3$), 3.08 (sept, *J* = 6.9 Hz, 4H, C*H*($CH_3$)$_2$), 2.95 (sept, *J* = 6.8 Hz, 8H, C*H*($CH_3$)$_2$), 1.50 (d, *J* = 6.9 Hz, 24H, CH(C*H*$_3$)$_2$),

1.37 (d, $J$ = 6.9 Hz, 24H, CH(C$H_3$)$_2$), 1.31 (d, $J$ = 6.9 Hz, 24H, CH(C$H_3$)$_2$) ppm. $^{13}$C{$^1$H} NMR (125.7 MHz, $C_6D_6$, 20 ˚C): δ = 225.5 (*C*O), 188.6 (*C*NR), 148.1, 146.6, 136.8, 134.4, 131.4, 130.0, 124.1, 120.9, 35.1, 31.3, 24.80, 24.77, 24.70 ppm. *Resonances for coordinated DME were not located. $^{11}$B NMR (160.4 MHz, $C_6D_6$, 20 ˚C): δ = N/A. $^{11}$B NMR (160.4 MHz, THF, 20 ˚C): δ = 44.3 ppm (br s). FT-IR ($C_6D_6$, KBr Windows, 25 ˚C): ν(C≡N) = 2082 (w), 1979 (vs) cm$^{-1}$, ν(C≡O) = 1928 (w), 1900 (m) cm$^{-1}$, ν($^{10}$B≡O) = 1660 (vw) cm$^{-1}$, ν($^{11}$B≡O) = 1609 (m) cm$^{-1}$, also 3047 (vw), 2962 (vs), 2934 (m), 2904 (w), 2869 (m), 1608 (w), 1573 (w), 1472 (vw), 1415 (w), 1384 (vw), 1361 (vw), 1240 (vw), 1243 (vw), 1149 (w), 1103 (vw), 1049 (w), 1006 (w), 941 (vw), 883 (m), 756 (m), 651 (w), 617 (w) cm$^{-1}$. FT-IR (THF, KBr Windows, 25 ˚C): ν(C≡N) = 2069 (m), 2026 (w), 1952 (vs) cm$^{-1}$, ν(C≡O) = 1893 (s), 1875 (s) cm$^{-1}$, ν($^{10}$B≡O) = 1744 (w) cm$^{-1}$, ν($^{11}$B≡O) = 1692 (m) cm$^{-1}$, also 3047 (vw), 2962 (vs), 2934 (m), 2904 (w), 2869 (m), 1608 (w), 1573 (w), 1472 (vw), 1415 (w), 1384 (vw), 1361 (vw), 1240 (vw), 1243 (vw), 1149 (w), 1103 (vw), 1049 (w), 1006 (w), 941 (vw), 883 (m), 756 (m), 651 (w), 617 (w) cm$^{-1}$.

**Preparation of NBu$_4$[Fe(BO)(CO)$_2$(CNAr$^{Tripp2}$)$_2$] (NBu$_4$[9]).** To a THF solution of **8** (5 mL) was slowly added a THF solution of NBu$_4$Cl (1.05 equiv., 2 mL), and the mixture was stirred for 45 minutes. The solvent was evaporated under vacuum, and the resulting solid was stirred in *n*-pentane revealing a white precipitate. The product dissolved in *n*-pentane was passed through Celite to remove LiCl. The volume was reduced to ~ 0.75 mL and ~0.05 mL benzene was added for recrystallization at –35 ˚C, which produced diffraction quality crystals of NBu$_4$[Fe(BO)(CO)$_2$(CNAr$^{Tripp2}$)$_2$] after 3 days. $^1$H NMR (499.8 MHz, $C_6D_6$, 20 ˚C): δ = 7.35 (s, 8H, *m*-Tripp), 7.08 (d, $J$ = 7.5 Hz, 4H, *m*-Ph), 6.91 (t, $J$ = 7.5 Hz, 2H, *p*-Ph), 3.14 (sept, $J$ = 6.9 Hz, 4H, C*H*(CH$_3$)$_2$), 3.08 (sept, $J$ = 6.9 Hz, 8H, C*H*(CH$_3$)$_2$), 1.55 (d, $J$ = 6.9 Hz, 24H, CH(C$H_3$)$_2$),

1.48 (d, $J$ = 6.9 Hz, 24H, CH(C$H_3$)$_2$), 1.34 (d, $J$ = 6.9 Hz, 24H, CH(C$H_3$)$_2$) ppm. *Resonances from the tetra-*n*-butylammonium cation were located as broad peaks centered at 2.58, 1.04, and 0.90 ppm with the fourth expected resonance obscured by the aliphatic doublet resonances of [9]$^-$. $^{13}$C{$^1$H} NMR (125.7 MHz, $C_6D_6$, 20 ˚C): δ = 220.1 (*C*O), 195.2 (*C*NR), 147.7, 146.6, 137.4, 135.0, 133.0, 130.2, 123.5, 121.4, 35.1, 31.4, 25.1, 24.7 ppm. *Resonances from the tetra-*n*-butylammonium cation were located as broad peaks centered at 58.1, 24.1, 19.9 and 14.1 ppm. $^{11}$B NMR (160.4 MHz, $C_6D_6$, 20 ˚C): δ = 42.9 ppm (br s). FT-IR ($C_6D_6$, KBr Windows, 25 ˚C): ν(C≡N) = 2062 (m), 2024 (w), 1943 (vs) cm$^{-1}$, ν(C≡O) = 1884 (s), 1848 (s) cm$^{-1}$, ν($^{10}$B≡O) = 1772 (w) cm$^{-1}$, ν($^{11}$B≡O) = 1720 (m) cm$^{-1}$, also 3047 (vw), 2962 (vs), 2934 (m), 2904 (w), 2869 (m), 1608 (w), 1573 (w), 1472 (vw), 1415 (w), 1384 (vw), 1361 (vw), 1240 (vw), 1243 (vw), 1149 (w), 1103 (vw), 1049 (w), 1006 (w), 941 (vw), 883 (m), 756 (m), 651 (w), 617 (w) cm$^{-1}$.

## 4.7 Details of Crystallographic Structure Determinations

**General.** Single X-ray structure determinations were performed at 100 K on Bruker Kappa diffractometers equipped with either a Mo or Cu radiation source and an APEX-II CCD area detector. All structures were solved via direct methods with SHELXS[50] and refined by full-matrix least-squares procedures using SHELXL[50] within the Olex2[51] software. All hydrogen atoms have been removed for clarity. Disordered components and co-crystallized solvent molecules are not shown for clarity.

Table 4.1. Crystallographic Data Collection and Refinement Information.

| Name | $Cs[Fe(BF_2)(CO)_2(CNAr^{Tripp2})_2]$ (**2**) | $Fe(BF_2)_2(CO)_2(CNAr^{Tripp2})_2$ (**3**) | $Fe(B(F)(DMAP))(CO)_2(CNAr^{Tripp2})_2$ (**4**)•1.8 $C_7H_8$ |
|---|---|---|---|
| Formula | $C_{76}H_{98}BCsF_2FeN_2O_2$ | $C_{76}H_{98}B_2F_4FeN_2O_2$ | $C_{95.6}H_{122.4}BFFeN_4O_2$ |
| Crystal System | Monoclinic | Monoclinic | Monoclinic |
| Space Group | $C2_1/c$ | $P2_1/n$ | $P2_1/c$ |
| *a*, Å | 18.7574(11) | 16.9225(9) | 14.7834(4) |
| *b*, Å | 15.6659(9) | 17.1531(9) | 32.4182(8) |
| *c,* Å | 25.2313(15) | 25.7017(13) | 17.9764(5) |
| α, deg | 90 | 90 | 90 |
| β, deg | 107.5700(10) | 107.4810(10) | 92.772(2) |
| γ, deg | 90 | 90 | 90 |
| V, $Å^3$ | 7068.5(7) | 7116.0(6) | 8605.1(4) |
| *Z* | 4 | 4 | 4 |
| Radiation (λ, Å) | Mo-Kα, 0.71073 | Mo-Kα, 0.71073 | Mo-Kα, 0.71073 |
| ρ (calcd.), $Mg/m^3$ | 1.230 | 1.143 | 1.116 |
| μ (Mo Kα), $mm^{-1}$ | 0.771 | 0.267 | 0.226 |
| Temp, K | 100 | 100 | 100 |
| θ max, deg | 25.435 | 25.735 | 25.392 |
| data/ parameters | 6537/485 | 13558/960 | 15797/971 |
| $R_1$ | 0.0347 | 0.0761 | 0.0685 |
| $wR_2$ | 0.0812 | 0.2029 | 0.1584 |
| GOF | 1.069 | 1.047 | 1.049 |

Table 4.2. Crystallographic Data Collection and Refinement Information.

| Name | $Fe(BN(SiMe_3)_2)(CO)_2(CNAr^{Tripp2})_2$ (**5**)•$C_6H_6$ | $Li[Fe(B(F)N(i\text{-}Pr)_2)(CO)_2(CNAr^{Tripp2})_2]$ (**6**)•1.75$Et_2O$ | $Cs[Fe\{BN(SiMe_3)\}(CO)_2(CNAr^{Tripp2})_2]$ (**7**) |
|---|---|---|---|
| Formula | $C_{88}H_{122}BFeN_3O_2Si_2$ | $C_{89}H_{129.5}BFFeLiN_3O_{3.75}$ | $C_{95.6}H_{122.4}BFFeN_4O_2$ |
| Crystal System | Triclinic | Triclinic | Monoclinic |
| Space Group | *P*–1 | *P*–1 | $P2_1/n$ |
| *a*, Å | 12.6768(14) | 12.6519(2) | 15.6847(5) |
| *b*, Å | 13.9335(12) | 14.7464(2) | 32.2948(11) |
| *c,* Å | 24.860(3) | 24.2692(4) | 17.7360(6) |
| α, deg | 85.385(3) | 76.6970(10) | 90 |
| β, deg | 86.433(3) | 80.8360(10) | 91.958(2) |
| γ, deg | 78.787(4) | 81.9470(10) | 90 |
| V, $Å^3$ | 4288.4(7) | 4368.91(12) | 8978.6(5) |
| *Z* | 2 | 2 | 4 |
| Radiation (λ, Å) | Mo-Kα, 0.71073 | Cu-Kα, 1.54178 | Mo-Kα, 0.71073 |
| ρ (calcd.), $Mg/m^3$ | 1.066 | 1.059 | 1.005 |
| μ (Mo Kα), $mm^{-1}$ | 0.249 | 1.753 | 0.619 |
| Temp, K | 100 | 100 | 100 |
| θ max, deg | 25.405 | 68.346 | 25.480 |
| data/ parameters | 15757/1072 | 15318/1042 | 16605/892 |
| $R_1$ | 0.0612 | 0.0719 | 0.0974 |
| $wR_2$ | 0.1550 | 0.2106 | 0.2046 |
| GOF | 1.019 | 1.052 | 1.196 |

Table 4.3. Crystallographic Data Collection and Refinement Information.

| Name | {[Li(DME)][Fe(BO)(CO)$_2$(CNAr$^{Tripp2}$)$_2$]}$_2$ (**8**)•DME | NBu$_4$[Fe(BO)(CO)$_2$(CNAr$^{Tripp2}$)$_2$] (NBu$_4$[**9**]) | Fe(BF)(CO)$_2$(CNAr$^{Tripp2}$)$_2$] (**1'**)•C$_6$H$_6$ |
|---|---|---|---|
| Formula | $C_{164}H_{226}B_2Fe_2Li_2N_4O_{12}$ | $C_{92}H_{134}BFeN_3O_3$ | $C_{82}H_{104}BFFeN_2O_2$ |
| Crystal System | Triclinic | Monoclinic | Triclinic |
| Space Group | *P*–1 | *P*2$_1$/*c* | *P*–1 |
| *a*, Å | 14.3145(10) | 21.348(2) | 15.2991(5) |
| *b*, Å | 15.2736(10) | 15.6788(15) | 16.4687(6) |
| *c,* Å | 20.9347(14) | 29.283(3) | 18.2117(6) |
| α, deg | 82.400(2) | 90 | 64.4580(10) |
| β, deg | 73.984(2) | 107.1300(10) | 76.7390(10) |
| γ, deg | 65.128(2) | 90 | 88.4430(10) |
| V, Å$^3$ | 3990.6(5) | 9366.5(15) | 4016.3(2) |
| *Z* | 2 | 4 | 2 |
| Radiation (λ, Å) | Mo-Kα, 0.71073 | Mo-Kα, 0.71073 | Mo-Kα, 0.71073 |
| ρ (calcd.), Mg/m$^3$ | 1.079 | 0.990 | 1.022 |
| μ (Mo Kα), mm$^{-1}$ | 0.238 | 0.205 | 0.232 |
| Temp, K | 100 | 100 | 100 |
| θ max, deg | 21.967 | 25.027 | 26.418 |
| data/ parameters | 9722/865 | 16441/975 | 16456/885 |
| $R_1$ | 0.0537 | 0.0552 | 0.0637 |
| $wR_2$ | 0.1092 | 0.1250 | 0.1599 |
| GOF | 1.022 | 1.016 | 1.026 |

## 4.8 Acknowledgments

**Chapter 4**: This chapter is currently in preparation as a manuscript by Drance, M. J.; Sears, J. D.; Gembicky, M; Rheingold, A. L.; Neidig, M. L.; Figueroa, J. S. The dissertation author is the first author of this paper.

## 4.9 References

(1) Schutzenberger, M. P. *Annales Chim. Physique (Paris)* **1868**, *15*, 100-106.

(2) Mond, L.; Langer, C.; Quincke, F. *J. Chem. Soc., Trans.* **1890**, *57* (0), 749–753.

(3) Werner, H. *Angew. Chem. Int. Ed. Engl.* **1990**, *29* (10), 1077–1089.

(4) Herrmann, W. A. *Journal of Organometallic Chemistry* **1990**, *383* (1-3), 21–44.

(5) Elian, M.; Hoffmann, R. *Inorg. Chem.* **1975**, *14* (5), 1058–1076.

(6) Ehlers, A. W.; Dapprich, S.; Vyboishchikov, S. F.; Frenking, G. *Organometallics* **1996**, *15* (1), 105–117.

(7) Cotton, F. A.; Kraihanzel, C. S. *J. Am. Chem. Soc.* **1962**, *84* (23), 4432–4438.

(8) Huang, H.; Hughes, R. P.; Landis, C. R.; Rheingold, A. L. *J. Am. Chem. Soc.* **2006**, *128* (23), 7454–7455.

(9) Huang, H.; Hughes, R. P.; Rheingold, A. L. *Dalton Trans.* **2011**, *40* (1), 47–55.

(10) Pell, C. J.; Zhu, Y.; Huacuja, R.; Herbert, D. E.; Hughes, R. P.; Ozerov, O. V. *Chem. Sci.* **2017**, *8* (4), 3178–3186.

(11) Braunschweig, H.; Radacki, K.; Schneider, A. *Science* **2010**, *328* (5976), 345–347.

(12) Uddin, J.; Boehme, C.; Frenking, G. *Organometallics* **2000**, *19* (4), 571–582.

(13) Cowley, A. H.; Lomelí, V.; Voigt, A. *J. Am. Chem. Soc.* **1998**, *120* (25), 6401–6402.

(14) Braunschweig, H.; Kollann, C.; Englert, U. *Angew. Chem. Int. Ed.* **1998**, *37* (22), 3179–3180.

(15) Braunschweig, H.; Rais, D. *Heteroatom Chemistry* **2005**, *16* (7), 566–571.

(16) Vidovic, D.; Pierce, G. A.; Aldridge, S. *Chem. Commun.* **2009**, *9* (10), 1157–1171.

(17) Braunschweig, H.; Dewhurst, R. D.; Schneider, A. *Chem. Rev.* **2010**, *110* (7), 3924–3957.

(18) Braunschweig, H.; Dewhurst, R. D.; Gessner, V. H. *Chem. Soc. Rev.* **2013**, *42* (8), 3197–3208.

(19) Ehlers, A. W.; Baerends, E. J.; Bickelhaupt, F. M.; Radius, U. *Chem. Eur. J.* **1998**, *4* (2), 210–221.

(20) Udo Radius; F Matthias Bickelhaupt; Andreas W Ehlers; Norman Goldberg, A.; Hoffmann, R. **1998**.

(21) Matthias Bickelhaupt, F.; Radius, U.; Ehlers, A. W.; Hoffmann, R.; Jan Baerends, E. *New J. Chem.* **1998**, *22* (1), 1–3.

(22) Timms, P. L. *J. Am. Chem. Soc.* **1967**, *89* (7), 1629–1632.

(23) Timms, P. L. *Acc. Chem. Res.* **1973**, *6* (4), 118–123.

.

(24) Wang, X.; Roos, B. O.; Andrews, L. *Angew. Chem. Int. Ed.* **2009**, *49* (1), 157–160.

(25) Wang, X.; Roos, B. O.; Andrews, L. *Chemical Communications* **2010**, *46* (10), 1646–1648.

(26) Xu, B.; Li, L.; Pu, Z.; Yu, W.; Li, W.; Wang, X. *Inorg. Chem.* **2019**, *58* (4), 2363–2371.

(27) Xu, B.; Li, W.; Pu, Z.; Yu, W.; Huang, T.; Cheng, J.; Wang, X. *Phys. Chem. Chem. Phys.* **2019**, *21* (46), 25577–25583.

(28) Vidovic, D.; Aldridge, S. *Angew. Chem. Int. Ed.* **2009**, *48* (20), 3669–3672.

(29) Carpenter, A. E.; Mokhtarzadeh, C. C.; Ripatti, D. S.; Havrylyuk, I.; Kamezawa, R.; Moore, C. E.; Rheingold, A. L.; Figueroa, J. S. *Inorg. Chem.* **2015**, *54* (6), 2936–2944.

(30) Drance, M. J.; Sears, J. D.; Mrse, A. M.; Moore, C. E.; Rheingold, A. L.; Neidig, M. L.; Figueroa, J. S. *Science* **2019**, *363* (6432), 1203–1205.

(31) Kerr, A.; Norman, N. C.; Orpen, A. G.; Quayle, M. J.; Rice, C. R.; Timms, P. L.; Whittell, G. R.; Kerr, A.; Marder, T. B. *Chemical Communications* **1998**, *0* (3), 319–320.

(32) Lu, N.; Norman, N. C.; Orpen, A. G.; Quayle, M. J.; Timms, P. L.; Whittell, G. R. *J. Chem. Soc., Dalton Trans.* **2000**, *0* (22), 4032–4037.

(33) Bauer, J.; Braunschweig, H.; Kraft, K.; Radacki, K. *Angew. Chem. Int. Ed.* **2011**, *50* (44), 10457–10460.

(34) Braunschweig, H.; Radacki, K.; Seeler, F.; Whittell, G. R. *Organometallics* **2006**, *25* (19), 4605–4610.

(35) Aldridge, S.; Jones, C.; Gans-Eichler, T.; Stasch, A.; Kays, D. L.; Coombs, N. D.; Willock, D. J. *Angew. Chem. Int. Ed. Engl.* **2006**, *45* (37), 6118–6122.

(36) Braunschweig, H.; Kramer, T.; Radacki, K.; Shang, R.; Siedler, E.; Werner, C. *Chemical Science* **2014**, *5* (6), 2271–2276.

(37) Braunschweig, H.; Radacki, K.; Rais, D.; Uttinger, K. *Angew. Chem. Int. Ed. Engl.* **2006**, *45* (1), 162–165.

(38) Addison, A. W.; Rao, T. N.; Reedijk, J.; van Rijn, J.; Verschoor, G. C. *J. Chem. Soc., Dalton Trans.* **1984**, *0* (7), 1349–1356.

(39) Braunschweig, H.; Kupfer, T.; Radacki, K.; Schneider, A.; Seeler, F.; Uttinger, K.; Wu, H. *J. Am. Chem. Soc.* **2008**, *130* (25), 7974–7983.

(40) Brand, J.; Braunschweig, H.; Dewhurst, R. D.; Hupp, F.; Lang, K. *Eur. J. Inorg. Chem.* **2015**, *2015* (15), 2592–2595.

(41) Brand, J.; Braunschweig, H.; Sen, S. S. *Acc. Chem. Res.* **2013**, *47* (1), 180–191.

(42) Braunschweig, H.; Radacki, K.; Schneider, A. *Chem. Commun. (Camb.)* **2010**, *46* (35), 6473–6475.

(43) Cotton, F. A.; Liehr, A. D.; Wilkinson, G. *Journal of Inorganic and Nuclear Chemistry* **1955**, *1* (3), 175–186.

(44) Beck, W.; Melnikoff, A.; Stahl, R. *Angew. Chem.* **1965**, *77* (16), 719–719.

(45) Steiner, T. *Crystallography Reviews* **2003**, *9* (2-3), 177–228.

(46) Armarego, W. L. F.; Chai, C. L. L. *Purification of Laboratory Chemicals*, 5th Ed.; *Elsevier* (2003).

(47) Pangborn, A. B.; Giardello, M. A.; Grubbs, R. H.; Rosen, R. K.; Timmers, F. J. *Organometallics* **1996**, *15*, 1518–1520.

(48) Fulmer, G. R.; Miller, A. J. M.; Sherden, N. H.; Gottlieb, H. E.; Nudelman, A;. Stoltz, B. M.; Bercaw, J. E.; Goldberg, K. I. *Organometallics* **2010**, *29*, 2176.

(49) Rosenau, C. P.; Jelier, B. J.; Gossert, A. D.; Togni, A. *Angew. Chem. Int. Ed.* **2018**, *57*, 9528–9533

(50) Sheldrick, G. M. *Acta Cryst.* **2008**, *A64*, 112.

(51) Dolomanov, O. V.; Bourhis, L. J.; Gildea, R. J.; Howard, J. A. K.; Puschmann, H. *J. Appl. Cryst.* **2009**, *42*, 339.

# Chapter 5

# Small Molecule Binding and Activation by a Functional Analogue of $Fe(CO)_4$

## 5.1 Introduction

The transient species $Fe(CO)_4$ has long been viewed as a prototypical reaction intermediate by organometallic chemists.[1-3] While $Fe(CO)_4$ was first mentioned in the literature in 1891 as the product formed upon passage of carbon monoxide over activated iron,[4] more accurate results in a subsequent report corrected the formula of this volatile iron carbonyl to $Fe(CO)_5$.[5] The existence of $Fe(CO)_4$ was postulated again 14 years later as the intermediate after CO dissociation in the decomposition of $Fe(CO)_5$ to $Fe_2(CO)_9$ in sunlight, the first reported photoreaction involving a metal carbonyl.[5,6] Following this observation, the photochemistry of $Fe(CO)_5$ was thoroughly explored throughout the 20$^{th}$ century, leading to its application in numerous catalytic processes such as olefin hydroformylation, hydrogenation, hydrosilylation, and isomerization.[7-10]

Due to its rich history, $Fe(CO)_5$ has also served as a model system for the advancements of techniques including matrix isolation,[11] time-resolved infrared spectroscopy (TRIR),[12] and electron diffraction.[13] The structure, bonding, and reactivity of the $Fe(CO)_4$ fragment have been consistent research topics for decades.[1-3,14-16] Given that a tetrahedral arrangement of ligands around a $d^8$ metal center is Jahn-Teller unstable, Burdett and Hoffmann predicted a $C_{2v}$ saw-horse geometry. Consequently, the two highest-lying metal-based orbitals are close in energy leading to a high-spin $S = 1$ electronic configuration.[17-19] Poliakoff provided direct experimental evidence of this in various matrices at 20 K by measuring the bond angles of photogenerated $Fe(CO)_4$ by IR spectroscopy in comparison with predicted values.[11] Additionally, bearing a triplet $^3B_2$ ground

state 4with an energetically accessible singlet $^1A_1$ excited state,[14] $Fe(CO)_4$ has also been used to examine the effect of spin-state on molecular structure and reactivity.[16,20-22]

Despite the exciting reaction chemistry available to the $Fe(CO)_4$ fragment such as alkane binding and E-H bond activation, the fleeting nature of this species and its reaction products has precluded detailed structural and stoichiometric reactivity studies.[11,16,23] A notable exception to this has been the unequivocal structure determination of the excited $^1A_1$ electronic state of $Fe(CO)_4$ in the gas phase using ultrafast electron diffraction.[13] The reactivity of $Fe(CO)_4$ has inspired the synthesis of a number of four-coordinate, formally iron(0) complexes utilizing carbenes, olefins, and/or phosphines. However, the electronic structures of these ligands relative to CO lead to dissimilar Fe d-orbital manifolds and reactivity divergent from $Fe(CO)_4$.[23-29]

Our group has found success in isolating analogues of classical unsaturated metal carbonyls (e.g. $Pd(CO)_2$, $Ni(CO)_3$, $Co(CO)_4$, $Mn(CO)_5$) through the use of sterically encumbering *m*-terphenyl isocyanides, which are isolobal to CO.[30-33] In an attempt to extend this strategy to iron, we reported the tetra-isocyano complex $Fe(N_2)(CNAr^{Mes2})_4$ ($Ar^{Mes2}$ = 2,6-(2,4,6- $Me_3C_6H_2)_2C_6H_3$), which ostensibly formed by $N_2$ trapping of the $Fe(CNAr^{Mes2})_4$ fragment. However, working in an argon-filled glovebox led to rapid product decomposition via intramolecular ligand activation.[34] It was later indicated by low level density functional theory (DFT) calculations that the predicted ground state electronic structure of the model complex $Fe(CNPh)_4$ is a singlet instead of the desired triplet spin state as a result of the increased σ-donor and diminished π-acceptor properties of aryl isocyanides relative to CO.[35,36] The more electron-rich $Fe(CNPh)_4$ was predicted to possess a higher lying $2a_1$ molecular orbital (Fe $d_{z2}$), which would encourage spin pairing in the $b_2$-symmetric orbital that is predominantly Fe $d_{xy}$ in character. This may partially account for the instability of $Fe(CNAr^{Mes2})_4$ despite a sterically crowded coordination sphere. In contrast, the

hypothetical molecule $Fe(CO)_2(CNPh)_2$ was predicted to possess a triplet ground state, like $Fe(CO)_4$. Accordingly, we report our efforts to stabilize a heteroleptic iron complex featuring both isocyanide and carbonyl ligands that effectively mimics the reactivity of $Fe(CO)_4$.

## 5.2 Dinitrogen Binding by an $FeL_4$ Fragment

We recently reported a series of iron complexes with a mixed ligand set of CO and the sterically encumbering isocyanide ($Ar^{Tripp2}$ = 2,6-(2,4,6-(*i*-Pr)$_3C_6H_2)_2C_6H_3$).[36,37] The formally iron(-II) species $K_2[Fe(CO)_2(CNAr^{Tripp2})_2]$ could be oxidized by molecular iodine ($I_2$) in an $N_2$ atmosphere to cleanly generate $Fe(N_2)(CO)_2(CNAr^{Tripp2})_2$ (**1**; Scheme 5.1). As in the case of $Fe(N_2)(CNAr^{Mes2})_4$, it is likely that a four-coordinate iron(0) species is formed fleetingly, but it is rapidly intercepted by $N_2$. Compound **1** has a trigonal bipyramidal geometry with axial isocyanides and an equatorial plane consisting of the two CO ligands and $N_2$. The bond between iron and $N_2$ appears weak based on a long internuclear Fe-N distance of 1.8850(33) Å and an unactivated N≡N triple bond (1.1059(41) Å). Additionally, the IR absorbance from the $N_2$ ligand of **1** occurs at 2194 $cm^{-1}$, indicating minimal Fe→N π backdonation due to the presence of strongly π-acidic CO and isocyanide ligands.[38] Notably, this stretch lies at nearly 130 $cm^{-1}$ higher frequency than the more electron rich $Fe(N_2)(CNAr^{Mes2})_4$[34] and 50-55 $cm^{-1}$ lower frequency than matrix-generated $Fe(N_2)(CO)_4$.[11] This is consistent with the intermediate σ-donor/π-acceptor ratio of a mixed ligand set, and it suggests that the electron density at iron in **1** more closely resembles that of $Fe(N_2)(CO)_4$ than $Fe(N_2)(CNAr^{Mes2})_4$.[35] These three isolobal species adopt analogous trigonal bipyramidal coordination geometry with $N_2$ bound at an equatorial site. Although $Fe(N_2)(CO)_4$ was originally thought to feature an axially bound $N_2$ ligand, it was later found to prefer equatorial coordination of $N_2$ (Figure 5.1).[11,39]

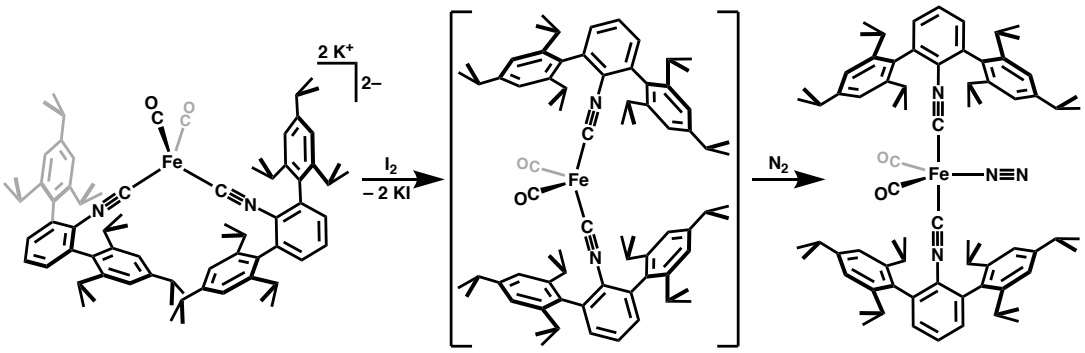


Scheme 5.1. Synthesis of $Fe(N_2)(CO)_2(CNAr^{Tripp2})_2$ (**1**) showing the proposed intermediacy of $Fe(CO)_2(CNAr^{Tripp2})_2$.

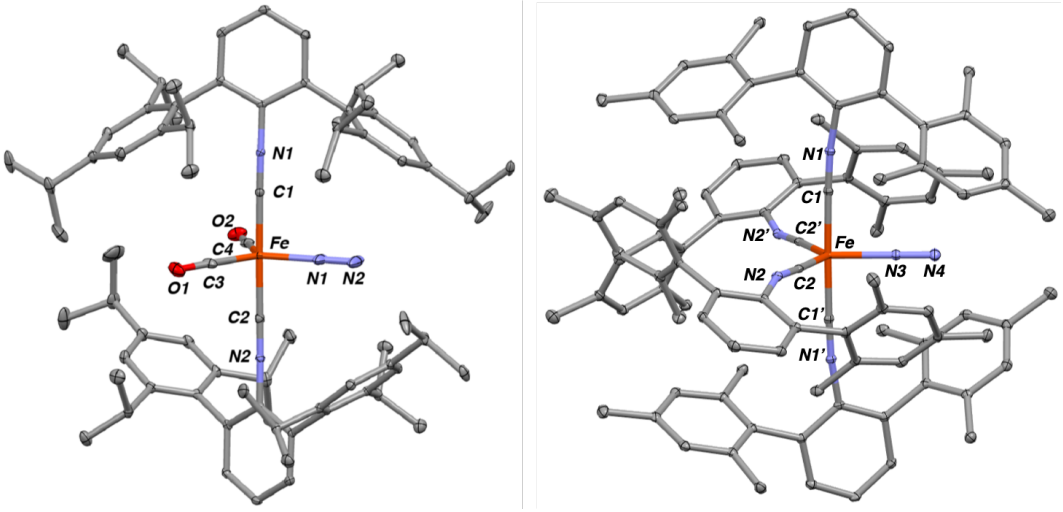


Figure 5.1. Solid-state structures of $Fe(N_2)(CO)_2(CNAr^{Tripp2})_2$ (**1**) and $Fe(N_2)(CNAr^{Mes2})_4$. *Note: The solid-state structure of $Fe(N_2)(CO)_4$ is not known, but polyethylene film matrix-isolation data suggest equatorial $N_2$ coordination.[39]

Complex **1** shows moderate stability in inert atmospheres and can be handled in solution at room temperature without noticeable diminution over the course of approximately 30 minutes. The only identifiable iron-containing products after the decomposition of **1** are $Fe(CO)_3(CNAr^{Tripp2})_2$ and $Fe(CO)_2(CNAr^{Tripp2})_3$, as assessed by $^1$H NMR spectroscopy and X-ray crystallography, which likely form via intermolecular ligand redistributions following $N_2$

dissociation. Conversely, $Fe(N_2)(CNAr^{Mes2})_4$ decomposes through an intramolecular ligand degradation pathway on a similar timescale, and $Fe(N_2)(CO)_4$ has a lifetime of significantly less than one second at room temperature.[34,39] Evidently, the larger steric profile of $CNAr^{Tripp2}$ discourages intramolecular decomposition processes for **1** while also kinetically stabilizing the labile $N_2$ ligand.

## 5.3 Small Molecule Activation by $Fe(N_2)(CO)_2(CNAr^{Tripp2})_2$

Given the apparent lability of the $N_2$ ligand, we reasoned that **1** would display analogous reactivity to $Fe(CO)_4$ in the presence of certain substrates. Indeed, exposing a $C_6D_6$ solution **1** to an atmosphere of $H_2$ in a J. Young tube led to an immediate lightening in color to pale yellow. The FTIR spectrum showed a disappearance of the $N_2$ stretch along with a *ca*. 25 $cm^{-1}$ blueshift of the asymmetric CN stretch, and the $^1H$ NMR spectrum revealed a single hydride resonance at $\delta_H = -9.46$ ppm. The product was determined by single crystal X-ray diffractometry to be *cis,cis,trans*-$H_2Fe(CO)_2(CNAr^{Tripp2})_2$ (**2**; Scheme 5.2, Figure 5.2) serving as an important analogue of $H_2Fe(CO)_4$, the first transition-metal hydride complex described in the literature.[40] $H_2Fe(CO)_4$ was first prepared through the Hieber base reaction between hydroxide ($OH^-$) and $Fe(CO)_5$,[41] which has been employed for molecular water-gas shift chemistry.[42] Additionally, matrix-isolated $Fe(CO)_4$ was shown to react with $H_2$ in the first instance of dihydrogen oxidative addition to a metal center under cryogenic conditions.[43] Later, polyethylene film matrix isolation allowed for the thermal reaction between $Fe(N_2)(CO)_4$ and $H_2$ at 210 K in a more direct analogy to the reaction between **1** and $H_2$ forming **2**.[39] Importantly, **2** is stable to vacuum at room temperature contrasting with $H_2Fe(CO)_4$, which liberates dihydrogen above –10 ˚C. Iron dihydrides of the type $H_2Fe(PR_3)_4$

and $H_2Fe(CO)_2(PR_3)_2$ have been crystallographically characterized; however, an important distinction is that they are derived from hydride and proton sources and not $H_2$.[44-49]

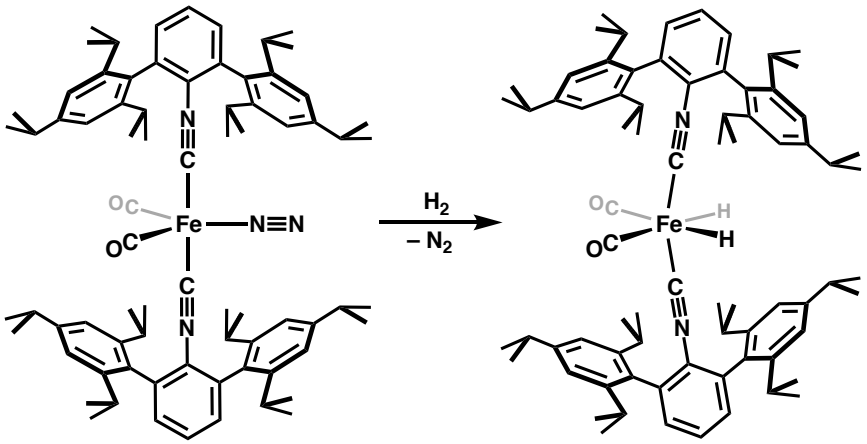


Scheme 5.2. Oxidative addition of $H_2$ by **1** to generate $H_2Fe(CO)_2(CNAr^{Tripp2})_2$ (**2**).

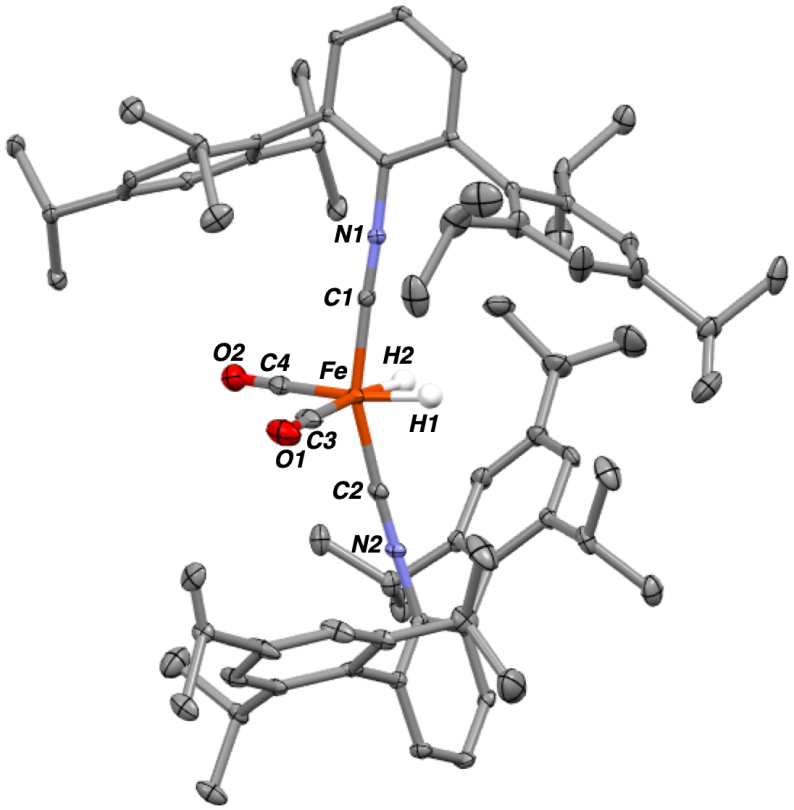


Figure 5.2. Solid-state structure of $H_2Fe(CO)_2(CNAr^{Tripp2})_2$ (**2**).

Unlike with $H_2$, the oxidative addition of Si–H bonds to matrix-isolated $Fe(CO)_4$ has not been reported despite the ability of $Fe(CO)_5$ to photochemically hydrosilylate alkenes, presumably due to a lack of thermal energy required to surpass the higher activation barrier for Si–H bond cleavage. However, photolysis or thermolysis of $Fe(CO)_5$ with $HSiCl_3$ or $HSiPh_3$ generates isolable $HFe(SiR_3)(CO)_4$ complexes, which have been spectroscopically characterized.[50,51] In order to glean definitive structural information from compounds of this type, **1** was treated with $HSiEt_3$ at room temperature. A hydride resonance was observed at $\delta_H = -9.45$ ppm, effectively the same chemical shift as **2**. Analysis of single crystals grown from a *n*-pentane/$Et_2O$ mixture revealed the product to be $HFe(SiEt_3)(CO)_2(CNAr^{Tripp2})_2$ (**3**; Scheme 5.3, Figure 5.3). Relative to **1**, the asymmetric νCN stretch of **3** shifts 20 $cm^{-1}$ to lower frequency, whereas both νCO stretches shift by about 40 $cm^{-1}$ to higher frequency. Similar results were obtained when the primary silane $H_3SiPh$ was added to **1** resulting in the clean formation of $HFe(H_2SiPh)(CO)_2(CNAr^{Tripp2})_2$ (**4**; Scheme 5.3, Figure 5.4) as confirmed by X-ray crystallography. It is worth noting that $Fe(N_2)(CNAr^{Mes2})_4$ has not been observed to oxidatively add $H_2$ or silanes, presumably as a result of steric congestion imposed by four encumbering *m*-terphenyl isocyanides preventing the rearrangement required to accommodate two more ligands on iron.

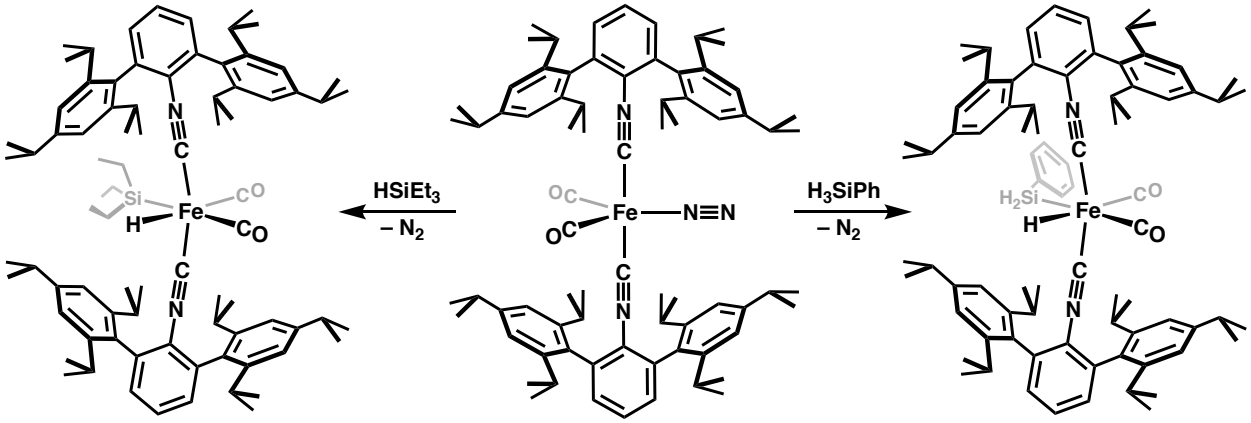


Scheme 5.3. Synthesis of $HFe(SiEt_3)(CO)_2(CNAr^{Tripp2})_2$ (**3**) and $HFe(H_2SiPh)(CO)_2(CNAr^{Tripp2})_2$ (**4**) by the oxidative addition of the corresponding silane.

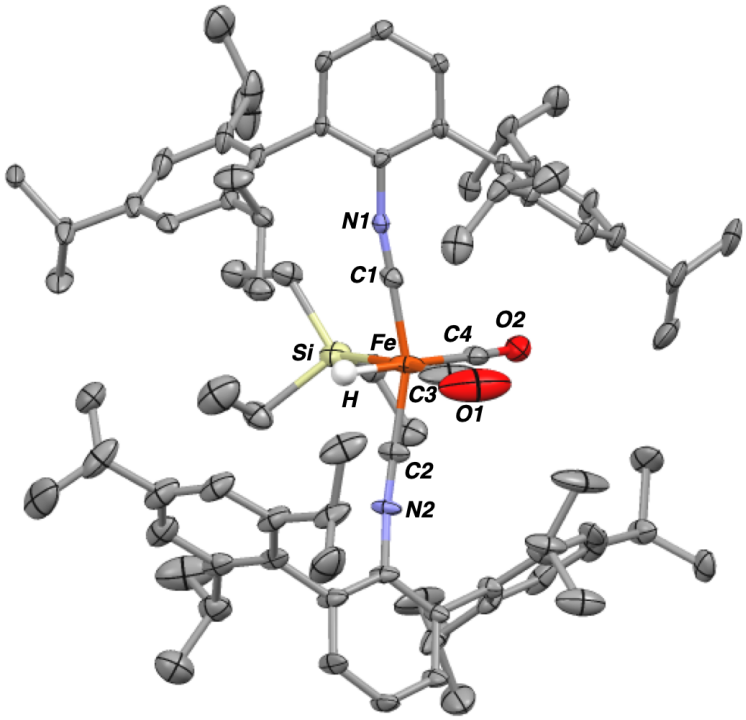


Figure 5.3. Solid-state structure of $HFe(SiEt_3)(CO)_2(CNAr^{Tripp2})_2$ (**3**).

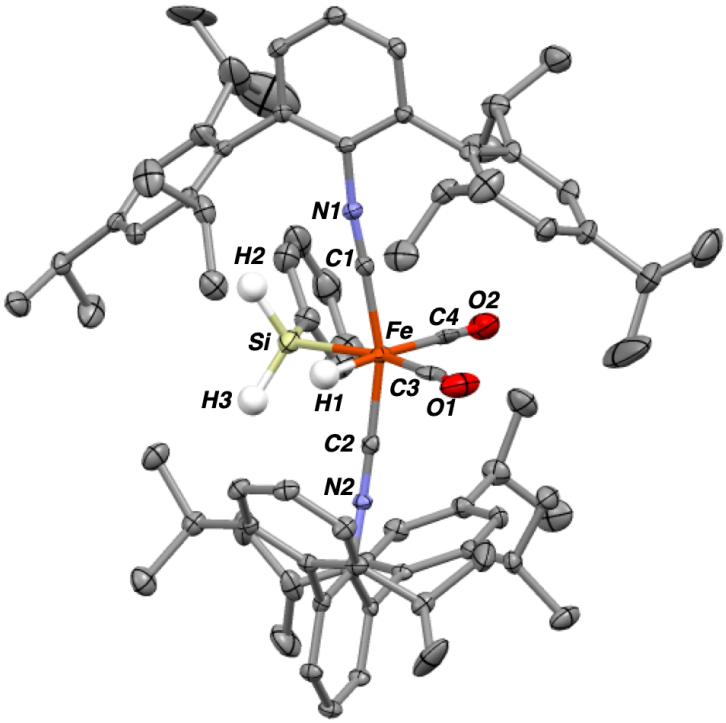


Figure 5.4. Solid-state structure of $HFe(H_2SiPh)(CO)_2(CNAr^{Tripp2})_2$ (**4**).

The above results show that **1** successfully recreates some of the chemistry performed by $Fe(CO)_4$, behaving as a stabilized source of a four-coordinate iron(0) fragment. This led us to explore reactions that have not been observed with $Fe(CO)_5$. Since $Fe(CO)_4$ is most commonly accessed by UV irradiation or at elevated temperatures, its reactivity with light- or temperature-sensitive substrates is not well defined. For example, reactions between iron carbonyls (i.e. $Fe_2(CO)_9$ and $Fe(CO)_5$) and white phosphorus ($P_4$) are largely phenomenological leading to multinuclear or polymeric products.[52,53] However, when **1** is treated with a toluene solution of 1.1 equivalents $P_4$, full conversion to a new major product displaying one $CNAr^{Tripp2}$ environment by $^1$H NMR and IR spectroscopy is achieved within 30 minutes. Additionally, two $^{31}$P resonances were observed at $\delta_P$ = –254.0 and –335.3 ppm . Structural determination from X-ray diffraction of orange crystals revealed $Fe(\kappa^2\text{-}P_4)(CO)_2(CNAr^{Tripp2})_2$ (**5**; Scheme 5.4, Figure 5.5), in which the

cleavage of one P–P bond of the tetrahedron occurs at iron creating a chelating butterfly $P_4$ unit. This activation mode of phosphorus has only been observed for group 4 and group 9 transition metals making compound **5** structurally unique among iron complexes. However, it is worth noting that three complexes of the formulation $Cp^*Co(\kappa^2\text{-}P_4)L$ have been fully characterized,[54-56] in line with the qualitative isolobal relationship between $[Fe(CO)_4]$ and [CpM(CO)] fragments (M = group 9 metal).[57]

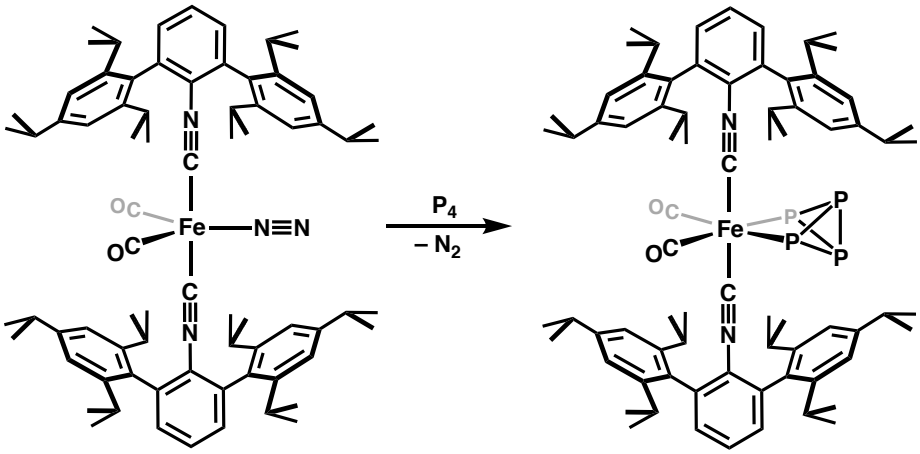


Scheme 5.4. P–P bond scission by **1** to form the butterfly $P_4$ complex $Fe(\kappa^2\text{-}P_4)(CO)_2(CNAr^{Tripp2})_2$ (**5**).

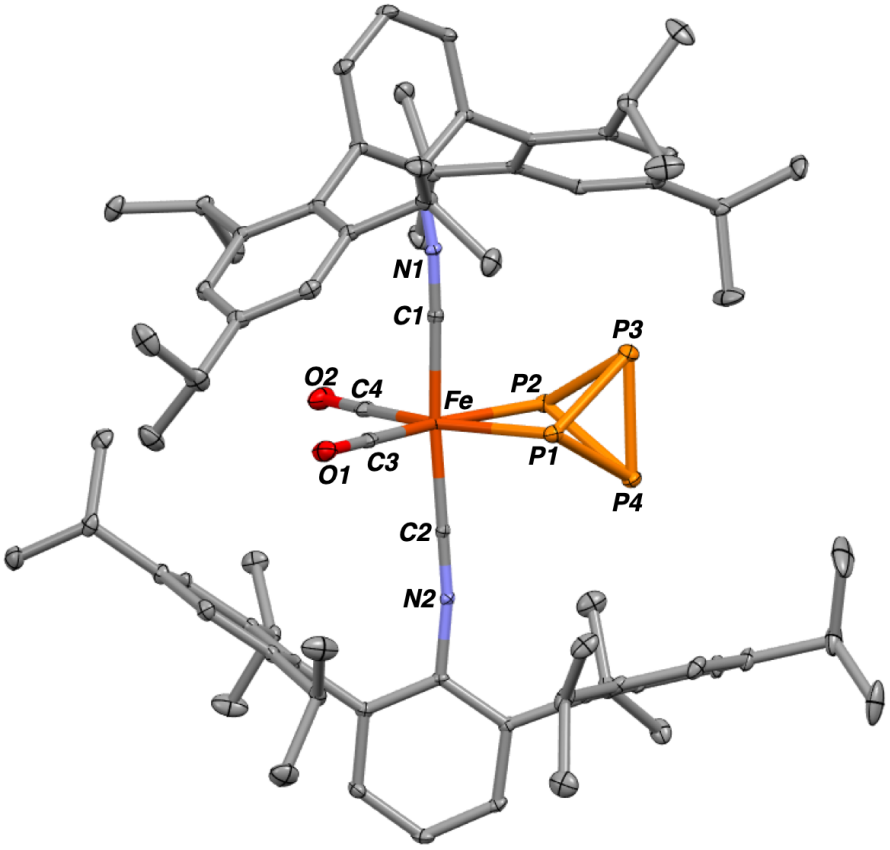


Figure 5.5. Solid-state structure of $Fe(\kappa^2\text{-}P_4)(CO)_2(CNAr^{Tripp2})_2$ (**5**).

The $Fe(CO)_4$ fragment has also not been shown to react with boranes. Preliminary findings of the treatment of **1** with catechol borane display spectroscopic signatures similar but not equivalent to dihydride complex **2** suggesting possible oxidative addition of the B–H bond. If verified, this compound would be only the second structurally characterized example of an iron hydrido-boryl complex.[58] Stoichiometric and potential catalytic investigations involving compounds **2**, **3**, **4**, and the presumed boryl complex are underway.

## 5.4 Unusual Solvent Binding by $[Fe(CO)_2(CNAr^{Tripp2})_2]$

Separately, it was noted that **1**, when handled under $N_2$, reversibly changed color from yellow-orange to brown upon exposure to vacuum in $Et_2O$ or THF solutions. **1** was brought into an argon-filled glovebox and stored at –35 ˚C in a *n*-pentane/THF mixture overnight, depositing dark yellow crystals from the brown solution. The species was determined to be $Fe(THF)(CO)_2(CNAr^{Tripp2})_2$ (**6**; Scheme 5.5, Figure 5.6) by X-ray diffraction, in which a molecule of THF had displaced $N_2$. The other ligands about iron rearrange such that the equatorial plane now consists of the two isocyanides and one CO ligand, and the molecular z-axis contains the other carbonyl ligand and THF. This likely occurs to maximize π-stabilization of the HOMO ($d_{xy}$) by placing three π-acidic ligands in the equatorial plane. While there are 291 crystallographically characterized iron complexes with THF as a ligand in the Cambridge Structural Data Base,[59] to our knowledge, **6** is the only example of THF binding to a formally iron(0) center.

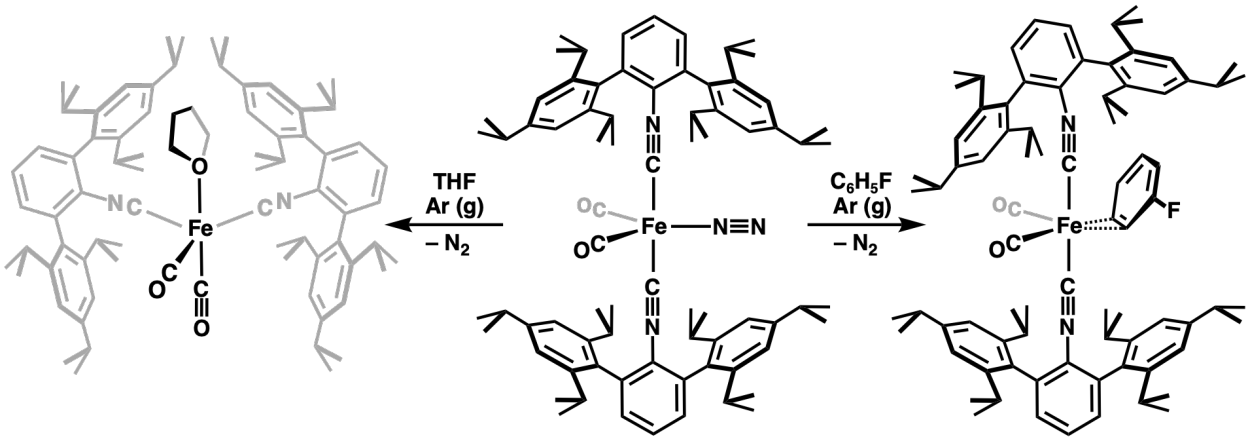


Scheme 5.5. Unique solvent binding by iron(0) in $Fe(THF)(CO)_2(CNAr^{Tripp2})_2$ (**6**) and $Fe(CO)_2(CNAr^{Tripp2})_2(\eta^2\text{-}(C,C)\text{-}C_6H_5F)$ (**7**).

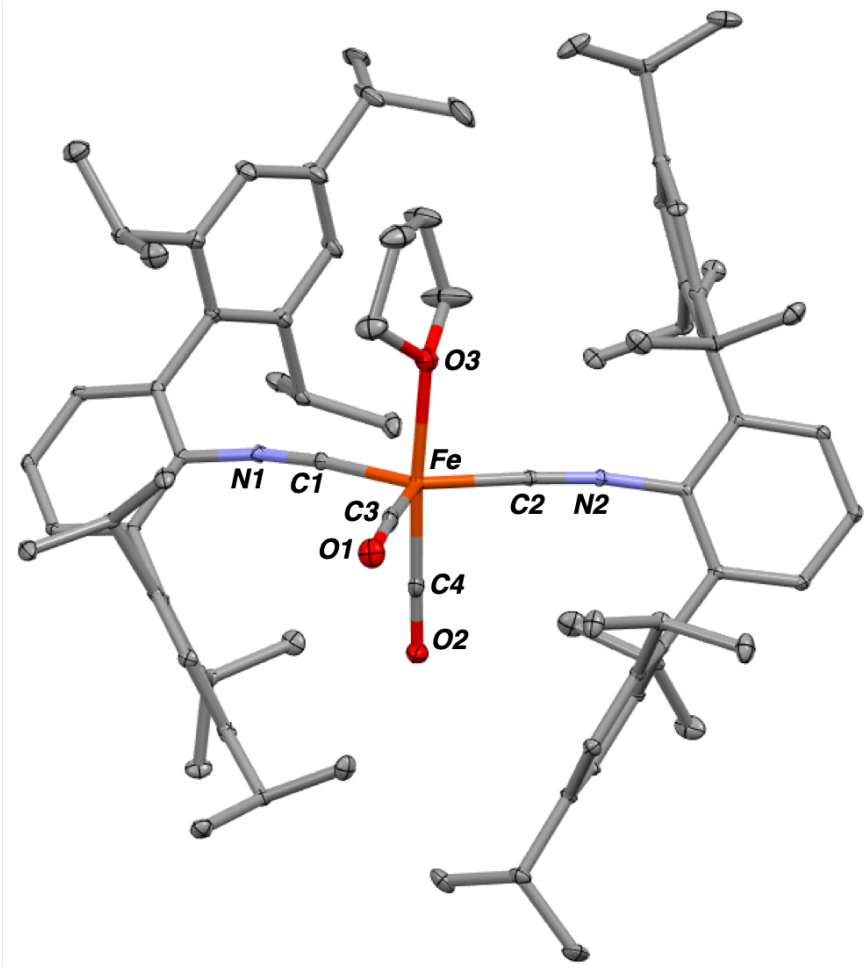


Figure 5.6. Solid-state structure of $Fe(THF)(CO)_2(CNAr^{Tripp2})_2$ (**6**).

In order to avoid $N_2$ and strongly coordinating solvents, the oxidation of $K_2[Fe(CO)_2(CNAr^{Tripp2})_2]$ was performed in thawing fluorobenzene ($C_6H_5F$) under Ar. The FTIR spectrum of the crude reaction mixture showed one major product with νCN and νCO stretches indicative of a new trigonal bipyramidal iron(0) complex. Single crystal X-ray analysis demonstrated the product to be $Fe(CO)_2(CNAr^{Tripp2})_2(\eta^2\text{-}(C,C)\text{-}C_6H_5F)$ (**7**; Figure 5.9), a rare example of an unsupported $\eta^2$-arene iron complex. The bond lengths in the fluorobenzene ring indicate that aromaticity is largely retained upon coordination to iron with only slight deviations to a pseudo-cyclohexatriene structure. **7** can also be generated by dissolving **1** in $C_6H_5F$ under argon and exposing to vacuum for *ca.* 5 minutes (Scheme 5.5). Despite minimal fluorobenzene activation apparent in the solid-state structure, leaving **7** dissolved in *n*-pentane for prolonged periods (> 1 month) at –35 ˚C deposited crystals of a new species $Fe(CO)_2(CNAr^{Tripp2})(\eta^4\text{-}(N,C,C,C)\text{-}Ar^{Tripp2}NC(H)C_6H_4F)$ formed formally from isocyanide insertion into an aryl C-H bond (Figure 5.8), which points to the potential for $Fe(CO)_2(CNAr^{Tripp2})_2$ to effect $sp^2$ C-H bond functionalization.

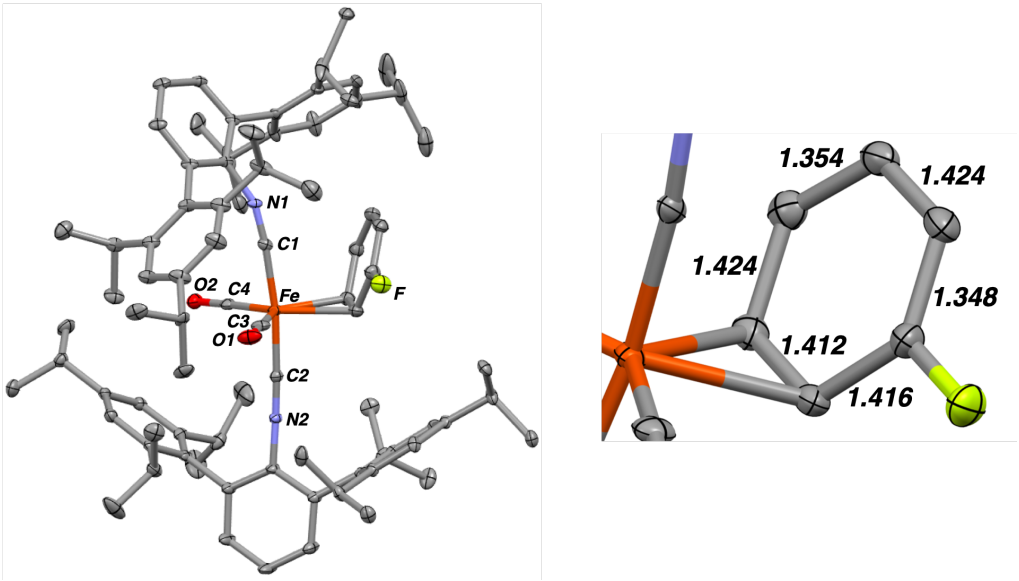


Figure 5.7. Solid-state structure of $Fe(CO)_2(CNAr^{Tripp2})_2(\eta^2\text{-}(C,C)\text{-}C_6H_5F)$ (**7**) (Left) and zoom-in depicting bond lengths of the bound arene (Right).

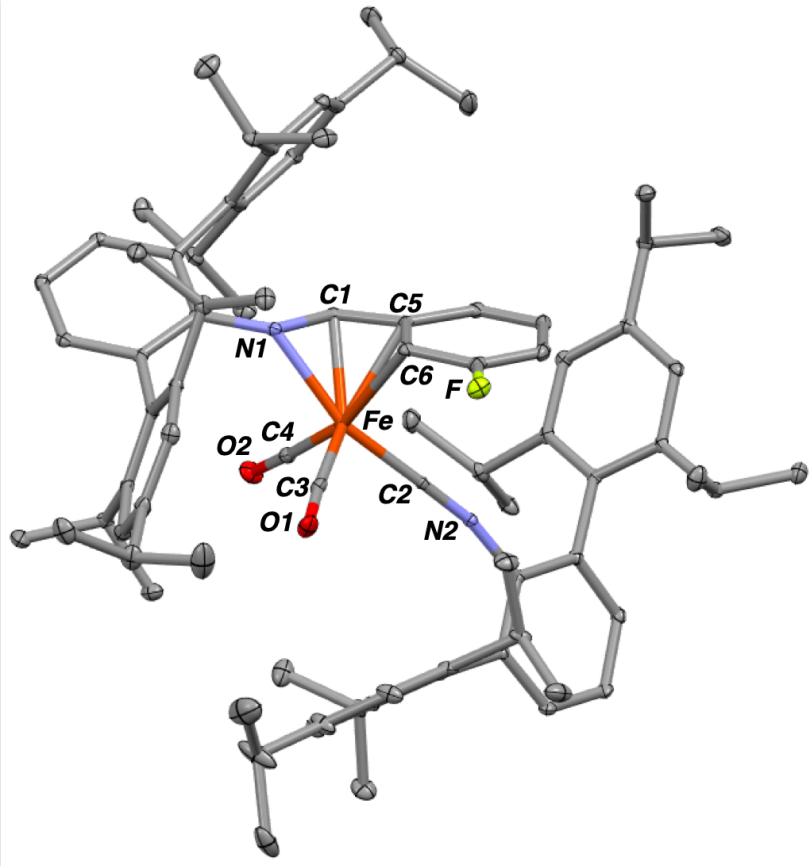


Figure 5.8. Decomposition of **7** by isocyanide insertion into an aryl C-H bond leading to $\eta^4$ coordination to iron.

## 5.5 Alternative Routes Toward $Fe(CO)_2(CNAr^{Tripp2})_2$

In addition to $I_2$ oxidation of the metallate $K_2[Fe(CO)_2(CNAr^{Tripp2})_2$, attempts at reduction of the $FeI_2(CO)_2(CNAr^{Tripp2})_2$ precursor were also employed. Varying the reaction conditions using sodium amalgam or potassium graphite as the reductant in toluene, $Et_2O$, THF, and combinations thereof led to intractable mixtures of iron products in multiple oxidation states according to IR spectroscopy. By using magnesium anthracene in toluene, conversion to a new major product was observed by IR as the solution turned from brown to bright red. Storage of the product mixture in *n*-pentane at –35 ˚C under Ar overnight gave a combination of orange, yellow, and colorless crystals. The yellow crystals were $Fe(CO)_3(CNAr^{Tripp2})_2$, and the colorless crystals were free anthracene based on unit cell determinations. However, X-ray crystallography identified the orange product as $Fe(CO)_2(CNAr^{Tripp2})_2(\eta^2\text{-}(C,C)\text{-}C_{14}H_{10})$ (**8**; Scheme 5.6, Figure 5.9). Like fluorobenzene adduct **7**, anthracene is bound to iron in a structurally unique $\eta^2$ fashion with minimal activation of the arene. One of the isocyanides distorts significantly from linear in order to accommodate the large arene ligand in the equatorial plane.

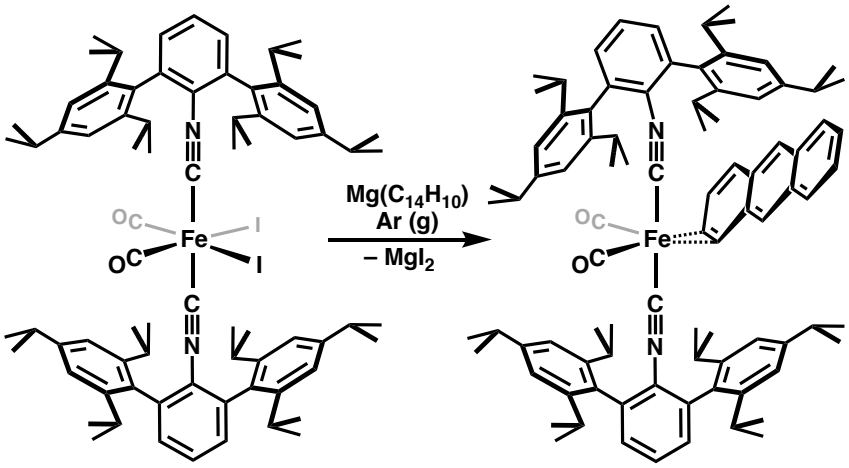


Scheme 5.6. Reduction of $FeI_2(CO)_2(CNAr^{Tripp2})_2$ with magnesium anthracene to yield $Fe(CO)_2(CNAr^{Tripp2})_2(\eta^2\text{-}(C,C)\text{-}C_{14}H_{10})$ (**9**).

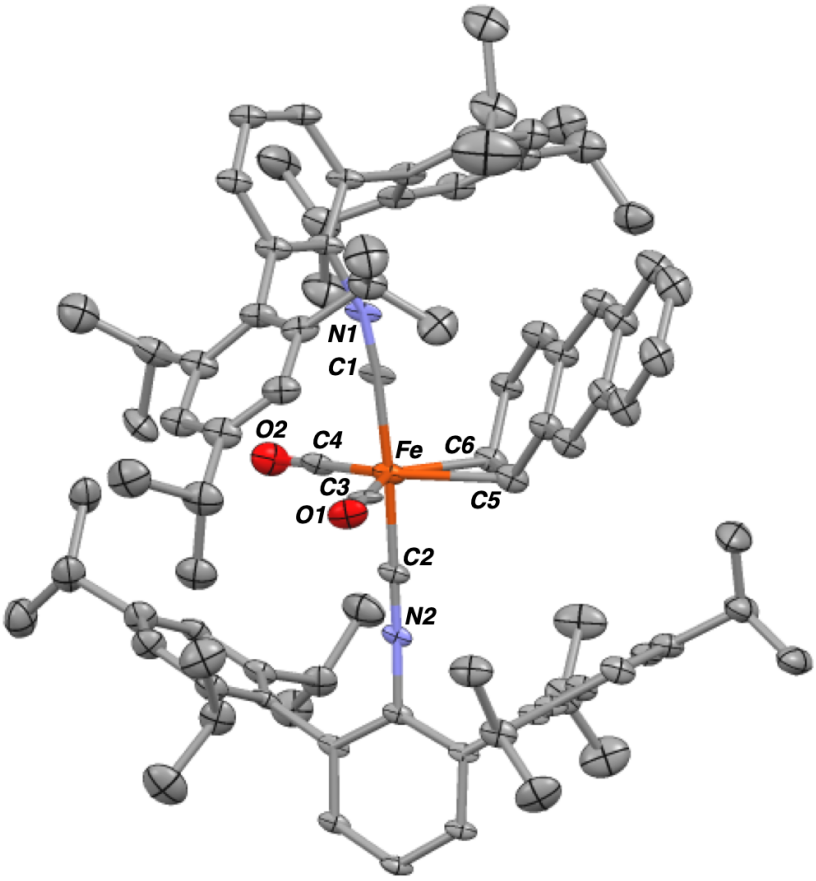


Figure 5.9. Solid-state structure of $Fe(CO)_2(CNAr^{Tripp2})_2(\eta^2\text{-}(C,C)\text{-}C_{14}H_{10})$ (**8**).

A promising path forward revisits the strategy used to synthesize $Fe(N_2)(CNAr^{Mes2})_4$. In that article, $[Fe(CNAr^{Mes2})_4]^{2-}$ was protonated to $[HFe(CNAr^{Mes2})_4]^-$, which was subsequently treated with methyl triflate (MeOTf) (triflate = trifluoromethanesulfonate, $[CF_3SO_3]^-$) to eliminate methane.[34] To that end, $K_2[Fe(CO)_2(CNAr^{Tripp2})_2]$ was treated with trimethylsilanol (TMSOH), and $K[HFe(CO)_2(CNAr^{Tripp2})_2]$ (**9**) was isolated in good yield. Fortuitously, **9** was found to be moderately soluble in *n*-pentane allowing for the exclusion of coordinating solvents. Contrastingly, $K_2[Fe(CO)_2(CNAr^{Tripp2})_2]$ and $FeI_2(CO)_2(CNAr^{Tripp2})_2$ are sparingly soluble in alkanes and require

the use of aromatic or ethereal solvents. Initial test reactions adding MeOTf in thawing *n*-pentane to thawing *n*-pentane solutions of **9** have not been successful in isolating an unsaturated iron complex. So far, the major products identified have been $Fe(CO)_2(CNAr^{Tripp2})_3$ and $Fe(CO)_3(CNAr^{Tripp2})_2$ as a result of ligand scrambling. Another species has also been identified by a low quality crystal structure as the divalent alkyl complex $Fe(CH_3)(OTf)(CO)_2(CNAr^{Tripp2})_2$ possibly originating from the oxidative addition of MeOTf by $Fe(CO)_2(CNAr^{Tripp2})_2$. Continued efforts to isolate this highly reactive unsaturated metal fragment are ongoing.

## 5.6 Concluding Remarks

The four-coordinate iron fragment $Fe(CO)_4$ has attracted continued attention from organometallic chemists for its ability to bind and activate a variety of small molecules as well as for its unusual high spin triplet electronic ground state. However, the transient nature of this intermediate species has inhibited detailed structural and stoichiometric reactivity studies. The work presented above describes our efforts toward the isolation of an analogue of $Fe(CO)_4$ using *m*-terphenyl isocyanides as sterically encumbering surrogates for CO. It was determined that previous investigations of $Fe(N_2)(CNAr^{Mes2})_4$ were not successful in modeling the behavior of $Fe(CO)_4$ for two main reasons. Firstly, the presence of four *m*-terphenyl substituents provided too much congestion such that the tetra-isocyano iron fragment could not accommodate oxidative addition products. Secondly, the higher σ-donor/π-acceptor ratio of isocyanides relative to CO led to a more electron-rich iron center destabilizing the desired $S = 1$ spin state and favoring a singlet electronic ground state. It was also predicted that the hypothetical molecule $Fe(CO)_2(CNAr^{Ph})_2$ would possess a triplet ground state, which led us to investigate $Fe(N_2)(CO)_2(CNAr^{Tripp2})_2$ (**1**) due

to the resistance of $CNAr^{Tripp2}$ to undergo intramolecular ligand degradation and electronic stabilization provided by two carbonyl ligands.

Complex **1** is isolobal to matrix-isolated $Fe(N_2)(CO)_4$, and the $N_2$ ligand of both species has been found to be substitutionally labile. In the absence of $N_2$, **1** binds two-electron donors such as THF and arenes in an $\eta^2$ fashion, highly unusual for iron(0) complexes. **1** also oxidatively adds E–H bonds (E = H, Si) in analogy to $Fe(CO)_4$ and contrasting with $Fe(N_2)(CNAr^{Mes2})_4$. Accordingly, we have claim diamagnetic compound **1** as a masked analogue of $Fe(CO)_4$ in the singlet spin state. The target $Fe(CO)_2(CNAr^{Tripp2})_2$ is likely within reach and worthy of further synthetic efforts in order to verify the predicted triplet ground state.

## 5.7 Synthetic Procedures and Characterization Data

**General Considerations.** All manipulations were carried out under an atmosphere of purified dinitrogen using standard Schlenk and glovebox techniques. Unless otherwise stated, reagent-grade starting materials were purchased from commercial sources and either used as received or purified by standard procedures.[60] Solvents were dried and deoxygenated according to standard procedures.[61] Benzene-$d_6$ (Cambridge Isotope Laboratories) was distilled from NaK alloy/benzophenone and stored over activated 3 Å molecular sieves for 2 d prior to use. Celite 405 (Fischer Scientific) was dried under vacuum (24 h) at a temperature above 250 ˚C and stored in a glovebox prior to use. Compounds $CNAr^{Tripp2}$ and $Fe(N_2)(CO)_2(CNAr^{Tripp2})_2$ were prepared as previously reported.[36,37]

Solution $^1H$ and $^{13}C\{^1H\}$ NMR spectra were recorded on a Varian Mercury 400 or a Varian X-SENS 500 spectrometer. $^1H$ and $^{13}C\{^1H\}$ chemical shifts are reported in ppm relative to $SiMe_4$ ($^1H$ and $^{13}C$ $\delta$ = 0.0 ppm) with reference to residual solvent resonances of 7.16 ppm ($^1H$) and

128.06 ppm ($^{13}C$) for $C_6D_6$. FTIR spectra were recorded on a Thermo-Nicolet iS10 FTIR spectrometer. Samples were prepared as KBr pellets or $C_6D_6$ or THF solutions injected into a ThermoFisher solution cell equipped with KBr windows. Solvent peaks were digitally subtracted from all solution FTIR spectra by comparison with an authentic solvent spectrum obtained prior to that of the sample. The following abbreviations were used for the intensities and characteristics of important IR absorption bands: vs = very strong, s = strong, m = medium, w = weak, vw = very weak; sh = shoulder.

**Preparation of $H_2Fe(CO)_2(CNAr^{Tripp2})_2$ (2).** In a J. Young NMR tube, a $C_6D_6$ solution of **1** was subjected to three freeze-pump-thaw cycles, and an atmosphere of $H_2$ was introduced. The color quickly lightened from orange to yellow. The product mixture was brought back into a nitrogen-filled glovebox, and volatiles were removed *in vacuo*. Single crystals were grown from *n*-hexane/benzene (15:1) at –35 ˚C overnight.

**Preparation of $HFe(SiEt_3)(CO)_2(CNAr^{Tripp2})_2$ (3).** To a $Et_2O$ solution of **1** was added a $Et_2O$ solution of $HSiEt_3$ (1.2 equiv.). The mixture was stirred for 15 minutes, after which time the solvent and excess silane were removed by vacuum. The yellow solid was dissolved in *n*-hexane/$Et_2O$ (10:1) for recrystallization at –35 ˚C overnight producing diffraction quality samples.

**Preparation of $HFe(H_2SiPh)(CO)_2(CNAr^{Tripp2})_2$ (4).** To a $Et_2O$ solution of **1** was added a $Et_2O$ solution of H3SiPh (1.2 equiv.). The mixture was stirred for 15 minutes, after which time the solvent and excess silane were removed by vacuum. Dissolution of the product in *n*-pentane/benzene and storage at –35 ˚C overnight deposited crystals suitable for diffraction studies.

**Preparation of Fe($\kappa^2$-$P_4$)(CO)$_2$(CNAr$^{Tripp2}$)$_2$ (5).** A toluene solution of $P_4$ (5 mL) was added to a thawing toluene solution of **1** (1 mL) and stirred for 30 min. The solvent was evaporated, and the resulting solid was dissolved into *n*-pentane. Single crystals formed within minutes of placing the vial into the –35 ˚C glovebox freezer.

**Preparation of Fe(THF)(CO)$_2$(CNAr$^{Tripp2}$)$_2$ (6).** Compound **1** was brought into an argon-filled glovebox as a solid. The vial headspace was evacuated of $N_2$, and THF was added as a solution in *n*-pentane. The solution immediately turned dark, and blackish-yellow crystals were grown from *n*-pentane at –35 ˚C overnight.

**Preparation of Fe(CO)$_2$(CNAr$^{Tripp2}$)$_2$($\eta^2$-(*C*,*C*)-$C_6H_5F$) (7).** In an argon-filled glovebox, $K_2$[Fe(CO)$_2$(CNAr$^{Tripp2}$)$_2$] was dissolved in fluorobenzene ($C_6H_5F$). Molecular iodine ($I_2$; 0.9 equiv.) was also dissolved in $C_6H_5F$, and both solutions were frozen. The $I_2$ solution was thawed and immediately added to the frozen solution of $K_2$[Fe(CO)$_2$(CNAr$^{Tripp2}$)$_2$]. The mixture was stirred at –35 ˚C for 30 min, after which time volatiles were removed *in vacuo* with the vial kept cold.

**Preparation of Fe(CO)$_2$(CNAr$^{Tripp2}$)$_2$($\eta^2$-(*C*,*C*)-$C_{14}H_{10}$) (8).** Magnesium anthracene (2 equiv.) was stirred in THF for 30 minutes prior to being added to a thawing THF solution of FeI$_2$(CO)$_2$(CNAr$^{Tripp2}$)$_2$. The mixture was stirred to room temperature for 30 minutes followed by solvent evaporation. The product mixture was extracted in *n*-pentane/$Et_2O$ (1:1) and crystallized from *n*-pentane/THF/toluene (10:1:1). Orange crystals of Fe(CO)$_2$(CNAr$^{Tripp2}$)$_2$($\eta^2$-(*C*,*C*)-$C_{14}H_{10}$) were selected by the Pasteur method.

## 5.8 Details of Crystallographic Structure Determinations

**General.** Single X-ray structure determinations were performed at 100 K on Bruker Kappa diffractometers equipped with Mo radiation source and an APEX-II CCD area detector. All structures were solved via direct methods with SHELXS[62] and refined by full-matrix least-squares procedures using SHELXL[62] within the Olex2[63] software. All hydrogen atoms have been removed for clarity. Disordered components and co-crystallized solvent molecules are not shown for clarity.

## 5.9 Acknowledgments

**Chapter 5**: This chapter is currently in preparation as a manuscript by Drance, M. J.; Gembicky, M; Rheingold, A. L.; Figueroa, J. S. The dissertation author is the first author of this paper.

## 5.10 References

(1) Wrighton, M. *Chem. Rev.* **1974**, *74* (4), 401–430.

(2) Poliakoff, M. *Chem. Soc. Rev.* **1978**, *7* (4), 527–540.

(3) Poliakoff, M.; Weitz, E. *Acc. Chem. Res.* **1987**, *20* (11), 408–414.

(4) Mond, L.; Quincke, F. *J. Chem. Soc., Trans.* **1891**, *59* (0), 604–607.

(5) Mond, L.; Langer, C. *J. Chem. Soc., Trans.* **1891**, *59* (0), 1090–1093.

(6) Dewar, J.; Jones, H. O. *Proceedings of the Royal Society of London Series a-Containing Papers of a Mathematical and Physical Character* **1905**, *76* (513), 558–577.

(7) Booth, B. L.; Goldwhite, H.; Haszeldine, R. N. *J. Chem. Soc., C* **1966**, *0* (0), 1447–1449.

(8) Harmon, R. E.; Gupta, S. K.; Brown, D. J. *Chem. Rev.* **1973**, *73* (1), 21–52.

(9) Schroeder, M. A.; Wrighton, M. S. *J. Am. Chem. Soc.* **1976**, *98* (2), 551–558.

(10) A Schroeder, M.; S Wrighton, M. *Journal of Organometallic Chemistry* **1977**, *128* (3), 345–358.

(11) Poliakoff, M.; Turner, J. J. *J. Chem. Soc., Dalton Trans.* **1974**, *0* (20), 2276–2285.

(12) Davies, B.; McNeish, A.; Poliakoff, M.; Turner, J. J. *J. Am. Chem. Soc.* **1977**, *99* (23), 7573–7579.

(13) Ihee, H.; Cao, J.; Zewail, A. H. *Angew. Chem. Int. Ed. Engl.* **2001**, *40* (8), 1532–1536.

(14) Poliakoff, M.; Turner, J. J. *Angew. Chem. Int. Ed.* **2001**, *40* (15), 2809–2812.

(15) Besora, M.; Carreon-Macedo, J.-L.; Cimas, Á.; Harvey, J. N. Advances in Inorganic Chemistry; Elsevier, 2009; Vol. 61, pp 573–623.

(16) Lomont, J. P.; Nguyen, S. C.; Harris, C. B. *Acc. Chem. Res.* **2014**, *47* (5), 1634–1642.

(17) Burdett, J. K. *J. Chem. Soc., Faraday Trans. 2* **1974**, *70* (0), 1599–1613.

(18) Burdett, J. K. *Inorg. Chem.* **1975**, *14* (2), 375–382.

(19) Elian, M.; Hoffmann, R. *Inorg. Chem.* **1975**, *14* (5), 1058–1076.

(20) Leadbeater, N. *Coordination Chemistry Reviews* **1999**, *188* (1), 35–70.

(21) Snee, P. T.; Payne, C. K.; Kotz, K. T.; Yang, H.; Harris, C. B. *J. Am. Chem. Soc.* **2001**, *123* (10), 2255–2264.

(22) Besora, M.; Carreon-Macedo, J.-L.; Cowan, A. J.; George, M. W.; Harvey, J. N.; Portius, P.; Ronayne, K. L.; Sun, X.-Z.; Towrie, M. *J. Am. Chem. Soc.* **2009**, *131* (10), 3583–3592.

(23) Hoberg, H.; Jenni, K.; Angermund, K.; Krüger, C. *Angew. Chem. Int. Ed.* **1987**, *26* (2), 153–155.

(24) Geier, S.; Goddard, R.; Holle, S.; Jolly, P. W.; Krüger, C.; Lutz, F. *Organometallics* **1997**, *16* (8), 1612–1620.

(25) Lavallo, V.; El-Batta, A.; Bertrand, G.; Grubbs, R. H. *Angew. Chem. Int. Ed.* **2010**, *50* (1), 268–271.

(26) Zhang, H.; Ouyang, Z.; Liu, Y.; Zhang, Q.; Wang, L.; Deng, L. *Angew. Chem. Int. Ed.* **2014**, *53* (32), 8432–8436.

(27) Hickey, A. K.; Lee, W.-T.; Chen, C.-H.; Pink, M.; Smith, J. M. *Organometallics* **2016**, *35* (17), 3069–3073.

(28) Burcher, B.; Sanders, K. J.; Benda, L.; Pintacuda, G.; Jeanneau, E.; Danopoulos, A. A.; Braunstein, P.; Olivier-Bourbigou, H.; Breuil, P.-A. R. *Organometallics* **2017**, *36* (3), 605–613.

(29) Casitas, A.; Krause, H.; Lutz, S.; Goddard, R.; Bill, E.; Fürstner, A. *Organometallics* **2017**, *37* (5), 729–739.

(30) Labios, L. A.; Millard, M. D.; Rheingold, A. L.; Figueroa, J. S. *J. Am. Chem. Soc.* **2009**, *131* (32), 11318–11319.

(31) Fox, B. J.; Millard, M. D.; DiPasquale, A. G.; Rheingold, A. L.; Figueroa, J. S. *Angew. Chem. Int. Ed.* **2009**, *48* (19), 3473–3477.

(32) Margulieux, G. W.; Weidemann, N.; Lacy, D. C.; Moore, C. E.; Rheingold, A. L.; Figueroa, J. S. *J. Am. Chem. Soc.* **2010**, *132* (14), 5033–5035.

(33) Agnew, D. W.; Moore, C. E.; Rheingold, A. L.; Figueroa, J. S. *Angew. Chem.* **2015**, *127* (43), 12864–12868.

(34) Mokhtarzadeh, C. C.; Margulieux, G. W.; Carpenter, A. E.; Weidemann, N.; Moore, C. E.; Rheingold, A. L.; Figueroa, J. S. *Inorg. Chem.* **2015**, *54* (11), 5579–5587.

(35) Cotton, F. A.; Zingales, F. *J. Am. Chem. Soc.* **1961**, *83* (2), 351–355.

(36) Carpenter, A. E.; Mokhtarzadeh, C. C.; Ripatti, D. S.; Havrylyuk, I.; Kamezawa, R.; Moore, C. E.; Rheingold, A. L.; Figueroa, J. S. *Inorg. Chem.* **2015**, *54* (6), 2936–2944.

(37) Drance, M. J.; Sears, J. D.; Mrse, A. M.; Moore, C. E.; Rheingold, A. L.; Neidig, M. L.; Figueroa, J. S. *Science* **2019**, *363* (6432), 1203–1205.

(38) Hazari, N. *Chem. Soc. Rev.* **2010**, *39* (11), 4044–4056.

(39) Cooper, A. I.; Poliakoff, M. *Chemical Physics Letters* **1993**, *212* (6), 611–616.

(40) Hieber, W.; Leutert, F. *Ber. dtsch. Chem. Ges. A/B* **1931**, *64* (11), 2832–2839.

(41) Hieber, W.; Leutert, F. *Z. Anorg. Allg. Chem.* **1932**, *204* (1-2), 145–164.

(42) Jacobs, G.; Davis, B. H. In *Catalysis*; Catalysis; Royal Society of Chemistry: Cambridge, 2007; Vol. 20, pp 122–285.

(43) Sweany, R. L. *J. Am. Chem. Soc.* **1981**, *103* (9), 2410–2412.

(44) Guggenberger, L. J.; Titus, D. D.; Flood, M. T.; Marsh, R. E.; Orio, A. A.; Gray, H. B. *J. Am. Chem. Soc.* **1972**, *94* (4), 1135–1143.

(45) Brunet, J.-J.; Kindela, F. B.; Labroue, D.; Neibecker, D. *Inorg. Chem.* **1990**, *29* (20), 4152–4153.

(46) Arion, V.; Brunet, J.-J.; Neibecker, D. *Inorg. Chem.* **2001**, *40* (11), 2628–2630.

(47) Summerscales, O. T.; Scott, B. L.; Viswanathan, H. S.; Sutton, A. D. *Inorganic Chemistry Communications* **2016**, *63*, 57–60.

(48) Maser, L.; Flosdorf, K.; Langer, R. *Journal of Organometallic Chemistry* **2015**, *791*, 6–12.

(49) Brunet, J.-J.; Chauvin, R.; Donnadieu, B.; Leglaye, P.; Neibecker, D. *Journal of Organometallic Chemistry* **1998**, *571* (1), 7–13.

(50) Jetz, W.; Graham, W. A. G. *J. Am. Chem. Soc.* **1969**, *91* (12), 3375–3376.

(51) Graham, W. A. G.; Jetz, W. *Inorg. Chem.* **1971**, *10* (1), 4–9.

(52) Schmid, G.; Kempny, H. P. *Z. Anorg. Allg. Chem.* **1977**, *432* (1), 160–166.

(53) Scheer, M.; Dargatz, M.; Schenzel, K.; Jones, P. G. *Journal of Organometallic Chemistry* **1992**, *435* (1-2), 123–132.

(54) Scherer, O. J.; Swarowsky, M.; Wolmershaeuser, G. *Organometallics* **1989**, *8* (3), 841–842.

(55) Dürr, S.; Ertler, D.; Radius, U. *Inorg. Chem.* **2012**, *51* (6), 3904–3909.

(56) Mokhtarzadeh, C. C.; Rheingold, A. L.; Figueroa, J. S. *Dalton Trans.* **2016**, *45* (37), 14561–14569.

(57) Hoffmann, R. *Angew. Chem. Int. Ed.* **1982**, *21* (10), 711–724.

(58) Dombray, T.; Werncke, C. G.; Jiang, S.; Grellier, M.; Vendier, L.; Bontemps, S.; Sortais, J.-B.; Sabo-Etienne, S.; Darcel, C. *J. Am. Chem. Soc.* **2015**, *137* (12), 4062–4065.

(59) Cambridge Structural Database (CSD), version 5.39 (November 2017)

(60) Armarego, W. L. F.; Chai, C. L. L. *Purification of Laboratory Chemicals*, 5th Ed.; *Elsevier*, **2003**.

(61) Pangborn, A. B.; Giardello, M. A.; Grubbs, R. H.; Rosen, R. K.; Timmers, F. J. *Organometallics*, **1996**, *15*, 1518–1520.

(62) Sheldrick, G. M. *Acta Cryst.* **2008**, *A64*, 112.

(63) Dolomanov, O. V.; Bourhis, L. J.; Gildea, R. J.; Howard, J. A. K.; Puschmann, H. *J. Appl. Cryst.* **2009**, *42*, 339.